SYNTHESIS AND CHARACTERIZATION OF MULTIFERROIC COMPOSITES AND THEIR POSSIBLE APPLICATION IN PHOTOVOLTAICS

Thesis Submitted for the Award of the Degree of

DOCTOR OF PHILOSOPHY

in

Physics

By

Rikky Sharma

Registration Number: 11815989

Supervised By

Dr. Deepak Basandrai (11873)

Professor

Department of Physics

Lovely Professional University

Jalandhar-Delhi, G.T. Road (NH-1),

Co-Supervised by

Dr. Rupam Mukherjee

Assistant professor

Department of Physics,

Presidency University, Bangalore,

Karnataka,150064, India

LOVELY PROFESSIONAL UNIVERSITY, PUNJAB

2025

DECLARATION

I, hereby declare that the presented work in the thesis entitled " **Synthesis and characterization of Multiferroic composites and their possible application in photovoltaics** " in fulfilment of the degree of Doctor of Philosophy (Ph.D.) is the outcome of the research work carried out by me under the supervision Dr. Deepak Basandrai, working as Assistant Professor, in the Department of Physics, School of Chemical Engineering and Physical Sciences of Lovely Professional University, Punjab, India. In keeping with the general practice of reporting scientific observations, due to acknowledgments have been made whenever work described here has been based on findings of another investigator. This work has not been submitted in part or full to any other University or Institution for the award of any degree.

Signature of scholar - 

Rikky Sharma
Reg. No: 11815989
Department of Physics
School of Chemical Engineering and Physical Sciences
Lovely Professional University
Jalandhar-Delhi, G.T. Road (NH-1),
Phagwara Punjab (INDIA)-144411
Date: 30-05-2025

CERTIFICATE

This is to certify that the work reported in the Ph.D. thesis entitled" **Synthesis and characterization of Multiferroic composites and their possible application in photovoltaics"** submitted in fulfillment of the requirement for the reward of degree of Doctor of Philosophy (Ph.D.) in the Department of Physics, School of Chemical Engineering and Physical Sciences of Lovely Professional University, is a research work carried out by **Rikky Sharma Reg. No: 11815989**, is a bonafide record of her original work carried out under my supervision and that no part of the thesis has been submitted for any other degree, diploma, or equivalent course.

Signature of supervisor

Dr. Deepak Basandrai (11873)
Associate Professor
Department of Physics
Lovely Professional University
Jalandhar-Delhi, G.T. Road (NH-1),

Signature of Co-Supervisor

Dr. Rupam Mukherjee
Assistant professor
Department of Physics,
Presidency University, Bangalore,
Karnataka,150064, India

Acknowledgment

My deepest gratitude goes out to Dr. Deepak Basandrai, my research mentor, for his continuous support, motivation, care, and critical corrections during my research. I will always be impressed by his vast and quick intellect, his ability to manage several projects at once, and his willingness to participate in all aspects of an experiment. Foremost, I would like to thank my Co-supervisor, Dr Rupam Mukherjee. He has provided guidance in my work while allowing me the freedom to work on what I was interested in. He has been an excellent mentor and very supportive throughout. I sincerely thank, my senior research associates, and colleagues, for guiding and assisting me in their methods during this research period. A hearty thanks to the whole faculty of the Lovely Professional University's physics department for their words of support. I want to convey my gratitude to Dr. Kailash Juglan (HOS) for his assistance and encouragement. Special thanks go out to the technical and non-technical employees, particularly Nithin Kumar Yadav, Ramesh Kumar, and Manoj Kumar from the physics and chemistry departments. My heartfelt gratitude is extended to Dr. Souivik Chatterjee and Sanat Kumar Adhikari (UGC-DAE Consortium for Scientific Research Kolkata Centre, India) and for their various contributions to the characterization process.

I would also like to thank my loving parents Ved Pardeep and Seema Sharma, who in addition to their support and encouragement, instilled in me the value of education and provided me with a great one. To my brother Rohit Sharma, I would want to convey my sincere gratitude. His continuous encouragement and support invaluable. To my dearest Grandma Premi Devi, your love has been a constant source of warmth and comfort throughout my life. I am incredibly grateful for your unwavering support and love.

Finally, I would like to thank my wife Mouli Mandal whose love, support and encouragement are without bounds. She has always been there for me through good times and bad and with her in my life, it is almost all good.

Rikky Sharma

Registration number: 11815989

Date: 30-05-2025

Table of content

List of Figures

List of Tables

Abstract

Multiferroics materials due to their exceptional properties hold huge potential for their applications in multifunctional, magnetic, and photovoltaic devices due to their unique properties. Researchers are actively exploring the ways to improve the electronic and magnetic strength of multiferroic materials so that they can be used for the development of next-generation devices with superior functionality, enabling miniaturization and integration into complex systems. While their photoelectric properties open doors for developing efficient solar cells. In our study, we opted for a composite system approach to enhance the overall multiferroic and optoelectronic properties of the multiferroic material. Firstly, we have synthesized a high-purity multiferroic material. The obtained multiferroic material is then used to make a multiferroic-based composite system where multiferroic material as a main matrix is used. The prepared composites have been investigated with the help of sophisticated instruments, for the morphological, electronic, magnetic, ferroelectric, and optoelectronic properties. The investigation suggested that enhanced properties of these composite systems may find their application in energy storage and photovoltaic devices. This opens the door to the creation of cutting-edge tools and uses across a range of technological domains. In our study we make various multiferroic nanoparticles and their composite systems are discussed as follows.

- $Bi_{(1-x)}\ Ba_{(x)}FeO_3$
- $Bi_{(0.9)}\ Ba_{(0.1)}\ Fe_{(1-x-y)}\ Co_{(x)}Al_{(y)}$
- $BiFeO_3$/NaCl
- $BiFeO_3$-$CoFe_2O_4$
- $Bi_{0.99}Nd_{0.01}Fe_2O_3$/ZnO

The sol-gel method is used to produce multiferroic material. The produced multiferroic material is used as a matrix and other materials as reinforcement are used to create a composite system with the help of mechanical grinding and press. The dielectric, magnetic, structural, optical, morphological, and ferroelectric properties were analysed using Impedance spectroscopy, Vibrating-Sample Magnetometer (VSM), X-ray powder diffraction (XRD), UV-Vis-NIR Spectroscopy, Field Emission Scanning Electron Microscope (FE-SEM), and ferroelectric loop tracer methods.

The Nanoparticles of Ba doped Bismuth ferrite was synthesized. The structural and morphological studies show the presence of Bismuth ferrite rhombohedral R3C group phase along with few impurity phases developed by the addition of Barium. The substitution of barium reduces crystallite size by 1.76 times. It is observed that the addition of Barium to $BiFeO_3$ has enhanced the Hc coercivity by 1.23 times as compared to undoped $BiFeO_3$. A similar trend is observed in the dielectric investigation where the substitution of Ba has a significant impact on materials dielectric.

Another nanoparticle has been fabricated of composition $Bi_{(0.9)}$ $Ba_{(0.1)}$ $Fe_{(1-x-y)}$ O_3 with $Co_{(x)}$, $Al_{(y)}$ as a dopant were used. The structural examination reveals the presence of $BiFeO_3$ belonging to rhombohedral phase along with the few impurity phases in the samples. The crystallite size is found to decrease along with the shrinkage in Lattice Constant. The SEM images show the formation of irregular and heterogeneous structures. It has been observed that the addition of Co followed by Al is found to reduce impurity phases. The presence of Co and Al is confirmed by EDX mapping. The dielectric response of the samples as a function of frequency is observed demonstrate the change in t dielectric constant and reduction in dielectric loss. The magnetic study reveals that subsequent addition Co and Al has offered improved magnetic properties attaining maximum Hc =1570 Oe at room temperature.

Composite systems consisting of ionic sodium chloride (NaCl) as a filler with varying weight percentages (x = 0%, 10%, 30%, and 50%) embedded into the matrix of multiferroic bismuth ferrite ($BiFeO_3$). The insertion of NaCl leads to the formation of secondary structural phases with particle grain size ranging from 0.5-1.5μm. The coercive field (Hc) is found to be maximum H_c = 79.18 Oe for the composite system with x = 10% in contrast to other composite samples. The electrical impedance study reveals that at a low-frequency regime, the dielectric permittivity has relatively increased for the composite systems compared to pure bismuth ferrite (BFO). Also, at low frequency the dielectric losses vary with filler percentages but remains comparable at the high-frequency limit, indicating a possible role in the energy storage application. Exponent (n) for frequency-dependent electrical conductivity is found to be large (n > 1) which is due to various degrees of the proximity of adjacent NaCl grains distributed in a multiferroic matrix.

The matrix of multiferroic $BiFeO_3$ (1-x) and $CoFe_2O_4$ (x) as a filler with varying weight fractions (x =10, 30, 50%) has been synthesized. The microstructure reveals that the filler

at a critical weight fraction of 30% forms a clustering network that spans the entire system. DC resistivity of the composite systems confirms the semiconducting behavior where the large change in resistivity is mainly attributed to scattering by grain boundaries between percolating clusters. The VSM analysis implies that saturation magnetization (M_s) in composite samples with x = 10% and 50 % increases to 17 emu/g and 35 emu/g respectively. The composite samples exhibit optical band gap below 3 eV offering applicability in photovoltaic devices. The impedance analysis showed the presence of severe trapped charges that lead to a depolarization effect in composites. However, the dielectric loss remains low for all composite systems till 10^4 Hz with the loss peak appearing around 10^5 Hz.

The composite system of $Bi_{0.99}Nd_{0.01}Fe_2O_3$ matrix and ZnO is prepared. The ZnO with cubic phase and BFO with rhombohedral phase were observed in the composite samples. On the introduction of a filler, ZnO nanoparticles were found to affect the grain structure and grain boundaries. The impedance analysis reveals the presence of large resistance offered by a composite maximum of 46.8 KΩ at x= 10%. The change in dielectric response in sample were observed at higher concentrations for (x= 5 %). The energy band gap in the composite sample exhibits significant dependence on ZnO concentration. The Ferroelectric investigation of the composite system shows that for x= 10% with P_r = 22.13 μc/cm^2 is the maximum achieved polarisation.

The prepared composite system showed up enhancement in electronic, magnetic, and optoelectronic properties. The finely tuned composite system may benefit the advances in the fabrication of multifunctional devices and find their potential applications in dielectric, photovoltaics, memory, and biomedical devices.

Outline of the thesis

This thesis was divided into five chapters, with **Chapter 1** briefly introducing the material and its type, and research ideas, including information on crystal structure and electronic properties and their scope in science and technology. The literature on the materials used is reviewed in **Chapter 2** describing ongoing progress and previous research in the relative field. Methods for synthesis and synthesized materials are provided in **Chapter 3**. The research techniques are also explained in **Chapter 4**. **Chapter 5** provides an in-depth investigation of the experimental results for each sample are given.

Chapter 1

Introduction

1.1 Multiferroics

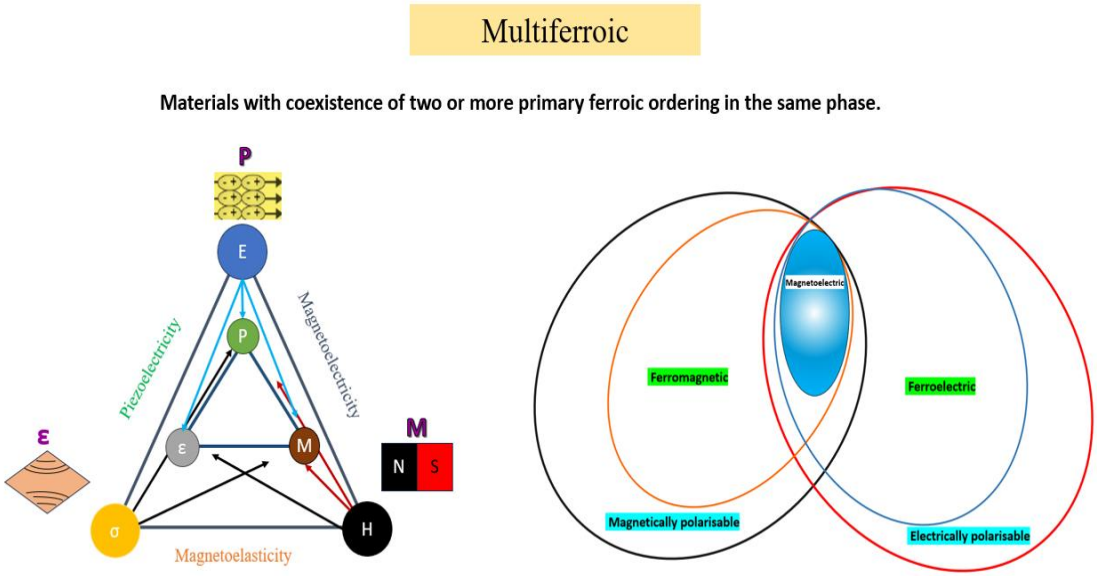

Fig.1.1 Multiferroic Materials

Multiferroic is an interesting class of materials that exhibit multiple ferroic ordering in a single material [1], [2], [3], [4]. From the perspective of device application, the magnetic and electronic properties are key factors of a material. The multiferroic material coexists with ferromagnetic, ferroelasticity and ferroelectricity which makes them an ideal candidate for a device application but it is observed that multiferroic materials exhibit these properties at different ordering temperatures which limits their use in device applications. Although, some well-known multiferroic such as $BiFeO_3$ [5], $YMnO_3$ [6] , $BiMnO_3$ [7] show multiferroic nature at room temperature yet they exhibit weak magnetic and electronic properties at room temperature. So, by improving magnetic and electric characteristics we can fabricate energy-efficient and new-generation multifunctional devices.

However, the existence of magnetoelectric, piezoelectric, and magnetoelasticity coupling as illustrated in Fig.1.1 opens the door for new kinds of multiferroic materials. This coupling allows to manipulate magnetic effect by applying electric field or external stress and vice versa. The magnetoelectric coupling is based on direct and indirect mechanism. In the case of direct coupling, the interaction between magnetic moments

and electric fields occurs through various mechanisms, such as spin-orbit coupling, where the orbital motion of electrons is influenced by their spin. The magnetic characteristics of a multiferroic material can be influence by using electric field and vice versa. Also by adjusting the electronic structure enables us to modify materials magnetic and electronic properties. Similarly, piezoelectric, and magnetoelasticity is a result of applied strain categorized as indirect coupling. The strain can influence the dipoles, which in turn may have an impact on the material's magnetic order and electric polarization. Similarly on applying an applied magnetics and electric field can cause a shift in the magnetic order, which can cause the crystal lattice to change position. This ability to regulate both magnetism and electricity with a single input creates amazing new possibilities for futuristic technology.

1.2 Ferroic Characteristics

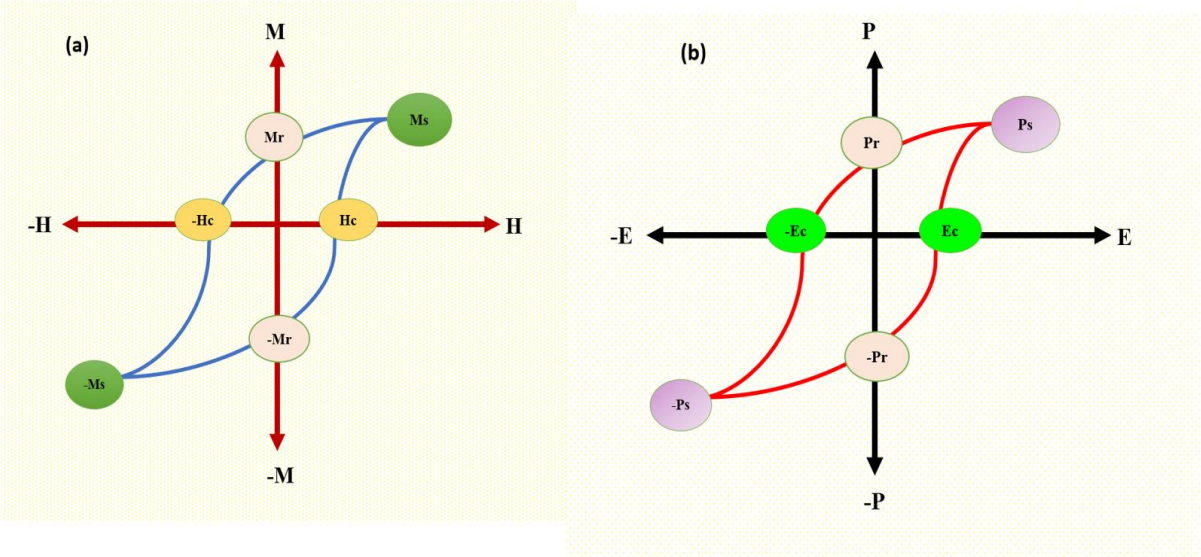

Fig.1.2 (a) M-H curve for ferromagnetic materials (b) P-E loop for ferroelectric materials.

There are four distinct kinds of ferroic characteristics: ferroelectric, ferroelastic, ferrotridicity, and ferromagnetic. Multiferroic material is described as a material having any of two or more types of ferroic ordering. To understand more about these different ferroic characteristics they are discussed below.

1.2.1 Ferromagnetic Characteristics

The term "ferromagnetism" first came from the magnetic characteristics of ferrite, it is a class of magnetic materials that exhibit permanent magnetic moment. The behaviour of magnetic domain lines in a magnetic substance is explained by the domain theory. These materials have the tendency to get magnetized under the effect of external magnetic field also they can store residual magnetic moment making them ideal for memory devices and permanent magnets. The various magnetic parameters like coercivity, retentivity, Bohr magnetons, and magnetic anisotropy constant can be analysed using B-H loop as shown in Fig.1.2 (a) also known as hysteresis loop.

1.2.2 Ferroelectric Characteristics

Ferroelectricity is the spontaneous polarization of a dipole when insulating material is induced between two conducting plates and electric field is applied. By changing the direction electric field of the ferroelectric material direction of polarisation can be reversed. The ferroelectric strength of a material can be analysed using P-E loop as shown in Fig.1.2 (b). These materials' alignment of charge spices makes them ideal for energy storage devices.

1.2.3 Ferroelastic Characteristics

The ferroelastic phenomena are based on internal strains that cause structural distortion where atoms are placed in a specific arrangement. On applying an external stress, the arrangement of atoms is displaced resulting in a different state.

1.2.4 Ferrotridicity Characteristics

This is a new kind of magnetic characteristics. It is different from ferromagnetism it involves microscopic vortices spinning in the same direction. The magnetization is produced when the direction of the vortices changes, breaking the time-reversal symmetry. However, as this property is new, an in-depth investigation is going on to uncover new methods of manipulating magnetism and their implementation in magnetic devices.

1.3 Structure

Ferromagnetic behaviour occurs due to the existence of partially occupied d orbitals; however, ferroelectric behaviour is due to an empty d orbital. This leads to a clear obstacle to the existence of such types of materials. This results in a blatant barrier to the existence of such kinds of materials. The multiferroic material's structure is responsible for the coexistence of ferroic ordering. Most multiferroics have perovskite ABO_3 shown in Fig.1.3. named after Russian mineralogist L.A. Perovskite, here O signifies oxygen and both A, B represent two cations. ABO_3 is a particularly intriguing class of material with a crystal structure comparable to calcium titanium oxide.

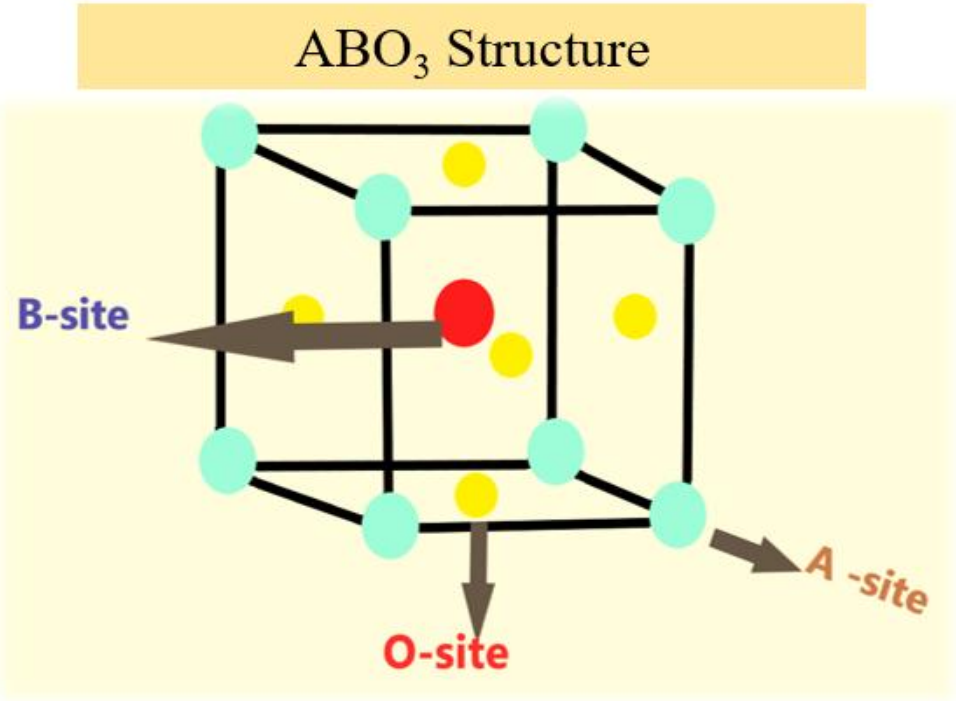

Fig.1.3 perovskite ABO_3 structure.

In perovskite the structure is generally cubic but distortion is common in structure and it depends upon the tolerance factor in equation 1 [8].

$$t = \frac{(r_a + r_o)}{\sqrt{2}(r_b + r_o)} \quad (1)$$

The ionic radii of the A and B is referred as r_a and r_b is the ionic radii of B ions, respectively, and r_0 is the ionic radii of oxygen, which is used further to determine the structure of the perovskite material. Perovskite does not typically have the perfect cubic structure, and this distortion results in several extremely intriguing features, including

ferroelectricity and multiferroic properties. Also, the tolerance factor can tell us about the structure of the material as represented in Table.1.

Table.1 Tolerance factor effect on structure.

Tolerance factor (t)	Effect	Possible structure
t > 1	A is larger than B cation	Hexagonal/ tetragonal
t lies between 0.9 to 1.0	Ideal conditions	Cubic
t lies between 0.7 to 0.9	A are smaller than B cations	Orthorhombic/ rhombohedral
t< 0.71	A and B cations are of similar size	Different structures

1.4 Types of Multiferroic Materials

Two primary categories for the multiferroic characteristics of distinct material systems result from different mechanisms known as Type-1 and Type-2. In Type 1 multiferroics feature weak coupling and separate origins for ferroelectricity and magnetism [9]. In case of Type-2 multiferroic materials, magnetism is created by ferroelectricity and vice versa with strong coupling. Fig.1.4 shows the classification of multiferroic and their various mechanism are discussed below.

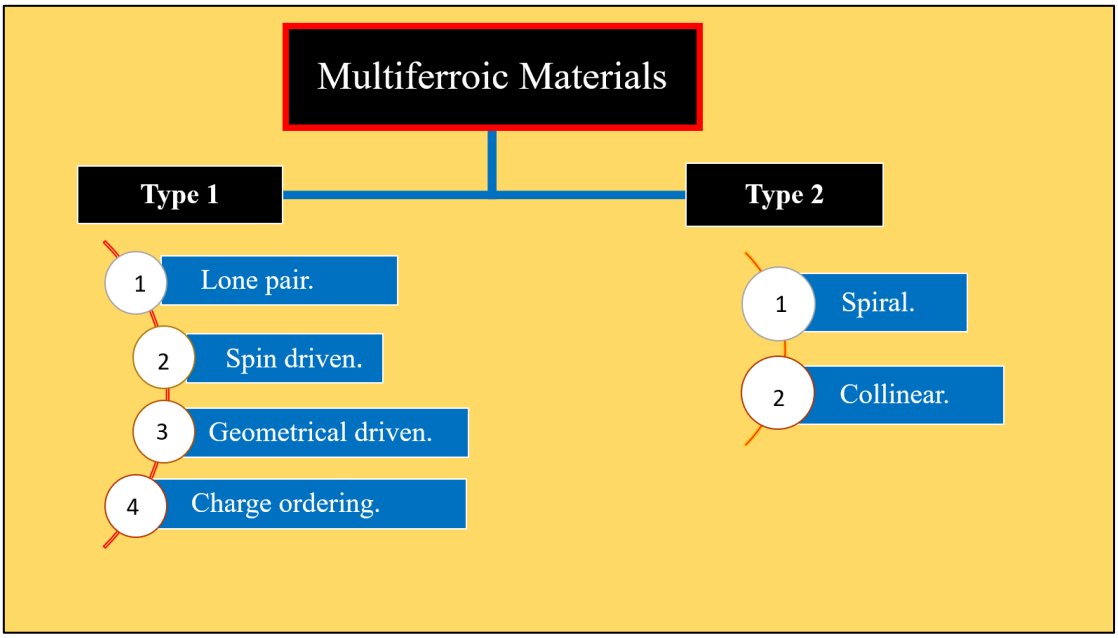

Fig.1.4 Types of multiferroic materials.

1.4.1 Type 1 multiferroics

In type 1 multiferroics, the origin of ferromagnetism and ferroelectricity exist independently. Type 1 multiferroics are simpler to create and integrate into current technology due to their simpler design. However, a lower correlation between their electric and magnetic properties and the degree of responsiveness limits the potential applications of these materials. The type 1 multiferroic are subcategorised based on the mechanisms behind their different ferroic orderings which are discussed below.

1.4.1.1 lone pair multiferroics

The source of ferroelectricity in case of lone pair multiferroics is attributed to the A-site cation, and the magnetic characteristics are attributed to the B-site due to incompletely filled d orbitals. The cation consists of an electron pair in their outermost shell which distorts the atomic arrangement due to the repulsion between them. Because of this distortion, an electric dipole moment is created, resulting in ferroelectric polarization.

However, the unpaired electrons due to the B site which are generally transition metals contribute to magnetic properties. For example, $BiFeO_3$ [10], $BiMnO_3$[11] , $PbVO_3$ [12] .

1.4.1.2 Spin driven

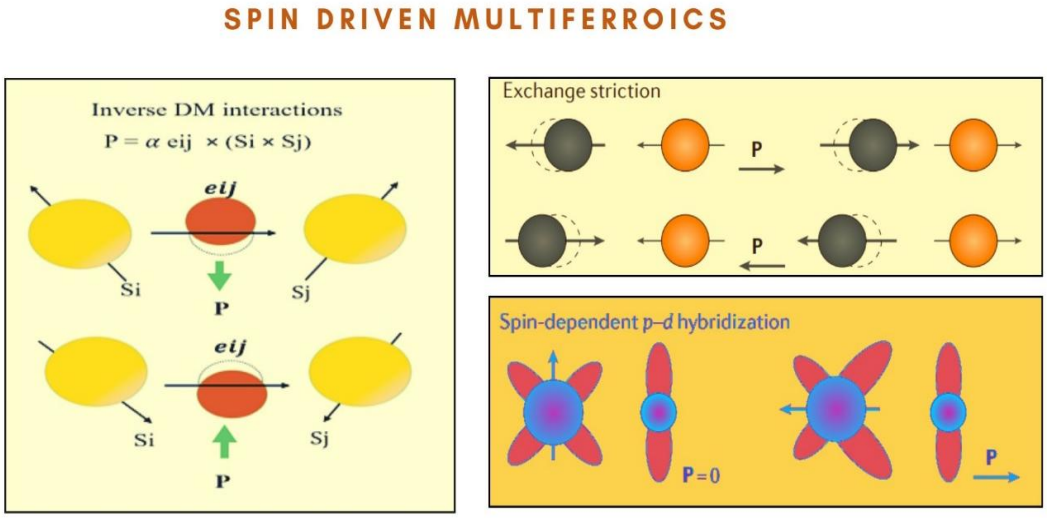

Fig.1.5 Spin-driven multiferroic materials [13].

The existence of multiferroicity in this scenario is due to the phenomenon of spin-orbit coupling. This origin is based on three microscopic mechanisms, as shown in Fig.1.5. Symmetric spin exchange, antisymmetric spin exchange, and spin-dependent p-d hybridization. The symmetric spin exchange comes into play when neighbouring spins that are aligned parallel or antiparallel interact with each other and create distortion in the crystal lattice. This distortion ends up breaking the symmetry thus resulting in ferroelectric polarization. However, the antisymmetric spin exchange also depends on neighbouring spin but it is independent of the alignment of spin. It encourages the spin to tilt out of alignment to break the symmetry. In Spin-dependent p-d hybridization, the distortion in nearby electrons is held responsible for the breaking of symmetry which result in induction of polarization. However, the contribution of the mechanism depends upon the material property and its crystal structure [14].

1.4.1.3 Geometrical driven

The structural phase transition factor is one of the reasons for the polar ferroelectric state. In this case, ionic shift and polar distortion are due to the steric effect. This steric effect is due to the geometrical distortion, strain and size effects etc which contribute to the

ferroelectric state. This type of mechanism is observed in the multiferroic ($BaMF_4$) barium fluorides. [15], [16], [17]

1.4.1.4 Charge ordering-

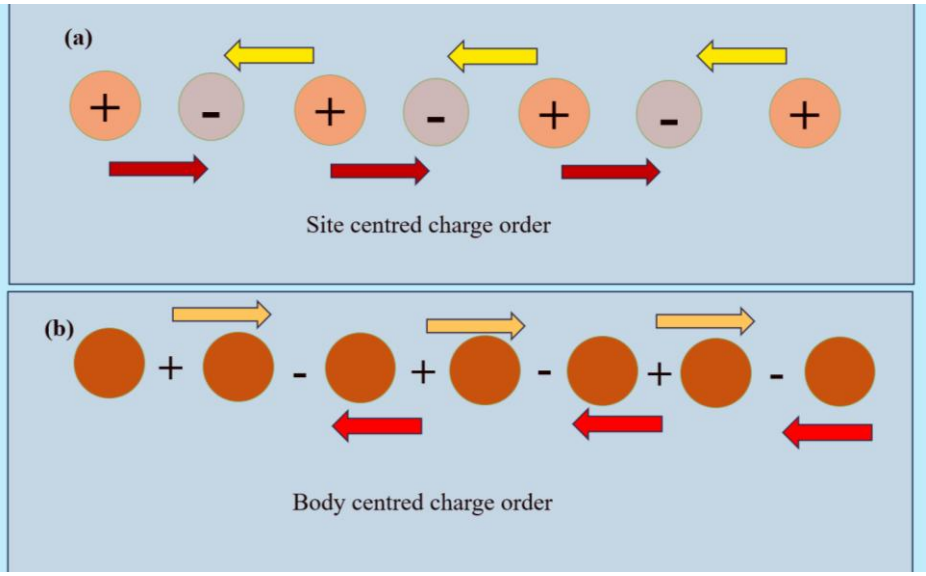

Fig1.6 Charge ordering mechanism in multiferroics.

The mechanism of multiferroicity in these materials is the broken inversion symmetry due to the co-existence of Site-centred charge ordering and Body-centred charge ordering [18]. In the case of site centred the electrons are located inside the lattice structure of a material at specific locations. This organizes the charges in an ordered manner, usually in a repeating pattern as shown in Fig.1.6 (a). However, body-centered ordering refers to a certain arrangement of atoms in a unit cell, with one atom positioned in the center and one at each corner as shown in Fig1.6 (b). For example, $LuFe_2O_4$ [19]

1.4.2 Type 2 multiferroics

Type 2 multiferroics exhibit an even more interesting interplay between magnetic and electric fields, indicating a stronger connection and potentially leading to new and more useful technologies. Type 2 multiferroic are classified into two categories discussed below.

1.4.2.1 Spinal

Spiral multiferroics are an intriguing subclass of multiferroic materials in which the magnetic spins create a corkscrew-like spiral pattern rather than aligning in one direction. Spiral multiferroics are being diligently studied for applications in spintronics, information storage devices, and novel forms of magnetoelectric sensors because of their

high magnetoelectric coupling and electrical controllability over magnetism. Some well-known spiral multiferroics are $TbMnO_3$ (Terbium Manganite), $Ni_3V_2O_8$ (Nickel Vanadate) $MnWO_4$ (Manganese Tungsten Oxide).

1.4.2.2 Collinear

Multiferroic materials with aligned magnetic spins in a single direction are known as collinear multiferroics. A certain kind of magnetic ordering known as a spiral spin can provide a mild ferroelectric effect even in this configuration. The crystal lattice deformation in these kinds of materials is what causes the weak ferroelectric effect. The material may become net electrically polarised because of this distortion, which can also change the locations of positive and negative ions. Some commonly known collinear multiferroics are Ca_3CoMnO_6 (Calcium Cobalt Manganese Oxide), and $RMnO_3$ (Rare Earth Manganite)**,** where R can be elements like Lu, Yb, and Y.

1.5 Opportunities

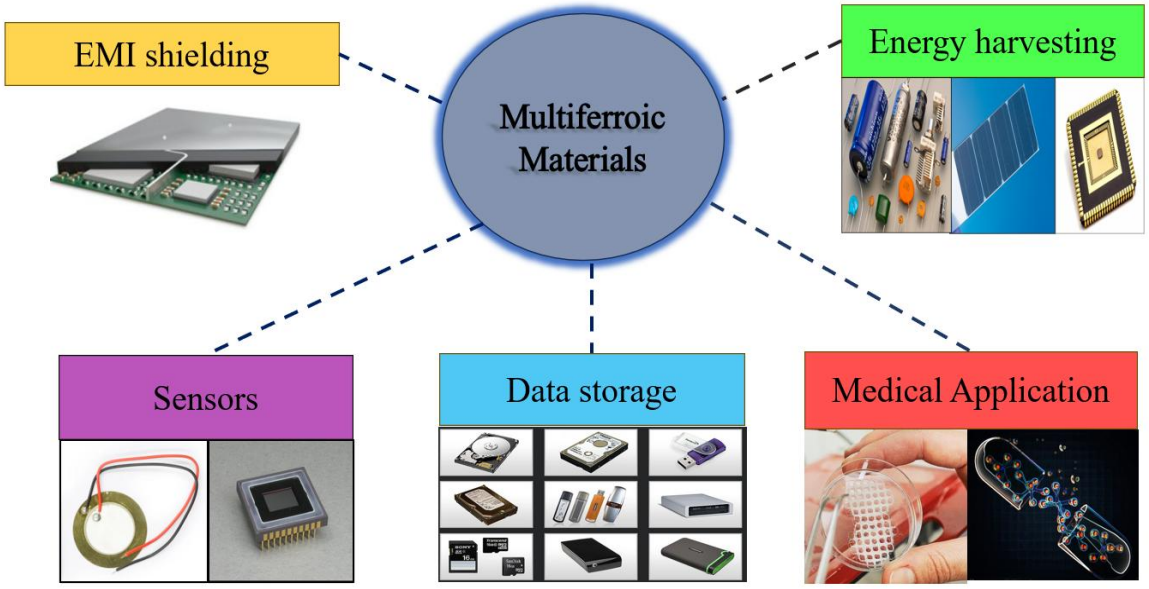

Fig.1.7 Application of multiferroic materials.

Multiferroic materials provide a multitude of possibilities because of (i) the special way in which they combine several ferroic characteristics. (ii) their distinctive feature such as the existence of large magnetoelectric coupling at room temperature. Multiferroic materials also show sustainability as shown in Fig.1.7 i.e. novel novel applications for

next-generation energy harvesting, memory, biological, and electronic technology [20], [21], [22], [23], [24], [25]. From the perspective of environmental safety, these materials are safe and mostly inorganic and can be synthesized at low manufacturing costs.

1.5.1 EMI shielding

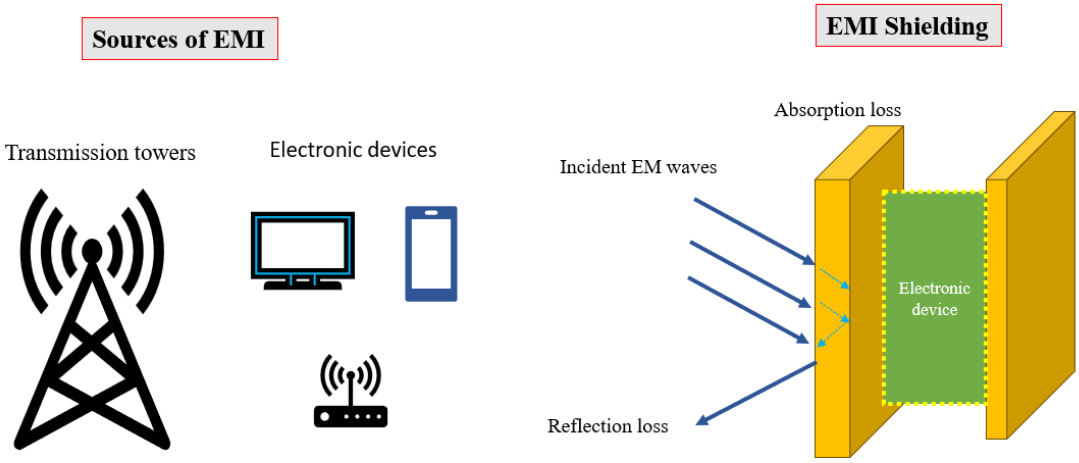

Fig.1.8 Multiferroics in EMI shielding.

Electromagnetic fields (EMF) are everywhere in the world. They originate from a variety of sources such as power lines, radios, and even other electronic gadgets. These electromagnetic fields (EMFs) can affect the delicate signals found in electronic equipment, resulting in malfunctions. Electronics are thus required to be shielded from this harmful electromagnetic interference (EMI). This shielding act as a barrier that blocks electromagnetic interference (EMI). Its components, which are magnetic or conductive, can act as this shielding to keep electronics safe from electromagnetic interference from the outside environment and to ensure proper operation illustrated in Fig.1.8.

Multiferroic materials because of their magnetoelectric interaction are used as materials for microwave absorption. Since a good electromagnetically suited material has a strong complementarity between both its permittivity and permeability, it regularly displays great microwave absorption. Researchers examined several types of multiferroic materials and their resulting composite systems, and they concluded that they exhibit substantial reflection losses, making them an effective choice of materials utilized in microwave absorption [26], [27], [28], [29], [30], [31], [32], [33], [34].

1.5.2 Energy Harvesting

Multiferroic materials offer a variety of applications due to their electronic properties in capacitors, transistors, photovoltaics, and spintronics.

1.5.2.1 Multiferroic in dielectrics

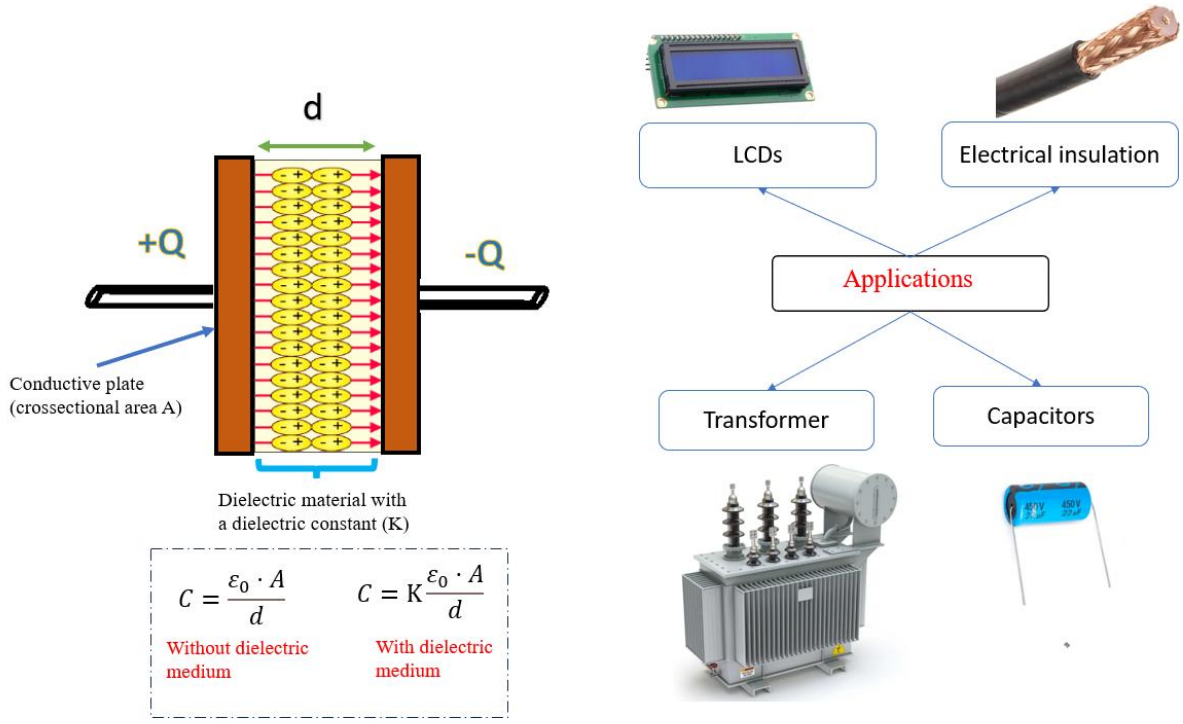

Fig.1. 9 Multiferroic in dielectrics.

Dielectric substances are commonly recognized for their ability to store energy. They are used in the fabrication of capacitors, batteries, and transformers. A dielectric material becomes polarized when placed in an external electric field, thus causing a movement of internal charges, as shown in Fig.1.9. However, the polarization that occurs in these materials is due to various mechanisms, such as ionic, space charge, and dipole. In the case of dielectric materials, one crucial factor when determining the strength of the material is the dielectric constant. Multiferroic materials, which are predominantly insulators, exhibit a large dielectric constant, making them essential for developing effective capacitors and various electronic devices.

Also, some multiferroic and their composite system such as $BaTiO_3$-$NiFe_2O_4$ [35], $BiFeO_3$ [36], $BaTiO3–CoFe_{1.8}Zn0.2O_4$ [37], $BaTiO_3$-GdO_3 [38] materials exhibit high dielectric constants (k), offering usage in capacitors. Also, the connection between the magnetic and electronic properties give rise to new possibilities for spintronic devices

new studies are carrying out to combine multiferroic in transistors and memory devices offering faster and more efficient devices [39], [40].

1.5.2.2 Multiferroics in Photovoltaics

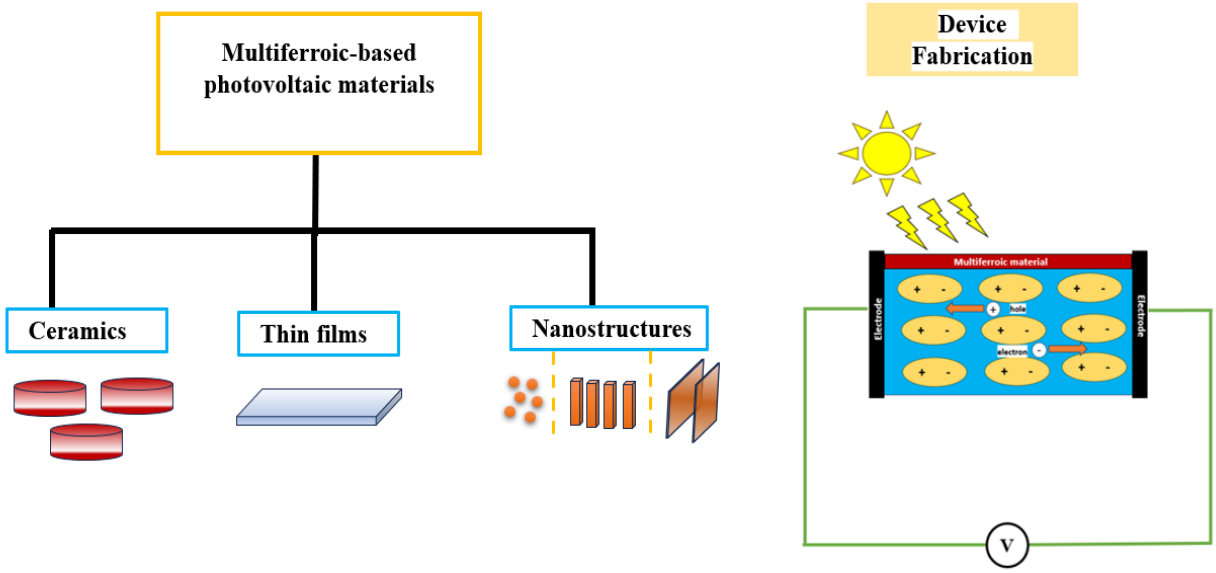

Fig.1.10 Multiferroics in Photovoltaics.

Multiferroics exhibit powerful magneto-optical effects, allowing significant changes in their optical properties—such as refractive index and absorption. The interaction of light's electric and magnetic components with the material's electric polarization and magnetization allow us to manipulate electric polarization and magnetization with external fields empowers active tuning of key optical parameters, including refractive index and absorption. This opens new avenues for applications in multiferroic based optical devices. The photovoltaic properties offered by multiferroic are very interesting where ferroelectric-driven polarization is held responsible for the generation of charge carriers. Unlike conventional p-n junction diodes, multiferroic-based materials operate based on the ferroelectric principle, which states that an electron-hole pair is produced when a photon from the sun is absorbed by a ferroelectric material illustrated in Fig.1.10. An internal field is produced because of significant inversion symmetry breaches, effectively maintaining the separation between photo-excited charge carriers, and producing a high open circuit voltage. Therefore, the output voltage is not limited to these materials. The high efficiencies, low potential material costs, and low processing costs of perovskite-based photovoltaics are indeed promising for futuristic purposes.

Perovskite solar cells are still promoted as the PV technology of the future, and much development work and research are invested into making this a reality Over the past years, several initiatives have been undertaken to develop these materials to produce energy, and ongoing efforts are being made to prepare them for industrial use [41].

1.5.3 Multiferroic in Data Storage

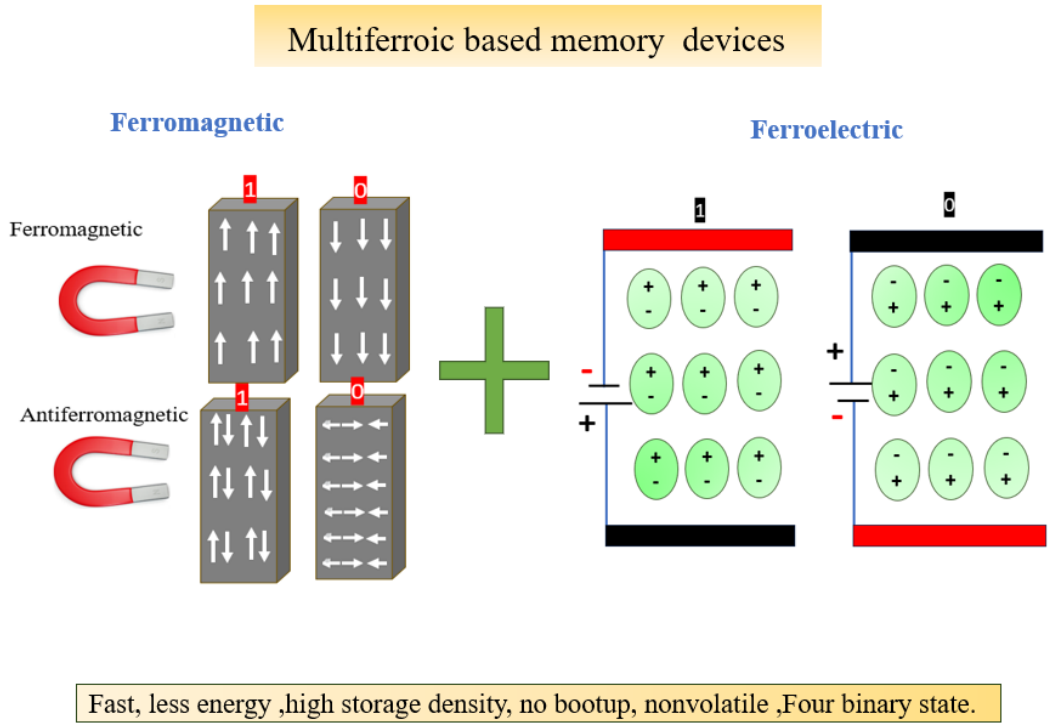

Fig1.11 Multiferroics in memory devices.

Memory devices are not only for computers, Smartphones, music players, cameras, and televisions all make use of them to store pictures, music, memories, and entertainment, which makes them essential in our digital world. These devices are composed of either ferroelectric or ferromagnetic materials. The polarization approach described in Fig.1.11 paired with an external field, is used to store data in the form of binary digits. However, magnetic, and ferroelectric memory devices have distinct benefits and limitations.

The multiferroic-based memory devices offer a mix of ferroic ordering. The main advantage of multiferroics is the interplay between their electrical and magnetic

properties which allows us to regulate the electronic state by external magnetic field and the other way around. Additionally, in conventional data storage, binary data (0 or 1) is represented by a single attribute, such as the magnetism found in hard drives. However, there are two knobs which can be manipulated by multiferroics: magnetic orientation and electric polarization. This offers up to four combined states as shown in Fig.1.11, which ultimately can increase data density. These qualities make multiferroic materials a superior option for low-power data storage device manufacturing since they require less energy to operate [42], [43], [44].

1.5.4 Multiferroic Sensors

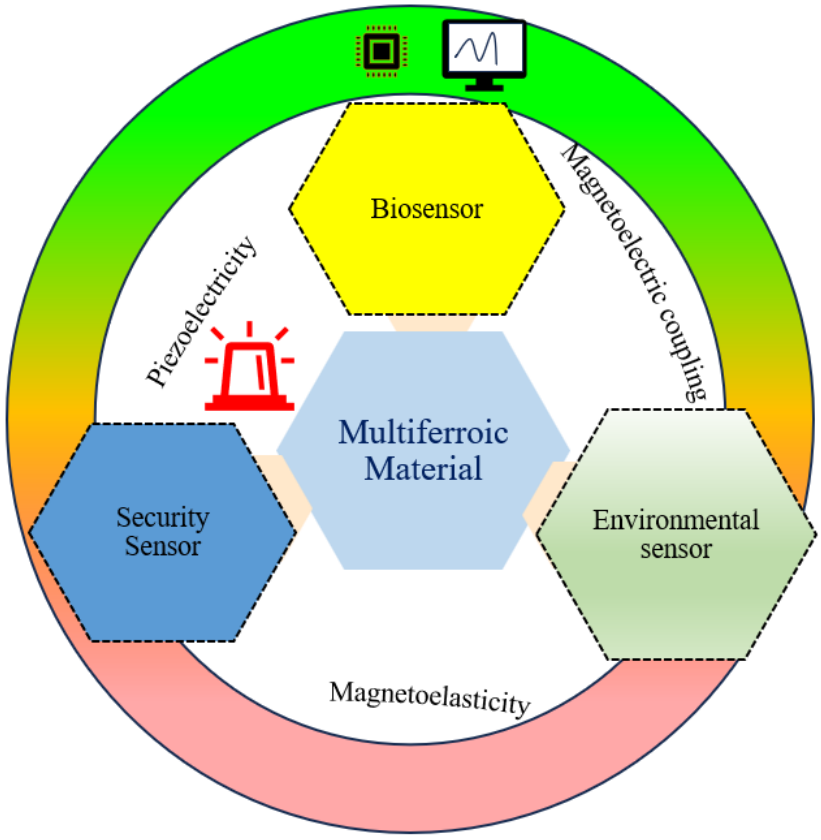

Fig.1.12 Multiferroics in sensor.

Sensors play a crucial role in our daily lives. They make sure that our devices function smoothly and properly. They can detect and respond to their surroundings making them useful for security, weather forecasting, and bio sensing as shown in Fig.1.12. It is possible for a single multiferroic sensor to simultaneously detect electric and magnetic fields thereby it possible to identify several signals at the same time [45]. It is observed

that sensitivity to magnetic fields in multiferroics is greatly amplified by the magnetoelectric coupling, making them useful for highly sensitive magnetic field sensors [46]. Some multiferroic materials have been found to change their electrical or magnetic features when they are subjected to pressure or mechanical strain making them ideal choice for sensor in biomedical application. These properties are evident enough to investigate multiferroic materials and make their potential application in sensors.

1.5.5 Medical application

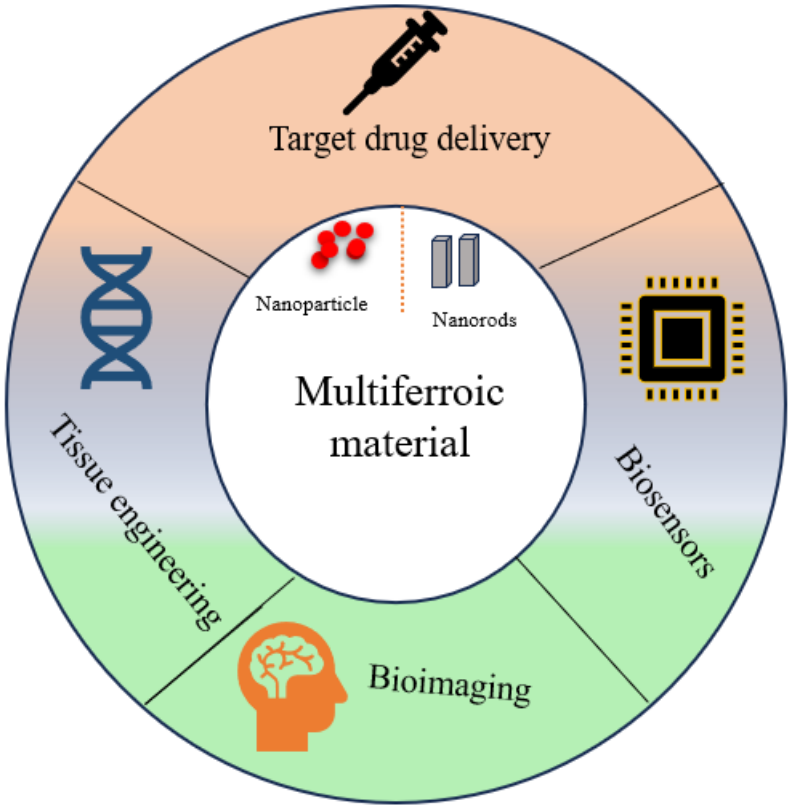

Fig.1.13 Multiferroics in memory devices.

Multiferroics materials has the capability to regulate electrical functions using a magnetic field which might be utilised in medical field. Various type of coupling in multiferroic materials offers the applicability of multiferroic materials in medical science [47] as shown in Fig.1.13. A few of these applications include target medication delivery [48], tissue regeneration [49], and magnetically controlled biosensors [50]. Researchers are now focusing on assuring biocompatibility, creating efficient delivery techniques, and improving material properties.

1.6 Progress in Multiferroic Materials

Researchers over the years have been actively exploring ways to improve the multiferroic materials and to maximize the potential of multiferroic material for device application. The multiferroic based thin films and nanostructures are fabricated to enhance their electronic and magnetic properties for their specific application. However, to enhance the properties of multiferroic materials are tailored using the two main mechanisms which are (i) Doping at A and B sites (ii) Composite system, both approaches have their advantages discussed as follows.

1.6.1Doping at A and B site

One method that has been investigated to improve a multiferroic material's multiferroic characteristics is doping the A and B sites. The doping enables us to modify the electronic band structure of a material by adding extra electrons or electron holes. This modification can impact on how the electrons interact, hence affecting the electrical and magnetic characteristics. Different-sized ions can cause strain in the crystal lattice during doping, which can change the magnetic ordering and perhaps improve the magnetoelectric interaction between the electrical and magnetic characteristics. It can create vacancies in the oxygen sublattice, impacting electrical conductivity and influencing magnetic properties through complex mechanisms. It is observed that addition of rare earth elements and transition in multiferroic materials has significantly enhanced their electronic and magnetic properties. Various researchers have investigated this approach by doping at the A or B site, simultaneously both sites to achieve enhanced multiferroic properties [14], [51], [52], [53], [54], [55], [56]. Nevertheless, while doping, a few important factors such as concentration, the development of undesirable secondary phases, and dopant selection should be considered. Overall, A-site and B-site doping may be used to tune and improve the multiferroic features of materials in several ways. Through dopant interaction, we may produce materials with improved functionality are useful for various device applications.

1.6.2 Composite system approach

In this approach a multiferroic material is used to make a composite system with another multiferroic or non-multiferroic material. In composite material each phase has independent performance and offer higher magnetoelectric coefficient compared to

single-phase multiferroics. This approach offers a variety of advantages over doping. We can construct composite systems with desired multiferroic characteristics by mixing different materials and designing the interface. Doping has a limited ability to alter the source material. With the help of composites, one can combine many materials, with different characteristics, to produce a final product with a unique set of characteristics. Also, the composite system with the combined features is superior to what either component might offer individually. The distribution and arrangement of the various components of a composite can be carefully controlled whereas in doping atoms distribute randomly which makes it possible to adjust the final properties. Composites can be designed to have multiple functionalities, especially for multiferroics which can exhibit magnetodielectric and magnetoelectric coupling. To do this, several multiferroic materials with complimentary and non-multiferroic characteristics are combined

Also, by combining the advantages of each material, we may get beyond their shortcomings, such as poor magnetoelectric coupling or undesirable secondary phases. It also leads to a large pool of possible materials making it possible to continuously explore and find new composite systems with remarkable multiferroic characteristics. This method significantly enhanced the overall characteristics of multiferroic materials [57], [58], [59], [60], [61], [62], [63], [64]. Despite the significant advantages, the composite system approach also faces certain challenges. For the composite system to operate consistently and dependably, optimal control and homogeneity of the interface qualities must be achieved. For practical applications, scalable and effective methods for creating high-quality composite systems with well-specified interfaces must be developed. More optimization and creativity will require a full grasp of the interactions between various materials and the impact of the interface on multiferroic behaviour. In summary, the use of composite systems presents a viable strategy for realizing the whole potential of multiferroics. We can produce innovative materials with specific qualities by mixing diverse materials. This will open new door for enhanced multiferroic materials which can be utilised in multifunctional devices, sensors, photovoltaics, and new memory devices.

1.7 Bismuth ferrite ($BiFeO_3$)

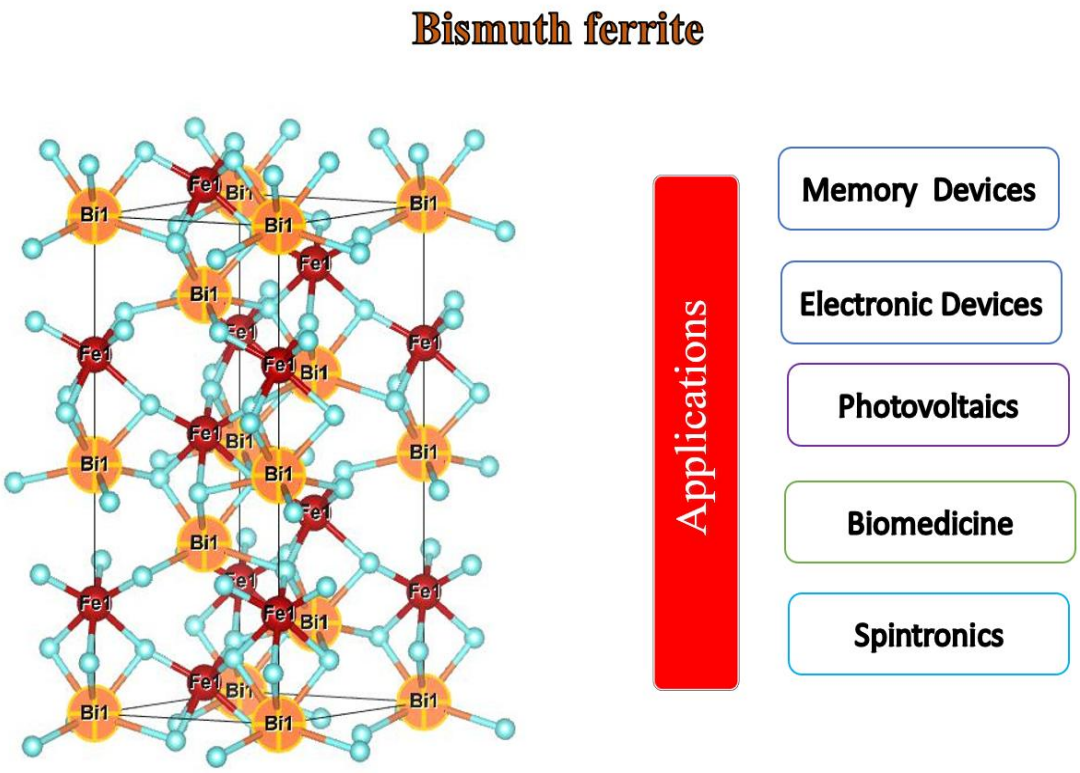

Fig1.14 Bismuth ferrite structure

The bismuth ferrite with chemical formula $BiFeO_3$, stands out a fascinating material that is classified as part of the multiferroics class. These materials are incredible because they respond differently to electric and magnetic fields because of their various ferroic qualities. When it comes to bismuth ferrite, it is both antiferromagnetic—that is, its magnetic moments are arranged in an opposite pattern—and ferroelectric, which means that an electric field can vary its electric polarization. To understand some more details let us have a close look at the structure of $BiFeO_3$ in Fig.1.14. We can observe that the A site has active lone pairs of Bi^{3+} with two 6s electrons not participating in the bond, which is responsible for the ferroelectric response. However, the B site Bi^{3+} ions are simultaneously available magnetic characteristics. The structure of BFO is a deformed

rhombohedral belonging to perovskite class. An octahedron comprising a smaller cation (B-site) encircles the big cation (A-site) in the centre, with oxygen anions occupying the spaces between them. Because of the tilting of the FeO_6 octahedron and the enormous size of the Bi^{3+} cation, the rhombohedral unit cell in BFO is somewhat deformed. This distortion is essential to its multiferroic characteristics. Bismuth ferrite in the forms such as doped bismuth ferrite, thin films, nanostructures, and ceramics are prepared for targeted applications. Also bismuth ferrite exhibit narrow bandgap and multiferroic ordering at room temperature making it suitable for optoelectronic devices making it a better alternative of led based photovoltaics. Nevertheless, there are still several drawbacks to bismuth ferrite, such as high leakage current and inefficiency, which restrict its applicability of this material. While research continues to be conducted to fully utilize bismuth ferrite's potential for utilizes in data storage, spintronics, sensors, and even solar cells, its unique combination of room temperature features makes it highly exciting for future innovation.

1.8 Cobalt ferrite ($CoFe_2O_4$)

Fig1.15 Cobalt ferrite structure and its application.

Cobalt ferrite is well well-known magnetic material it has a variety of electrical, thermal, and magnetic characteristics, making it a useful filler material option. The inverse spinel

structure is one of the interesting structures seen in Fig,1.15. In this arrangement, cobalt (Co^{2+}) ions fill semi octahedral sites, and (Fe^{3+}) ions fill remaining sites. This specific arrangement of cations is resulting in exclusive magnetic and electric properties of cobalt ferrite. These features when paired with a multiferroic matrix can be advantageous for enhancing multiferroic material which can be utilised in various applications, including electromagnetic shielding and magnetic memory [65]. The high magnetic strength o of cobalt ferrite can influence bismuth ferrite magnetic properties which can be employed in target drug delivery [66]. Cobalt ferrite is affordable and non-hazardous since it can be made using a simple chemical process [67] and in an environmentally friendly manner [68]. These qualities make this material an ideal choice for making composite system with multiferroic material.

1.9 Sodium Chloride (NaCl)

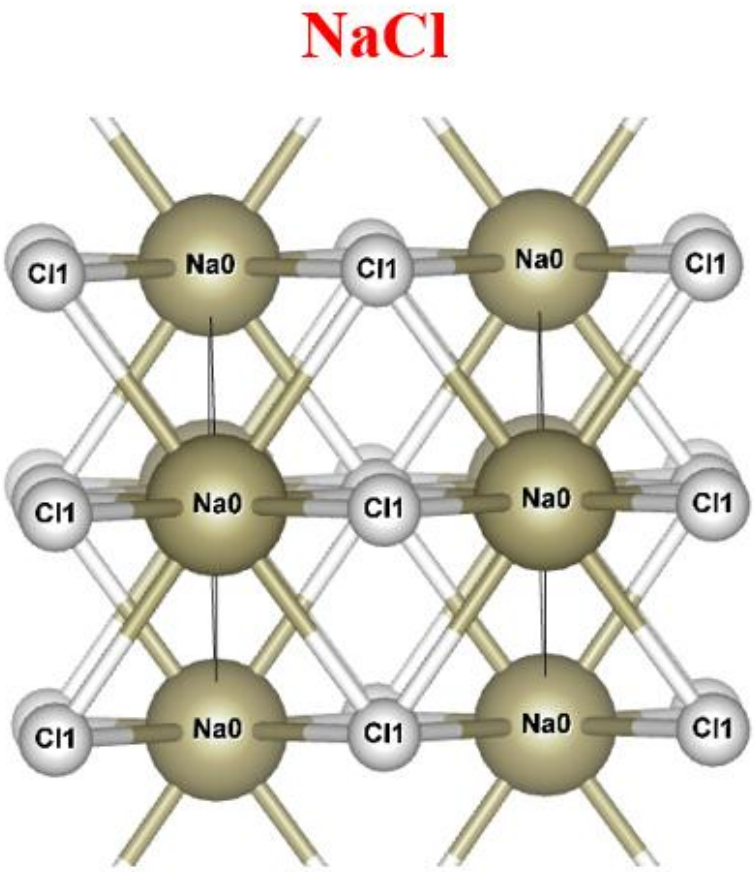

Fig1.16 Sodium Chloride structure

Sodium chloride, or NaCl as it is more well known, is readily accessible in big quantities. This material exhibits a cubic structure as shown in Fig.1. 16 with a face-centered cubic (FCC), producing a cubic crystal lattice. In this lattice, each sodium ion is covered by six chloride ions, and vice versa. There is not enough research on the addiction of NaCl as a reinforcement. However, few studies suggested that the addition of NaCl [69] for the desired purpose can be used to manipulate the properties of matrix elements [70]. So, it should be interesting to see the roleplay on ionic material in a multiferroic matrix. The composite system could be beneficial to enhance moisture barrier, electrical conductivity, and magnetic characteristics etc.

1.10 Zinc Oxide (ZnO)

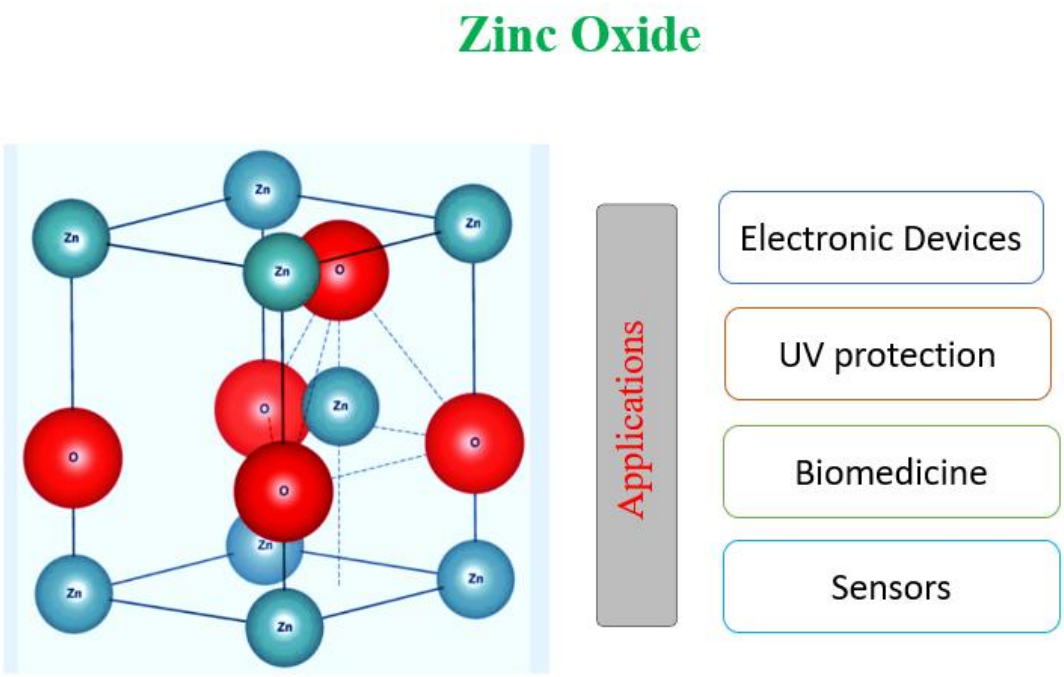

Fig1.17 Bismuth ferrite structure

As seen in Fig. 1.17, zinc oxide (ZnO) normally forms part of the hexagonal crystal structure. packed with oxygen anions (O^{2-}) and zinc cations (Zn^{2+}). The distinctive characteristics of zinc oxide (ZnO) nanoparticles have made them an attractive choice as a filler material which can variety of applications. ZnO nanoparticles can be beneficial

for electrical conductivity, dielectric properties, and mechanical strength [71]. This allows for the creation of composites with tailored electrical functionalities. It is observed that the addition of ZnO as filler results in the creation oxygen vacancies which significantly changed the magnetic properties [72]. ZnO nanoparticles also exhibit antibacterial [73] and UV absorption properties [74] properties making it beneficial for medical applications. These reported properties make this material a better choice to make composite with other material offering improved composite material. Thus, the addition of ZnO as a filler is helpful in achieving desired electronic and magnetic properties for targeted application.

Chapter 2
Literature review

Dabas et al (2025) In this comprehensive report, researchers delve into the fascinating properties of multiferroic materials, highlighting their potential applications in sensor-based electronic devices. The remarkable advancements in two-dimensional multiferroics have captivated the interest of scientists, driving efforts to design more efficient and energy-saving sensors tailored for diverse fields, including electronics, magnetics, and biomedicine. Moreover, the enhanced optical characteristics of these multiferroic materials under visible light offer promising avenues for innovation and development. As researchers explore the intricate interplay between magnetic and electric properties in these materials, the future holds exciting possibilities for smarter, more versatile sensors that could revolutionize various applications across multiple domains. [75]

Ahmed et al. (2025) The multiferroic-based composites with PbZr0.52Ti0.48O3 as a filler with variable composition were fabricated. The synthesized samples are then investigated using structural, ferroic, and magnetoelectric properties. The magnetoelectric coefficient up to 8.45 mV cm^{-1}Oe has been observed in the samples. The investigated study reports strain strain-mediated magnetoelectric effect resulting in fine multiferroic properties suitable for device application.[76]

Bochenek et al. (2024) In this study, researchers created a composite system using two multiferroic materials $BaTiO_3$ (Barium Titanate) and strontium, chromium doped PZT (Lead Zirconate Titanate) with low magnetic values. The impact on electrical properties on modifying the ferroelectric matrix in various composite material is observed. The $BaFe_{12}O_{19}$ phase are observed in samples which is due to the combination of excess iron and Ba. The ferroelectric analysis reveals that at larger concentrations of barium titanate, maximal electric polarization is attained, whereas at lower concentrations, ferroelectric qualities are reduced. These outcomes indicate that on controlling the amount of ferroelectric element in multiferroic composites allows for optimal final parameters with desirable characteristics ideal for electronic applications [77].

Ao et al. (2024) The author of this study described how to create multi-ferroelectric fluid utilising a ball milling technique and beginning materials made of Cobalt ferrite and strontium doped barium titanate that were fabricated via sol-gel process. Several samples with various weight fractions have undergone systematic investigation. A link between the dielectric characteristics and the volume fraction is noticed. Where at 5% volume percent, permittivity reaches its maximum value. The magnetodielectric coefficient, where a maximum value of 27.1% is reported, is similarly impacted by the changing weight fraction. The result from cyclic voltmeter shows that at greater weight fractions the samples exhibit unsystematic dielectric characteristics; the curve is smoother and less distorted than at lower concentrations [78] .

Xu et al. (2023) The presented study addressed the effect of Gd and Co-doped bismuth ferrite. The doped system is subsequently used to form a thin film to explore optical and other properties. The present investigation examines the concentration of $Bi_{0.9}Gd_{0.1}Fe_{1-x}Co_xO_3$ (x = 0, 0.05, 0.1, 0.15). In contrast, the magnetic investigation shows that the incorporation of Gd has improved magnetic properties with a maximum Ms = 21 emu/cm^3, which agrees with smaller grain sizes as seen in the morphological analysis. Optical measurement shows that as the doping level increases, the bandgap value drops from 2.4 eV to 1.89 eV. A polarization value of 22 μC/cm^2 is measured. The study suggests that altering the bandgap and ferroelectric characteristics can be an efficient method to enhance ferroelectric photovoltaic and other optoelectronic effects [79].

Yao et al. (2023) The increased multiferroic characteristics of a composite sample based on a BiFeO3/BaTiO3 perovskite were reported by the author. The ferroic characteristics of the composite samples are discovered to be influenced by the variation in sintering temperature. Maximum remanent polarization (Pr) of 1.62 μC/with a clearly defined loop was observed at ambient sintering temperature. On the other hand, significant leakage current is observed at different temperatures, leading to an irregular hysteresis loop. A similar trend is seen in the magnetic response, where the Mr increases with change in temperature, reaches its maximum of 0.16 emu/g at 750^0 C, and then falls to 0.02 emu/g [80].

Sharma et al. (2023) To create Gd-doped Bismuth ferrite with varying Gd (Gadolinium) percentage sol-gel route is opted. The presence of distorted orthorhombic structures is validated by XRD analysis. There decrease in lattice parameters was observed on increasing Gd concentration. The particle size ranging from 16 to 70 nm is observed from microstructural investigations. The specimen with Gd (x = 0.15) exhibited the highest saturation, Ms = 0.185 (emu/g). At high frequencies, all samples have equivalent dielectric properties. However, different reactions have been noticed in the low-frequency range. Overall, the sample with concentration Gd (x = 0.15) appears to be finely matched for implementation in multifunctional devices [81].

Tazzayet et al. (2022) This works report synthesis of $BiFeO_3$ and $Bi_2Fe_4O_9$ nanoparticles by a hydrothermal synthesis method. The SEM images obtained confirmed a marked shift in the morphology for $BiFeO_3$ and $Bi_2Fe_4O_9$, with the former having clustered nanoparticles with diameters below 10 nm. Under solar radiation, the photocatalytic activity of $BiFeO_3$ and $Bi_2Fe_4O_9$ reaches 61% and 83% after 3 hours, respectively. The superior absorption of $Bi_2Fe_4O_9$ over $BiFeO_3$, notably for light with energy above 2.65 eV, accounts for its higher efficiency despite its larger size and higher bandgap [82].

Mahajan et al. (2021) The composite of system $0.94(Bi_{0.5}Na_{0.5}TiO_3)–0.06BaTiO_3$ is reported where three sample samples are undergone through different processing methods. The investigation shows that the samples show different electrical properties which are due to the phase transition. This study highlights the significance of the pre-processing stages on materials electronic properties [83].

Verma et al. (2021) The paper reports the outcome of calcination on Bismuth ferrite which are fabricated with the aid of sol-gel method. It suggests that calcination result in decreased crystallite size thus altering the electronic properties. In this work different calcination temperatures are used for nanoparticles that were synthesized. An anomaly is observed where results suggest that temperature has a negative correlation with the secondary phase, but that temperature additionally triggers a rise in crystallite sizes [84].

Suresh et al. (2021) This paper presents a thorough analysis of various characteristics of Lanthanum, Holmium and Cobalt doped $BiFeO_3$ ceramic polycrystals. The creation of secondary phases decreases quickly and promotes grain growth as the doping concentration of substitutional elements rises. On adding the cobalt at A-site in $BiFeO_3$, the crystal structure is deformed but retains its rhombohedral space group R3c. The lattice experienced considerable distortion because of the replaced ions' differing ionic radii, which has a substantial effect on the electronic characteristics. When La content was added, there was a noticeable change in dielectric permittivity. Also, the dielectric losses are lowered on adding dopant. However, the substitution of La and Co rise the HC (coercivity) attributed to the antiferromagnetic coupling among Holmium and Fe sublattice. The M-H hysteresis loops show that the samples are ferromagnetic at low temperatures. At low temperatures, the magnetic compensation temperature phenomenon is revealed by the magnetization curves [85].

Khan et al. (2021) The work reports the synthesis and investigation of $BiFeO_3$–$CaTiO_3$ (CTO) composite was created with the aid of sol-gel method. The existence of a rhombohedral structure at low filler concentration is confirmed by structural analysis. However, at higher concentration a combination of rhombohedral and orthorhombic phases was observed in structure. Homogeneous, non-uniform, randomly orientated grains with a drop in grain size after $x = 0.2$ are observed in the FESEM pictures. At high temperatures, an unusual shift in tangent loss and dielectric permittivity was noted for all compositions, which was linked to the impact of structural phase transition. The conductivity upsurges with growing filler concentration, it may be inferred that addition of filler increases the number of charge carriers, which in turn raises ac conductivity. The magnetic properties at room temperature for composite samples demonstrate the material's modest ferromagnetic character. It is observed that at higher concentration of CTO the sample exhibit only negative magneto-dielectric coupling, while for low concentration and Pure sample shows both positive and negative magneto-dielectric coupling [86].

Siddiqui et al. (2021) The bismuth ferrite nanoparticles consist with particle size of 13 nm are synthesized using the sol-gel method. The photo-degradation of Rhodamine-B, a typical industrial contaminant, was accomplished using the nanoparticles. The catalyst

demonstrates the dye's capacity to degrade in both naturally occurring pH and visible light environments. Owing to the BFO nanoparticles' wide surface area and tiny band gap, the substrate molecules are efficiently adsorbed on the catalyst's surface, creating a hole in the conduction band. After 180 minutes, the catalyst degraded nearly 94% of the dye at room temperature using just 0.02 g of catalyst [87].

Comarago et al. (2020) In this report researcher explored the effect of co-substitution on Ba(1-x) $Na_xNi_x/2TiO_3$ ceramics. Oxygen vacancies are present, according to an XPS investigation. The bandgap energy is also decreasing according to the optical characteristics. The dielectric constant's relationship to temperature was investigated. The result demonstrated that when the concentration of dopant is increased the dielectric constant is reduced. These change in electronic properties impact is attributed to the enhanced oxygen vacancies, which also cause the decrement in the material's grain size and polarizability [88].

Zheng D et al. (2020) The study reports the impacts of impurity phase on multiferroic composite system. The composite system of $BaTiO_3$ and BaNbCrO3 are sintered and then examined for structural and electronic properties. The structural instigation reveals the phase shift from tetragonal to the cubic. The band gap between 3.1 eV to 2.1 eV is observed. These findings suggest an alternative option for lead free compound for optoelectronic application [89].

Sharma et al. (2020) In comparison to undoped BFO, this study demonstrated good ferroelectric characteristics. This study examines the various properties of composite system consist of cobalt doped Bismuth ferrite and Lead titanate, produced through a straight forward sol-gel method. The structural investigation that the samples having rhombohedral phases and tetragonal phases are present in the samples. It is established that Co^{2+} doping significantly improves the magnetic characteristics, which are attributed to structural modifications. Because the DC current density is reduced by co-doping, ferroelectric characteristics are also improved. The multiferroic characteristics of this compound at ambient temperature point to a promising future for magnetoelectric technology [90].

Rehman et al. (2020) The cobalt and Samarium doped composites samples are prepared using sol-gel method. The occurrence of crystalline rhombohedral structure were revealed by the structural analysis. The magnetic investigation reveals that the M_s =3.2 emu/g, and M_r=1.5 emu/g, is achieved in the composite samples. The sample are found exhibit improvement in Pmax=12.5 μC/cm^2 and P_r=7.5 μC/cm^2 on adding the dopants. Also, the electronic analysis shows that result implied that electronic conductivity and resistivity are improved. This study concluded that co-doped samples exhibit overall enhanced properties which can be used for efficient electronic and photovoltaic devices [91].

Wang N et al. (2020) This is a review report which signify importance of multiferroic Bismuth ferrite. The morphology, architectures, characteristics, and possible applications of BFO nanoparticles in multiferroic devices with unique functions were all thoroughly explored by the authors in this review. This reports the chances and difficulties in the respective field. This review is helpful in ongoing advances and persuade further scientists to investigate BFO nanomaterials and create new possibilities in future [92].

Rehman et al. (2020) The paper reports how Cobalt as a dopant on Bismuth ferrite and its properties. The dielectric analysis discloses that the incorporation of dopant has improved the conductivity and magnetic properties with maximum Ms = 7.8 emu/g observed. It was discovered that the cobalt-doped BFO's crystallite size reduced to 45 nm. The result implies that the addition of cobalt as a dopant has significantly enhanced the magnetic and electronic properties [93].

Shenn et al. (2020) The reported work discusses the effects of zinc concentrations on Bismuth ferrite based thin film on the dielectric characteristics, oxygen vacuum concentration, ferroelectricity, structure, leakage current, and leakage process. The ferroelectric investigation confirms that the sample has exhibits polarization 82.4 μC/cm^2, have improved remanent polarization. Additionally, there was coercive field with value 887 kV/cm were found in the samples. This study suggests that appropriate Zn doping has been demonstrated to promote the emergence of BFZO film grains by

lowering the oxygen vacancies and reducing current leakage and significantly, improving the ferroelectric characteristics of the thin films [94].

Cao et al. (2020) The study reports that Al-doped Bismuth ferrite with varying weight percentage were synthesized using the sol-gel approach. Every sample have an R3c space group and a rhombohedral structure. Low dielectric loss (tanδ) and dielectric constant were achieved through grain refining and enhanced electric characteristics brought about by al-doping. Reduced leakage current was the result of the lower particle size. The calculated resistivity of samples was 3.71 × 106 Ω·m. The sample exhibit coercive field of 43.7 kV/cm and enhancement in polarization with P_r =1.93 μC/cm^2, suggesting that the system may find viable applications [95].

Spaldin et al. (2019) This is a review article provide a detailed insight view of multiferroic material and various ongoing advances in the respective field are discussed. It suggests that researchers should place the highest priority on multiferroic material which can exhibit strong ferroelectric and magnetic coupling, minimal leakage with high remanent magnetic moment. To Resolve the need of better room-temperature multiferroics by the discovery of new materials and synthesis of novel materials is made easier by the combination of experimental and theoretical understanding. It would be extremely helpful to create new pathways for synthesis of materials with strong magnetoelectric coupling and get closer to the limitations of and overcome those limitation [3].

Song et al. (2019) The paper reports the overall characteristic analysis of indium doped gallium ferrite are investigated for various concentration. The solid-state reaction is used to create gallium ferrite. The rise in lattice parameters upon doping is confirmed by the structural analysis employing X-ray diffraction. Indium doping causes distortion, which causes polarization to rise. With indium = 0.05, the magnetization is observed to be at its highest. This report suggests that indium as a dopant has successfully enhanced properties of multiferroic bismuth ferrite [96].

Arti et al. (2019) The study reported the improvement in optical properties of Praseodymium (Pr) incorporated Bismuth ferrite. The ceramic samples are produced

using the sol-gel technique. The study reported increment in dielectric constant via increasing doping concentration. The doping also boosted its ferroelectric property. The optical band gap is reduced to 2.27 eV on the addition of Praseodymium. The finely tuned nanoparticle can be employed in energy storage and photovoltaic devices [24].

Peng et al. (2019) The paper reports the dielectric behavior of a composite system of two multiferroic materials. Ceramics made of $BiFe_{1-x}Al_x$-$BaTiO_3$ were created using the solid-state method. The sample exhibits improved spontaneous polarization and remnant polarization. It is observed that this enhancement was dominated by the role that structure played in the process. The disorder of Fe and Al doping is confirmed by Mossbauer spectra. The dielectric constant's thermal development is also impacted by this. The grain boundary effect were held responsible for the relaxation process observed in impedance spectra. These findings suggested the role of structures in describing various properties in case of ferroelectric materials [97].

Merina et al. (2019) The paper reports the synthesis of bismuth ferrite nanoparticles. To fabricate Sol-gel method was used. The produced bismuth ferrite nanoparticles were further investigated. According to XRD characterization data, bismuth ferrite ($BiFeO_3$) nanoparticles have a rhomboid-centered structure. Morphological analysis reveals change in particle size at high annealing temperature. The surface analysis verifies that the bismuth ferrite nanoparticles with diameter in the range of 81 nm are synthesized [98].

Bismibanu et al. (2018) A Sono chemical technique was utilized to effectively synthesize $BiFeO_3$ nanoparticles. The BFO sample's rhombohedral structure was verified by the XRD examination. The produced nano size particle is also confirmed by structural investigation using TEM. The BFO nanoparticles' ferromagnetic nature was confirmed by the ABK plot, and the saturation magnetization (Ms) of 63emu/g was discovered. The ferroelectric behavior was detected by the P-E loop tracer, and reduced leakage current was observed in the samples. The study signify the importance of processing route for desired application [99].

Gaikwad et al. (2017) The modification in the perovskite material using a spinel ferrite $ZnFe_2O_4$. The observed magnetic, ferroelectric, and dielectric properties are found to be influenced by the presence of Zinc ferrite where the magnetic strength is increased by 7 times with a reduction in leakage current. This suggests that the composite approach is beneficial to overcome the challenges offered by pristine BFO resulting in modified functionality of material at room temperature [100].

Liu et al. (2017) The author presented some new developments in perovskite multiferroics that combine theoretical and experimental research. These outstanding outcomes demonstrate that strain engineering is a successful approach for achieving multiferroicity. Thin-film materials are needed as they can exhibits various electronic properties for smaller microelectronic devices. A key component in multiferroicity is the BO_6 deformation. The author proposed that for perovskite multiferroics to improve the band gap and recover leakage current, a thorough knowledge of the relationship between various factors such as structural deformation, electronic conductivity and electromagnetic coupling is required. The author also recommended developing some basic and conventional methods because the analysis of the multiferroic material requires some specialized equipment [101].

Wu et al. (2017) The A site doping in Bismuth Ferrite, where Barium is doped at several concentrations (x = 0, 0.05, 0.10, 0.15, and 0.20), is reported in the paper. Raman spectra further support the structural analysis's findings that Ba-doped content inhibited the development of the impurity phase present in these nanoparticles. The spectroscopical investigation observe that the Ba-doped affected the dual valence states of Fe^{3+} and Fe^{2+} which reduced the oxygen vacancies. The addition of dopant tailored the magnetic parameters, and a decrease in leakage current density was seen for Ba (0.2). These findings imply that bismuth ferrite multiferroic qualities are significantly improved by Ba-doping and that Ba-doped BFO nanoparticles are suitable options for dielectric energy storage and spintronics[102].

El-desoky et al. (2016) The outcome of barium doping on the structure of bismuth ferrite and its physical properties is reported. The samples are prepared using solid state method. On analyzing the magnetic properties, it is noticed that addition of dopant has enhanced

the remanent magnetization by 18 times in comparison to pristine bismuth ferrite. Also, on exploring the effect of substitution on electronic properties sample with aremanent polarization of 89 $\mu C/cm^2$. The obtained result signify that Ba doped bismuth ferrite nanoparticles have the potential to employed in device application[103].

Godara et al. (2015) The addition of Ba, Nb, Co as dopants in a significant amount has altered the ferroelectric properties by reducing leakage current up to three orders of magnitude and conductivity behavior is very similar to that of an ohmic device. Oxygen vacancies appeared to have significantly decreased at high concentration of dopants. With increasing doping levels and remnant polarization, the ferroelectric loop's saturation level improves from by 1.5 times in doped samples [55].

Wang l et al. (2013) The material reports low-temperature synthesis using a process using solid-state precursors at low temperatures is used to create $BiFeO_3$ nanoparticles. The morphological investigation shows that average length of the particle form increases from 80 to 100 nm as the annealing temperature is raised. From the UV-vis spectral analysis it is observed that as the particle size increases band gap is reduced and the absorption edge shifts towards red color[104].

Wongmaneerung et al. (2013) This study reports the fabrication of multiferroic composites system consisting of antiferromagnetic bismuth ferrite as a filler and ferroelectric lead titanate as a reinforcement. The materials were produced with the aid of solid-state sintering method. Interestingly, the magnetic analysis exposed that the composites exhibit superparamagnetic behavior due to the antiferromagnetic nature of bismuth ferrite and paramagnetic nature of ferroelectric lead titanate. However, on increasing the lead titanate concentration the magnetic saturation of composite samples is decreased [105].

Lan et al. (2011) This study reports the investigation of composite system consist of lanthanum doped multiferroic bismuth ferrite ceramics. The solid-state reaction process is used to fabricate the composite system. The prepared materials are then investigated for structural and, morphological analysis. Both samples showed rhombohedral distorted perovskite structure. The sample consist of homogenous and small grains size is observed

in lanthanum and zirconium doped bismuth ferrite prior to other samples. The sample are found to have greater magnetization, which was attributed to the structural transition. The magnetic investigation reveals the enhancement in coercivity in the composite samples. However, there is no change in the Neel temperature as it remains the same in both systems which is 355 ^{0}C [106].

Wang et al. (2011) This study reports the synthesis of Bismuth ferrite nanoparticle using citric and tartaric acids as chelating agents with the sol gel method. These obtained nanoparticles were subsequently calcined at a low temperature. The study shows that magnetic properties of the samples are linked to the size of nanoparticles. On the precursors and creation mechanism of the nanoparticles employed in the studies, proposals are offered. This method suggests a different potential mechanism to control the morphology and can be easily adapted to other systems. This technique is effective for low temperature synthesis compared to conventionally used high temperatures techniques [107] .

Wang.et.al 2011 The paper describes the fabrication of pure-phase BFO nanoparticles using the sol-gel technique, where different chelating agent are used for the synthesis. The study presents the effect of chelating agent on the final product. The magnetic and structural characteristics of the synthesized nanoparticles are investigated. Morphological investigation indicates that the nanoparticles are less than 30 nm in size. The findings show that with the help of citric acid, the required results are obtained at low temperatures [108].

Osinska et al. (2011) This study discusses the fabrication of ceramic composites made of $BiFeO_3$//$Bi_4Ti_3O_{12}$ (BF//BiT) ceramic at a variety of concentrations. The synthesis is carried out using the traditional mixed-oxide technique. The analysis of these composite samples shows that the creation of additional structural phases is associated with an increase in barium titanate concentration. According to the dielectric investigation, the ceramic composite exhibits a rapid rise in dielectric permittivity up to 10% of concentration. This anomaly is generated by the percolation phenomenon, which drops the value of dielectric permittivity when the maximum percolation threshold is achieved [109].

Spaldin et al. (2010) This is a review article which reports the progress and future scopes done in multiferroics and it also provide a detailed study of two perovskite materials LaMnO3 and BiMnO3 based on their electronic magnetic and structural properties is discussed which emerges the d^0 rule. As a result, asymmetry is created by B-O bonding in BiMnO3. This study with great attention to detail answered why d-0ness is strongly favored [110].

Ghosh et al. (2005) The paper reports the production of bismuth ferrite using a ferrioxalate precursor technique. The produced nanoparticles have a diameter of around 10 nm. The bismuth ferrite produced using the ferrioxalate precursor approach is shown to have less impurity phases than bismuth ferrite obtained by solid-state reaction. This suggests that nitric and oxalic acids may be important factors in the alteration of structural characteristics [111].

Ramadass. n. d et al. (1978) An investigation on the structural and other physical characteristics of oxides of the ABO3 type was conducted. It has been found that several factors, including ion size, electrical configuration, and preparative condition, govern these properties. These oxides' simple cubic structure is somewhat distorted and extremely uncommon. The tolerance factor affects the distortion. The B-O interaction is what gives the electrical characteristics. The metallic properties of LaCaO3 gradually become more prominent after adding strontium or lanthanum[112].

Recent advances in multiferroic materials have focused on enhancing their magnetic, ferroelectric, and photocatalytic properties through various doping methods, composites, and synthesis techniques. Table 1 summarizes key findings from recent studies, highlighting variations in magnetization, polarization, bandgap, and photocatalytic performance. This comparison aids in identifying materials best suited for applications like magnetoelectric sensors and visible-light photocatalysts.

Study	Investigated System	Key Findings	Significance
Ahmed et al. (2025) [76]	$PbZr_{0.52}Ti_{0.48}O_3$-based composite	Magnetoelectric coefficient: **8.45 mV cm^{-1}Oe**	High ME coupling for sensors
Ao et al. (2024) [78]	$CoFe_2O_4$ + Sr-doped $BaTiO_3$	Magnetodielectric coefficient: **27.1%**, Permittivity max at 5% vol.	Strong dielectric-magnetic interaction
Xu et al. (2023) [79]	$Bi_{0.9}Gd_{0.1}Fe_1{-}xCoxO_3$	Ms: **21 emu/cm³**, Bandgap drop: **2.4 → 1.89 eV**, Polarization: **22 µC/cm²**	Improved magnetic & optical properties
Sharma et al. (2023) [81]	Gd-doped $BiFeO_3$	Ms: **0.185 emu/g** @ x=0.15	Best match for multifunctional devices
Yao et al. (2023) [80]	$BiFeO_3/BaTiO_3$	Pr: **1.62 µC/cm²**, Mr: **0.16 → 0.02 emu/g** (temp dependent)	Enhanced ferroic performance with sintering control
Tazzayet et al. (2022) [82]	$BiFeO_3$ vs. $Bi_2Fe_4O_9$	Photocatalytic degradation: **61% vs. 83%**, Bandgap: $Bi_2Fe_4O_9$ > 2.65 eV	$Bi_2Fe_4O_9$ better for photocatalysis
Siddiqui et al. (2021) [87]	BFO nanoparticles	Dye degradation: **94% in 180 min** @ room temp	Excellent photocatalytic efficiency
Rehman et al. (2020) [91]	Co, Sm-doped BFO	Ms: **3.2 emu/g**, Pr: **7.5 µC/cm²**	Enhanced magnetic and ferroelectric synergy
Shenn et al. (2020) [94]	Zn-doped BF thin films	Polarization: **82.4 µC/cm²**, Coercive field: **887 kV/cm**	Strongest ferroelectric response
Bismibanu et al. (2018) [99]	$BiFeO_3$ nanoparticles	Ms: **63 emu/g**	Exceptional ferromagnetic strength

Table.2 Key findings from recent studies on multiferroic composite materials.

2.2 Research Gap

Multiferroic materials due to their multiple ferroic ordering are promising candidates for application in various devices. Despite the exciting possibilities, there are several challenges [3], [113] which are identified from the literature stated below.

- Few multiferroic materials such as pure bismuth ferrite shows weak electronic and magnetic properties at room temperature. Hence to enhance their electromagnetic properties doped/composites are required to achieve their potential application in electronic and magnetic memory devices.
- The existence of structural defects and oxygen vacancies in multiferroic leads to outflow of current. Thus, it is necessary to reduce leakage current in multiferroic materials to make them more stable and efficient for energy storage devices.
- The led based multiferroic materials are toxic in nature having severe side effect. On the other side, bismuth based multiferroic are better alternative owe to their non-toxic nature and biocompatibility.
- It is observed that multiferroic materials are sensitive to various physical condition such as temperature, stress and strain. So, it is necessary to optimize techniques for compatibility and cost effectiveness of multiferroic material to make them suitable for device applications.

So, by overcoming the existing challenges we can utilise multiferroic materials to create energy efficient devices used to make next generation storage devices, sensors,

biomedical devices, and lead-free alternative for photovoltaics. The reported work is focused on synthesizing high-quality multiferroic. The synthesized multiferroic material is then used to make composite materials. materials and how introduction of another material to a multiferroic material can influence its phase, microstructure, electronic and magnetic properties.

2.3 Objective of the proposed study

1) To synthesize multiferroic nano-particles.
2) Interwoven of synthesized nano-particles and other materials to make composites.
3) Characterization of composite system for structural and magnetic, optoelectronic, and dielectric properties.
4) To study percolative behavior and find the percolation threshold in the composite system

2.4 Expected outcomes

The goal of the research is to make multiferroic composite system by integrating various materials with distinct properties. The composed materials are expected to have enhance electronic, magnetic, and optoelectronic property. These modified composite systems can offer enhanced performance, efficiency which significantly advance the development of multifunctional devices, memory devices, energy storage and photovoltaics.

Chapter 3

Methodology

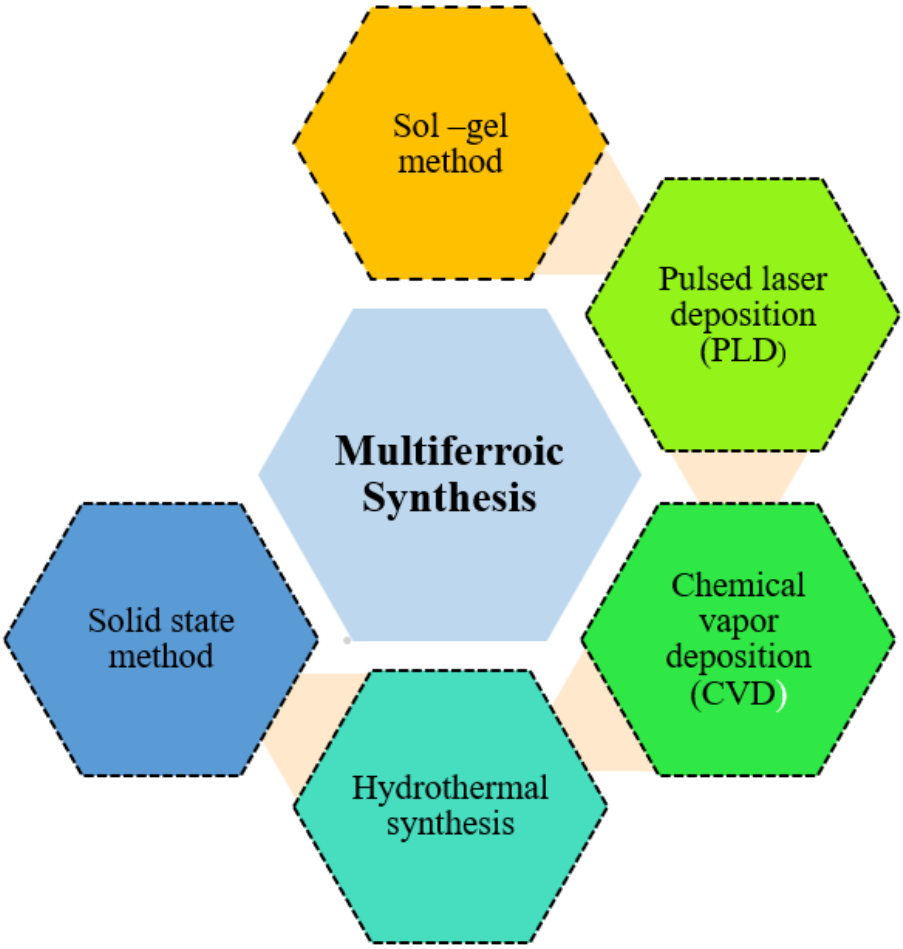

Fig.3.1.1 Synthesis method for multiferroic materials.

3.1 Method of synthesis

Multiferroic materials are synthesized using a variety of techniques as shown in Fig.3.1.1 which include hydrothermal synthesis, physical vapor deposition, chemical vapor deposition, pulsed laser deposition, sol-gel, and solid-state reaction. [114], [115] . It is observed from previous studies that in comparison to sol gel method the other synthesis routes have several drawbacks, including slow reaction rates, high energy needs, and inhomogeneity. These drawbacks can significantly limit their practical applicability and the quality of the synthesized materials. Particularly for multiferroic materials based on perovskites, where it is discovered that the structure is temperature-sensitive. On the other hand, sol gel method offers various advantageous such as low production cost, low

operating temperature, high purity product etc. These advantageous encourage to adopt this methodology for the purpose of our study.

3.1.1 Sol-gel method

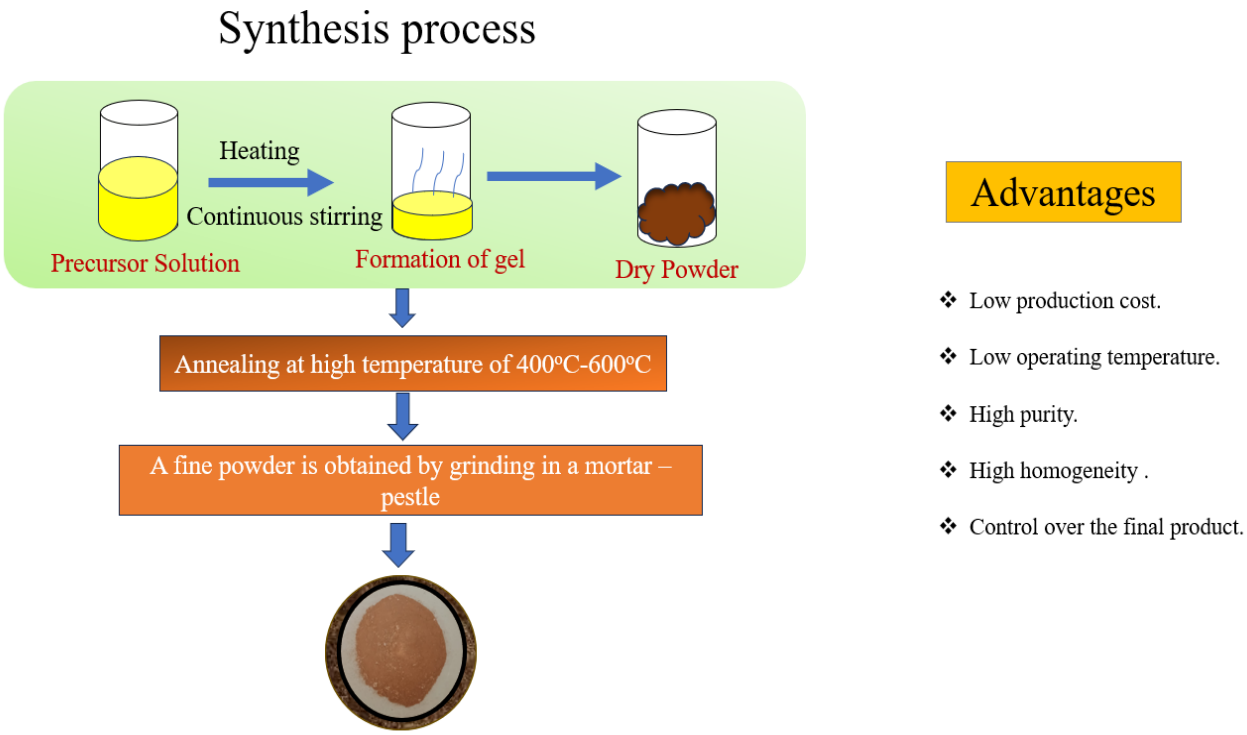

Fig.3.1.2 A schematic illustration of processing stages in sol-gel method.

The sol-gel method is a chemical method used to synthesize multiferroic materials at low temperatures using a precursor solution involving various stages shown in Fig.3.1.2. The process includes a precursor solution in a stochiometric ratio which is then allowed to heat with continuous stirring using a magnetic stirrer. After a few hours of heating, the fluid is subsequently transformed into a gel. To remove any remaining impurities, the resulting powder is next annealed at a high temperature for a short period before being allowed to cool at normal temperature. This process offers various benefits such as, including low cost, low working temperature, control over morphology, low amount of contamination, and high-quality materials [116], [117]. Because of its flexibility, this technique is used in a wide array of industries, including biomedical engineering and material science to fabricate various high-quality materials.

3.2 Making Composite system

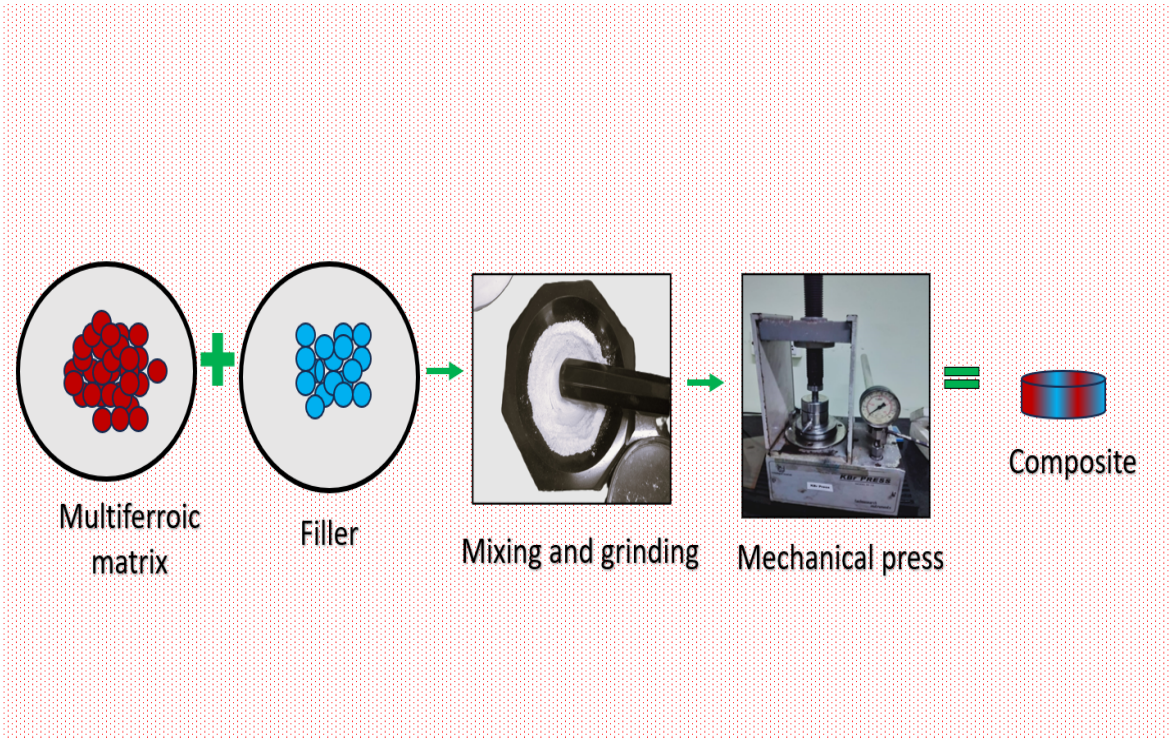

Fig.3.2 A schematic representation of the preparation of composite.

The composite system is made using a multiferroic matrix which is embedded with a filler. The filler and matrix in varying weight fractions are grinding together with the help of mortar and pestle. Pellets are formed by mechanically pressing the fine powder using a KBR dye press as illustrated in Fig.3.2. The pellets are then investigated for structural, electronic, magnetic properties and other properties. Fillers are known to affect the multiferroic response in the matrix's strength or direction, according to an earlier study. More functions can be achieved in a material by fusing the filler's contribution with the intrinsic features of the multiferroic. In certain cases, fillers can enhance the multiferroic's processing properties, which facilitates device fabrication.

3.3 Preparation of Bismuth ferrite/ NaCl composites.

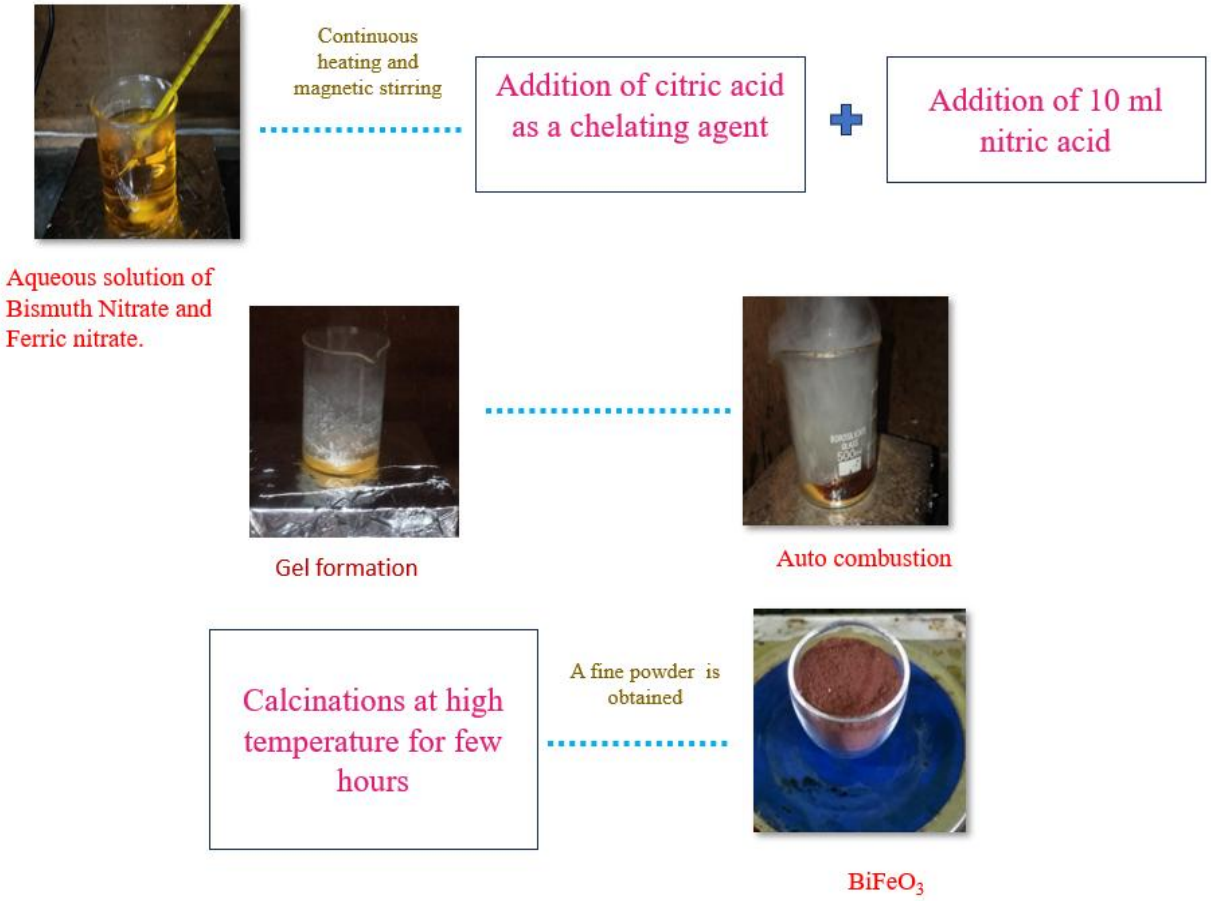

Fig.3.3.1 Synthesis of Bismuth ferrite nanoparticles.

The sol-gel method shown in Fig.3.3.1 is used to synthesize Bismuth ferrite nanoparticles. This technique is important and easy as it has the advantage of synthesizing nanoparticles of different morphologies at much lower temperatures [24, 25]. Nitrated-based compounds such as Bismuth nitrate pentahydrate [$Bi(NO_3)_3 \cdot 5H_2O$] and Ferric (III) nitrate Nonahydrate[$Fe(NO_3)3 \cdot 9H_2O$] from Loba Chemie of AR grade are used to make an aqueous solution with 200 ml deionized water. The obtained solution is then heated with continuous stirring at 60-70°C. The citric acid in 1:1.5 is used as a chelating agent followed by 10 ml of nitric acid (HNo_3). The entire mixture is heated to 150° C while being continuously stirred to form a gel, and then it undergoes auto combustion. The resultant powder is next ground using a mortar and pestle into a fine powder. After that, the powder is annealed for 4 hours at 450° C.

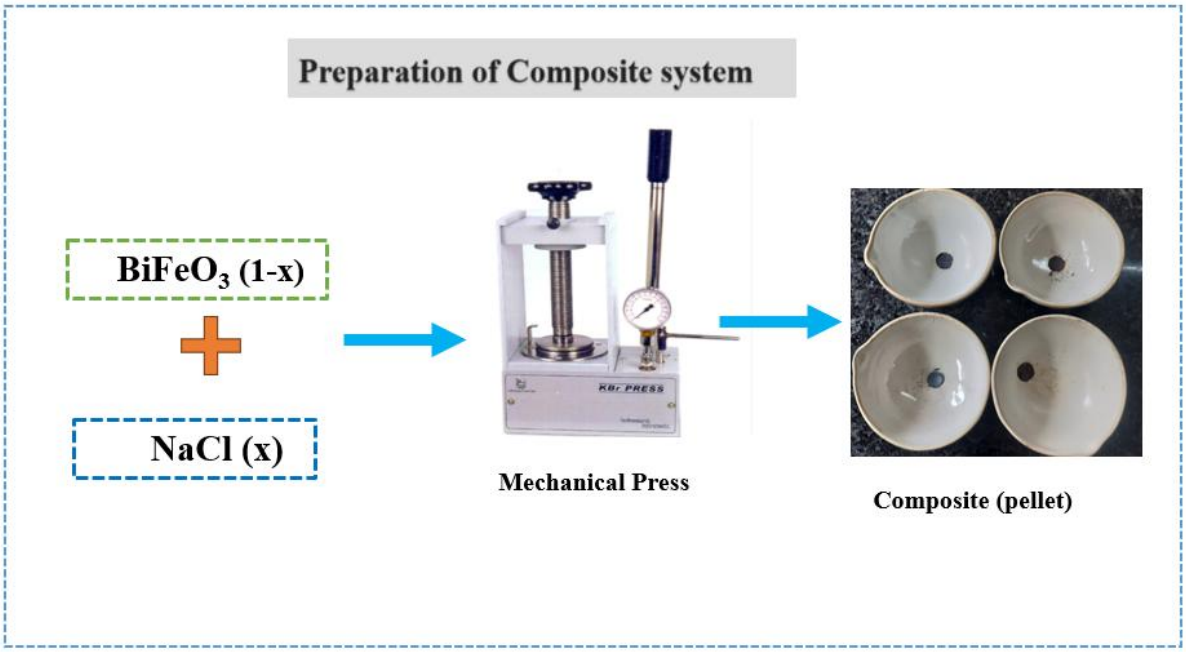

Fig.3.3.2 Preparation of composite system of Bismuth ferrite and Sodium Chloride.

To create a composite system with NaCl, the produced nanoparticles of bismuth ferrite are subsequently used as a matrix element described in Fig.3.3.2. The composite is made with high-purity powdered NaCl from Loba Chemie (99.5% purity). There is no purifying process used for the NaCl. A KBr dye press is used to create composite pellets at a pressure of 20 Torr in a dehumidifying environment. The composites were formed according to wt% using the equation mx = m (1-x) in weight percent, and m is the total weight of material used to prepare composites of X=0%, 10%, 30%, and 50%. Prior to measurement, the produced composite pellets are finally annealed in a muffle furnace at 750 ° C for two hours. After that, they are allowed to cool at a rate of 1° C per minute to room temperature.

3.4 Preparation of Bismuth ferrite/ Cobalt ferrite composites.

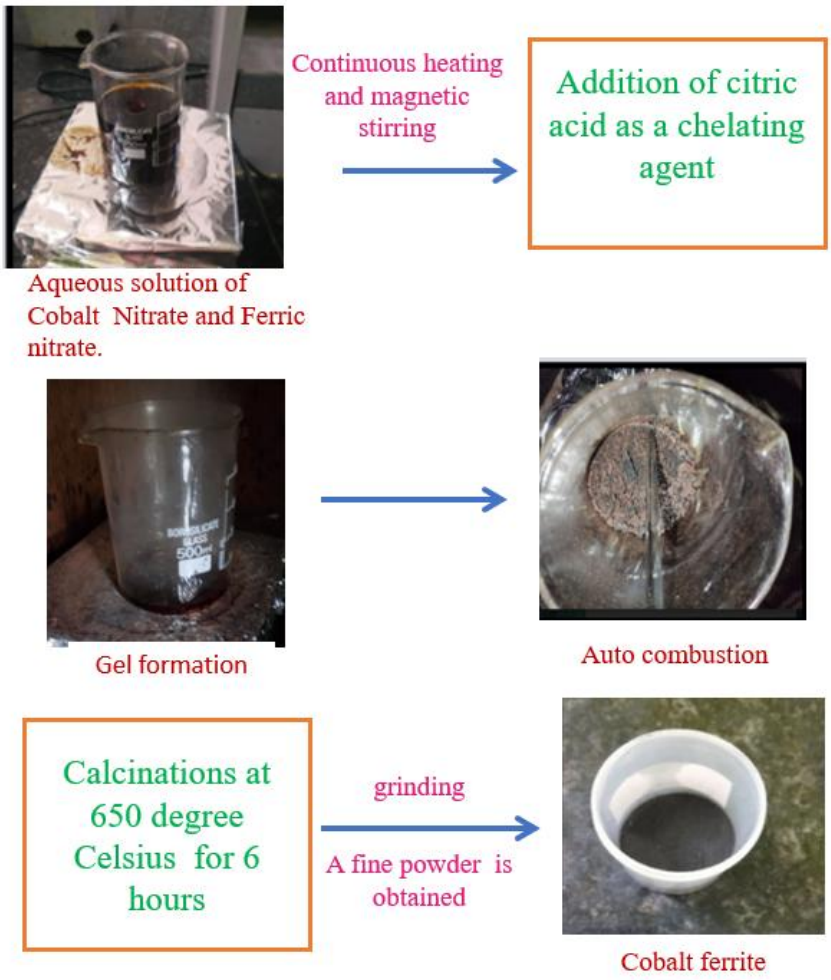

Fig3.4.1 Synthesis of Cobalt ferrite.

The sol-gel method is adapted [116], [117], [118] to synthesize bismuth ferrite (as mentioned in Fig.3.3.1) and cobalt ferrite nanoparticles. This technique is important and easy as it has the advantage of synthesizing nanoparticles of different morphologies at much lower temperatures. Nitrate-based compounds such as Bismuth nitrate pentahydrate [Bi $(NO_3)_3 \cdot 5H_2O$], Ferric nitrate [Fe $(NO_3)_3 \cdot 9H_2O$], and Cobalt Nitrate Hexahydrate [Co $(NO_3)_3 \cdot 6H_2O$] are used as precursors separately. Fig.3.4.1 shows the synthesis of cobalt ferrite. The aqueous-based solution is used for the synthesis where citric acid in 1:1.5 and 15 ml of nitric acid is used in equal proportion for both the precursor solutions. The entire solution is heated at 70-80 °C with continuous stirring to

form a gel, followed by auto-combustion. The obtained powder is then crushed into fine powder by mortar and pestle. The powder is then annealed at 450° C for 4 hours.

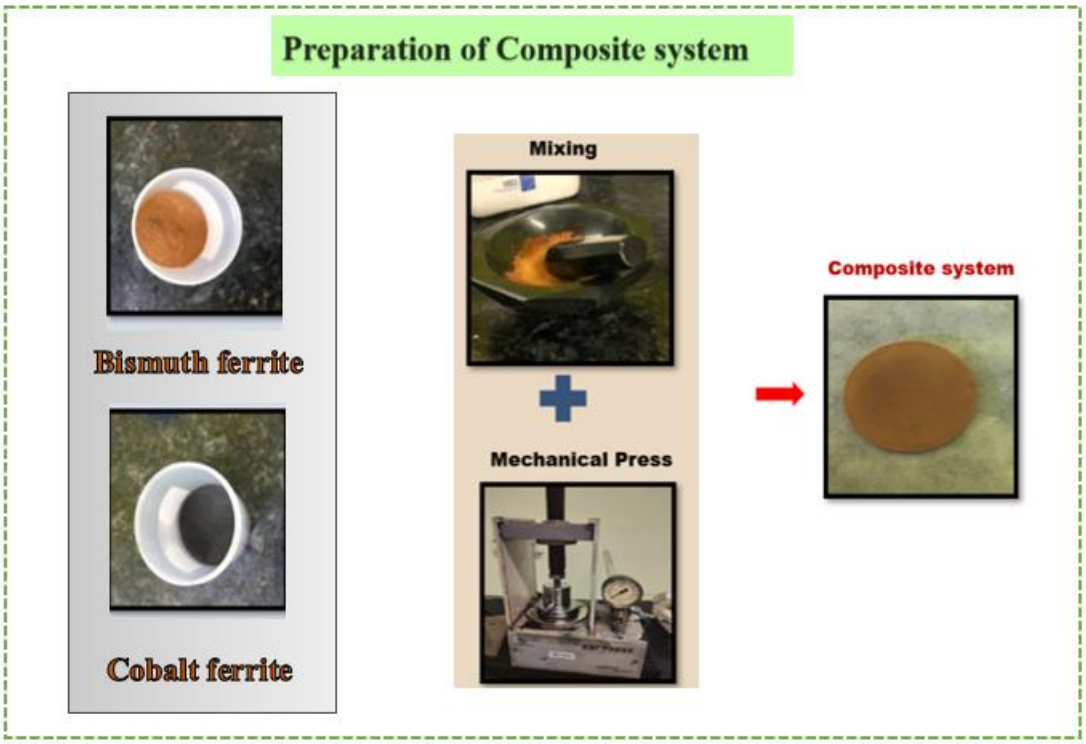

Fig3.4.2 Preparation of $BiFeO_3$ and $CoFe_2O_4$ composites.

The nanoparticles obtained from bismuth ferrite and cobalt ferrite are then used to form a composite system. Composite pellets are made with the help of a KBr dye press at a pressure of 20 Torr in the dehumidifying atmosphere as shown in Fig.3.4.2. Several systems are made with varying filler weight percentages x = 10%, 30%, and 50%. The obtained composite pellets were finally annealed to 650 ° C for 2 hours in a muffle furnace before measurement, which was then allowed to cool at a rate of 1°C per minute to room temperature.

3.5 Preparation of Co $_{(x)}$, Al $_{(y)}$ into Bi $_{(0.9)}$ Ba $_{(0.1)}$ Fe $_{(1-x-y)}$ O_3.

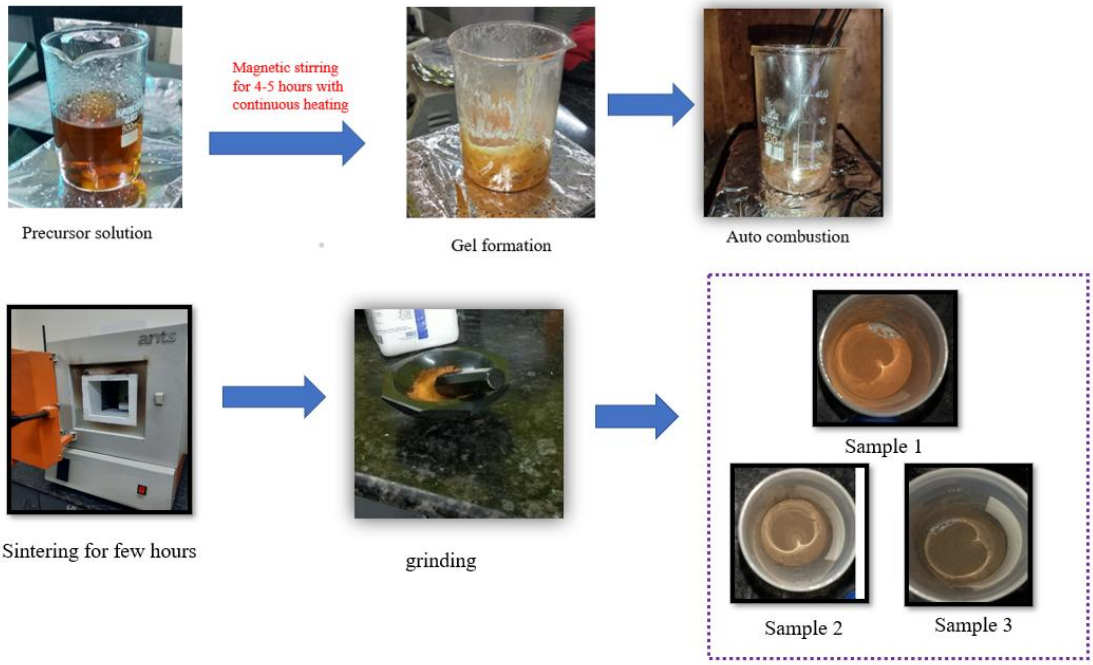

Fig3.5 Synthesis of tertiary doped $BiFeO_3$ nanoparticles.

The synthesis of Barium doped Bismuth ferrite is done using sol gel method. To synthesize chemical such as Bismuth nitrate, Ferric Nitrate, Barium Nitrate, and citric acid. An aqueous solution is prepared with the help of these chemical. The prepared solution is vigorously heated with continuous stirring. Afterwards, citric acid in ratio 1:1.5 as a chelating agent followed by HNO_3 (nitric acid) is added to the solution. The solution is transformed into a gel. On further heating auto combustion occurs which results in a fine powder. The obtained Nanoparticles in powdered form are pre-sintered at 200^o C for 2 Hours and afterward sintered at 500^o C for 3 hours. Further to add Cobalt at and aluminium the chemicals used are Bismuth nitrate, Ferric Nitrate, Aluminium nitrate, Cobalt nitrate, Barium Nitrate, and citric acid from Loba Chemie. The nitrates in a stoichiometric ratio are dissolved in an aqueous solution with deionized water for all precursor solution. Citric acid is used as a chelating agent followed by HNO_3 (nitric acid). The solution is then heated at 70^o C with continuous stirring with a magnetic stirrer. The solution is then followed by auto combustion to give powder as shown in Fig.3.5. The obtained powder is then crushed into a fine powder with the help of a mortar pestle. The similar calcination procedure is followed as for Ba doped Bismuth ferrite where Nanoparticles in powdered form are pre-sintered at 200^o C for 2 Hours and afterward sintered at 500^o C for 3 hours. Then obtained and allowed to cool up

to room temperature the they are subjected to performed an experimental characterisation. The sample Bi $_{(0.9)}$ Ba $_{(0.1)}$ Fe $_{(0.99-x-y)}$ Co $_{(x)}$ Al $_{(y)}$O3 with composition (x, y = 0), (x=0.1, y = 0) and (x = y = 0.1) is named as sample 1, sample 2 and sample 3 respectively.

3.6 Preparation of $Bi_{0.99}Nd_{0.01}FeO_3$ /Zinc oxide composite

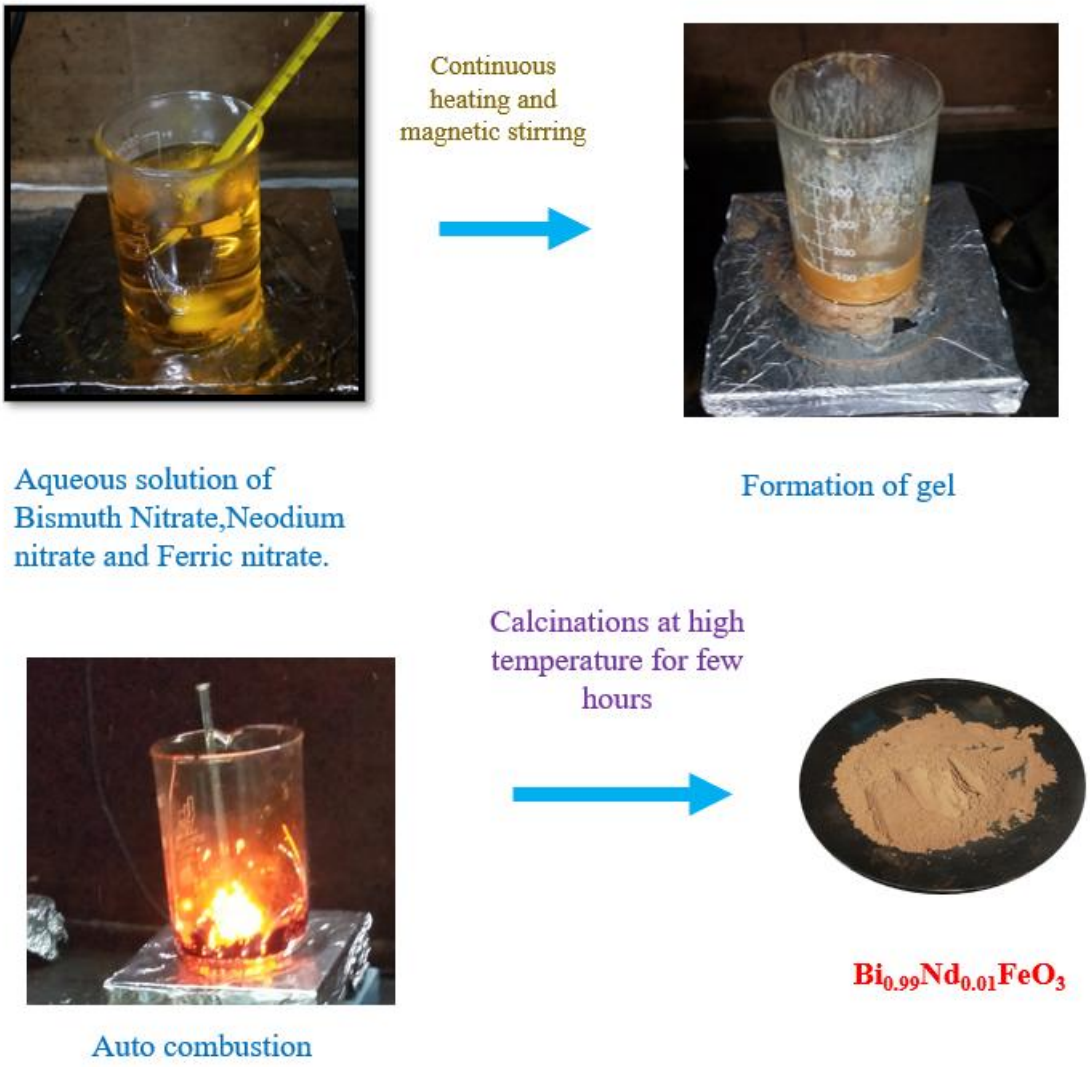

Fig.3.6.1 Synthesis of Neodymium doped $BiFeO_3$ nanoparticles.

The sol-gel method is adapted [116], [117], [118] to synthesize $Bi_{1-x}Nd_xFeO_3$ (x= 0.01) and Zinc oxide nanoparticles. This method is simple and useful since it can create nanoparticles with a variation of morphologies at suggestively lower temperatures. For $Bi_{1-x}Nd_xFeO_3$ (x= 0.01)/ Nitrate-based compounds such as Bismuth nitrate pentahydrate

[Bi $(NO_3)_3 \cdot 5H_2O$], Ferric nitrate [Fe $(NO_3)_3 \cdot 9H_2O$], and Neodium Nitrate hexahydrate, [Nd $(NO_3)_3 \cdot 6H_2O$] are used as precursors separately. For the synthesis, an aqueous-based solution is utilized, with 1:1.5 citric acid and 15 ml of nitric acid being added in equal amounts for the precursor solutions described in Fig.3.6.1. The entire solution is heated at 70-80 °C with continuous stirring to form a gel, followed by auto-combustion. The obtained powder is then crushed into fine powder by mortar and pestle. The powder is then annealed at 450° C for 4 hours.

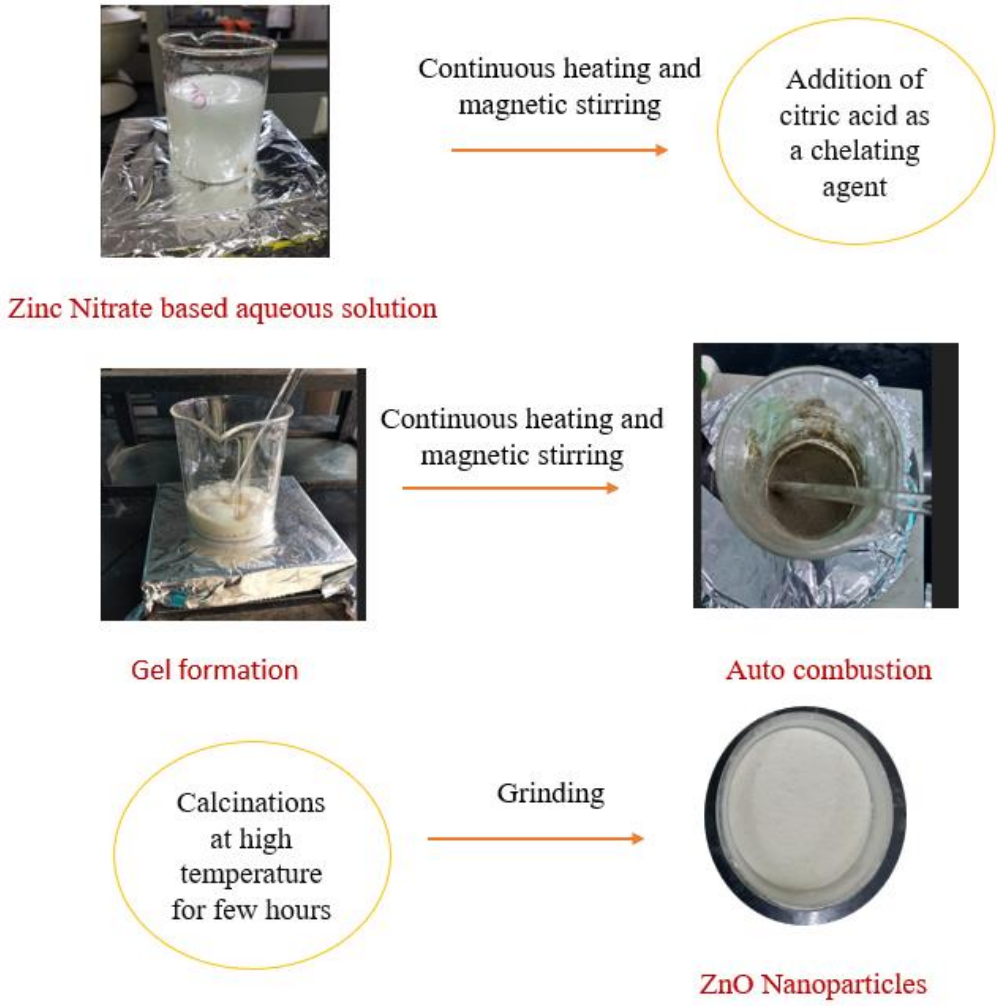

Fig 3.6.2 Synthesis of Zinc Oxide nanoparticles.

Similarly, for zinc oxide, Zinc nitrate hexahydrate [Zn $(NO_3)_2 6H_2O$] and distilled water are used as solutions in Fig.3.6.2. The entire solution is then heated to 70-80 °C while being stirred continuously to produce a gel, which is subsequently auto-combusted. The acquired powder is next crushed into fine powder with a mortar and pestle. The powder is then annealed at 500 °C for five hours to obtain Zinc oxide nanoparticles.

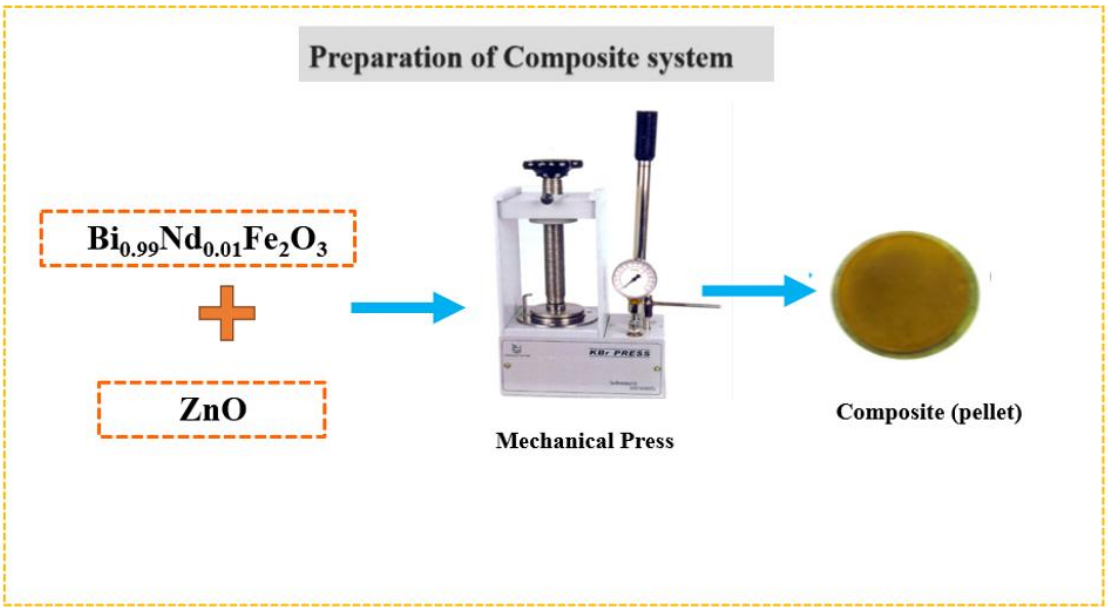

Fig 3.6.3 Preparation of $Bi_{0.99}Nd_{0.01}Fe_2O_3$ and Zinc Oxide nanoparticles.

The nanoparticles obtained from $Bi_{0.99}Nd_{0.01}Fe_2O_3$ and Zinc oxide nanoparticles are then used to form a composite system. Composite pellets are made with the help of a KBr dye press at a pressure of 20 Torr in the dehumidifying atmosphere. Several composite systems are made with a matrix of $Bi_{0.99}Nd_{0.01}Fe_2O_3$ (1-x) and ZnO (x) as fillers with weight percentages (x = 0%, 5%, 10%, 15%) shown in Fig.3.6.3. The obtained composite pellets were finally annealed to 500 ° C for 2 hours in a muffle furnace before measurement, which is then allowed to cool at a rate of 1°C per minute to room temperature.

Chapter 4

Characterisation Technique

4.1 XRD

The X-ray diffraction is essential technique in defining the physical and structural characteristics of materials like chemicals, powdered materials, and thin films. Additionally, it is utilized to gather data on crystallographic information, composition, structural analysis, and crystallite size. Nevertheless, several other factors, including stress, strain, and lattice constant can be determined from this technique.

The simple production of constructive interference of the monochromatic X-rays obtained from the structure of sample material is the foundation for the operation of the XRD tool. The cathode ray tube generates x-rays, which are then separated out to create monochromatic radiations, which are then collected and concentrated in the direction of the sample. The initial interaction occurs between X-rays and sample material. A certain number of photons are diverted from their intended course by an X-ray strike, resulting in the production of a constructive and destructive interference diffraction pattern on the detector. The constructive interference between the various planes and the mirror image of the incident X-ray results in formation of peaks known as Bragg's peak as shown in Fig.4.1. The formation of constructive interference happens only if the phase shift is acquired as a multiple of 2λ. This situation is explained based on Braggs law i.e n λ = 2dsinθ.

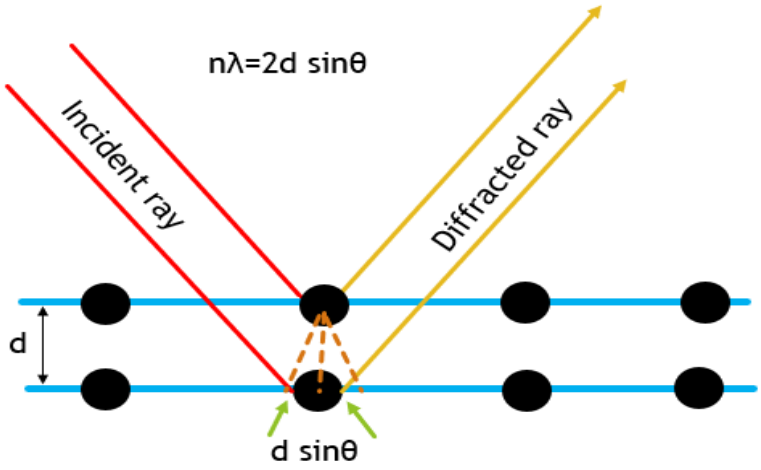

Fig 4.1 shows the schematic representation of Braggs law.

Working –

A source of X-ray radiation that generates radiation with the proper wavelength is built into the apparatus. The primary characteristics of the target substance, such as Fe, Cr, Cu, and Mo, are represented by the radiation's Kα and Kβ wavelengths. Using a monochromator and filter, the device's wavelength is adjusted. The primary purpose of the filters and monochromator is to allow Kβwavelength radiation to pass while absorbing extraneous Kα wavelength emissions Slits are used to monitor and alter the shape of the incident beam. Between the incident ray and the detector, a sample holder is positioned to allow the detector to pick up the diffracted beam.The X-Ray impulses are then captured and analyzed by a detector, which further converts the input signals into a count rate. These values are then entered into a computer and the data is examined using analysis programs such as Xpowder, Xpert High Score and Full proof.

4.2 FE-SEM

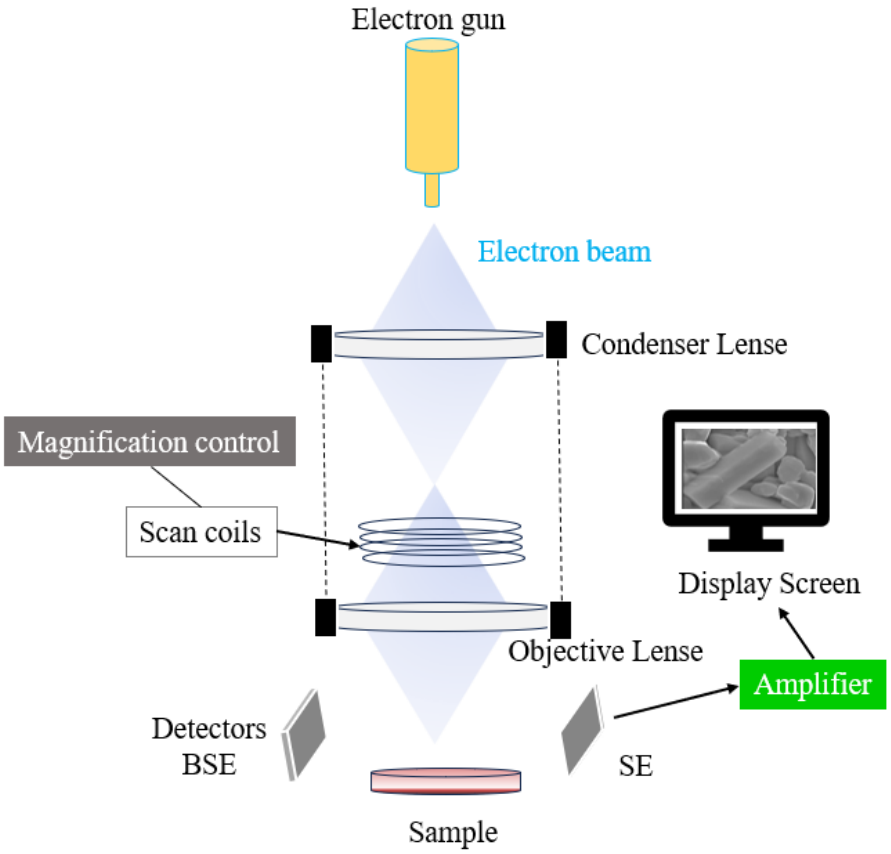

Fig4.2 shows different component of FESEM.

While light is used in structural and molecular spectroscopies, electrons are employed in FESEM. At the microscope's apex, electrons are employed to produce electron beams. Through a perpendicular channel maintained by vacuum, this electron beam travels through the microscope. After passing via lenses and electromagnetic fields, the electron beam is subsequently directed towards the sample. When electron beam falls on the sample, some electrons and x-rays are ejected and tare picked up by the detectors as secondary electrons and backscattered electrons. These signals are then converted into signals that are displayed on the screen as an image. While secondary electrons originate from within the sample material's atoms and emerge from the inelastic collision of the incident light, however the back-scattered electrons are obtained when electron from the material undergo elastic collision with the incident beam. It also gives information on the tiny impurities that exist inside the sample and the elemental compositions. It is utilised in the investigation of the thickness for the changed coatings and in the determination of structural homogeneity.

4.3 EDX

The elemental mapping tool is a non-destructive means of obtaining both qualitative and quantitative data. It provides information on the spatial distribution of constituents in the form of elemental ratios and details about their composition. With EDX mapping, elemental concentrations can be accumulated very quickly from either points or lines, and the results can also be downloaded as maps. Displaying the peaks next to the elements that are constructing the material composition in an analytical spectrum, it gives the ratio details.

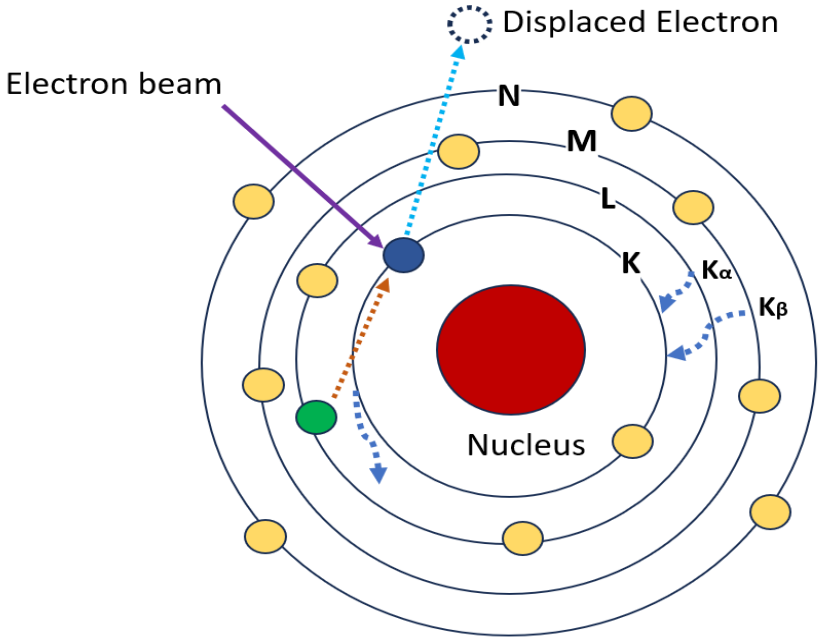

Fig.4.3 shows working mechanism of EDX.

The EDX operates based on Moseley's Law, which states that high energy electro-magnetic X-rays expel core electrons from atoms that are not found in their outermost shell. This establishes and validates the existence of the first-hand relationship between an atom's atomic number and its light frequency. A hole is created in the network when an electron is withdrawn, and this hole needs to be replaced by a high-energy electron. As the electron relaxes, this also results in the energy being released. This energy was released during the relaxation reaction, which has distinct values for every element in the periodic table. In this manner, the incident x-ray attack on the sample material can be used to determine the pre-existing elements and their percentage.

4.4 UV-Vis Spectrometer

UV-Visible spectroscopy is an effective technique that measures how much ultraviolet and visible light a material absorbs to examine its optoelectronic properties. It's a fast, inexpensive, and informative method of analysing a range of samples. To investigate it, the sample is put in a specific kind of transparent container termed as a cuvette and then subjected to light. While exposed to light, the sample's electrons are excited by light energy to high and low energy levels, which is depending on the sample's characteristics. It also causes it to absorb and reflect specific wavelengths of light. Afterwards, the

wavelength-dependent plot of this abortion and reflectance spectrum is generated. With the help of absorption spectrum, which shows the relationship between absorbance and wavelength, we can find the onset of absorption corresponding to the energy. This energy, also referred to as the band gap energy which is necessary for transition of electrons between valence and conduction band. The band gap is one of the key factors for understanding the optical properties and potential applications o in devices such as solar cells. The information from this technique is also used in chemistry, biomedicine, and food sciences

4.5 VSM

It is called as vibrating sample magnetometers (VSMs) are used to assess a material's magnetic characteristics in relation to temperature, time, and magnetic field. It functions by vibrating a sample placed inside a strong magnetic field. This magnetic field influence the presence of another magnetic material by generating a voltage in a nearby coil in corresponds with Faraday's Law. The magnetic moment of the sample, can be measured through determining this voltage by the VSM. A VSM can easily hold single crystals, thin films, solids, liquids, and powders. The magnetic inquiry is a computer-based automated process that utilises data control and analysis tools. In our case we have used powdered samples which are coated in a Teflon tape.

4.6 Impedance Spectroscopy

It is an effective method used for analysing various electronic and dielectric properties. This technique offers several advantages as it can reveal information about the electrochemical dynamics at an electrified interface in a single test. These basic processes include those that drive the corrosion of metals and alloys, power commercial batteries, and drive the electrochemical biosensors. The subject material is provided by a sinusoidal voltage of amplitude 1 Volt. The parameters obtained Z' and Z'' referred in terms of real and imaginary parts of complex impedance are measured. The various dielectric parameters such as real part (ε') and loss (tan δ) can be measured using the equation given below [120].

$$Z^* = Z' - iZ'' \quad (2)$$

$$\varepsilon' = \frac{Z''}{\omega c_o Z^2} \quad (3)$$

$$\varepsilon'' = \frac{Z'}{\omega c_o Z^2} \quad (4)$$

$$tan\delta = \frac{\varepsilon''}{\varepsilon'} \qquad (5)$$

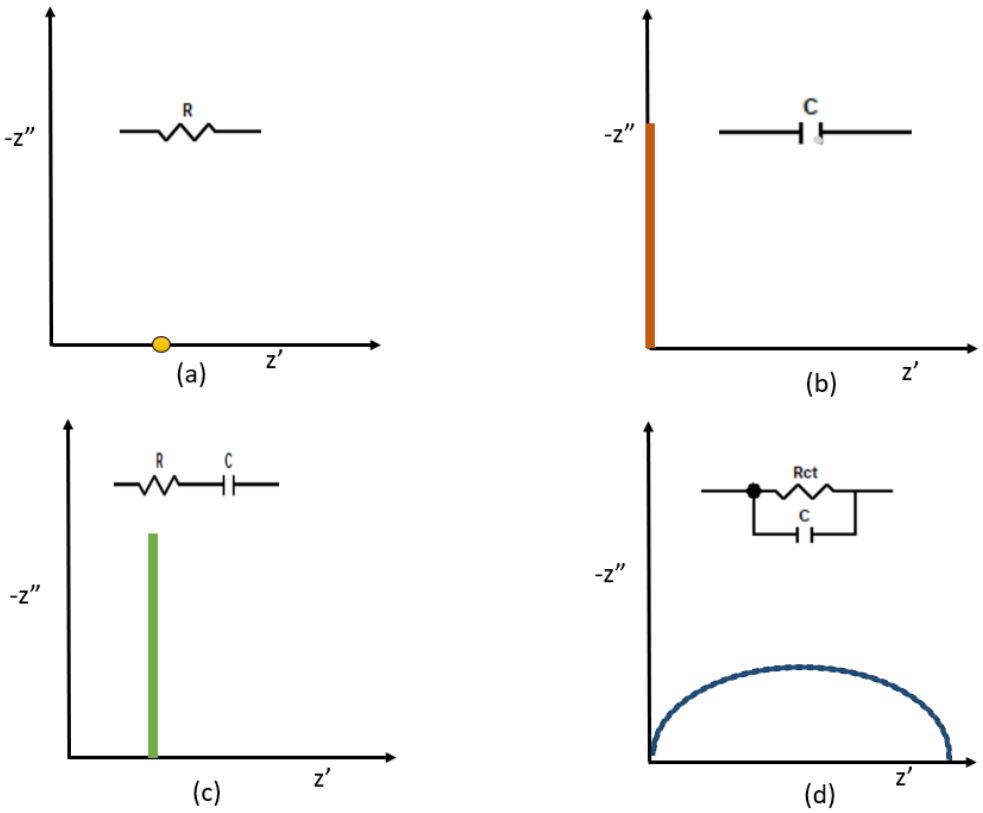

Fig.4.4 shows Nyquist plot and circuit for different type of materials.

The frequency response is plotted for the magnitude Z' and Z'' also known as the Nyquist plot at high and low frequency regimes. It is very helpful in understanding the mechanism of charging process in the provided material. The obtained data is then fitted into an equivalent circuit to calculate electronic parameters. The Fig.4.4. shows some typical Nyquist plot with the equivalent circuit for different materials. Thus, from the nature of the plot we can classify the materials characteristics.

4.7 P-E loop

Fig.4.5 The 4 K CCR instrument setup for P-E loop measurement.

The ferroelectric examination of the samples cryocooler model SRDK-205 circuit via 4 K CCR at 5 K-300 K. The chosen mode of sample used to examine by making pellets. The samples in the pellet form as electrodes by applying silver paste and connecting wires. The samples via making an electrode system have undergone an electric field to investigate the electronic properties. The observed polarization data in the form a loop is plotted with the help of computer software. This P-E loop provides the crucial information about the ferroelectric characteristics such as P_r (remanent polarisation). In our case the multiferroic materials exhibits ferroelectric based polarisation so it is crucial to determine ferroelectric parameters. The instrument can also be used to measure the ferroelectric parameters with variations in temperature, voltage, and frequency.

Chapter 5
Result and discussion

5.1 The addition of an ionic filler to the matrix of bismuth ferrite.

5.1.1 Introduction

Combining dielectric permittivity and multiferroic behaviour offers up probable uses in a variety of fields, including biomedical science and multifunctional microelectronic devices[2, 3]. The multiferroic material BiFeO3 is an appropriate choice for dielectric energy storage devices because of its strong magnetoelectric coupling at room temperature[122]. In BFO, the lone pair electrons from the bismuth (Bi^{3+}) ion (in its $6s^2$ state) on the A site are known to be responsible for ferroelectricity at high temperatures. As BFO is a popular material for research, scientists have discovered additional ways it can be multiferroic. These mechanisms, beyond the lone pair electrons, involve the arrangement of atoms (geometry) in both single and mixed-phase forms of BFO. These geometric factors can significantly improve the material's capability to accumulate electrical energy (permittivity) across various temperature ranges [5, 6]. However, additional techniques such as chemical doping and altering the shape of nanoparticles have also greatly enhanced BFO's electromagnetic properties[7–12]. According to recent studies by Remya et al., perovskite BiFeO3's electrical and magnetic properties are improved when the structure of the material was modified.[124]. However, the unstable perovskite phase of BFO makes preparation difficult and contributes to poor dielectric constant and significant dielectric loss.[128]. A recent study found that incorporating 30% of h-BFO nanoparticles into a PVDF-HFP matrix significantly enhances the composite's performance. This improvement is attributed to the strong interaction among the nanoparticles and the polymer matrix, leading to both high remanent polarization and reduced dielectric loss. [14, 15]. BFO-$MnFe_3O_4$ and BFO-$CaTiO_3$ composites are reported to have better magneto-dielectric properties, which means their magnetic and electrical properties change more significantly with [16 - 18]. A significant obstacle in creating these composite materials was that the BFO nanoparticles tended to agglomerate within the matrix material. This agglomeration bounds the dielectric constant of the composite below 100. To enhance the permittivity inclusion of dipole is an effective way [134] where permittivity ranging up to 10^5 is obtained [135].

In addition, the incorporation of metal halide to perovskite got lot of attention recently. [21, 22]. It is observed that adding halide ions to hybrid organic-inorganic perovskites can change their crystal structure. Therefore, it impacts the electronic and other properties of the material.[23, 24]. These modifications led us to clarify how and why the presence of an ionic medium impacts the electrical and magnetic properties of the multiferroic BFO [137].

This study explores a novel composite system: a combination of the multiferroic material BFO (and ionic compound sodium chloride (NaCl). As far as we know, this specific combination has not been investigated before. We created thin pellets by incorporating NaCl, an alkali-metal halide, as a filler material into a matrix of multiferroic BFO nanoparticles. The amount of NaCl filler varied, with weight percentages of 0%, 10%, 30%, and 50% used. In NaCl, the ions are arranged in a symmetrical structure that minimizes the repulsive force between their electrons. We expect the existence of these ions to significantly impact the microstructure, electrical properties, and magnetic properties of the composite material, particularly at room temperature.

5.1.2 Instrumentation

X-ray diffraction method is employed to analyse synthesised composite material in terms of phase purity. Cu-K radiation ranges of from 20º-70º were used to record the XRD (BRUKER). JEOL (FE-SEM) is used to analyse the microstructure, and magnification levels range from 25 to 1000000. By the help of VSM (Vibrating Sample Magnetometer) having magnetic field ranging from -21 to 21 KOe at normal temperature magnetic characteristics of the produced samples are examined. The Nyquist plot and dielectric properties are analysed using the METROHM together with the FRA32M-Impedance analyser, which operates in the 10 Hz–1 MHz range.

5.1.3 XRD analysis

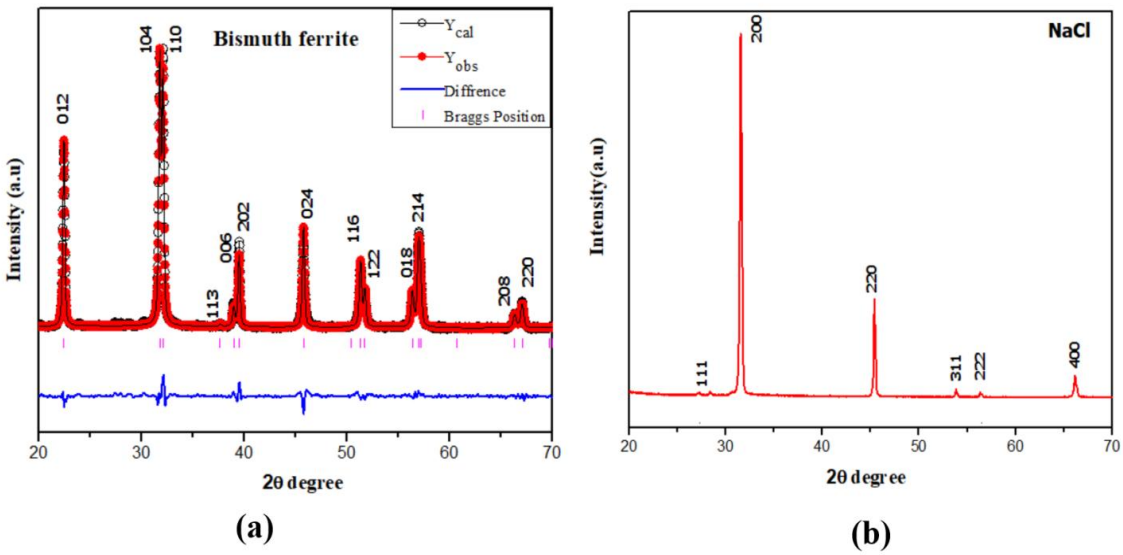

Fig.5.1.1 *XRD pattern of (a) as-prepared Bismuth ferrite and (b) NaCl.*

By measuring the powder XRD, the phase purity and crystallinity of the synthesized Bismuth Ferrite and selected NaCl were evaluated. The XRD analysis Fig.5.1.1 (a) confirms the development of Bismuth ferrite while the phase identification with the help of Rietveld refinement using Full Proof software. The presence of sharp peaks specify the crystalline nature of the material matches well with the single phase belonging to the R3C group with COD 96-210-2910. NaCl is known to have crystalline nature with a cubic phase. Similar results are obtained from the XRD of NaCl in Fig.1. (b) as taken with sharp crystalline peaks similar to COD 96-430-0181. The lattice constant is calculated with the help of the following equation 1[138]. The obtained parameters such as lattice constants and crystallite size for as-prepared BFO and NaCl are shown in Table.3.

$$\frac{1}{d} = \frac{4}{3}\left(\frac{h^2+kh+k^2}{a^2}\right) + \frac{l^2}{c^2} \qquad (6)$$

Lattice Constant	a	b	c
BFO	5.57	5.57	13.86
NaCl	5.6344	5.6344	5.6344

Table.3 The lattice constant of synthesized BFO and NaCl.

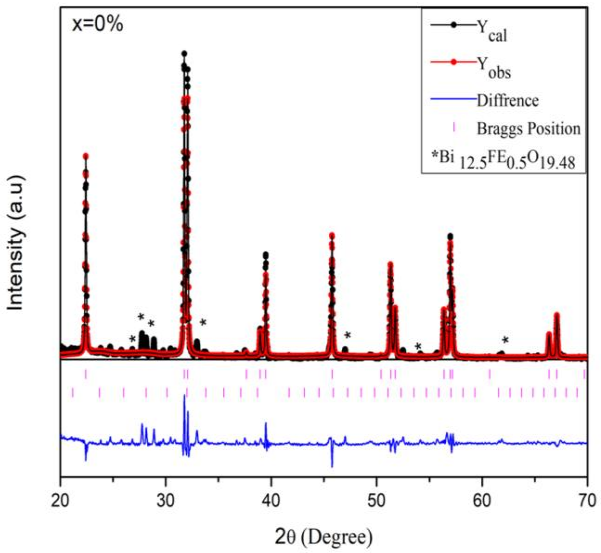

(a)

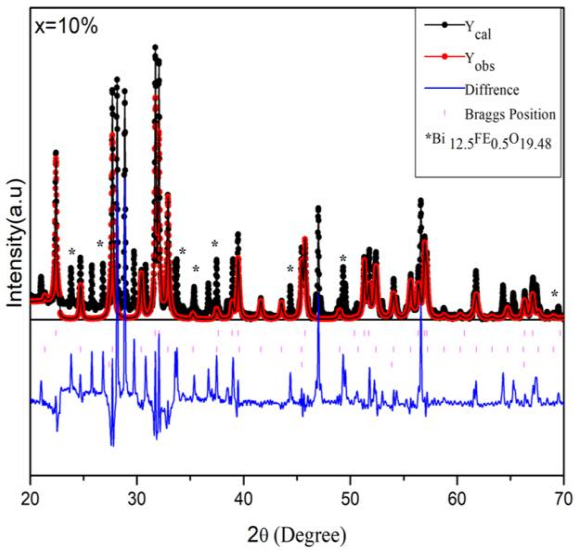

(b)

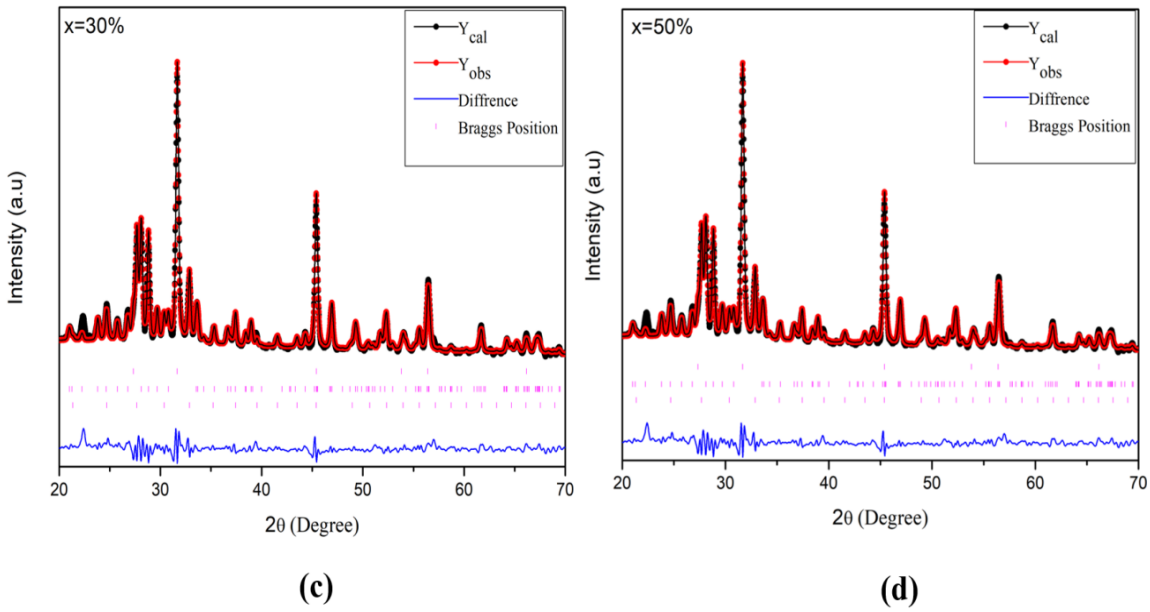

(c) **(d)**

Fig.5.1.2 (a) XRD retrieved pattern for x=0%, (b) XRD retrieved pattern for x=10%, (c) XRD retrieved pattern for x=30%, (d) XRD retrieved pattern for x=50%.

The XRD analysis is carried out for BFO-x NaCl (x= 0, 10, 30, 50%) composite systems post-annealing the morphology of the structure is discovered to be greatly influenced by the annealing temperature, and several research studies have found that the lattice constant rises as the annealing temperature upsurges [84], [139], [140]. Similar behavior for BFO (x=0%) is seen in Fig.5.1.2 (a) where production of secondary phases in BFO, consisting of the phases Bismuth Ferrite (BFO) with and Selenite (Bi12.5Fe0.5O19.48), is induced by the high-temperature annealing procedure. In addition to NaCl, the phased purity is affected by lowering the crystallinity of bismuth ferrite along with peak shifting to a lower angle. Fig.5.1.2 (b) shows the retrieved XRD pattern of the x = 10% sample consisting of individual Phases of Bismuth Ferrite, Selenite, and NaCl.

The computation reveals that the lattice constants rise for the composite systems with x=0% and 10%, as shown in Table.3. The XRD pattern of the composite system x = 30% and 50% is shown in Fig.5.1.2 (c) and (d) respectively. The analysis also confirms that at a high percentage of NaCl reinforcement along with annealing, the BFO phase changes where the low crystallinity peaks are mostly related to selenite and $Bi_2Fe_4O_9$ with COD 96-153-0919, although no change or shift in NaCl peaks is observed. The result shows that the phase change is prominent with an increase in the percentage of NaCl. Annealing at a high temperature is found to affect phase purity. In contrast, the phase of $BiFeO_3$

entirely transforms into other well-known phases of $Bi_2Fe_4O_9$ with lattice constants mentioned in Table. 4 for composite systems with x=30% and 50%.

Table.4 The lattice constant of the composite system.

Sample	X=0%	X=10%	X=30%	X=50%
Lattice constant	a=b=5.755, c=13.86	a=b=5.5772, c=13.86	a=7.981, b=8.450, c=6.01	a=7.9733, b=8.440, c=6.003

These findings suggest that the addition of NaCl alters the crystallinity and morphology. These results imply that the morphology and crystallinity are changed by the addition of NaCl. The impact of filler on phase transition was detected in our case at lower temperatures than those reported by other studies, which stated that phase transition occurs around 820^0 C [141]. The observed phase transition for the above-mentioned composite systems is investigated to provide further information on the structure's magnetic and electronic properties.

5.1.4 Morphology

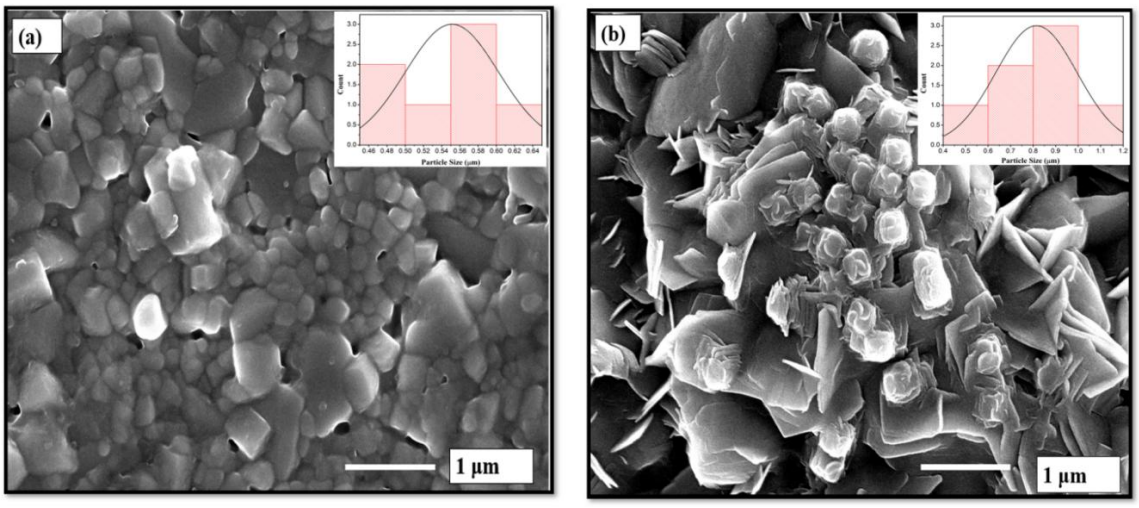

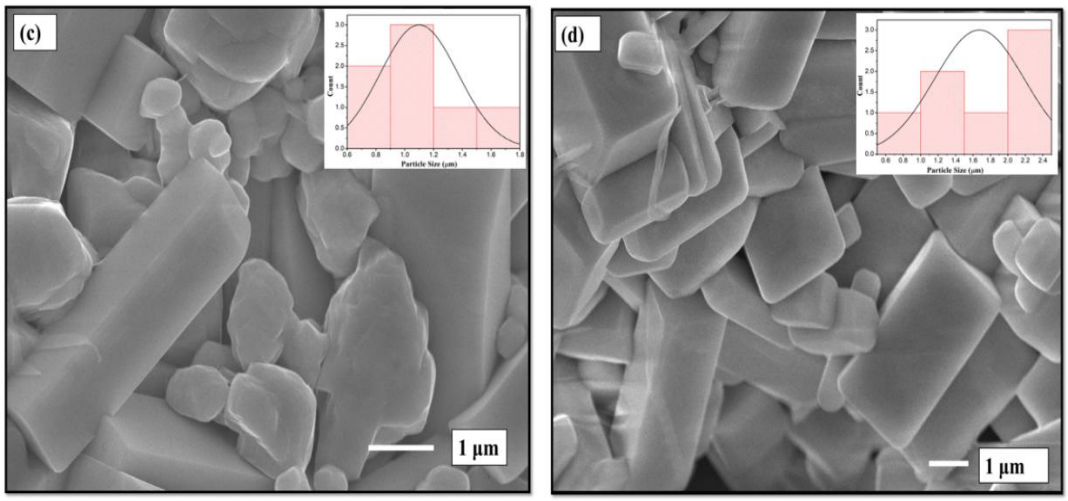

Fig.5.1.3(a) The SEM images for x=0%, (b) The SEM images for x=10%, (c) The SEM images for x=30%), (d) The SEM images for x=50%.

Fig.5.1.3 shows the magnified images of the composite sample post-annealing with the help of a field emission scanning electron microscope revealing grain formation in (x=0%) in the absence of filler with an inhomogeneous shape of a particle with empty voids. Annealing does cause the particle size to rise [142], here we observe in Fig.5.1.3 that the average grain size of particles is found to be in the range of 0.5µm-1.5µm. On introducing filler, we observe a change in morphology with flower petal shape with unstable phases makes a good agreement with the obtained XRD results. The formation of different Phases is mainly attributed to the competition between crystal nucleation and growth [143]. Fig.5.1.3 (c) and (d) show that the morphology is more well-defined at higher concentrations, with a rod-shaped structure connected to $Bi_2Fe_4O_9$ that is identical to the report and is in good accord with the XRD data we collected [144]. The presence of NaCl inferred the decrease in the melt's viscosity and improved the mobility of its components, culminating as we increase the weight percentage in a structure with a clearly defined rod shape [145]. The morphological alterations seen in the composites' XRD pictures and phase transformation for those composites are consistent.

5.1.5 Magnetic properties

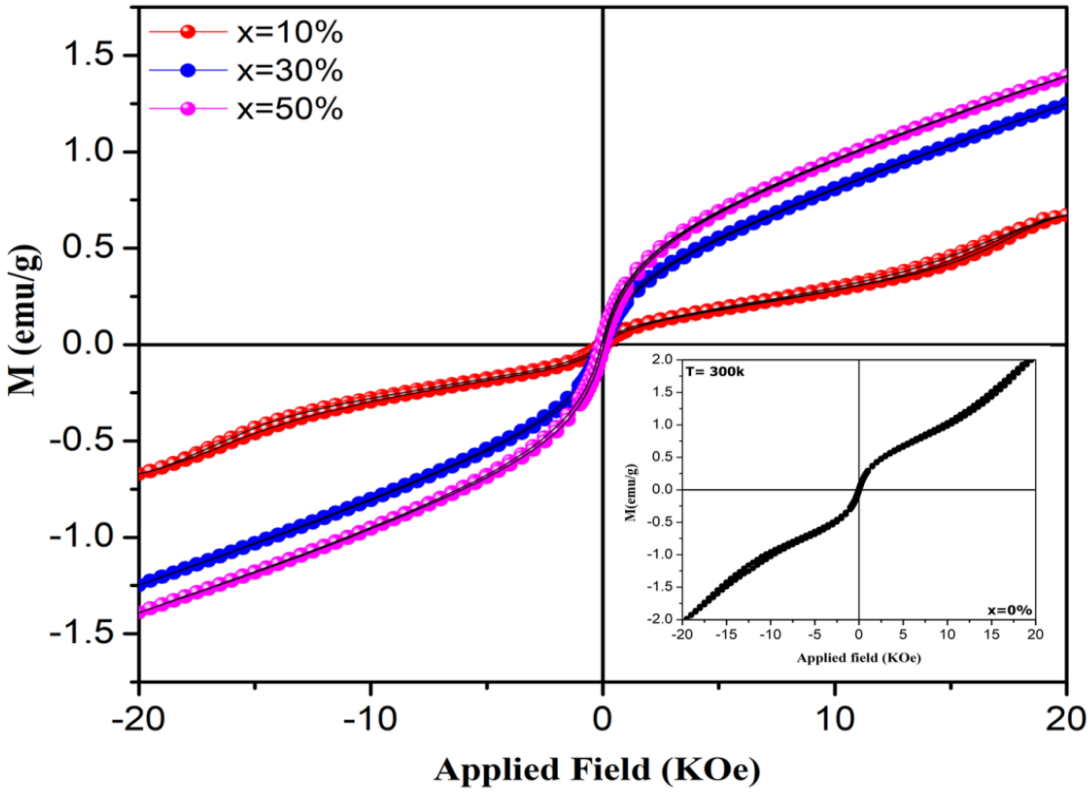

Fig.5.1.4 shows the hysteresis loop for x= 0% (inset) 10%, 30%, 50%.

The room temperature magnetic properties are investigated with the help of a Vibrating Sample Magnetometer as shown in Fig.5.1.4. The composites are subjected to a high magnetic field ranging from -20 to +20 KOe. The various parameters such as Retentivity (**M_r**), Saturation (M_s), and Squareness Ratio (M_r/M_s),) are calculated from the observed magnetization data listed in Table 5. The analysis reveals a composite showing that the sample has weak magnetic nature as reported in previous studies [24] favoring antiferromagnetic nature induced by Dzyaloshinskii -Moriya interactions [90]. Fig.5.1.5 (a) - (d) shows a thin hysteresis loop and the attained magnetic parameters are listed in Table.4.

Table.5 Magnetic parameters obtained from VSM.

Sample	H_c Average (Oe)	M_r Average (emu/g)	M_s Average (emu/g)	M_r/M_s
x=0 %	44.55	1.895	0.063	0.009
x=10%	79.18	0.008	0.02	0.013
x=30%	57.99	0.0195	0.037	0.016
x=50%	57.54	0.02	0.041	0.019

The parameters such as coercive field and remnant magnetization are found to be sensitive to the weight fraction of NaCl in the composite systems at room temperature. The improved magnetism in x = 10, 30, and 50% compared to the BFO sample (x = 0%) is attributed to the transition and distortion in crystal structure resulting in spiral spin modulation [85], [146] and enhanced oxygen vacancies [147]. As from the above result for x=10%, the coercive field H_c is found to be 79.18 Oe which is the highest compared to other samples. The presence of mixed phases in the composite system is held responsible for the spiral spin modulation that affects magnetization. Also, the co-existence of multi-phase affects the Fe-O-Fe bond resulting in enhanced magnetic properties [148]. However, the filler used is diamagnetic therefore no large increment in the H_c can be expected.

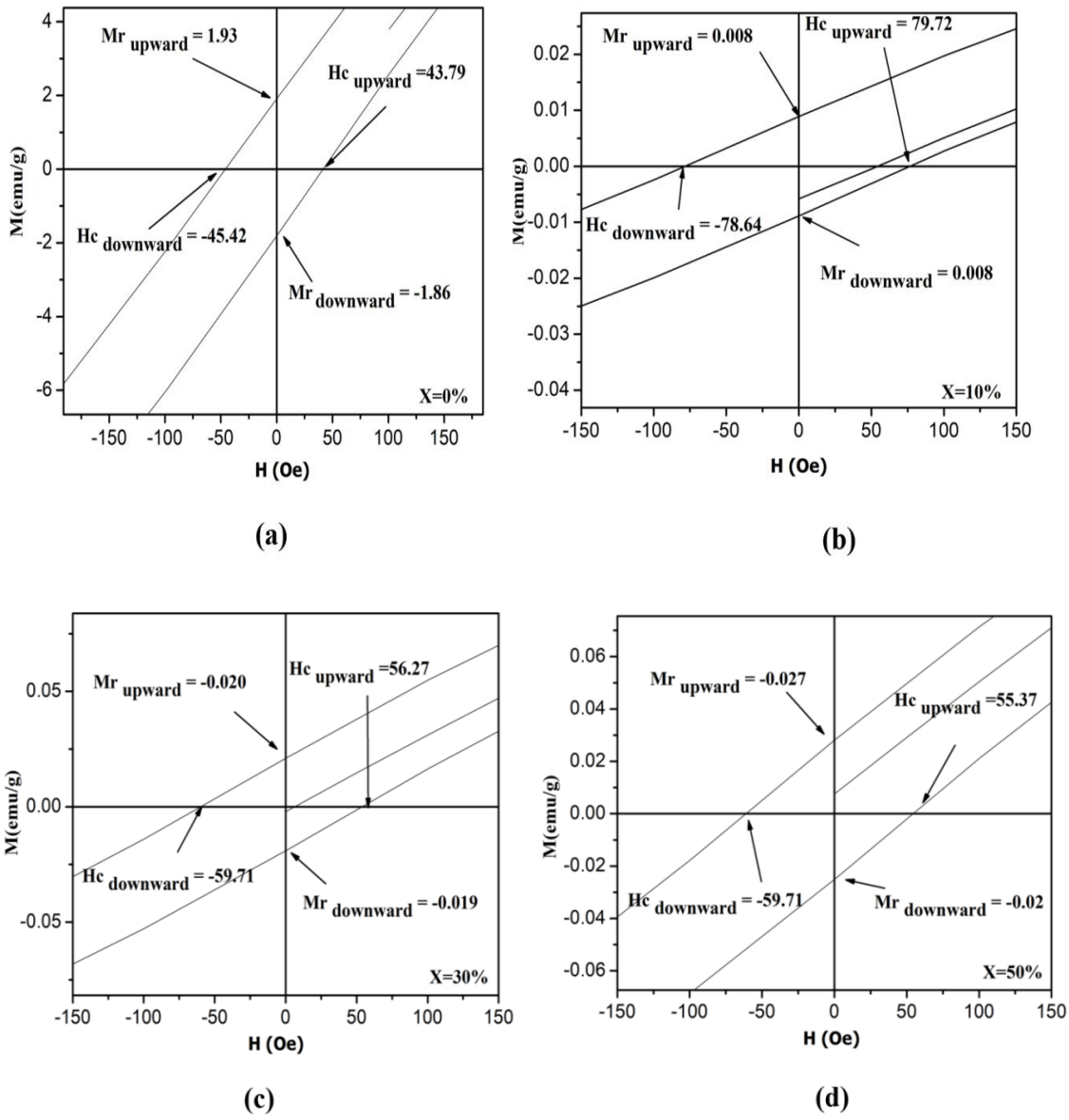

Fig.5.1.5 The enlarged view hysteresis loop for x=0%, (b) The enlarged view hysteresis loop for x=10%, (c) The enlarged view hysteresis loop for x=30%, (d) The enlarged view hysteresis loop for x=50%.

The XRD result also confirms that for x=30% and 50%, the rhombohedral phase vanishes resulting in net magnetization due to the secondary phases only. It is observed that in $Bi_2Fe_4O_9$ antiferromagnetic nature is dominant at high magnetization [149]. The squareness ratio is very small and less than 0.5 confirming the random orientation of the domain in the system domains [150]. Moreover, the increased oxygen vacancy [151]defects in BFO may alter the spacing between the Fe ions [53], break the super-

exchange interactions of Fe^{3+}-O_2 -Fe^{3+}, and introduce the Dzyaloshinskii-Moriya (DM) interaction, resulting in a weak ferromagnetic nature. The fabrication of magnetically based devices may make use of the modified magnetic characteristics [92].

5.1.6 Impedance Analysis

5.1.6.1 Nyquist plot

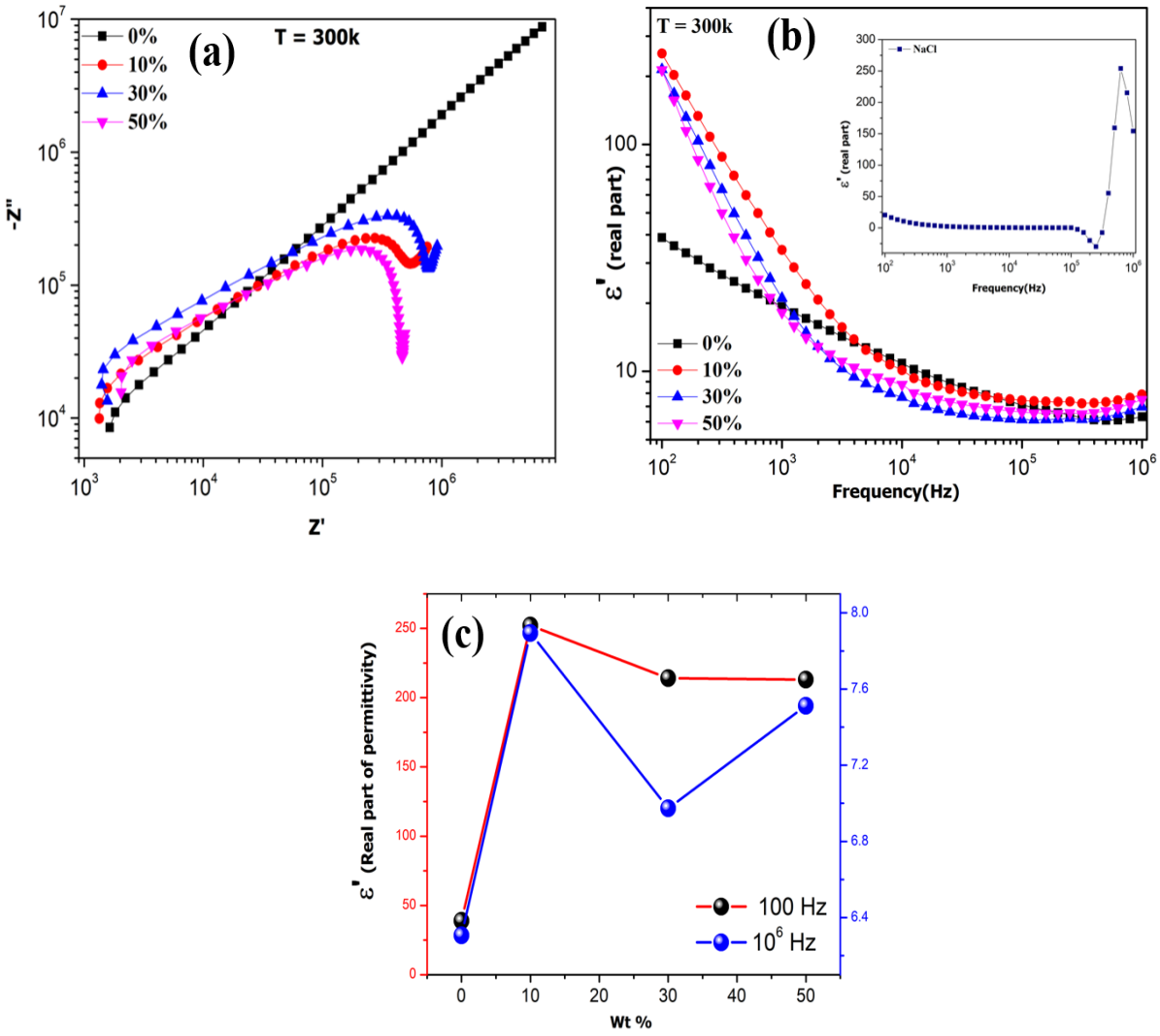

Fig.5.1.6 (a)The Nyquist plot for complex impedance was calculated for the composite system (b)The real part of permittivity is a function of Frequency and (c) variation of the real part of permittivity with wt %.

The composite system in the pellet form is subjected to analysis of the electronic properties using impedance spectroscopy. The composite is subjected to a sinusoidal voltage of amplitude 1 Volt. The complex impedance Z' and Z'' in terms of real and

imaginary parts are measured. The Dielectric constant for the real part (ε') and loss (tan δ) is also calculated with the help of given equations [120].

$$Z^* = Z' - iZ'' \quad (2)$$

$$\varepsilon' = \frac{Z''}{\omega c_o Z^2} \quad (3)$$

$$\varepsilon`` = \frac{Z'}{\omega c_o Z^2} \quad (4)$$

$$tan\delta = \frac{\varepsilon''}{\varepsilon'} \quad (5)$$

The Nyquist plot as shown in Fig.5.1.6 (a) is plotted for the composite system at room temperature with frequency ranging from 100Hz to 1MHz.

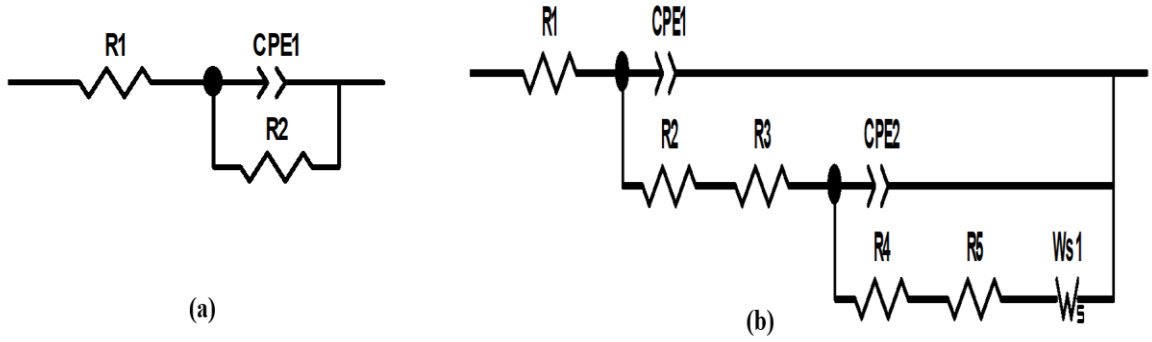

Fig.5.1.7 Equivalent circuit purposed for fitting of EIS obtained from (a) for x= 0% (b) for composite systems (x=10,30,50%).

The impedance spectra have been analysed followed by an equivalent circuit in Fig.5.1.7 (a), (b) The circuit consists of a resistance followed by a double parallel combination of a constant phase element (CPE) and a resistance. The presence of an oblique line is associated with the Warburg impedance. The parameters calculated using the fitting are listed in Table.5. The pure sample (x= 0%) exhibits a linear behaviour indicating good capacitive behaviour throughout the entire frequency range. The formation of two arcs is evident from the plot which further implies that on NaCl addition, grain boundaries are formed in between BFO grains. The formation of a semi-circular arc for x=10%, 30%, and 50% is a direct consequence of spatial heterogeneity, thus changing the charge dynamics in the composite system considerably. However, as the dopant percentage increases, the magnitude of the real part of Z^* tends to decline due to the interfacial grain boundary effect which facilitates the charge modulation at the interface. The blocking

effect between the particles causes the resistance R1 to grow with filler percentage at x=10% and 30%, while the resistance R1 decreases at x=50% in relation to the lower percentage of BFO.

Table.6 The calculated parameters were obtained from an equivalent circuit.

Sample	R_1 (ohm)	CPE_1T (F)	CPE_1P (F)	R_2 (ohm)	$R_3 \times 10^6$ (ohm)	$CPE_2T \times 10^{-10}$ (F)	CPE_2P (F)	$R_4 \times 10^6$ (ohm)	$R_5 \times 0^6$ (ohm)	Ws-R $\times 10^6$	Ws-T	Ws-P
X=10%	6443	5.44×10^{-11}	0.90	5.30970	8.47	4.05	0.25	9.35	0.60	3.19	31.03	0.119
X=30%	8205	2.4×10^{-11}	0.93	746660	2.7	1.55	0.49	3.69	0.29	3.91	57.06	0.1665
X=50%	5553	2.17×10^{-11}	0.93	418930	0.11	1.55	0.72	0.58	1.99	3.36	0.082	0.015

5.1.6.2 Dielectric constant and Losses

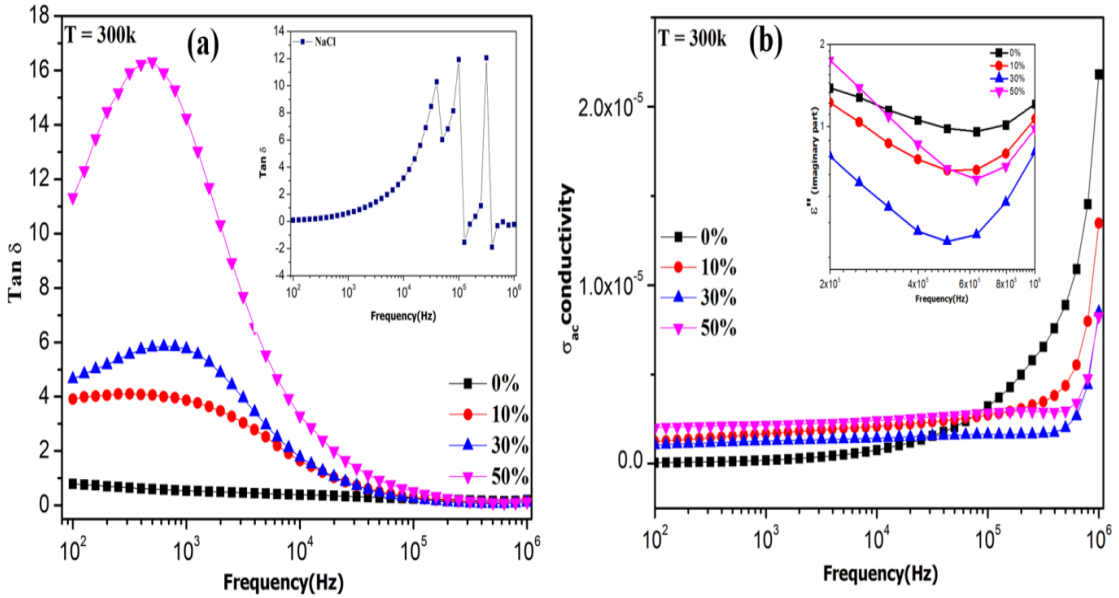

Fig.5.1.8 (a) The dielectric loss as a function of Frequency (b) The AC conductivity as a function of frequency, inset ε'' (imaginary part of permittivity) variation in high-frequency regime.

The real part of the electrical permittivity (ε') of the material associated to the dielectric constant which helps the charge to build up in a system. A material's capacity to polarise under the effect of an applied field is also stated by its real part of permittivity. The dielectric constant with varying frequency at room temperature has been described here for composite systems.

Fig.5.1.6 (b) demonstrate that permittivity (real part) of the samples has a significant change at the low-frequency regime and tends to upsurge with the increase in NaCl filler. Weak dependency between frequency and dielectric permittivity is observed for pure BFO whereas, for x > 10%, the dependence becomes stronger at a low-frequency regime as shown in Fig.5.1.6 (b). This is primarily ascribed to the formation of different phases at different concentrations of NaCl. The ferrites have been found to have large dielectric constant in the low-frequency region because of ion accumulation close to the interface, thus in the composite systems, the addition of ionic filler results in value of dielectric constant by one-fold. Electric dipole relaxation on changing the frequency commonly exhibits this type of electrical on approaching the high-frequency regime because of the Maxwell-Wagner effect [34, 35]. This also signifies that the dipole is far more responsive to the applied field at inferior frequencies, leading to a larger dielectric value [153].

However, in the high-frequency area, the polarization caused by the accumulation of ionic charge carriers reduces due to the high periodic setback of the electric field, which causes the reduction in the value of ε' [154]. In addition, the effect of increasing filler percentage makes the system more disordered due to which the frequency-dependent real part of permittivity attains a plateau at high frequency. The inset of Fig.5.1.6 (b) displays the flat frequency dependence of dielectric permittivity of NaCl till 10^5 Hz at room temperature afterward there is a sharp increase of permittivity followed by another regime where permittivity decreases. This strange variation of the dielectric constant can be attributed to the ionic contribution of NaCl similar to complex halide perovskite where various mechanisms such as optical response, ionic space charge effect, and the presence of dipolar spices play a vital role in determining the charge dynamics[155].

As a result, it is conferred that in the prepared system, a high dielectric constant result from a growth in the number of dipolar species as the weight percentage of NaCl increases and other hetero-phases present in the system. Fig.5.1.6 (c) shows the discrepancy of the real part of permittivity as a function of the weight percentage of NaCl. Similar behaviour in the variation is observed for both low and high-frequency regimes. From the plot, it is found that at around X= 10%, a peak in the permittivity appears which suggests a percolation-type behaviour [156]. Above the peak point, the permittivity decreases which further indicates the formation of a conducting path through which charge percolates in the system.

Fig.5.1. 8 (a) illustrate the observed change in dielectric loss as a function of frequency at 300 K. It is found that for X = 0%, the dielectric loss is less than 1 with no peak observed, indicating an efficient dielectric energy storage material. On the other hand, the composite systems with X > 0% show increased dielectric losses followed by a peak at a frequency close to 10^3 Hz also reported in previous studies [86]. This behaviour is caused by the predominating ohmic components and maxima at a certain frequency that matches the rotation of the molecules and leads to the greatest amount of power transfer [157]. In this area, capacitor behaviour is predominant. The peak of the dielectric loss at the 1 KHz regime does not show any significant shifts with an increase in filler percentage, suggesting that the packing of the molecules is loosened with an increase in NaCl percentage, resulting in a comparable relaxation period [47].

In Fig.5.1. 8 (a) inset it shows the dielectric loss for NaCl as a function of frequency. It is found that dielectric loss leans towards high magnitude in the intermediate frequency

range beyond which the loss becomes noisier. This shows that at high-frequency regime, the ions in the crystal structure of NaCl displaces, thus increasing the possibility of the generation of polarons.

5.1.6.3 Ac conductivity

The organized motion of weakly bonded charged particles in our disordered system observed in Fig.5.1. 8 (b) under the influence of an electric field. Electrical conductivity is one of the key properties that is affected by the various charge carriers such as electrons and holes , cations and anions that regulate conduction process, along with their response to frequency [159].

From equation $\sigma_{ac} = \varepsilon''\omega c_0$, the relationships between σ_{ac} conductivity and frequency are plotted in Fig.5.1. 8 (b). The flat plateau in the conductivity at low frequency mainly signifies dc conductivity followed by an increase in conductivity at high frequency with a steep slope. It is also found that for X = 0% (BFO), the rise in ac conductivity takes place at a lower frequency as compared to composite with NaCl. The relationship between conductivity and frequency is explained based on large and small polaron models [37, 38]. In most cases, the conductivity's frequency dependency follows Josher's power law $\sigma_{ac} = \sigma_{dc} + A\omega^n$ [161].

Here n (exponent) is the slope having significance in diverse interpretations, applications, and models and relates to the polarization mechanism which includes a full contribution from the effects of mobile charges. In our case, the value of n (fitting not shown here) is found to vary between 0.9 - 2. The large value of n (n > 1) usually suggests that a dynamic related to the bound charge mechanism due to the disorderliness in the material predominates in the composite system [54, 55]. Moreover, the same behaviour and similar order of conductivity for x > 0% signify that the ac conductivity is independent of the details of the disorder in the extreme disordered limit which is when local random mobilities span many orders of magnitude. The imaginary part of dielectric permittivity also shows an upturn at the same frequency where AC conductivity rises significantly. This behaviour is revealed in the inset of Fig.5.1. 8 (b). This signifies that ac conductivity reflects an underlying percolation behaviour in the composite system.

This reasonable speculation has urged us to carry out a temperature-dependent study on the percolative composite system. The density and size of the grains greatly affect the electrical characteristics. Moreover, the multiple phases present in the system, as found from XRD, can tweak the percolation threshold which in turn can influence electrical

conductivity in BFO-x NaCl. The observed electronic response shows interesting results that can be used to enhance the overall properties of the ionic composite system and may find their practical application in electronic devices.

Conclusion

In summary, we have fabricated bismuth ferrite nanoparticles of high purity by sol-gel process. The effect of annealing temperature results in the formation of secondary phases. X-ray diffraction and FE-SEM have further confirmed the change in microstructure and morphology of matrix BFO with the increasing weight percentage of ionic filler NaCl, indicating the production of secondary phases of BFO. Further on adding the filler, it is observed that the R3C Bismuth ferrite structure is very sensitive to filler weight percentage with phase transformation to prominent phase belonging to $Bi_2Fe_4O_9$ at (X = 30%, 50%). The formation of secondary phases and phase transformation are also evident in FE-SEM images with an increment in size of particle.

The magnetic parameter is also influenced by the integration of NaCl at ambient temperature which may be due to the coupling between the morphology and intrinsic magnetic moment of BFO. Further, the increase in coercivity with the addition of halide filler in the BFO matrix indicates improved coupling among the nanoparticles which can further pave an indigenous path for the potential application in memory devices and fabrication of sensor-based electronic devices. From the CIA (complex impedance Analysis) measurement, it is found that the presence of NaCl is largely responsible for the rapid change in dielectric characteristics.

By introducing NaCl as an ionic filler, we were able to enhance the dielectric permittivity by a factor of 6 at low frequency with the peak appearing around X = 10%. The introduction of filler causes disorder in the composite, yielding a large exponent n ~ 1.6 of σ_{ac} conductivity. Optimizing the size and morphology of grains can improve the electronic properties significantly. This study is evidence that the presence of NaCl alters the microstructural, dielectric, and magnetic properties which urges the investigation of such halide-based composite systems to benefit desired properties. The improved dielectric and magnetic properties may find practical application in the fabrication of electronic and energy storage devices.

5.2 The addition of Cobalt ferrite to the matrix of bismuth ferrite.

Multiferroics belongs to a class of materials that exhibits two or more primary ferroic ordering, thus making them a suitable contender for numerous applications like spintronics, microsensors, and storage devices[1–4]. $BiFeO_3$, bismuth ferrite (BFO) is one of the renowned multiferroic materials whose lone electron pairs of Bi^{3+} lead to ferroelectric behavior and ordering of Fe^{3+} leads to G-type antiferromagnetic behavior. The simultaneous presence of both electrical and magnetic polarization at room temperature leads to strong magnetoelectric coupling which further offers a extensive choice of applications in electromagnetic transducers, biomedical applications, and solar cells for energy generation [4–7]. However, the intriguing properties of perovskite-structured BFO are strongly dependent on the fabrication process which has a direct impact on the coupling coefficient, thus making it weak. Moreover, the existence of large leakage current, high transition temperature, and small magnetization limit its potential usage in scientific applications. Various methods such as substitutional doping, surface modification, and multilayer with imperfect interfaces have been adapted in order to advance the properties of multiferroic BFO materials [8–14]. Further, for better utilization of multiferroic materials in commercial technologies, the large magnetoelectric coupling over vast range of temperature is required. The lack of consistent and desired properties in so-far investigated multiferroic materials at wide temperature range have shifted our attention to nano-composite systems.

In addition, it has also known that as ccompared to single-phase materials, composite systems are prone to have synergistic effect that leads to remarkable magnetoelectric coupling due to the product tensor properties [168]. The interfacial phenomena between the nanoparticles of the constituent phases in composites is helpful in developing multifunctional devices like spintronics with high efficiency and fast electric and magnetic switching. However, magnetoelectric effect in percolation based composite systems have not been studied in details till date. In our work, $CoFe_2O_4$ (CFO) nanoparticles are embedded into the matrix of BFO in order to investigate the effect on structural and other properties in the percolative composite system. The CFO is well known for its high magnetic coercivity, strong crystalline anisotropy, high curie temperature, chemical stability and mechanical hardness [169]. The addition of magnetic

cobalt ferrite is anticipated to increase the net magnetic and ferroelectric properties of bismuth ferrite, thus enhancing the magnetoelectric effect [170]. So far, composite systems such as $BiFeO_{3:}$ $MnFe_2O_4$, $BiFeO_3$: Co_2FeO_4, $BaTiO_3$: $BiFeO_3$ and $BiFeO_3$: RGO have been investigated for different natures of electronic, magnetic and dielectric properties [16–19]. Despite the fact that multiferroic compounds are known to be sensitive to temperature, composition, and other chemical aspects, these studies lack the focus on the tunability of ferroelectric properties as a changing weight percentage of the constituent particles at wide temperature range [23–25].

Hence, it will be interesting to look on the structural composite of a spinel cobalt ferrite - $CoFe_2O_4$ and a multiferroic perovskite BFO, where the variation of magnetoelectric coupling effect arises from the increasing size of percolating cluster of CFO leading to different degree of electrical and magnetic properties in the composite system. It is well established that several variables, including the weight percentage of crystallinity, morphology, and particle size are crucial in determining the composite's overall characteristics. Here, both materials are synthesized under the same circumstances following the same route for preparation using the same chelating agent. Nanocomposites consisting of CFO as filler in BFO matrix, with filler weight percentage (x) as 10%, 30% and 50% have been prepared by mechanical blending and were pressed into pellets afterwards samples are heated in furnace at 650 ^{0}C for 2 hours. The findings of the experiment will enable us to better comprehend how sensitive the BFO Matrix is to the weight percent of CFO and how this factor affects the electrical, dielectric, and magnetic properties. The CFO-BFO composite system will enable us to adjust the multiferroic characteristic to our specific needs for room temperature applications involving magnetic, electrical, and spintronic devices.

5.2.1 Instrumentation

The synthesized nanoparticles are characterized by X-ray diffraction for phase purity. The XRD (BRUKER) was recorded using Cu-K radiation ranges from 20^o-70^o with a step size of 0.02 degrees at room temperature. The microstructure is analyzed using JEOL (FE-SEM) and EDX spectroscopy with magnification ranging from 25 to 1000000 is performed. The magnetic properties of the prepared sample are analyzed with the help of a VSM (Vibrating sample magnetometer) with the field ranging from -21 to 21 KOe at room temperature. The Zeta potential analyzer from MALVAREN is used to calculate Zeta potential. The SES DFp-03 Probe instrument is used to measure temperature-

dependent resistivity. The METROHM and the FRA32M-Impedance analyzer ranging from 10 Hz to 1MHz are used to analyze the dielectric properties. The ferroelectric properties (P–E) hysteresis are carried using a cryocooler model SRDK-205 circuit via 4 K CCR in temperature and frequency range of 5 K - 300 K and 50 Hz - 250 Hz respectively.

5.2.2 Structural analysis

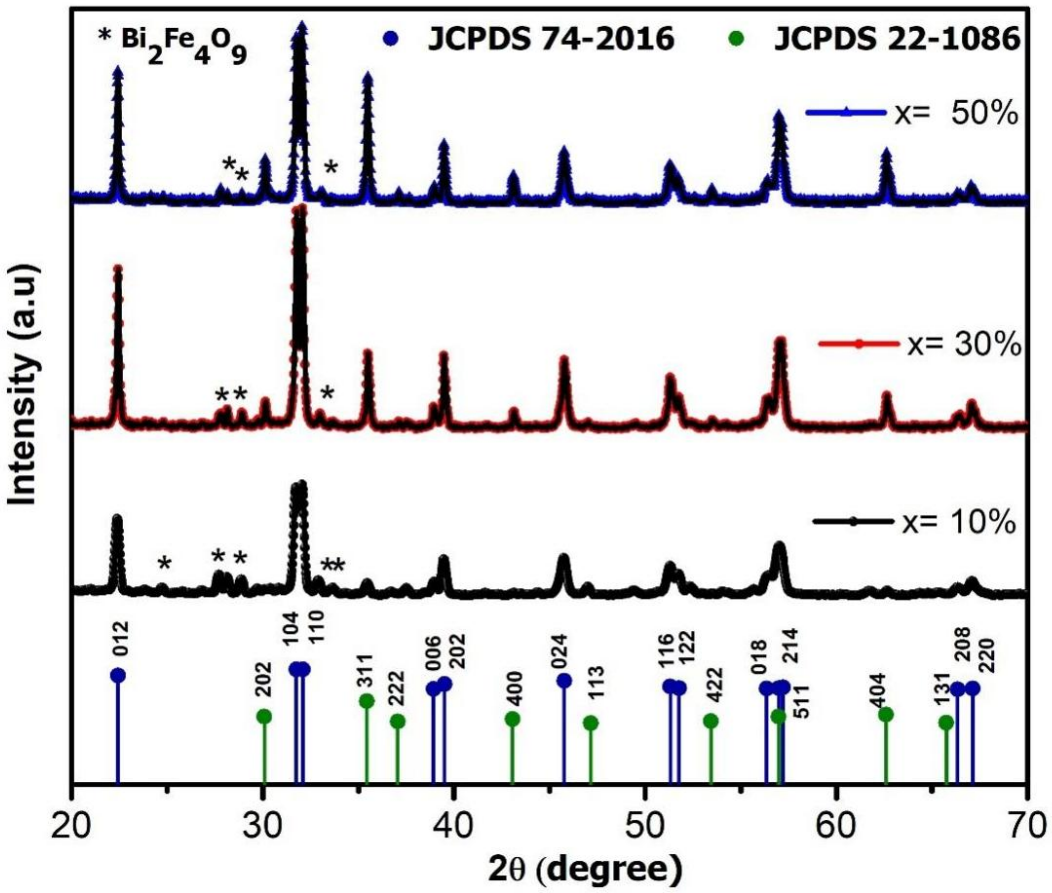

Fig.5.2.1 XRD retrieved pattern for x=10%, x=30%, x=50% along with JCPDS.

The composite system is subjected to XRD in Fig.5.2.1 with step sizes of 0.002 and 2θ spanning from 20^0 to 70^0 at room temperature. With the aid of X powder and X pert high score, the data phase is identified. XRD data of every composite system is presented along with the JCPDS card in Fig5.2.1. The diffraction peak shown in Fig 5.2.1 demonstrates that $BiFeO_3$ with JCPDS (74-216) phase belonging to R3C - rhombohedral and $CoFe_2O_4$ 22-1086 belonging to cubic phase with JCPDS (22-108) are present. Bismuth ferrite is found to be sensitive to heating temperature and the morphology of the

structure is found to be greatly influenced by the annealing temperature. Several researchers have found that on changing the heating temperature lattice constant are greatly affected [23], [25 –27]. In CFO - BFO composite system, it leads to the formation of $Bi_2Fe_4O_9$ with the JCPDS (74-1098) phase (not shown here). The peak shift as observed in the identity peaks of $BiFeO_3$ (140, 110) for x = (10%, 30%, 50%) are positioned at (31.70, 32.04), (31.75, 32.07) and (31.72, 32.08) respectively. Along with the peak shift that is associated with $CoFe_2O_4$ [172] distinctive peak (311) was observed at (35.45), (35.9) and (35.46) correspondingly. The intensity peaks corresponding to $CoFe_2O_4$ with index (311) (400) and (404) are found to increase with the filler percentage. The presence of sharp diffraction peaks is evident of crystalline characteristics of the sample.

The crystallite size is determined by the equation

$$d = \frac{k\lambda}{\beta Cos\theta} \quad (6)$$

Where k is the shape factor, λ is the wavelength of the target anode which is around 1.05 A^0, θ is the Bragg's angle and β is the full-width half maximum (FWHM).

Table.7 It shows the observed values of lattice constant and crystallite size of composite systems.

BFO: xCFO		X=10	X=30	X=50
Lattice constant	BFO	a=b = 5.58, c = 13.86	a=b = 5.58, c = 13.86	a=b = 5.58, c = 13.86
	CFO	a = b = c = 8.39	a = b = c = 8.39	a =b =c = 8.38
d (nm)	BFO	35.05	35.46	37.24
	CFO	20.17	33.36	47.10

From Table.6. the crystallite size of the sample is found below 50 nm. The FWHM (β) belonging to peaks of Bismuth ferrite indicated that there had been a noticeable shift in crystallite size. However, the increase in crystallite size on adding $CoFe_2O_4$ is observed. This is due to the influence of an increase in the weight % of $CoFe_2O_4$ generated by nanoparticle agglomeration caused by the large surface area of the particle, or it could be connected to the magnetic moment that forces the particles to gravitate towards one another [173]. Fig.5.2.1 depicts that by adding filler, it is found that the $Bi_2Fe_4O_9$ peaks are affected, which lowers the impurity phase. The reduction in impurity phases is a direct result of the occupation of vacant vacancies by Cobalt atoms [174] which become more dominant as the filler percentage increases.

5.2.3 Morphological analysis

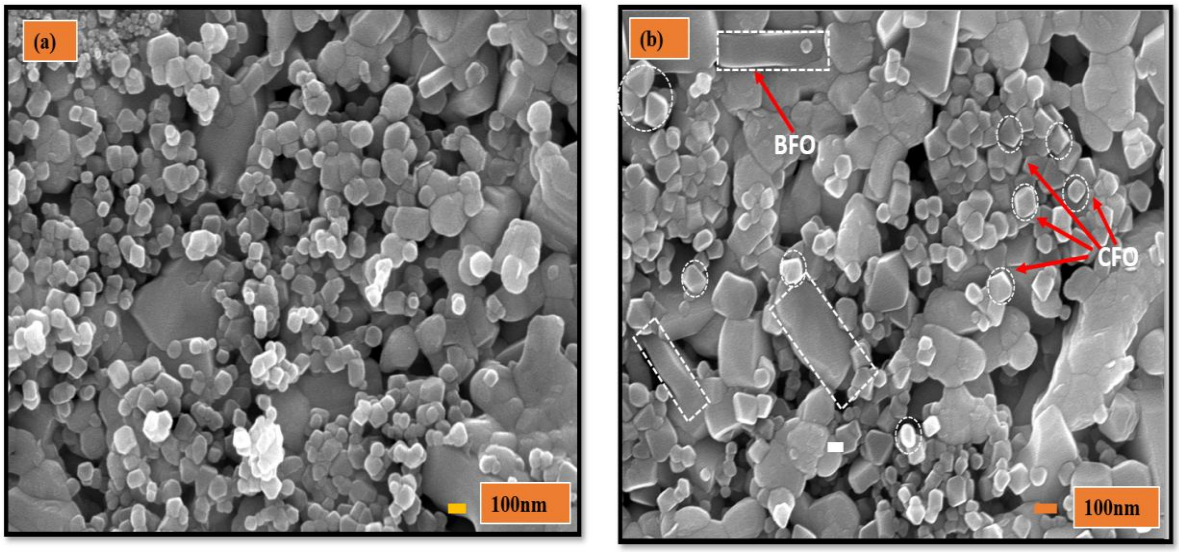

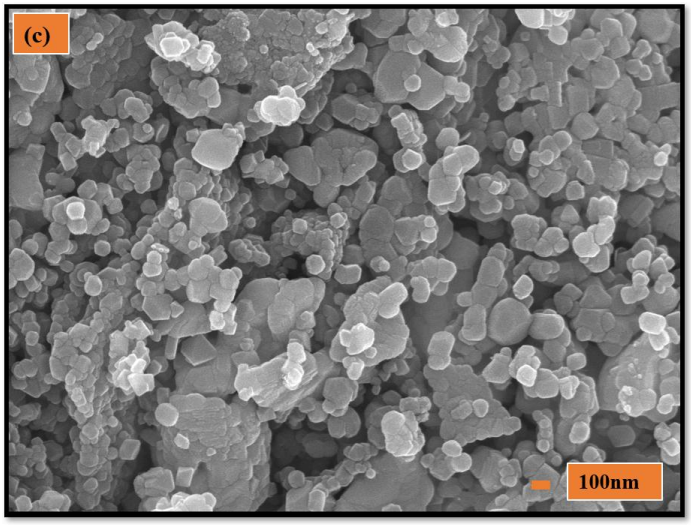

Fig.5.2.2 (a) The magnified "SEM" images of composite samples for X = 10%, (b) The SEM images for X = 30%, (c) The SEM images for X = 50%.

In the Fig.5.2.2 (a, b, c) the magnified SEM images of the post-annealed composite sample corresponding to x = 10%, 30%, and 50% are shown. The grain size of BFO and CFO is found to be around 400 nm and 80 nm respectively with the help of Image J software (not shown here) with rod-shaped structure belonging to BFO [144]. It is observed that the system consists of mostly cubic dense particles with uneven sizes where some particles exist independently and some get amalgamated. In Fig.5.2.2 (b) observed for x=30% some phases are relevant for the specific phases of BFO and CFO are shown which are not clearly visible at x=50%. Also, on introducing filler, we observe increase in clustering with additional phases caused by the bigger surface area of cobalt ferrite. Also it can be associated and chemical reaction or inter-diffusion between the two phases makes a good agreement with the obtained XRD results. The formation of different Phases is mainly attributed to the competition between crystal nucleation and growth [143]. Fig.5.2.2 (a) and (b) show a rod-shaped structure connected to $Bi_2Fe_4O_9$ that is identical to the report and in good accord with the XRD data we collected [144]. The morphological alterations seen in the composites' XRD pictures and phase transformation for those composites are consistent.

5.2.4 Elemental analysis

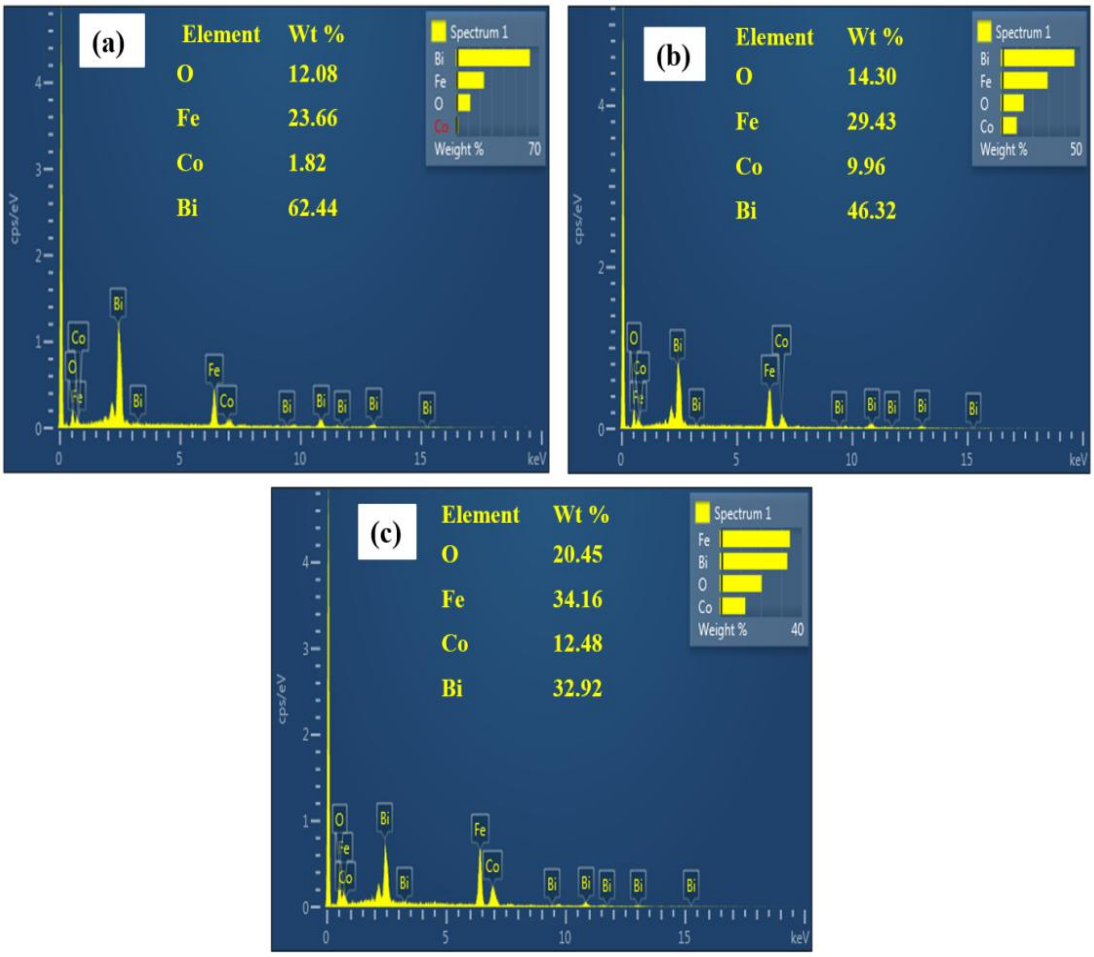

Fig.5.2.3 The Energy dispersive X-ray spectra with atomic weight percentage for composite samples (a) X = 10%, (b) X = 30%, (c) X = 50%.

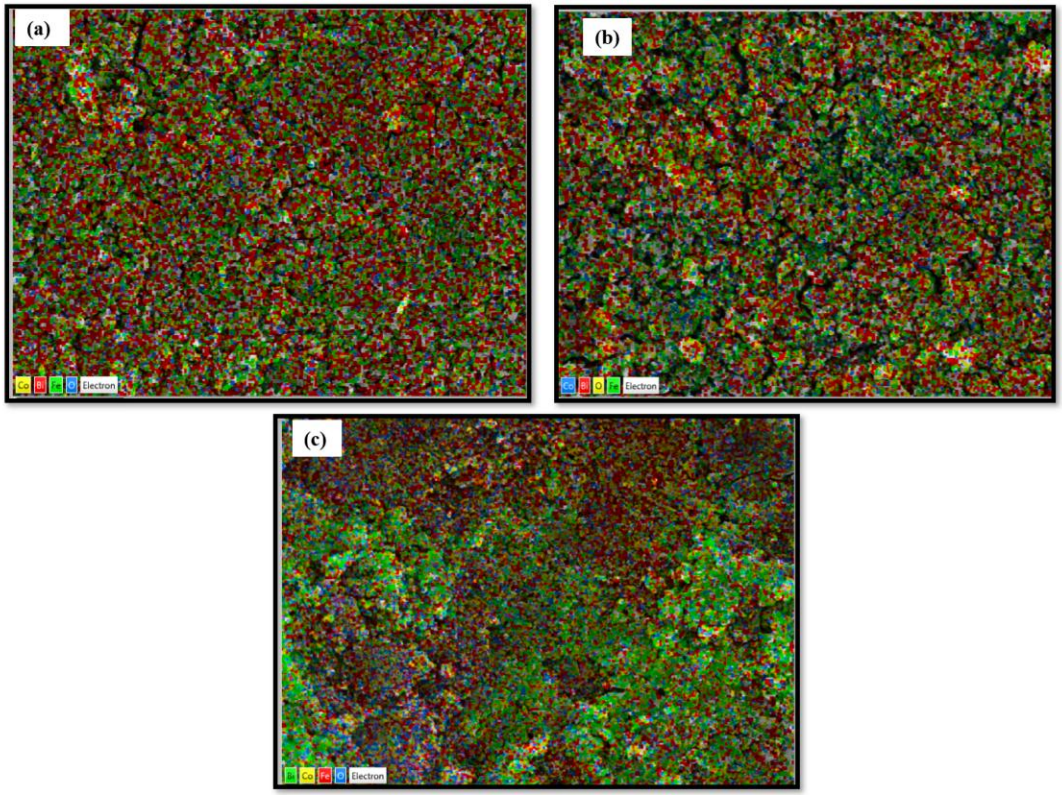

Fig.5.2.4 (a) The Energy dispersive X-ray mapping for composite samples X = 10%, (b) X = 30%, (c) X = 50%.

Fig.5.2.3 (a-c) illustrates the EDX analysis showing the occurrence of the host and the filler elements incorporated in samples. The varying atomic percentage corresponding to the samples is evidence of experimental stoichiometric composition. No additional impurity is detected in the EDX spectra. The elemental distribution throughout the composite samples and the corresponding mapping is shown in Fig.5.2.4. It is detected that at a lower percentage (x=10%) the dispersal of Bi and Fe is prominent with the presence of Co very limited, however for (x=30%) the Co distribution from $CoFe_2O_4$ seems to form a percolating cluster that spans the entire sample.

5.2.5 Zeta potential

The composite system is dissolved in distilled water and subjected to ultrasonication for 15 minutes resulting in a colloidal solution. Zeta potential is carried out for a composed sample for the determination of the surface charge of particles in a colloidal solution. The surface of a charged particle will attract a small layer of the opposing charge and securely attach it to create the Stern layer, a liquid layer. An electrical double layer will arise because of the particle's interaction with an outer diffuse layer of loosely linked ions when it diffuses in solution. Charged particles moving across the sample solution towards

the electrode along with applied electric field are counted and used to calculate the double layer's electrical potential. The Zeta potential (mv) for x = (10%, 30%, 50%) is 23.8, 24.9, 18.9 respectively. Zeta potential is an important tool for comprehending how particles interact with surfaces. The zeta potential of nanoparticles, for instance, is essential in defining how they interact with biological tissues and cells in the field of biomaterials. Additionally, it has an impact on how molecules adsorb onto surfaces, which has ramifications for industries like chemical catalysis and wastewater treatment. By examining the zeta potential of surfaces and particles, scientists may learn more about the interactions between these systems and create plans to control those interactions for a range of purposes. The zeta potential ranging from +30to -30 mv indicate good dispersion stability. The observed values are lowered below 30 mv with an increase in weight percentage indicating good stability which ensures that repulsive forces of particles are strong enough to maintain stability of dispersion. The colloidal solution of such material exhibiting magnetic and electronic properties has potential application in biomedical science[175].

5.2.6 Electrical Characterization

5.2.6.1 DC resistivity

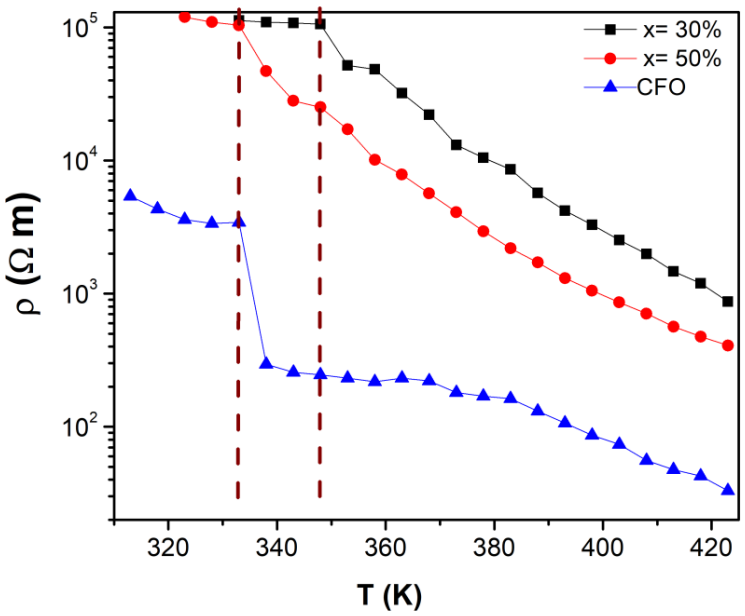

Fig.5.2.5 The transition in Resistivity of composite samples X = 30%, (b) X = 50%, (c) cobalt ferrite as a function of temperature.

Temperature-dependent resistivity of as prepared CFO and composite system for x = 30% and 50% is shown in the semi-log plot of Fig.5.2.5. From the plot, it is found that the resistivity of CFO (Blue legend) exhibits a sharp jump at ~ 332 K but saturates to ~ 6×10^3 Ω m at 320 K. The staircase type resistivity implies the presence of two different Arrhenius type conductivity at two separate temperature (T) regime. The one for T < 332K shows weaker slope and the other one for T > 332K shows strong temperature dependence with higher slope. Moreover, CFO being a semiconducting material shows reduction in resistivity with rise in temperature which also approves the presence of thermally activated charge carriers (Fe^{2+} and Co^{2+}) with enhanced mobility, which leads to a greater electron transfer from one ion to another [176].

The resistivity of BFO is found to be much higher than the compliance value of our source meter. For the composite system with filler x = 30 and 50%, the resistivity has increased to around 10^5 Ω m at 320 K and decreases linearly beyond 348 K with temperature. The large value of resistivity in the composites around 330 K is mainly due to the scattering of charge carriers at the boundary between conducting CFO and insulating BFO. Moreover, it is also found that with the increase in filler concentration (x), decline in resistivity is observed above 348 K, but remains comparable for x=30 and 50% below 332 K. This implies that CFO as conductive filler creates an isolated conducting island in the matrix of BFO where the size of isolated islands is increasing with the increase in x [177].

This behavior is commonly observed in percolative composite systems where the resistivity of the composites is mainly explained by the percolation phenomenon. Below x =30%, the resistivity of the composite was high enough to be detected by our measuring meters, thus indicating non-conducting behavior at low filler fractions. This indicates that x= 30% may be the critical weight fraction at which the classical percolation threshold exists. Above this, there is a growing infinite percolating cluster where the conduction is mainly governed by infinite clusters of CFO nanoparticles. This type of electrical transition is well understood by the percolation phenomenon where the geometrical phase transition between conducting CFO and insulating BFO helps to develop a conducting channel or cluster which spans the entire system. To investigate further on this conducting behavior, ac behavior is studied on these composite systems.

5.2.6.2 Impedance analysis

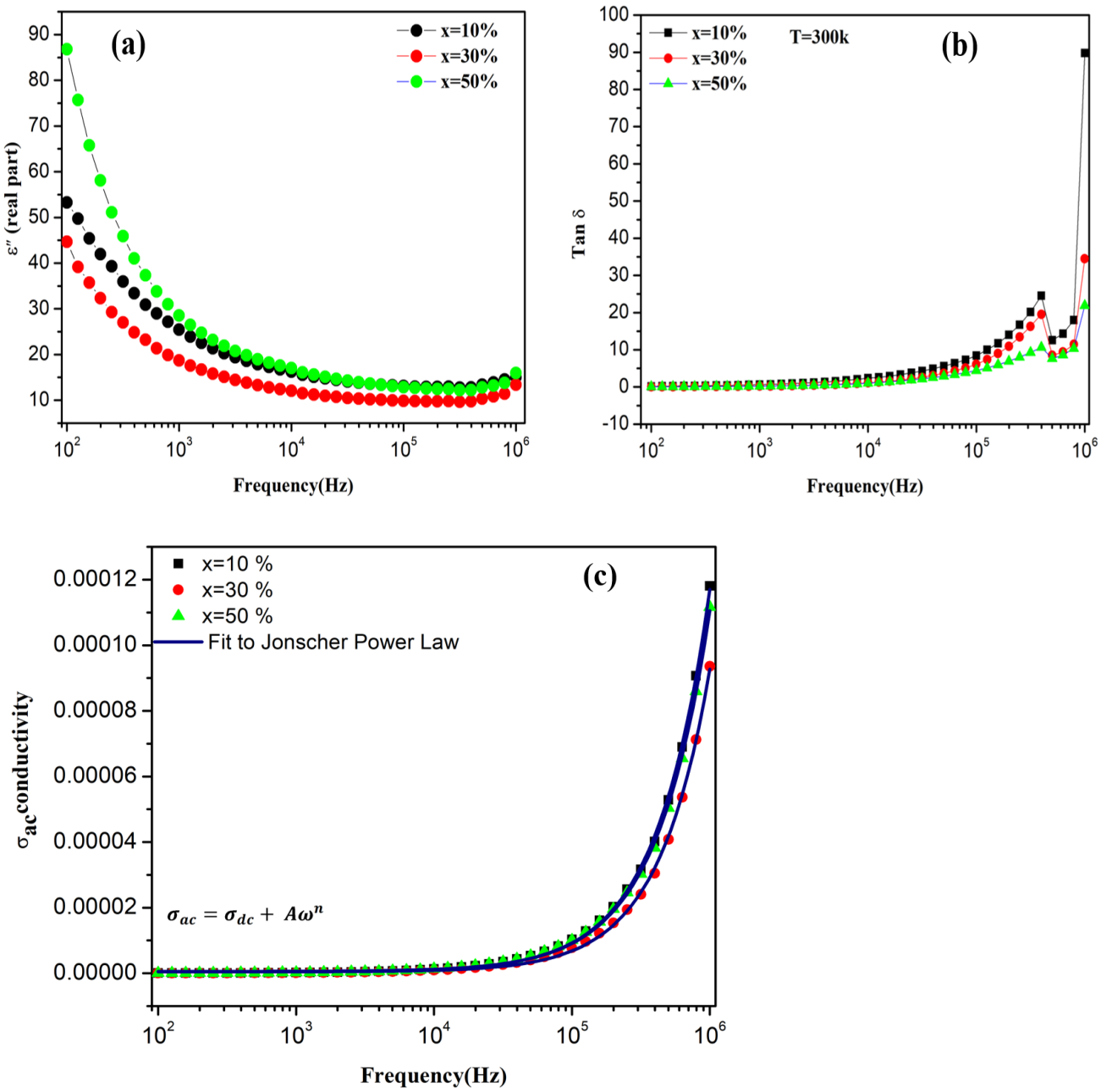

Fig.5.2.6 The (a) ε" (real part of permittivity) as a function frequency, (b), dielectric loss as a function of Frequency (c) AC conductivity as a function of frequency for composite samples (a) X = 10%, (b) X = 30%, (c) X = 50%.

The composite systems in the pellet form are subjected to alternating currents in order to analyze the ac electrical properties. The composites are feeded with input sinusoidal voltage of amplitude 1 V. The complex impedance Z as measured is found in terms of

real and imaginary parts and the ac conductivity has been calculated with the help of the following equations [120].

$$\varepsilon' = \frac{Z''}{\omega c_0 Z^2} \qquad (3)$$

$$tan\delta = \frac{\varepsilon''}{\varepsilon'} \qquad (5)$$

$$\sigma_{ac} = \varepsilon''\omega c_0 \qquad (7)$$

Fig.5.2.6 displays the real part of the electrical permittivity (ε') of the material at room temperature with variable frequency which is related to the dielectric constant that helps the charge to build up in a system. A material's capacity to polarize in answer to the applied field is also referred by its real part of permittivity.

In Fig.5.2.6 it is noticed that the permittivity (real part) follows a strong frequency-dependent performance at a low-frequency regime and becomes independent to high frequency. At low frequencies, the permittivity is mostly affected by the dc conductivity of the charge carriers which exhibits Maxwell-Wagner effect at the contact region between the conducting electrode and the sample, leading to faster drop. Whereas at the high-frequency regime, the electric dipole relaxation time increases as compared to the period of the input ac voltage, leading to a slower reduction of dielectric constant [36],[103], [178]. Real part of permittivity attains a value of around 90 and 45 at 100 Hz for x = 50 and 30% respectively. Among the composites with x = 10, 30 and 50%, the real part of permittivity is found to be weaker for x=30% which is mainly due to the maximum screening of polarized BFO by conducting CFO nanoparticles at this concentration. For x = 50%, clustering of CFO nanoparticles leads to large conducting islands separated by BFO grains. As a result, it yields high value of dielectric constant at low frequency which is a consequence of charge accumulation at grain boundaries.

Fig.5.2.6 shows frequency-dependent dielectric loss which directly represents the extent of leakage current or unused energy. The loss remains relatively low till 10^4 Hz above which it increases, indicating the composites will be efficient for high-frequency applications. Moreover, the relaxation peak for all the composite systems appears at the same frequency, indicating the same charge dynamics among the systems [153]. The dielectric material at high frequency may not be able to respond quickly enough to the rapidly changing electric field thus resulting in the lag of polarization causing energy loss in the form of dielectric loss. Around 1 MHz, the dielectric loss shoots up which is due to the dipolar relaxation and physical displacement of charge carriers within the

composite system. As a result, it is concluded that in our composite system, the difference in dielectric constant is mainly due to the onset of the percolating cluster, above which a large magnitude of dielectric permittivity is observed.

AC conductivity is one of the key properties which is driven by the types of charge carriers and its frequency response that rule the conduction process, such as electrons and holes or cations and anions [159]. From equation 7, the relationships between σ_{ac} conductivity and frequency are plotted in Fig.5.2.6 (c) The flat plateau in the conductivity at low frequency mainly signifies space-charge effect which leads to huge drop in voltage and decrease of electric field in the bulk. This space-charge in turn can build large electrical polarization that led to enhancement of dielectric permittivity at low frequency. As frequency increases, the conductivity tends to rise at high frequency with a steep slope, following a power law behavior with frequency. Moreover, the lagging in ac conductivity as found from the plot for x =30% is mainly due to formation of finite clusters of CFO nanoparticles in matrix of BFO. At this concentration, which is at the vicinity of percolation threshold, allows the charge carrier hopping between percolation clusters but is much affected by the presence of polarized BFO particles where the transition between two different relaxations becomes more significant at high frequency. Whereas above x= 30%, there is a complete formation of infinite percolating cluster and the hopping of carriers is less affected by the polarized matrix.

Since BFO is a perovskite material, the relationship between conductivity and frequency can also be explained on the basis of large and small polaron models[93], [138], [179] In most cases, the frequency dependency follows Josher's power law $\sigma_{ac} = \sigma_{dc} + A\omega^n$ [64] The fitting shown in Fig.5.2.6 (b) is overlaid on the experimental data as per Josher's power law behavior. Here, n (exponent) is the slope that has significance in diverse applications and models which mainly relates to the polarization mechanism that includes a full contribution from the effects of mobile charges. In our case, the value of n (fitting not shown here) is found to vary between $1 < n < 2$ suggesting intermediate disorder in the system which is mainly governed by the percolation phenomenon [180].

The parameters obtained for dc and ac part are listed in Table.8. The difference in the magnitude mainly appears due to the different measuring techniques (four probe and two probe) that were adopted. Also, as the conductivity is co-related to dielectric loss, the direct relationship is observed in the frequency range 10^5 hz where both rises significantly. The imaginary part of the dielectric permittivity also shows an upturn at

the same frequency where ac conductivity rises significantly. However, some other aspects such as morphology, size, and density may influence the conductivity in our system.

Table.8 The calculated ac and dc conductivity part.

Sample	σ_{dc}(Sm^{-1})	σ_{ac}(Sm^{-1})	n
X=10%	5.05219 x 10^{-7}	2.66337 x 10^{-12}	1.12
X= 30 %	4.3338 x 10^{-7}	1.19512 x 10^{-12}	1.16
X=50%	5.45281 x 10^{-7}	3.07018 x 10^{-12}	1.11

5.2.7 Magnetic analysis

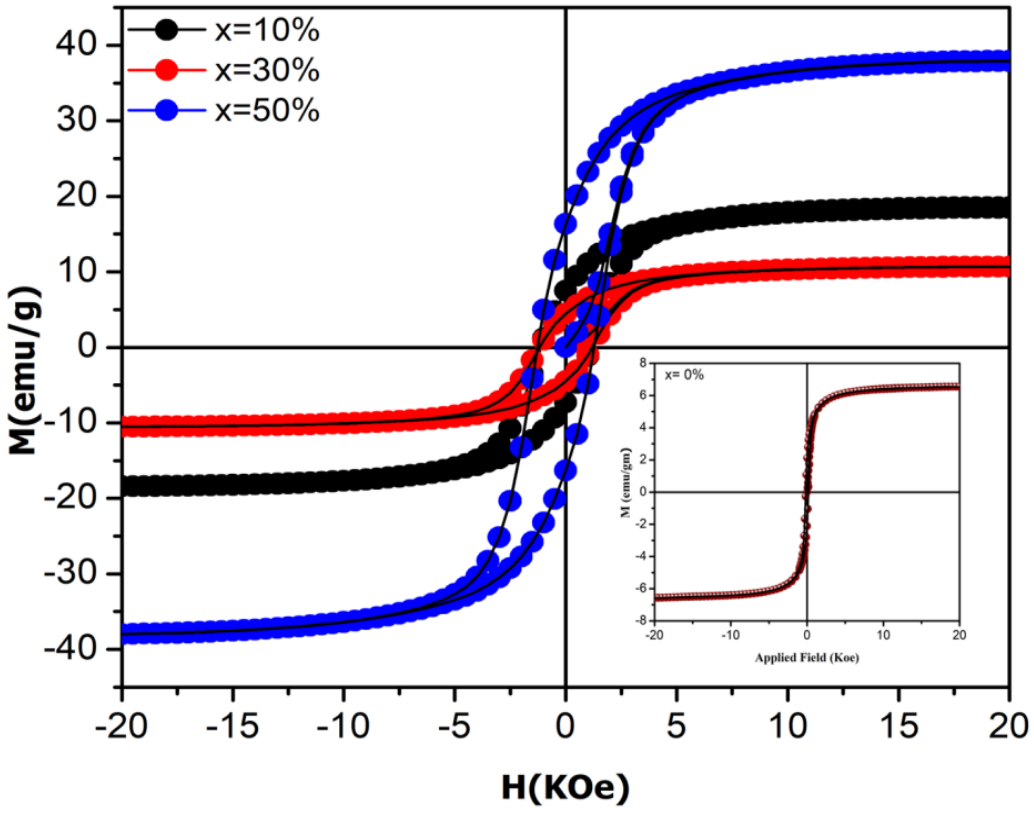

Fig.5.2.7 shows the hysteresis loop for x= 10%, 30%, 50%, inset shows magnetization of as-prepared $BiFeO_3$.

The room temperature magnetic properties are investigated with the help of a Vibrating Sample Magnetometer. The composites are subjected to a magnetic field ranging from -

20 to +20 KOe. Fig.5.2.7 demonstrates that the samples have a well-defined hysteresis loop indicating a hard magnetic nature. The inset of Fig.5.2.7 clearly shows that the as-prepared $BiFeO_3$ has weak magnetic nature as reported in previous studies [24] favoring the antiferromagnetic nature induced by Dzyaloshinskii - Moriya interactions [90]. The various parameters such as retentivity (M_r), saturation (M_s), squareness ratio (M_r/M_s), coercivity (H_c), Bohr magneton (μ_b), and magneto crystalline anisotropy (H_a) are obtained from VSM data as listed in Fig.5.2.8.

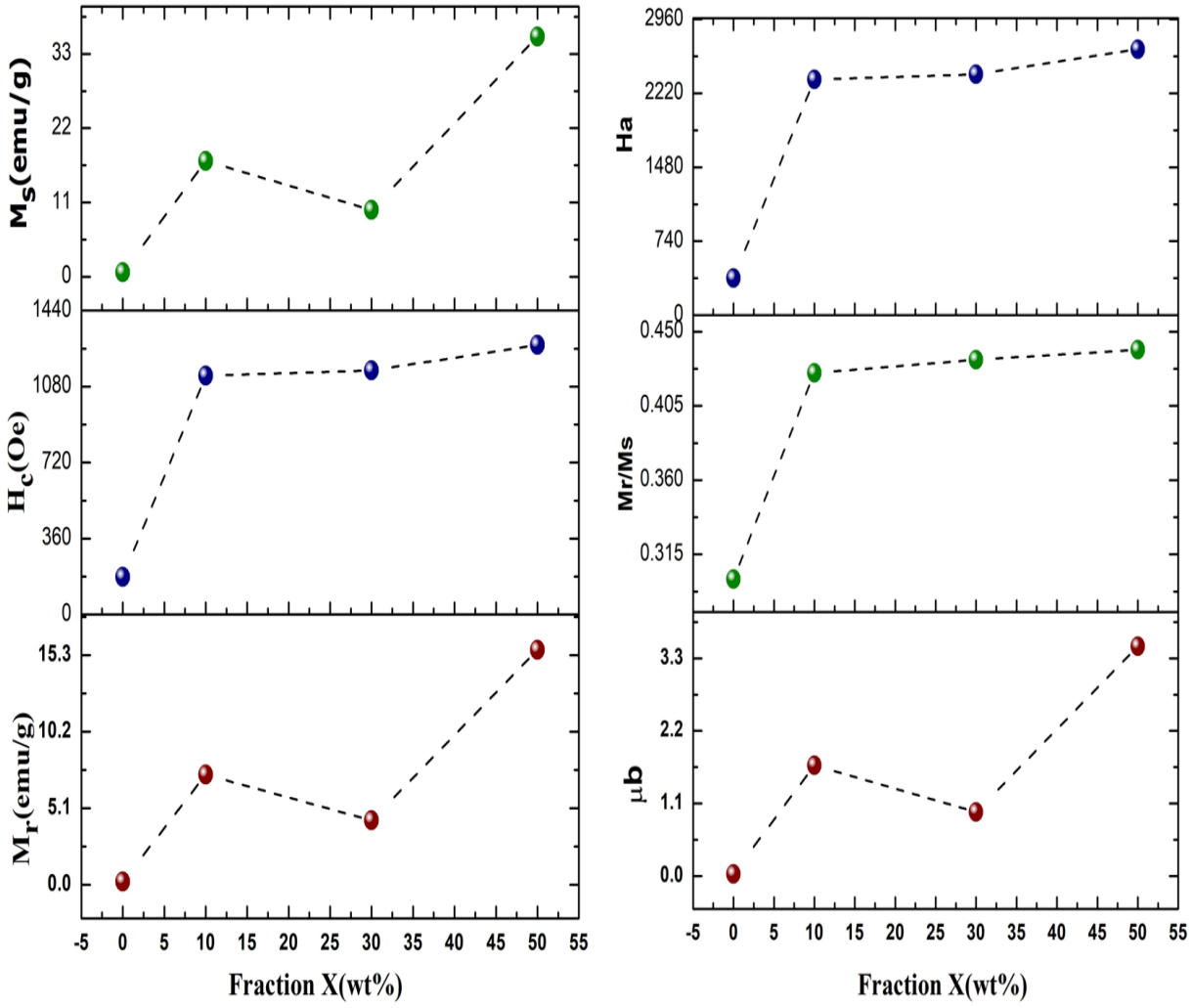

Fig.5.2.8 The magnetic parameters such as retentivity (M_r), saturation (M_s), ssquareness ratio (M_r/M_s), ccoercivity (H_c), Bohr magneton (μ_b), and magneto crystalline anisotropy (H_a) as a function of weight fraction.

As cobalt ferrite is a ferromagnetic material and bismuth ferrite is antiferromagnetic, it implies that the incorporation of magnetic CFO is expected to advance the magnetic

properties in the composite system. However, it is found that the saturation and remanent magnetization is reduced for x = 30%. This anomaly may be due to the bifacial alignment of the magnetic domains, indicating mutual interparticle interaction among BFO and CFO nanoparticles is maximum at critical weight fraction x= 30% also reported in previous studies [171], [181]. Also, the squareness ratio as found suggests that all samples have a random orientation of domains [150] thus reducing M_r and M_s in this case. For x=50% the addition of magnetic fillers favors the increment in magnetic response in the composite system. However, the H_c keeps on increasing with the fill percentage in the samples which indicates the dependence of Hc on the composite. The sample qualified in the category of Hard magnetic material as it shows a high rate of coercivity in contrast to $BiFeO_3$ only This behavior might find potential application in magnetic devices working at room temperature [182].

5 .2.8 Optical bandgap

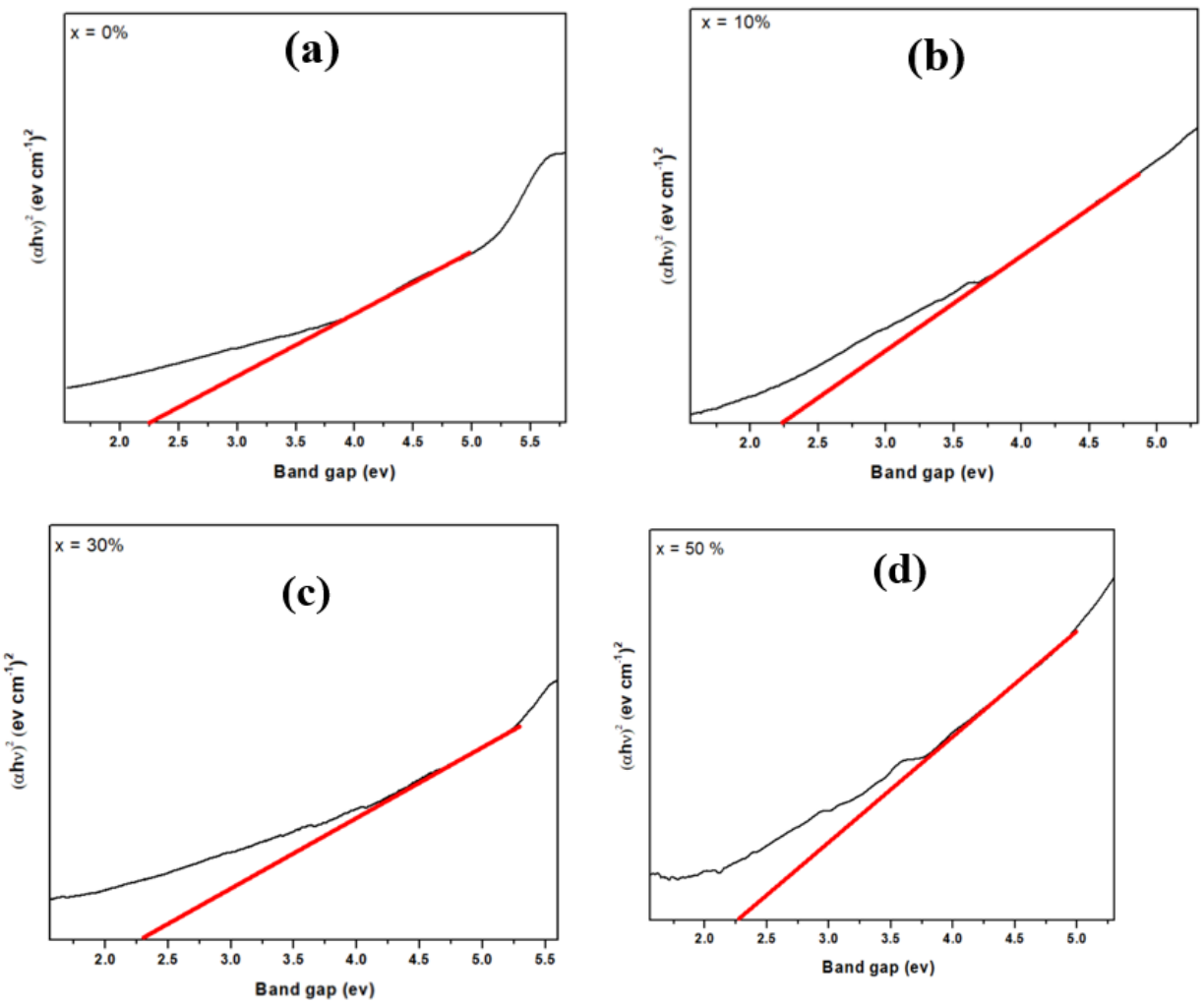

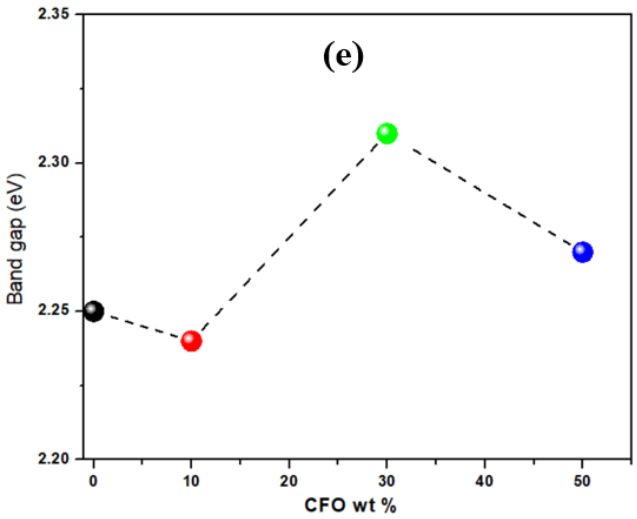

Fig.5.2.9 Band gap calculation for samples (a) X= 0%, (b) X= 10%, (c) X= 30%, (d) X= 50%., (e) Band gap as a function of weight percentage.

The samples are exposed to absorption and transmission spectra over the wavelength ranges of 200–800 nm to examine the photoelectric response. The band gap is calculated using the Tauc plot method since the band gap and optical transmittance characteristics are correlated. Eq. 4 is used to calculate the band gap [183].

$$\alpha h\nu = B(h\nu - E_g) \quad (8)$$

Where B is aporportionality constant, E_g refers to bandgap, hν is the photon energy, and α is the provided absorption coefficient. From Fig.5.2.9 (a-d), the estimated values for the composite system x= (0%, 10%, 30%, and 50%) are 2.25 eV, 2.23eV, 2.32eV, and 2.27 eV, respectively. From Fig.5.2.9 (e) the observed values indicate that at a lower weight percentage, the composite system exhibits a good optical response. The increment in band gap at x = 30% is due to interaction between CFO and BFO as observed in structural and electronic analysis. These results suggest that these composite systems exhibit good optoelectronic properties and may find their practical application in photovoltaics.

5.2.9 Ferroelectric Analysis

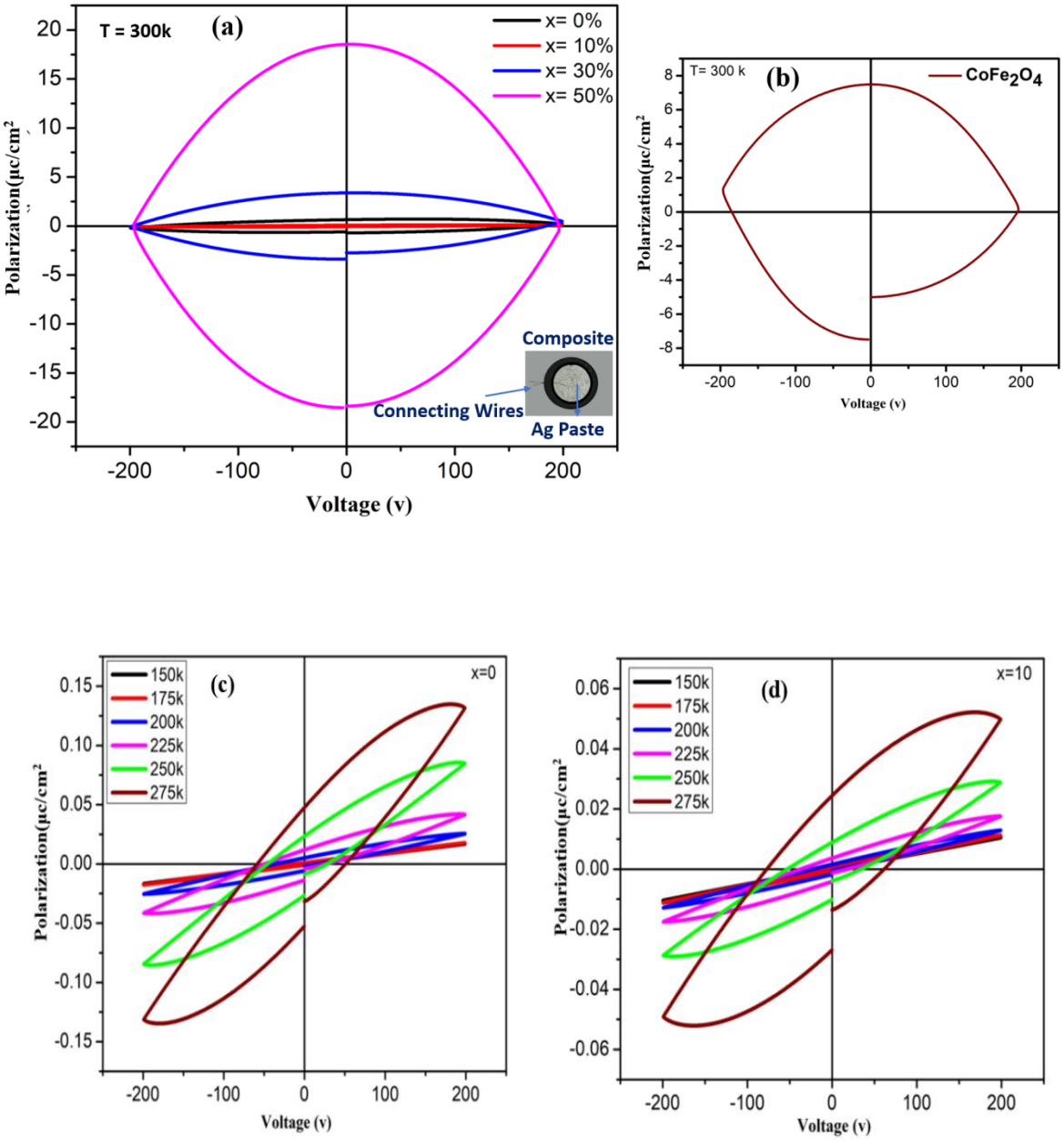

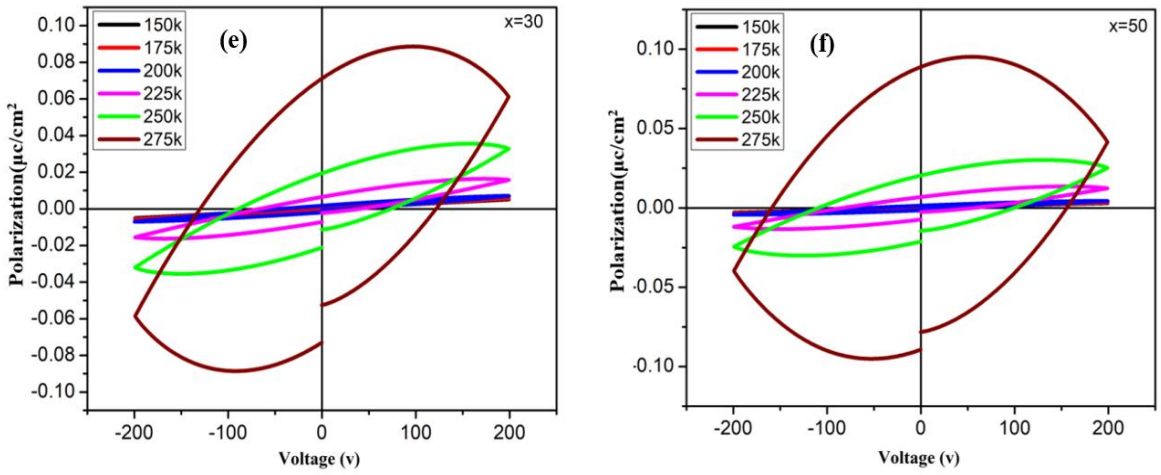

Fig.5.2.10 P-E loop at room temperature for Sample(a) BFO (b) CFO, P-E loop with varying temperature for Sample (c) X= 0%, (d) X= 10%, (e) X= 30%, (f) X= 50%.

In the Fig.5.2.10 (a), (b) it shows the ferroelectric study of the composite systems where voltage-dependent polarization is analyzed at room temperature. As bismuth ferrite is an intrinsic multiferroic compound, it has simultaneous magnetic and electric ordering at 300 K[184]. For x = 0% ($BiFeO_3$), the shape of the loop represents that of the lossy capacitor, indicating low leakage current whereas with the increase of CFO filler, the shape of the polarization loop changes from oblate to spheroid because of the depolarization effect. Due to the capture of charge carriers in the composites, they tend to depolarize with input voltage at normal temperature. This implies that at x = 50%, the presence of a considerable amount of leakage current converts the composite system into an ideal resistor as found in the Fig.5.2.10 (b). The inset shows the fabrication of a pellet with silver electrodes and conducting wires for experimental measurements.

Fig.5.2.10 (b) shows an asymmetric loop with a huge leakage current in cobalt ferrite at room temperature. The large magnitude of polarization and its related asymmetry arises mainly due to the presence of conducting charges of certain polarity whose polarization response differs when voltage is swiped from positive to negative polarity. It is observed that the merging of filler increases the loop area, thus, increasing the charge leakage in composite samples. Fig. 7 (c, d, e, f) shows polarization variation along with the voltage with a range of 200 V and frequency 10 Hz at different low temperatures corresponding to composites x = (0, 10, 30, 50) respectively. As the temperature is lowered below 300 K for any value of x, it is observed that it affects the ferroelectric properties to a greater

extent by affecting the loop parameters resulting in a well-defined loop at such temperatures. It is also noticed that on lowering the temperature, the leakage current decreases. At 275 K, the polarization is found to be maximum (0.13 μc/cm^2) for x = 0% which reduces to 0.05 μc/cm^2 for x = 10%. The reduction in the magnitude of polarization is attributed to the screening of electric dipoles by conducting CFO nanoparticles. For x = 30 and 50%, the polarization attains a convex shape which implies the formation of percolating clusters by trapped charges in the composites.

Moreover, for temperatures below 275 K, the magnitude of polarization further shrinks down that is mainly due to the freezing of charge carriers leading to enlarged relaxation time. For all the composite systems till 250 k, a similar tendency is seen, below which the moment of dipoles is constrained, making the paralytic kind of behaviour more prevalent and causing the hysteresis loop to slim. The temperature-dependent variation of saturation polarization is observed for all the composite systems. The thermally activated behavior of dipoles followed by an exponential increase is observed. The observed PE loop shows a monotonous increase in electrical coercivity with temperature for the composite systems [185]. A kink is observed at x = 30% at 250 K and 275 K which is more prominent for 275 K. The magnitude of saturation polarization as a function of varying weight percentages at temperatures 250 K shows that polarization for x= 10% is 0.049 μc/cm^2 and for x=30% is observed as 0.061 μc/cm^2 and at 275 K for x= 10% is 0.028 μc/cm^2 and for x=30% is observed as 0.030 μc/cm^2, beyond which the polarization decreases. This further confirms that the incorporation of CFO can affect the properties of BFO, thus making the composite system suitable for versatile applications.

Conclusions

In this work, bismuth ferrite and cobalt ferrite are prepared using the sol-gel method followed by fabricating composite systems with varying wt% of CFO nanoparticles. Bismuth ferrite with R3C structure and cobalt Ferrite with cubic phase is confirmed by X-ray diffraction along with some impurity peaks of $Bi_2Fe_4O_9$. SEM images confirm the presence of a percolating cluster at x = 30%. The stability of the composite-based solution is found more stable at a low percentage as compared to x=50%. The complex impedance spectroscopy confirms the presence of the screening effect at x=30% which makes the dielectric constant weaker on varying frequencies. The dielectric loss is found to remain low for all the composites till 10^4 Hz, thus making it a promising energy storage material.

The VSM analysis reveals that the addition of a magnetic CFO increases the overall magnetization non-monotonically with maximum M_r = 35.57(emu/gm) and H_c= 1277 Oe. The ferroelectric loop investigation shows that the ferroelectric properties are changed with the addition of cobalt ferrite nanoparticles. Beyond x=30%, the composite system changes from a lossy capacitor to an ideal resistor, indicating the formation of a conducting percolating cluster that spans the composite system. The multiferroic characteristics of this interacting composite as found at ambient condition indicates tremendous promise for the advances in magnetic memory devices and electronic sensor devices.

5.3 Substitutional effect of Ba doping on the properties $BiFeO_3$.

5.3.1 Introduction

Bismuth Ferrite is a multiferroic material which is known to have different ferroic properties in a single-phase[186] and have a distorted perovskite structure [2] .In contrast to other multiferroic bismuth ferrite one of the interesting candidate for multifunctional devices due to magnetoelectric coupling at room temperature and narrow band gap[1], [10], [164]. The effect of phase purity, shape and size is found to have influence on electronic properties of bismuth ferrite. The previous study suggest that sol-gel method is effective and cost-efficient way to achieve material with desirable properties [116], [117], [119], [187], [188]. Despite of that multiferroic having strong electronic and magnetic is a significant challenge, multiple investigation shows that substitution of dopant can overcome this obstacle [3], [189]. The various investigation by researchers is evident that substitution at A and B site in multiferroics is beneficial in achieving desired material properties [190]. The addition of dopant can affect several factors like such as structural deformation, vacancies, and particle size. These factors play a vital role in deciding materials overall characteristics [138], [191]. The reported work shows the synthesis of Ba doped Bismuth ferrite using sol gel method and how doping can influence the structural, magnetic, and dielectric properties at room temperature. The modified multiferroic material can be utilised for various device application.

5.3.2 Characterization

The synthesized nanoparticles are investigated for structural analysis with the help of X-ray diffraction. The morphological examination along with estimated particle size of the prepared samples is intended by Field electron Microscope (FE-SEM). To investigate the magnetization of the materials at room temperature the Vibrating sample magnetometry (VSM) is used. The materials have undergone a magnetic field ranging from -20000 to +20000 oe. The electronic properties are investigated using METROHM and the FRA32M-Impedance analyzer ranging from 1000 Hz to 1MHz.

5.3.3 XRD analysis

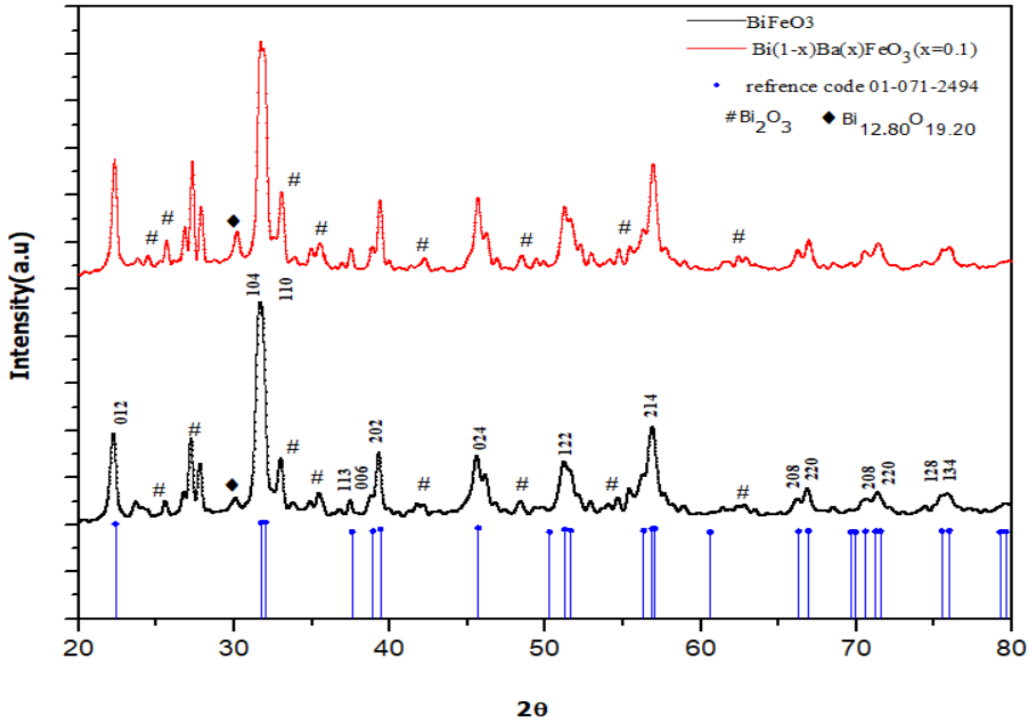

Fig.5.3.1. Xrd pattern of $Bi_{(1-x)}Ba_{(x)}FeO_3$ with x = 0, 0.1

The Fig. 5.3.1 displays obtained diffraction pattern of the prepared samples. The observed diffraction pattern indicates strong reflection of rhombohedral hexagonal structure peaks belonging to the R3C group (ICSD-01-071-2494). However, some impurity phases of bismuth oxide correspond to (ICSD-00-027-0053), and (ICSD-01-077-0868) were also observed in the samples. The development of these secondary phases is due to the metastable, low decomposition temperature, off-stoichiometric which cause the evaporation of Bi_2O_3 [192].

The estimation of crystalize size is done via using the Scherrer formula [193].

$$D = \frac{k\lambda}{\beta \cos\theta} \qquad (1)$$

The lattice parameter was calculated based on structural parameter using equation [138]

$$\frac{1}{d} = \frac{4}{3}\left(\frac{h^2+kh+k^2}{a^2}\right) + \frac{l^2}{c^2} \quad (6)$$

The obtained lattice parameter along with the estimated crystallite size are listed in Table.9. The greater ionic radii of dopant have significantly influenced the lattice parameters resulting in reduced crystallite size

Table.9 shows the calculated lattice parameters and crystallite size.

Sample	a	b	c	Crystallite size (nm)
X=0	5.582	5.582	13.886	38.048
X=0.1	5.604	5.604	13.9828	21.593

5.3.4 Surface morphology

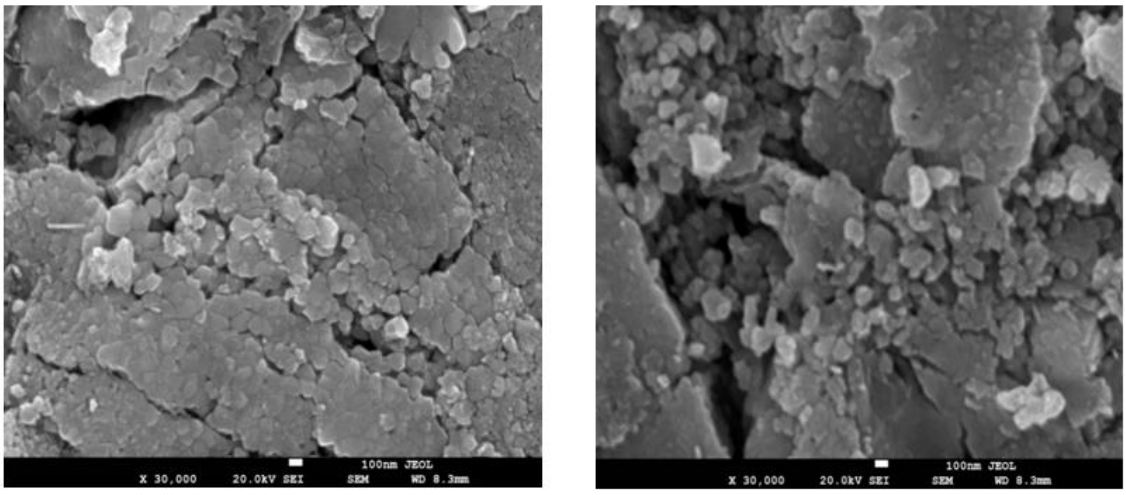

(a) (b)

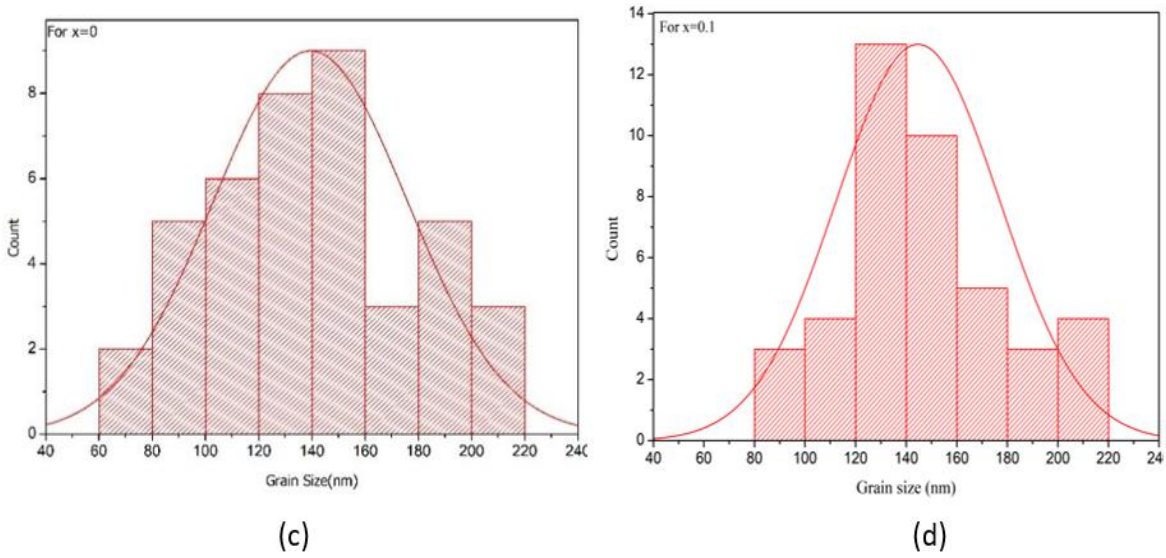

Fig.5.3.2 The SEM images of (a) $Bi_{(1-x)}Ba_{(x)}FeO_3$ with x = 0, (b) $Bi_{(1-x)}Ba_{(x)}FeO_3$ with 0.1 a (c) distribution of grain size for $Bi_{(1-x)}Ba_{(x)}FeO_3$ with x = 0 (d) distribution of grain size for $Bi_{(1-x)}Ba_{(x)}FeO_3$ with x = 0.1.

The nanoparticles are analysed for the morphological study Fig.5.3.2(a, b) shows the FESEM images of $Bi_{(1-x)}Ba_{(x)}FeO_3$ with x = 0, 0.1 at 30000X magnification. We employed these SEM images to analyse the distribution of grain sizes across the samples as shown in Fig5.3.2 (c, d). Interestingly, the introduction of barium (Ba) dopant resulted in an observable growth in grain size compared to the undoped sample. As both samples were synthesized under identical processing conditions, this variation in size of grain can be directly ascribed to the presence of Ba dopant [191], [194], [195]. This morphological analysis provides valuable insights into the impact of Ba substitution on the microstructure of the material, particularly with regards to grain size. To further understand the effect of dopant on the prepared samples are investigated for magnetic and electronic characteristics.

5.3.5 Magnetic Properties

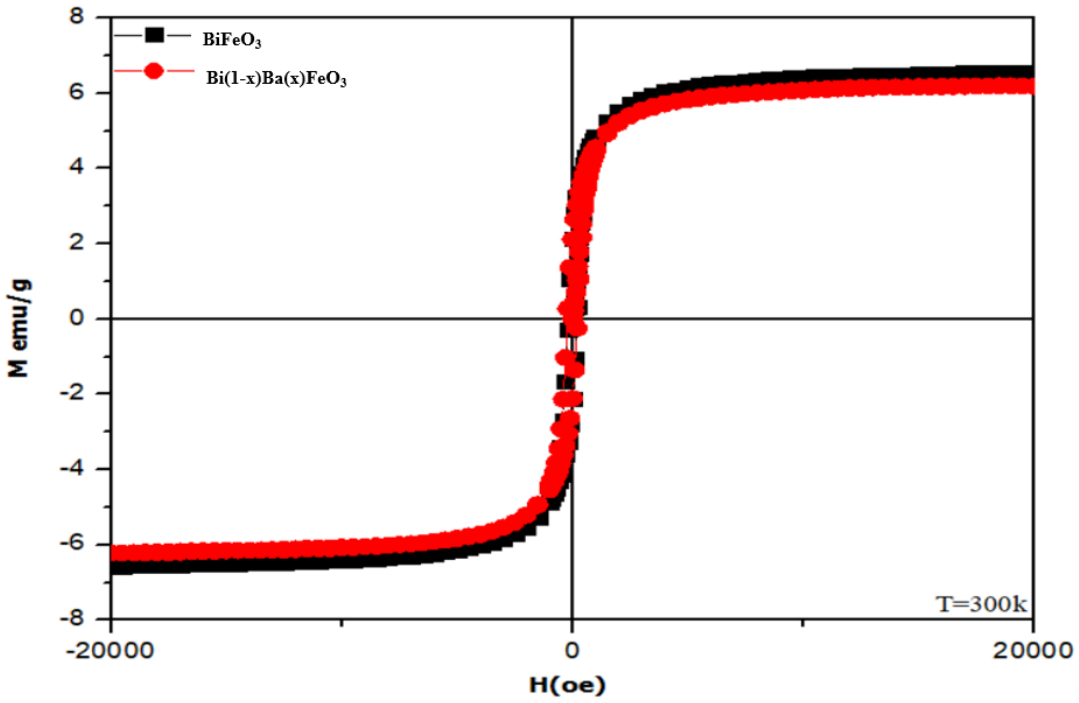

Fig.5.3.3 The room temperature magnetism of $Bi_{(1-x)}Ba_{(x)}FeO_3$ with x = 0, 0.1

Fig.5.3.3 shows the hysteresis loop $Bi_{(1-x)}Ba_{(x)}FeO_3$ with x = 0, 0.1 at room temperature with magnetic fields ranges from -2 tesla to 2 tesla. The observed magnetic hysteresis is found to be very thin loop indicating weak magnetic response by the material. The magnified view of loop shown in Fig.5.3.4 (a,b) is used to obtain magnetic parameters which are listed in Table.10. While bismuth oxide impurities are not magnetic, the observed net magnetization can be attributed solely to the bismuth ferrite phase [142]. The abrupt change in magnetization, potentially due to variations in Fe^{+2} and oxygen valency's distribution within the material. So, it can be said that the exchange interaction between Bi and Ba cations and grain size effect observed in morphological analysis it increases the net magnetization [52].

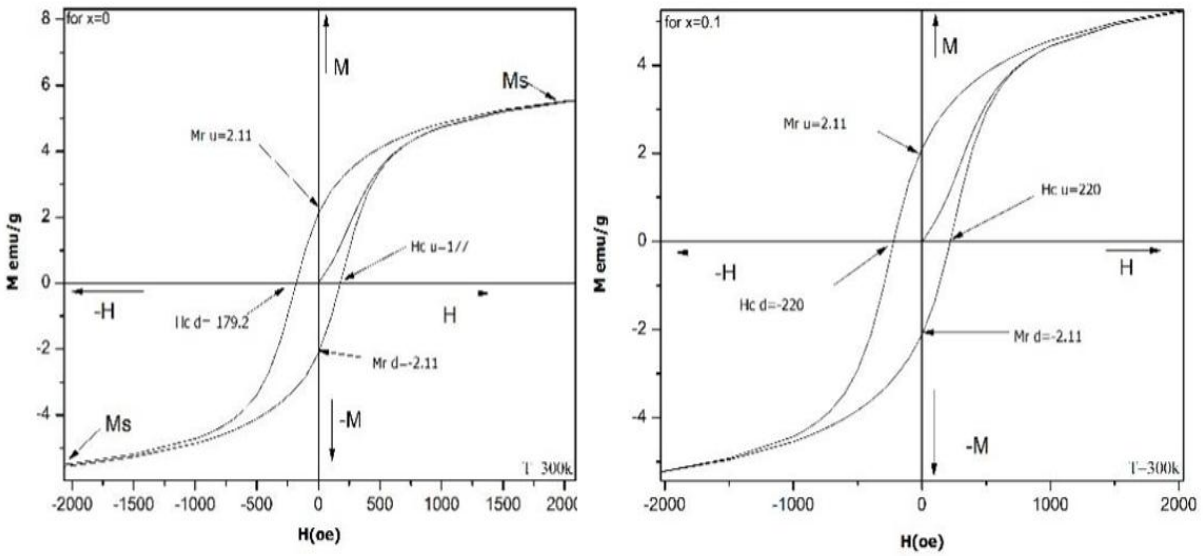

Fig.5.3.4 (a, b) shows the enlarged view of the hysteresis loop.

Table.10 shows obtained magnetic parameters.

Sample (x)	M s (Emu/g)	M r (emu/g)	H c (Oe)
0.0	6.55	2.11	178.23
0.1	6.20	2.11	220.182

5.3.6 Dielectric analysis

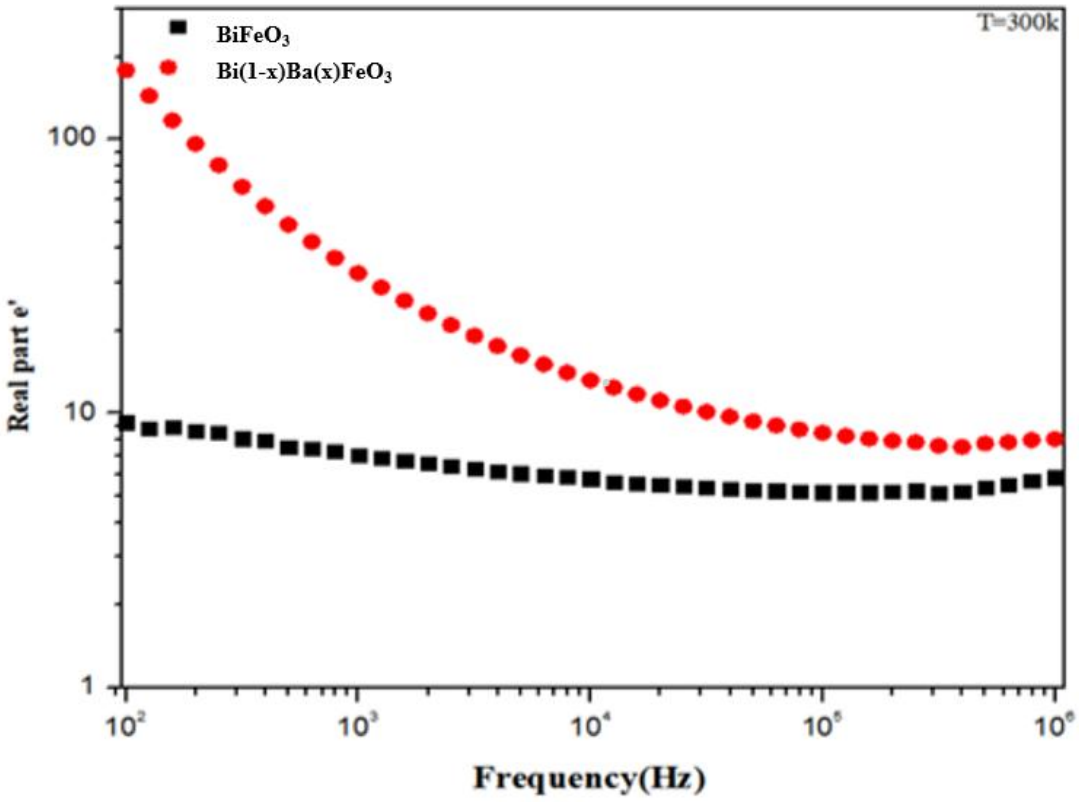

Fig.5.3.5 shows the real part of permittivity for the samples $Bi_{(1-x)}Ba_{(x)}FeO_3$ with x =0, 0.1.

The nanoparticles are then subjected to sinusoidal voltage. The dielectric parameters such as dielectric constant (ε′), dielectric loss (tan δ) is calculated with the help of impedance measurement Z (complex impedance) consists of Z′, Z′′ i.e., real, and imaginary part [120]. Fig.5.3.5 shows the calculated dielectric constant. In this type of material, the dielectric constant shows a decline at higher frequencies due Maxwell-Wagner relaxation process[120], [152]. Interestingly, the dielectric constant of the undoped sample remains relatively unchanged across the frequency range. However, the Ba-substituted sample exhibits consistently higher dielectric constant values. This difference in behaviour at low frequencies is attributed to the presence of phase impurities and variations in oxygen valency within the Ba-doped material.

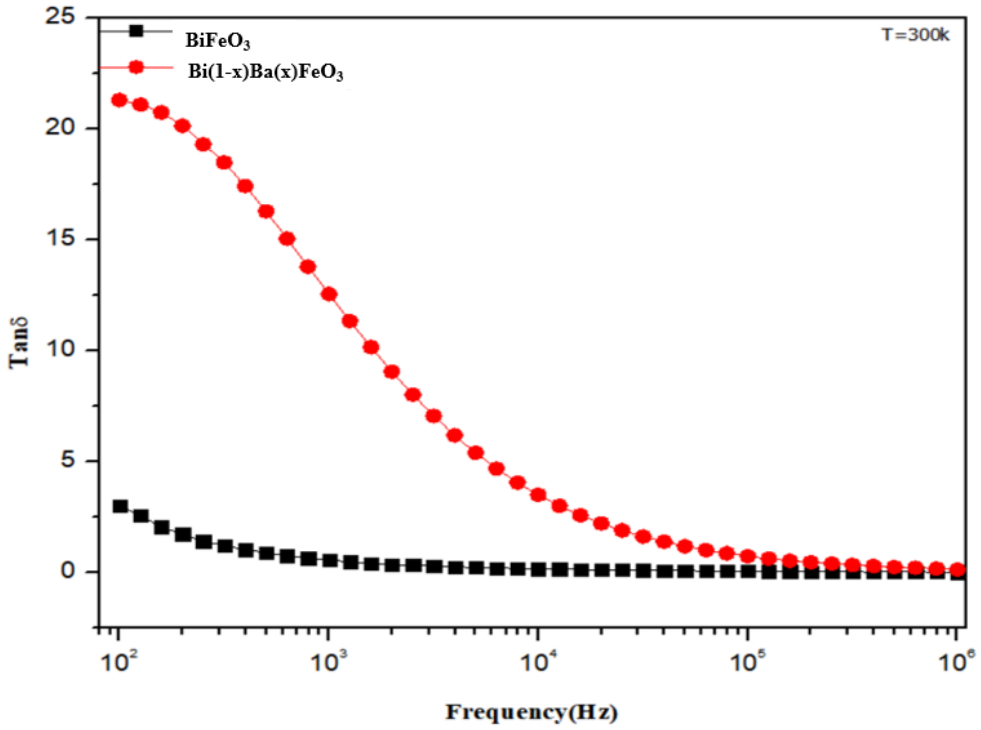

Fig.5.3.6 shows the dielectric loss for the samples $Bi_{(1-x)}Ba_{(x)}FeO_3$ with x =0, 0.1.

The energy loss for observed samples is illustrated in Fig.5.3.6. The observation indicate that Ba substitution has led to increase the dielectric losses. The dielectric losses were found sensitive to numerous factors such as stoichiometry, annealing temperature, geometric arrangement, and composition [196]. On addition grains, defects, and impurities can also results in high resistance at the grain boundaries[126]. The observed samples exhibit irregular grain size and other phase impurities which is also confirmed by microstructure analysis. The increment in dielectric losses as Ba is incorporated is due to modified structural properties of Bismuth ferrite which strongly agree with the observed XRD analysis and morphological analysis. So, we need high energy for the exchange interaction between the ions. However, at higher frequencies both systems show similar response.

Conclusion

The successful synthesis of Ba doped Bismuth ferrite nanoparticles via a sol-gel method are produced. The X-ray diffraction examination confirms the formation of a rhombohedral crystal structure with the R3c space group. The morphology study reveals that samples are spherically dense with fine grain boundaries. Intriguingly, the

introduction of Barium cations at A site induces a lattice strain due to the size variation between Bi3+ and Ba2+ leading to an observed increase in grain size. Furthermore, magnetic investigation reveals a significant enhancement in the coercivity of the Ba-doped system compared to pristine BiFeO3. Dielectric analysis unveils a notable increase in energy losses with Ba substitution. The observed enhancement in room temperature physical properties, particularly the tuneable magnetic behaviour and dielectric response, underscores the potential for tailored modifications in BiFeO3 through controlled Ba doping. These findings pave the way for the exploration of these Ba-doped BiFeO3 nanoparticles in various technological applications, including magnetoelectric devices, multiferroic memory elements, and high-frequency capacitors.

5.4 Investigation of Cobalt and Aluminium doped $Bi_{(0.9)}$ $Ba_{(0.1)}$ FeO_3.

5.4.1 Introduction

Due to the presence of two or more fundamental ferroic orderings, multiferroics [1, 2] are well-known materials and an excellent choice for a variety of electrical devices [3]. Due to its low band gap and robust magnetoelectric coupling at ambient temperature, bismuth ferrite is a well-known multiferroic with a wide range of applications in electronic devices, medicinal applications, and solar cells [4–8]. Its potential applications are constrained by the existence of substantial leakage current, a high transition temperature, and a modest magnetization. These materials are more dependable for use in electronic and magnetic devices because they have strong magnetic characteristics and strong, stable electronic properties at room temperature. Many researchers over the world have developed various mechanisms to adjust the properties of multiferroic materials such as doping, and composite, anisotropy change, synthesis mechanism [3]. The structure plays a vital part in deciding the properties of the materials by tailoring the microstructure and morphology we can interplay with such material by replacing A and B cations [197]. Although the perovskite Phase in multiferroic Bismuth ferrite is very sensitive the interplay of structural disorder is considered one of the key features to improve electronic properties. Various studies reported that the incorporation of other Anion and Cation enhanced the overall physical properties[191], [198]. The incorporation of Ba into Bi is found to influence the multiferroic and dielectric properties [191], [195], [199], [200]. This implies that the choice of a suitable dopant can finely tune the required properties. In this study, we have synthesized $Bi_{(0.9)}$ $Ba_{(0.1)}$ $Fe_{(0.9-x-y)}$

$Co_{(x)}$ $Al_{(y)}O_3$ for (x, y = 0), (x = 0.1, y = 0) and (x = y = 0.1) using the sol-gel process as it offers various advantages over another synthesis route[116], [117], [118]. Both Al for its electronic[151], [201], [202] and Co[90], [167] for its magnetic are well known for their physical properties so they are expected to enhance the overall electronic properties in the incidence of Ba. The purpose of the study is to enhance the electronic and room temperature and their significant effect on the microstructure and may find their potential application in device fabrication.

5.4.2 Instrumentation

The synthesized powdered sample are characterized by X-ray diffraction for phase purity and microstructure properties. The XRD (BRUKER) was recorded using Cu- K radiation ranges from 20°-70°. The microstructure is analysed using JEOL (FE-SEM) and EDX with magnification ranging from 25 to 1000000. The magnetic properties of the prepared sample are analysed with the help of a VSM (Vibrating sample magnetometer) with the field ranging from -21 to 21 KOe at room temperature. The METROHM along with the FRA32M-Impedance analyser ranging from 100 Hz to 1MHz is used to analyse the dielectric properties.

5.4.3 XRD analysis

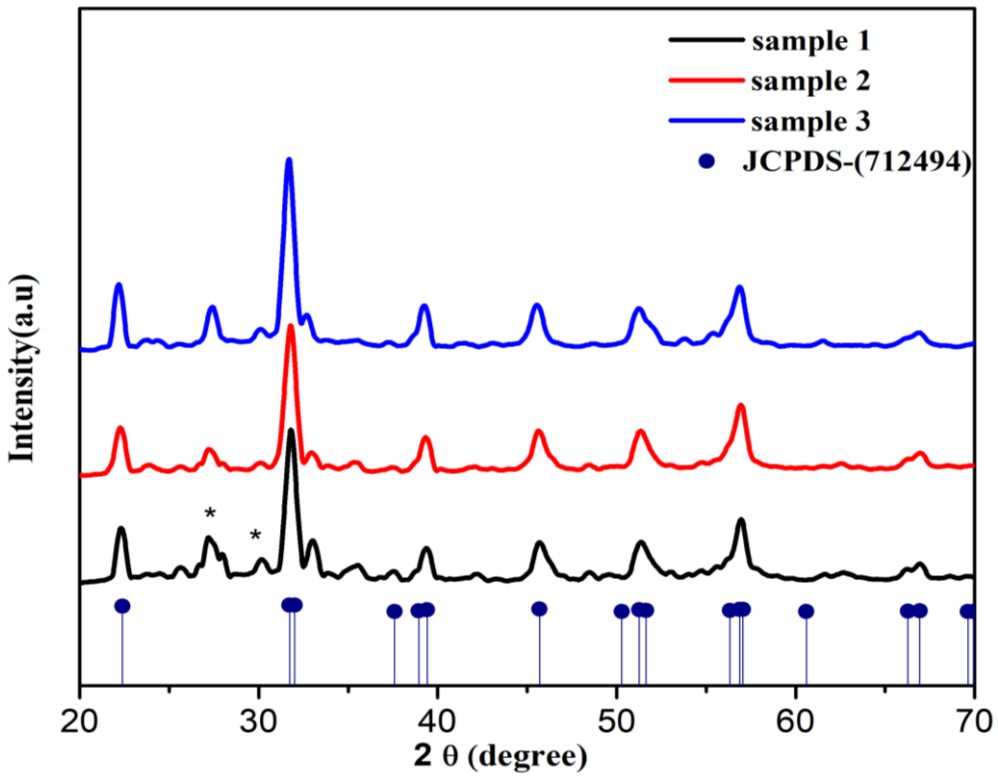

Fig.5.4.1 The observed XRD patterns of samples indexed with JCPDS.

The formation of Bismuth ferrite with rhombohedral R3C corresponds to JCPDS (712494). However, the impurity phases of Bi_2O_3 like JCPDS (761730) and $Bi_2Fe_4O_9$ corresponding to the JCPDS card (250090) are present in the system. X Powder is used to match the phases. Bi2O3's metastability, off-stoichiometry, low peritectic breakdown temperature, or volatilization are alleged to be the causes of secondary phase production [192]. Fig.5.4.1 shows the plotted XRD pattern corresponding to samples 1, and 2,3. The lattice constant is calculated with the help of equation 6 [138]

$$\frac{1}{d^2} = \frac{4}{3}\left(\frac{h^2+kh+k^2}{a^2}\right) + \frac{l^2}{c^2} \qquad (6)$$

The Crystallite Size is determined by the equation

$$d = \frac{k\lambda}{\beta Cos\theta} \qquad (2)$$

Where k is the Shape factor is the wavelength of target anode =1.05 A^0 and β is FWHM. The angle used is the Braggs angle(θ). The obtained parameters such -as lattice constant, and crystallite size are shown in Table.11

Table. 11 *The calculated lattice parameter from XRD data.*

Sample name	2θ	hkl	d (A)	D (nm)	Lattice constant
Sample 1	31.80	110	2.811	19.71	a=b=5.622, c=13.73
Sample 2	31.76	110	2.815	19.88	a=b=5.63, c=13.78
Sample 3	31.60	110	2.966	12.158	a=b=5.93, c=12.90

The perovskite structure is present in all the samples as per listed in Table.11 with corresponding 2θ values. There is evidence of the peak's relative displacement. The calculated values for the lattice constant are found to be decreased indicating the

occupation of empty Fe sites by Al and Co [203]. With the addition of aluminium, it is discovered that the crystallite size is reduced. The tolerance factor plays an important role in the structural interplay. Barium has larger atomic radii than Bismuth emerging distortion in the structure cause the formation of impurity phases. The smaller atomic radii of Al and Co, however, make it easier for them to occupy the vacant sites, which reduces the amount of impurity phases in Bi_2O_3.

5.4.4 Morphology

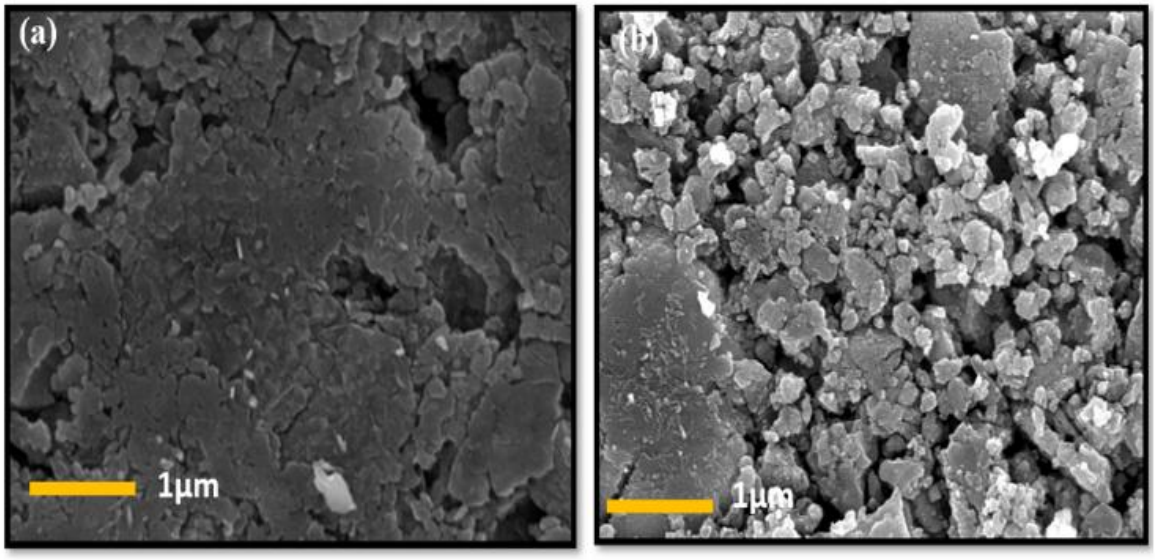

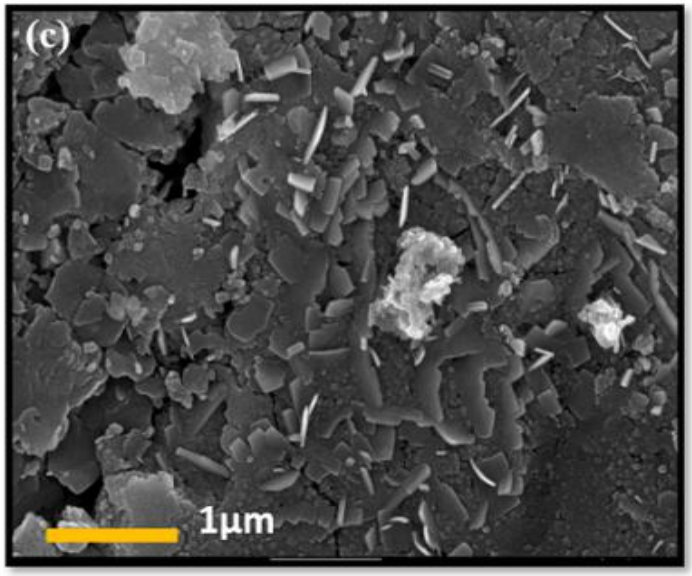

Fig.5.4.2 (a) The SEM images for sample 1, (b) The SEM images for sample 2, (c) The SEM images for sample 3.

The SEM images of the samples at 200000 magnifications for a scale of 1µm are carried out. In Fig.5.4.2 (a-c) the images show the presence of fine-grains with uneven size distribution. The results from XRD support the change in morphology attributed to crystal nucleation growth [143]. The variation in size is observed from the SEM images. The addition of Al further reduces the resultant powder's porosity, which is made more porous by the integration of Co.

5.4.5 EDX mapping

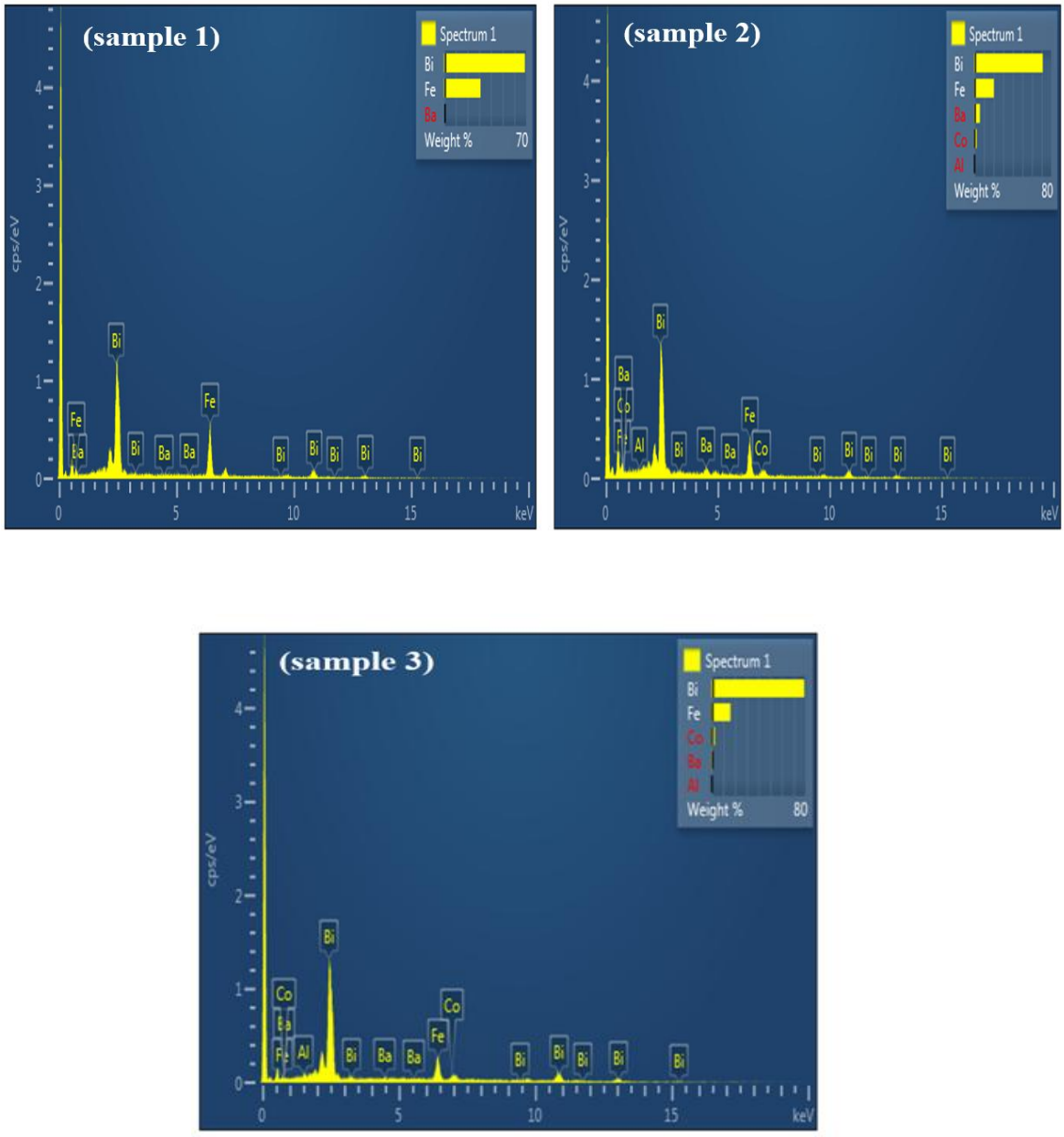

Fig.5.4.3 shows the obtained EDX of sample 1,2 and 3.

Table.12 Atomic percentage obtained from EDX.

Sample 1	Atomic %	Sample 2	Atomic %	Sample 3	Atomic %
Fe	62.78	**Fe**	46.10	**Al**	3.32
Ba	0.01	**Co**	5.52	**Fe**	38.50
Bi	37.21	**Ba**	5.42	**Co**	6.28
Total	100.00	**Bi**	42.96	**Ba**	1.52
		Total	100.00	**Bi**	50.38
				Total	100.00

Fig.5.4.3 illustrates the EDX analysis confirms the existence of the host and incorporated elements in the samples. However, the atomic percentage corresponding to the samples is evidence of retained stoichiometric composition and foreign impurities are present. Table.12 illustrates the change in atomic percentage with the incorporation of a dopant.

5.4.6 Magnetism

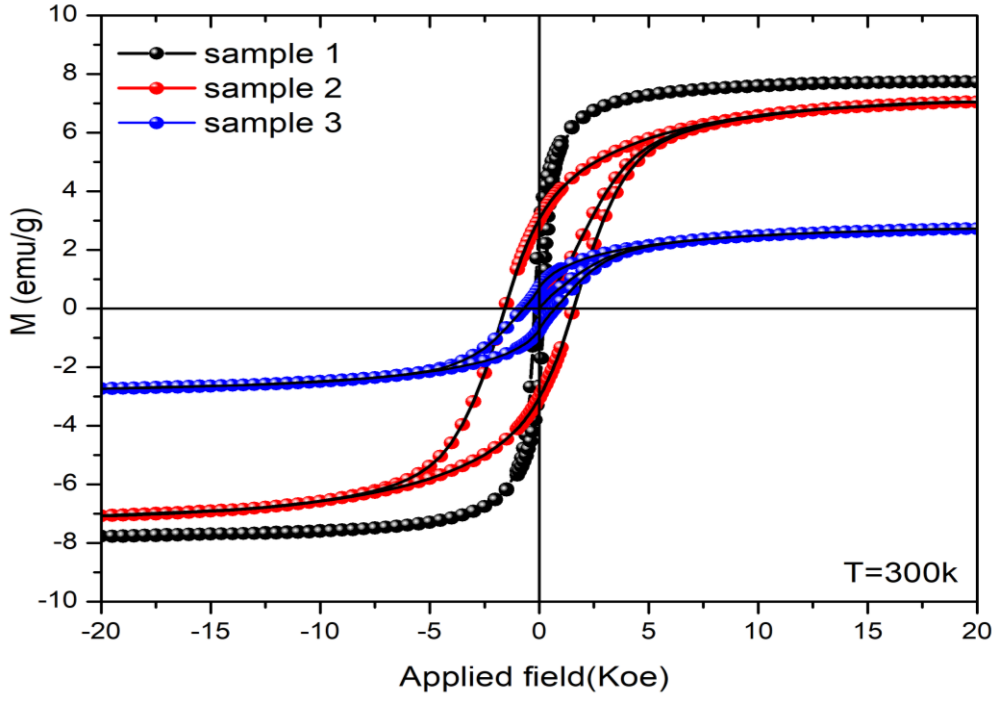

Fig.5.4 4 shows the hysteresis loop for (a) sample 1, (b) sample 3, and (c) sample 3.

The room temperature magnetic properties are investigated with the help of a Vibrating Sample Magnetometer as shown in Fig.5.4.4. The samples are subjected to a high magnetic field ranging from -20 to +20 KOe. Fig.5.4.4 shows the enhanced magnetic parameter and the acquired magnetic values for Samples 2 and 3. The obtained parameters from the ferromagnetic loop are shown in Table.122. Although the impurities of Bismuth oxide do not contribute to magnetism at room temperature [142] resulting in net magnetization due to the bismuth ferrite only. This demonstrates that the sudden change in magnetism is caused by the structure's variable oxygen and Fe valency distribution [52]. The squareness ratio confirms that there is the presence of random orientation of magnetic domains [150]. Also, it has been found that incorporation of Al has significantly changed the magnetic properties by reducing the retentivity. These samples qualify as hard magnetic materials because of their strong coercivity. These materials are excellent for magnetic memory devices and magnets due to their enhanced magnetic characteristics.

Table.13 *The calculated magnetic parameter from the Hysteresis loop.*

Sample code	Mr (emu/gm)	Ms (emu/gm)	Hc (Oe)	Mr/Ms
1	2.11	6.2	220	0.34
2	2.43	5.64	1570	0.43
3	0.57	4.3	709	0.132

5.4.7 Dielectric properties

The synthesized powdered samples are subjected to analyse dielectric properties using impedance spectroscopy. The samples in the form of pellets without any binder are subjected to a sinusoidal voltage. The complex impedance Z’ and Z’’ in terms of real and imaginary parts is measured [120].

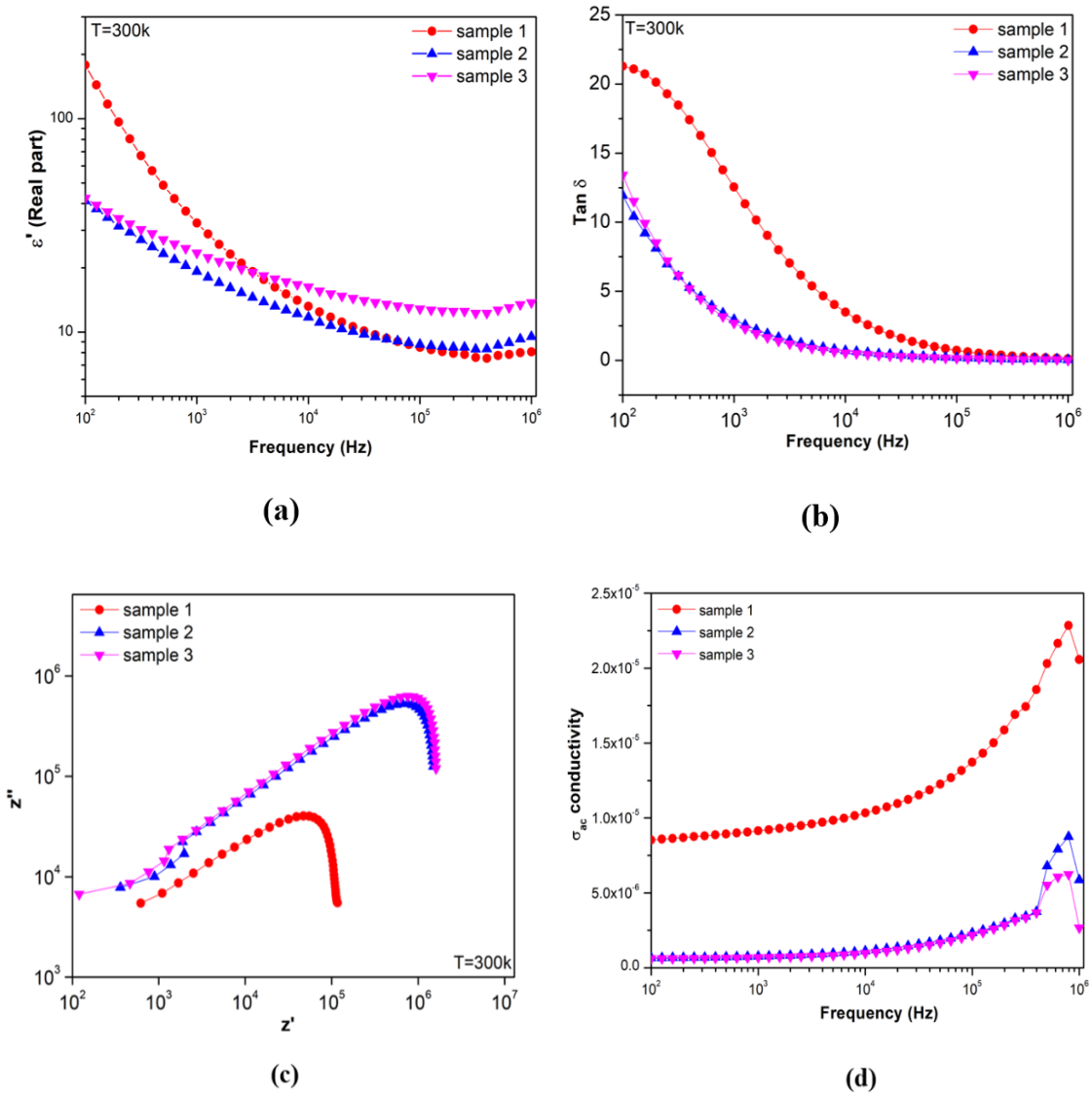

Fig.5.4.5 (a) The real part of dielectric constant (b) The dielectric response as a function of frequency. (c) The Nyquist plot for complex impedance (b) Conductivity as s function of frequency.

Fig.5.4.5 (a) demonstrates the real portion of permittivity using frequency variation. The real portion of a material's electrical permittivity (/) is correlated with the dielectric constant, which promotes the accumulation of charge in a system. From fig. 5 (a) it is observed that reduction in the magnitude of dielectric constant at higher frequencies which has been observed in such types of materials due to the Maxwell -Wagner effect [120], [152]. The system's dipolar spices contribute to the dielectric response at lower frequency areas, but at higher frequencies, it is seen to be nearly constant with no

reaction. Also, from Fig.5.4.2 it is observed that samples are having inhomogeneous grain and grain boundaries. Thus, the space charge effect is the primary cause of the dielectric response [128].

The maximum value of dielectric constant was obtained for sample1.This enlarge value is attributed to the incorporation of Ba. However, a large decrease in ε' is observed with the introduction of Co. Further on adding Al it does not show much change. The phase impurities and oxygen valency created by Co may be responsible as the inhomogeneous grain are observed in Fig.5.4.2. Also Fig. Fig.5.4.5(b) shows that the dielectric losses are reduced for sample 1, 2 and higher for sample 3. This is due to the change is composition, structure, and formation of new oxygen vacancies as it is common with Bismuth ferrite which is also confirmed by Table. 2 [196].

The composite system's Nyquist plot, as depicted in Fig. Fig.5.4.5(c), is plotted at room temperature with frequencies ranging from 100Hz to 1MHz. Due to the interfacial grain boundary effect, which promotes charge modulation at the interface, the the real part of Z* tends to decrease as the dopant percentage rises. The plot clearly shows the establishment of two arcs, which further suggests that on adding dopant, grain boundaries occur in between BFO grains. As a direct result of spatial heterogeneity, significantly altering the charge dynamics in our composite system.

From equation $\sigma_{ac} = \varepsilon''\omega c_0$, the relationships between σ_{ac} conductivity plotted in Fig.5.4.5 (d) with varying frequency which reveals that samples having high resistance. The obtained results from XRD and SEM shows that grains, defects, and impurities are there resulting in high resistance at the grain boundaries [126]. From Fig.5.4.5 (d) indicate that the ac conductivity changes abruptly in high frequency region for sample 2 and 3 showing the presence of traces of conductive metal ions corresponding to Al and Cobalt. Electronic devices may benefit from the improved dielectric properties at room temperature.

Conclusion

The structural analysis reveals the presence of Bismuth ferrite accompanied by impurity phases. The lattice constant and other parameters are calculated and are found to be affected by the incorporation of Al and Co. The impurity phases are found to decrease with a change in composition which is evident in the occupation of empty Fe sites by Al and cobalt. The production of non-uniform grains and an uneven size distribution in the

structure are both seen in the SEM images. The room temperature magnetic parameters such as Coercivity, retentivity, and squareness ratio is calculated are and obtained from the Hysteresis loop obtained from VSM. The impedance Spectroscopy calculated dielectric response as a function of frequency. The insertion of a dopant element has significantly changed the dielectric properties. It has been observed that dielectric losses are reduced but decrease the dielectric constant as well. The improved dielectric and magnetic properties make these materials suitable candidates for device application.

5.5 Composite system of $Bi_{0.99}Nd_{0.1}Fe_2O_3$/ ZnO

5.5.1 Introduction

The search for novel compounds with distinct and flexible properties has prompted researchers to investigate multifunctional materials that exhibit fine control of electrical and magnetic properties in miniaturized smart devices. Multiferroics are materials that exhibit both ferroelectric and ferromagnetic characteristics concurrently in a single phase[204]. The presence of both the ferroic properties in a material simultaneously has received a lot of consideration in the development of non-volatile memory devices, ultrafast optoelectronic devices, spintronics, transducers, solar cells for energy generation [205], biomedical applications [20], [21], [121], [164]. Till date, $BiFeO_3$ (BFO) is one of the most premeditated single-phase multiferroic material that exhibit magnetic and other electronic characteristics at ambient temperature [206]. It has ferroelectricity at 643 K Curie temperature and anti-ferromagnetism at 1143 K Neel temperature. Its perovskite crystal structure is deformed and rhombohedral, of the ABO3 type, with an R3c space group[207]. A-sites in BFO are typically held by Bi^{3+} ions, which promote the steadiness of ferroelectricity in deformed structures, whereas B- sites are filled by transition metal ions (Fe), which contribute to magnetism. The unoccupied d^0 orbital causes ferroelectricity in multiferroics, whereas partially filled d^n orbitals cause ferromagnetism[208]. Ferroelectricity can, however, be formed by the stereochemical activity of Bi^{3+} ions, whereas Fe^{3+} ions cause ferromagnetism in BFO. Many fractional replacements of rare-earth ions at A sites and transition metal ions at B sites can significantly improve electrical and magnetic characteristics[209]. Ferroelectricity is

caused by the displacement of Bi^{3+} and Fe^{3+} cations along the [111] planar direction, which is off-centered to the oxygen octahedron[209]. Even though BFO exhibits versatile properties for device applications, its real-world applicability is limited by the occurrence of contamination and impurity phases in the synthesis process. The unwanted impurity phases grown during synthesis lead tosome unfavourable condition, such as weak magneto-electric coupling, high tangent loss, structural distortion, high current leakage and other secondary phase formations, which later affect the dielectric permittivity, ferroelectric, electrical resistivity, and magnetization of the material[210]. To solve the drawbacks of single-phase Bismuth Ferrite, research has been carried out by doping rare earth elements (Nd, Sm Tb, La, Y, Gd, , and so on) at the A-site of Ferroic materials to improve their properties[206][211][212][213][214].

Various reports observe that doping has effectively enhanced the overall properties of the Bismuth ferrite. Shisode et al. has reported synthesis of $Bi_{1-x}Sr_xFeO_3$ (x = 0.05, 0.15, 0.25) by sol-gel auto-combustion method in which for x = 0.15, the polarization value of 4.801 C/cm^2 is achieved that indicates partially saturated nature of the loop[215]. Hu and colleagues reported that $Bi_{1-x}Gd_xFeO_3$ films coated on $Pt/Ti/SiO_2/Si$ substrates found to have improved electric remanent polarization ($Pr > 70\ \mu Ccm^{-2}$)[216]. Li et al. found that Mg^{2+}-doped $BiFeO_3$ has improved magnetic and ferroelectric characteristics and these compounds are ideal for memory devices and magnetoelectric device applications[217]. Das et al. prepared bismuth ferrite samples co-doped with nonmagnetic and magnetic elements at various sites respectively. Similarly co-doped samples were found to exhibit higher electric polarization and utmost resistivity at normal temperature, which is attributed to the decreased leakage current and oxygen vacancy [218], [219]. Sahu et al. synthesized Nd-doped BFO (x=0.5-0.8) by solid-state method. It is observed that inclusion of Nd enhances the electronic properties of all samples. The obtained Nyquist plot displays the involvement of bulk material properties. The power law guides the study of AC conductivity and frequency. The stability factor reduces as dopant Nd concentration rises[220].

Based on current results, it is found that neodymium (Nd) may be a promising dopant to boost overall characteristics, which can find practical applications in device-based applications. However, the doping concentration must be kept low since larger Nd concentrations are found to reduce the multiferroic characteristics of bismuth ferrite [221]. The composite system approach is one of the keys to unlocking the potential of multiferroic materials. By far several characteristics have been discovered to be advanced

in BFO-based composited structures, including optical, ferroelectric, and magnetic by the stimulus of the heterostructure interface [58], [60], [169], [177], [222], [223], [224], [225], [226]. Several studies have been conducted on combining BFO with other materials like metal oxide such as Fe_3O_4 [227], NiO[228], etc. It observed that BFO/ZnO based thin film displays the peak polarization of 46.7 μCcm^{-2} and ZnO/BFO thin film shows the enlarged value of 2Pr of 18.47μCcm^{-2}[229]. Also zinc oxide (ZnO), is a semiconducting oxide with a piezoelectric wurtzite structure and permanent spontaneous polarization and its enormous active adsorption sites, superior electronic mobility, and flexible morphology making it interesting to researchers as a useful material.

Our current study focuses on the composite system Nd doped BFO with composition $Bi_{0.99}Nd_{0.1}Fe_2O_3$/ZnO where ZnO is used as a filler with varying weight fractions (p = 0%, 5%, 10%, and 15%). Here, we investigate the effect of Nd doping on the structural, magnetic, and impedance characteristics of a $Bi_{0.99}Nd_{0.01}Fe_2O_3$/ZnO composite at room temperature. The study points to a significant improvement in the composite's electrical and ferroelectric characteristics at room temperature and thus can serve as a possible candidate for energy storage devices and other applications.

5.5.1 Instrumentation

The synthesized nanoparticles are characterized by X-ray diffraction for phase purity. The XRD (BRUKER) was recorded using Cu-K radiation ranges from 20^o-70^o with a step size of 0.02 ^{0}. The microstructure is analysed using JEOL (FE-SEM) and EDX spectroscopy with magnification ranging from 25 to 1000000 is performed METROHM and the FRA32M-Impedance analyzer ranging from 1000 Hz to 1MHz are used to analyze the dielectric properties. The optoelectronic properties are examined using a UV spectrometer. The ferroelectric properties (P–E) hysteresis are carried using a cryocooler model SRDK-205 circuit via 4 K CCR in temperature and frequency range of 5 K - 300 K and 50 Hz - 250 Hz respectively.

5.5.2. Structural analysis

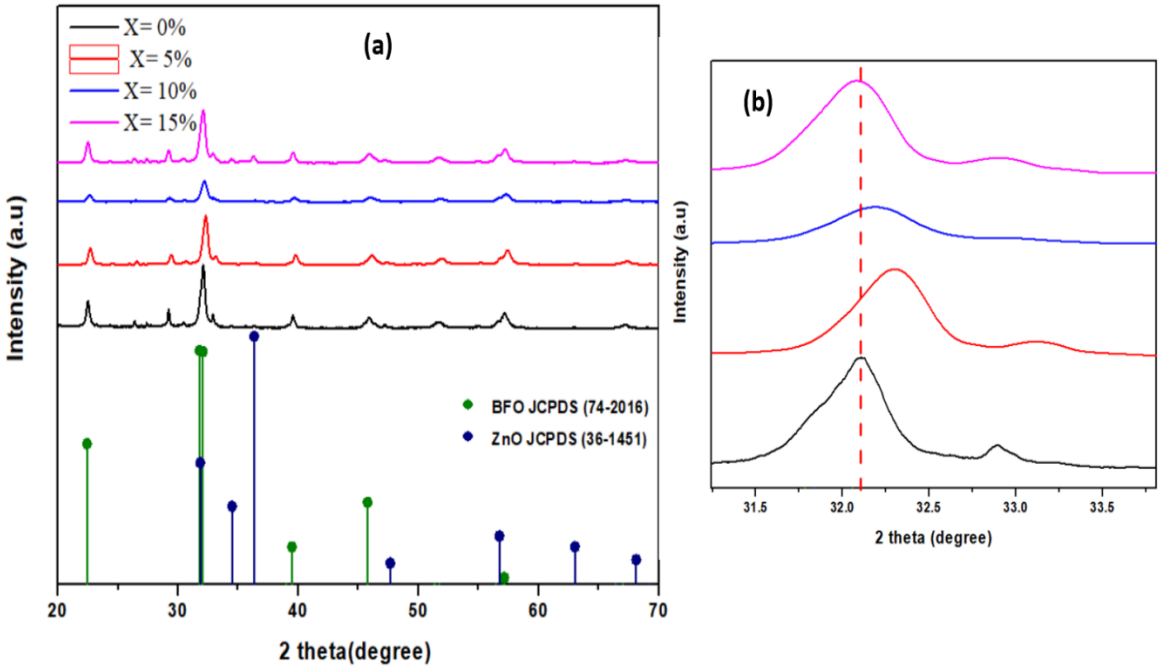

Fig.5.5.1 (a) XRD retrieved pattern for x=10%, x=30%, x=50% along with JCPDS. (b) Peak shift for $Bi_{1-x}Nd_xFeO_3$ with change in composition.

The composite system is subjected to XRD as shown in fig. 2 with step sizes of 0.002 ^{0} and 2θ spanning from 20^0 to 70^0. With the aid of X powder and X pert high score, the data phase is identified. XRD data of every composite system is presented along with the JCPDS card in Fig.5.5.1 (a).

The diffraction peak shown in Fig.5.5.1 (a) demonstrates that $BiFeO_3$ with JCPDS (74-2016) phase belonging to R3C - rhombohedral having lattice constant a = b = 5.58 A^0 c= 13.867 A^0 are present. It has been observed that identity peak belonging to rhombohedral Bismuth ferrite is found to be sensitive to temperature and composition resulting in changes in crystallite size, lattice constant l[84], [119], [140], [142]. The presence of Neodymium results in the formation of secondary phases [144]. The phase identification reveals that ZnO belonging to cubic phase with JCPDS (36-1451) with lattice constant a = b = 3.249 A^0 c= 5.207 A^0 are present. The presence of sharp diffraction peaks is evident in the crystalline characteristics of the prepared composites. The equation1 determines the crystallite size

$$d = \frac{k\lambda}{\beta Cos\theta} \quad (6)$$

Where k is the shape factor, λ is the wavelength of the target anode which is around 1.05 A^0, θ is the Bragg's angle and β is the full-width half maximum (FWHM). The crystallite size of the sample x = 0%, 5%,1 0%, 15%, is found to be 20nm, 15nm, 14nm, and 17nm respectively. It is noted in Fig.5.5.1 (b) that in samples diffraction peak changes to a higher angle with the introduction of the filler, but at greater concentrations, the peak shifts towards a lower 2 theta value. The observed change makes a good agreement with the lattice parameters that were estimated.

5.5.3 Morphological analysis

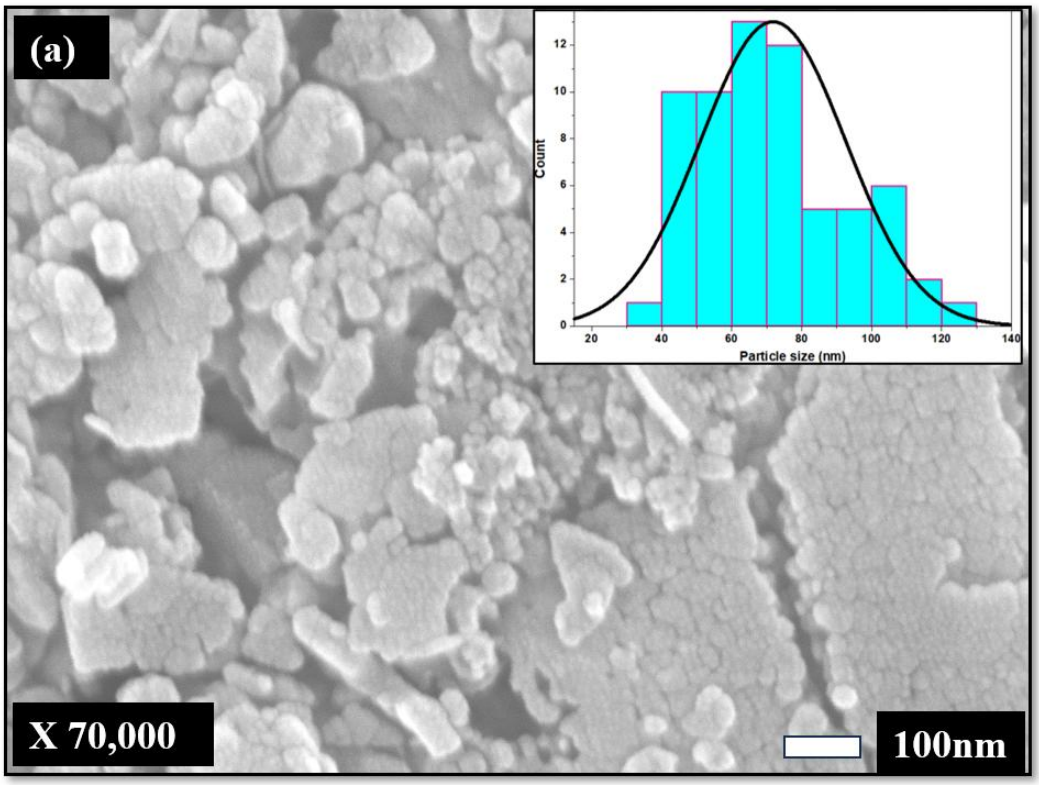

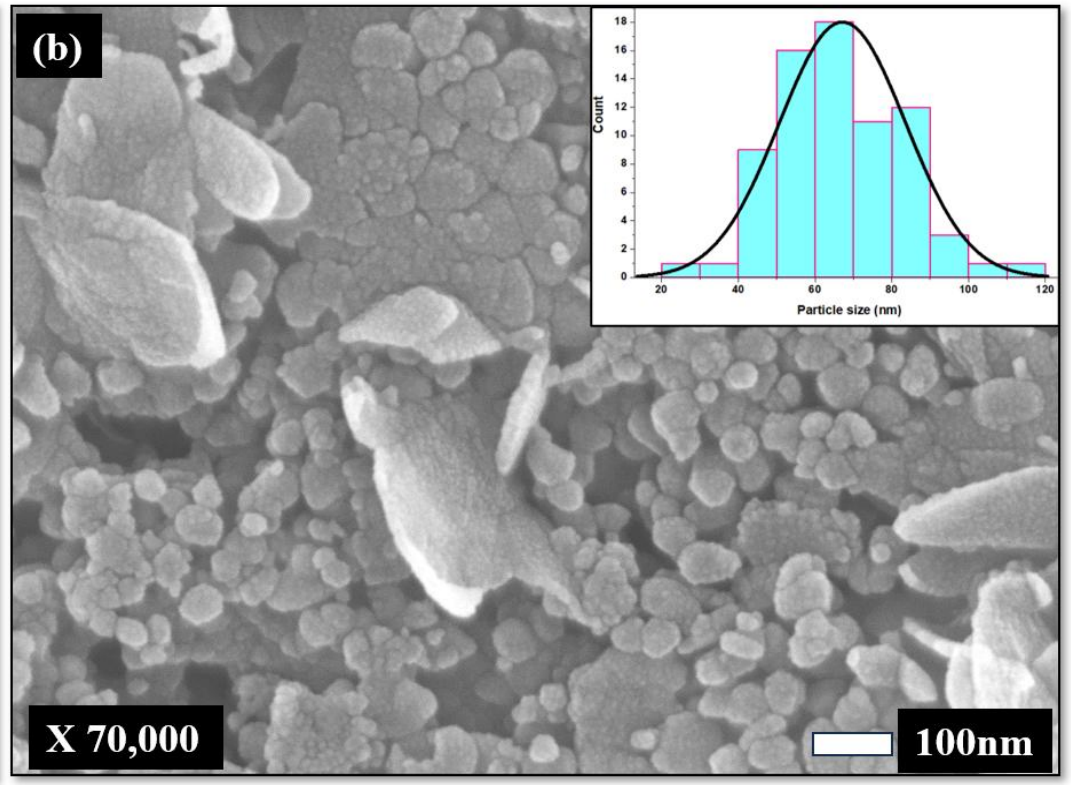

Fig.5.5.2 (a) The magnified "SEM" images of composite samples for X = 0%, (b) The SEM images for X = 15%.

Fig.5.5.2 (a, b,) shows the magnified SEM images of the post-annealed composite sample corresponding to x = 0%, and 15%. The average size of the nanoparticle observed is below 100 nm which results system consisting of mostly spherical dense particles with uneven sizes where some particles exist independently and some get amalgamated. The voids between the grains are visible in both samples. Even at large weight fractions, the average particle size remains unchanged when ZnO is added as a filler. However, A morphological change brought about by a chemical reaction or inter-phase diffusion has been seen with the introduction of filler, and this observation aligns well with the acquired XRD data. The primary reason for the creation of distinct phases is the competition between crystal nucleation and growth [143]. The phase transition and morphological changes seen in the XRD images of the composites are consistent.

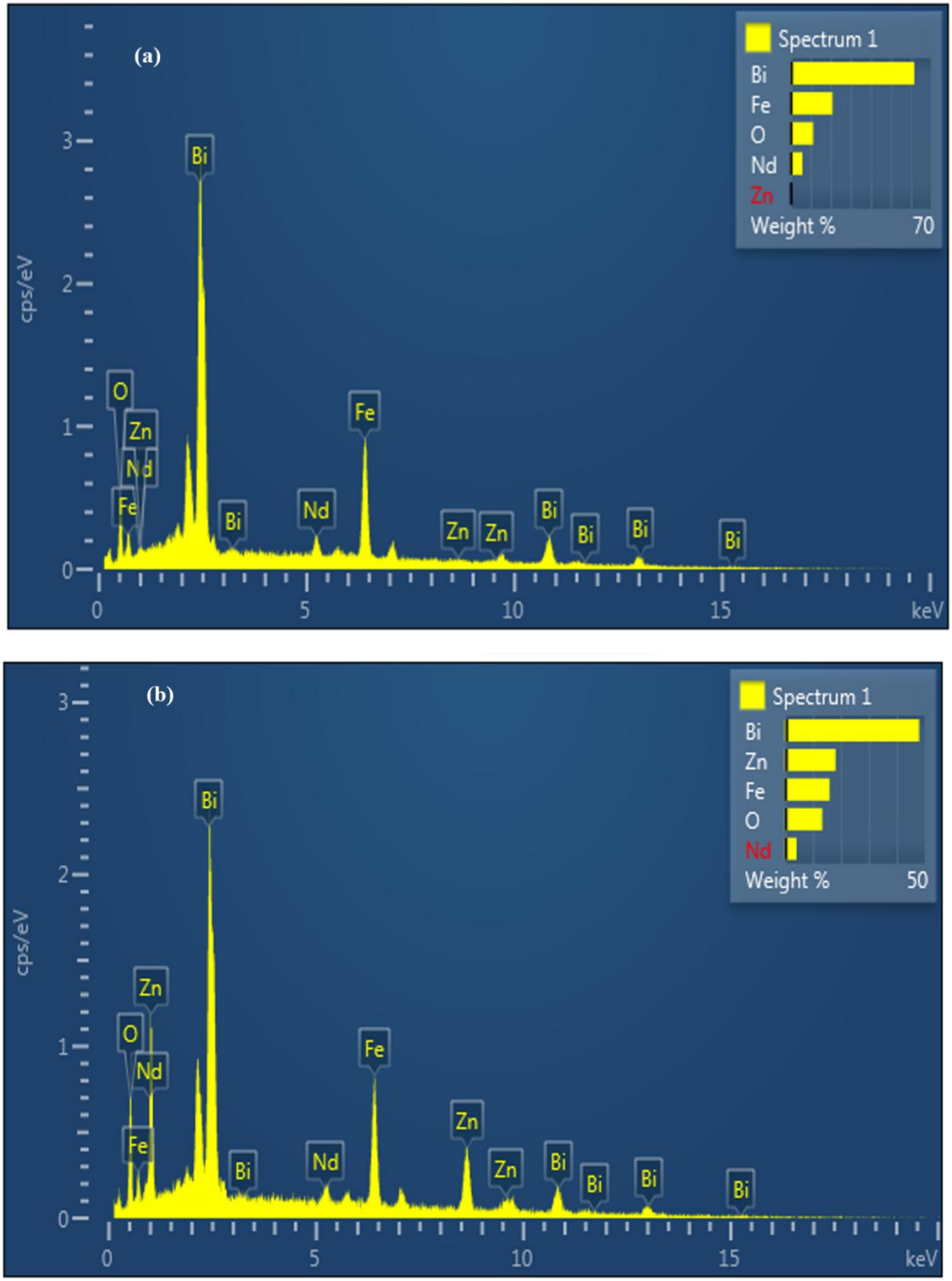

Fig.5.5.3 (a) The EDX of composite samples for X = 0%, (b) for X = 15%.

Table.14 Elemental wt. percentage obtained from EDX spectra.

Sample	Wt.%	Wt.%	Wt.%	Wt.%	Wt.%	Total %
	Bi	Nd	Zn	Fe	O	
O%	20.85	2.93	0	26.42	49.80	100
15%	13.79	1.78	15.67	17.27	50.49	100

Fig.5.5.3 (a), (b) shows the obtained electric dispersive X-ray for the composite sample x=0%and x=15%. The EDX analysis shows that elements like Bi, Nd, Fe, Zn, and O coincide with the composition of the system acquired for observation. The atomic wt% of elements are listed in Table.14 The samples' EDAX analysis produced quantifiable results. It is determined that the Nd-doped $BiFeO_3$/ZnO composite samples were successfully formed and that there are no foreign impurities.

5.4.4 Impedance analysis

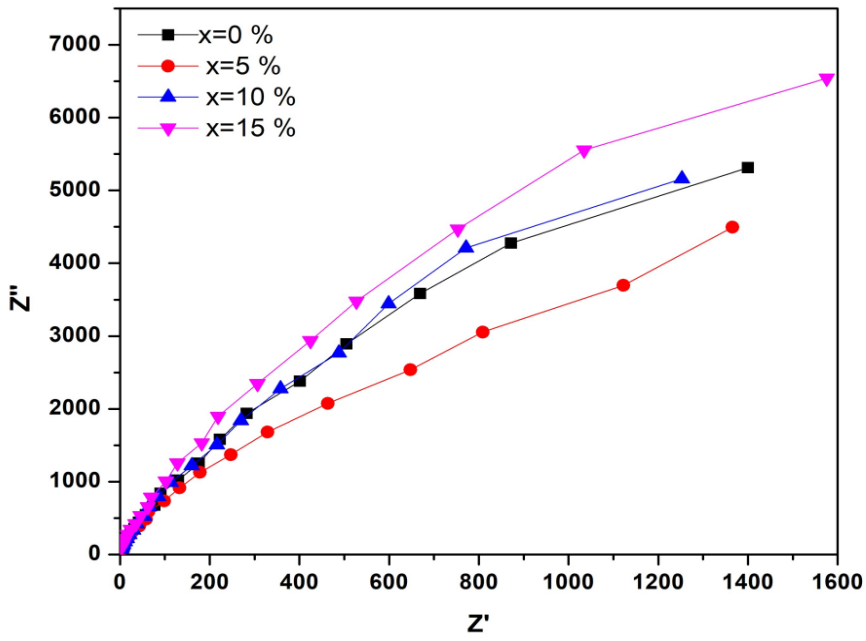

Fig.5.5.4 The Nyquist plot for composite samples X= 0%, 5%, 10%, 15%.

Alternating currents are applied to the composite systems to examine the electrical characteristics. A sinusoidal voltage with an amplitude of one volt is delivered into the composites. The complex impedance Z as measured is found in terms of real and imaginary parts to observe the Nyquist plot in Fig.5.5.5. The partial semi-circular arcs observed in all the samples are caused by the significant resistance at low frequencies. So, it can be concluded, that most of these complete resistances coincide with the grain boundary of the nanoparticles [230].To further investigate an equivalent circuit is derived for all the samples.

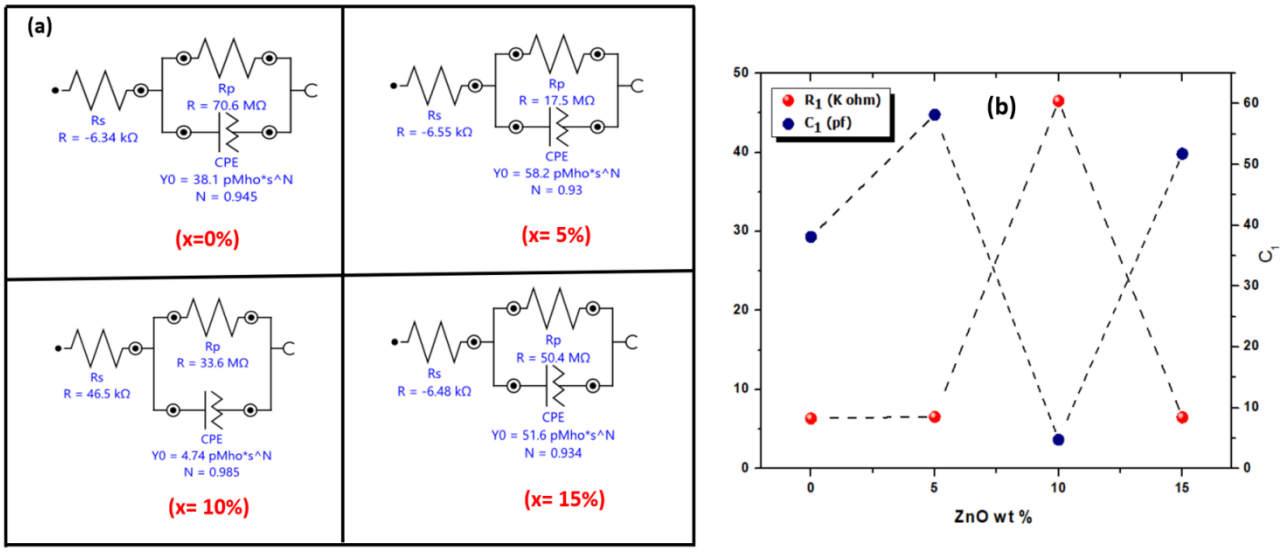

Fig.5.5.5 (a) The equivalent circuit obtained for composite samples X= 0%, 5%, 10%, 15%. (b) The obtained value of Resistance and capacitance as a function of weight percentage.

The impedance spectra have been analysed followed by an equivalent circuit shown in Fig.5.5.5 (a). The circuit is made up of a resistance, a constant phase element (CPE), and another resistance combined in parallel. It is observed that the system consists of a large resistance. The obtained value of resistance R_1 and capacitance C_1 is in Fig.5.5.5 (b) as a function of weight percentage is also derived which shows that R_1= 46.5 KΩ is maximum for x=10% and C_1 = 4.74 pF is minimum. To investigate the dielectric characteristics of the samples following formulas have been used. [120].

$$\varepsilon' = \frac{Z''}{\omega c_o Z^2} \qquad (3)$$

$$tan\delta = \frac{\varepsilon''}{\varepsilon'} \qquad (5)$$

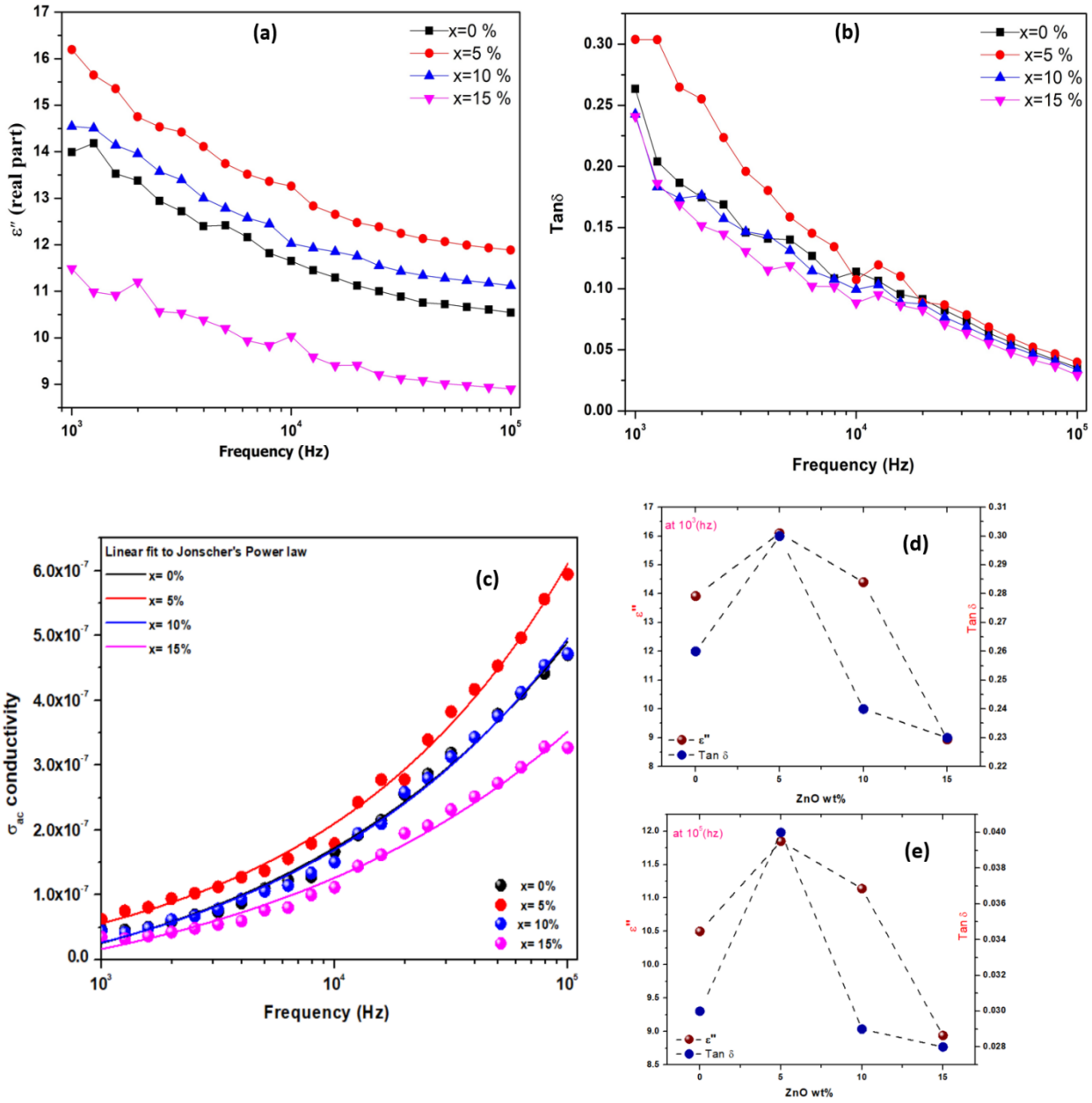

Fig.5.5.6. The (a) ε'' (real part of permittivity) as a function of frequency, (b) dielectric loss as a function of Frequency(c) AC conductivity as a function of frequency for composite samples X= 0%, 5%, 10%, 15%. (d) dielectric constant and loss as a function of wt.% at low frequency (e) dielectric constant and loss as a function of wt.% at high frequency.

A material's capacity to polarize in answer to an electric field is also stated by its real part of permittivity. Fig.5.5.6. (a) shows the frequency-dependent real part of the electrical permittivity ($\varepsilon^{/}$) of the material at room temperature which corresponds to the dielectric constant that helps the charge to build up in a system. The observation shows that on

introducing the filler at x= 5% the maximum value of the dielectric constant is observed. However, at higher concentrations, the value is decreased significantly. Fig.5.5.6. (a) clearly shows that the real part of the permittivity follows a strong frequency-dependent behavior at a low-frequency regime and becomes independent at high frequency. The addition of ZnO has increased the dielectric constant up to an extent however at higher weight percentages the increment in conducting charge species further reduced the overall dielectric constant.

The system's dissipated energy is tanδ. Energy is delivered into a capacitive system, which stores some energy, releases it for the device, and loses some energy in the process. Therefore, these losses should be reduced for the devices' increased stability. The losses are calculated using eq.4. Fig.5.5.6. (b) shows that the dielectric loss is a function of frequency where it is observed that losses are reduced for x = 10%, 15%. Here both the dielectric constant and dielectric loss follow the same trend where it is observed that at low frequencies, the permittivity is mostly affected by the DC conductivity of the charge carriers which exhibits the Maxwell-Wagner effect at the interface between the conducting electrode and the sample, leading to a faster drop. Whereas at the high-frequency regime, the electric dipole relaxation time increases as compared to the period of the input AC voltage, leading to a reduction of dielectric constant and dielectric loss [36],[103], [178]. From Fig.5.5.6 (d), (e) we observed a significant change in dielectric properties at low and high-frequency regions by the addition of ZnO as a filler.

In most cases, the conductivity's frequency dependency follows Josher's power law $\sigma_{ac} = \sigma_{dc} + A\omega^n$ [48]. Fig.5.5.6. shows the fitting of observed ac conductivity with Josher's power with variable frequency range for all samples. The fitting shows that obtained data is in accord with Josher's power law indicating various charge mechanisms [231]. The slope in this case, denoted by the dimensionless term "n," is significant in a variety of models, applications, and interpretations. It is related to the polarization process, which incorporates the whole contribution of mobile charge effects.

The calculated values of ac and dc parts of conductivity are shown in Table.15. In our case, the value of n is found to vary between 0.9 - 1. The increase in the value of n typically indicates that the composite system is dominated by a dynamic related to the certain charge mechanism caused by disarrangement in the materials. [54, 55]. From Fig.5.5.6. (c) it is detected that in all the composite systems, the value of $n < 1$ suggests that the system is stable at low and high-frequency regimes. The composite system's

improved electrical and dielectric qualities indicate that energy storage devices may benefit from its use.

Table.15 The calculated AC and Dc conductivity part.

Sample	$\sigma_{dc}(Sm^{-1})$	$\sigma_{ac}(Sm^{-1})$	n
X=0%	1.0×10^{-7}	6.68×10^{-9}	0.99203
X= 5 %	4.02×10^{-8}	2.56×10^{-9}	0.99423
X=10%	8.57×10^{-8}	4.93×10^{-9}	0.99258
X=15%	8.84×10^{-8}	6.86×10^{-9}	0.98604

5.5.5 Ferroelectric properties

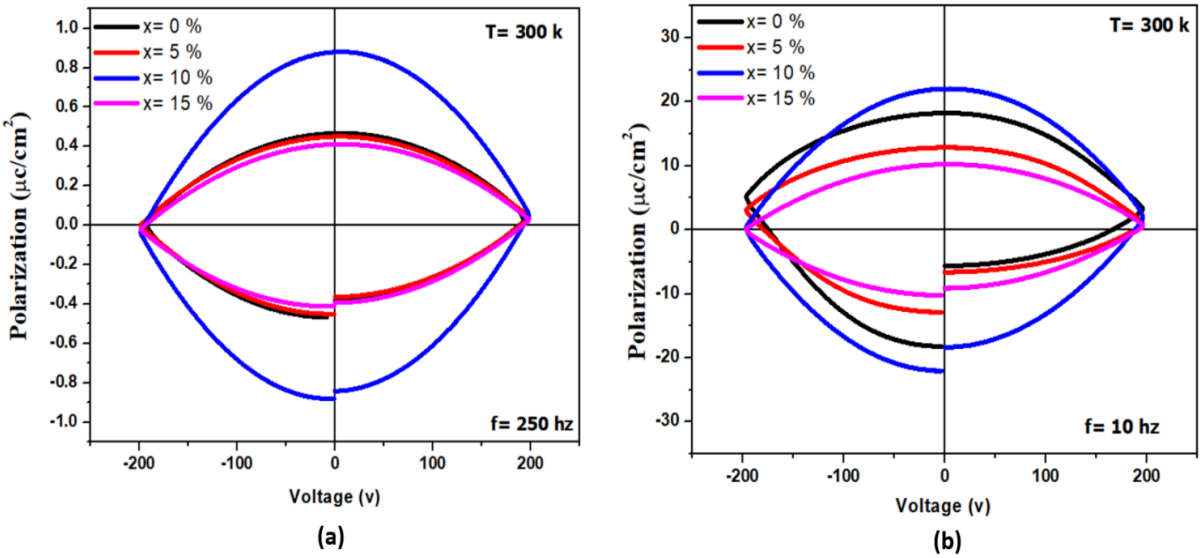

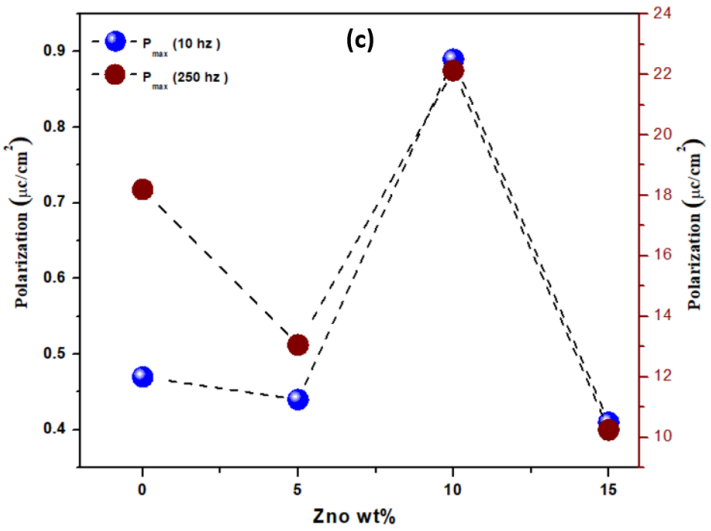

Fig.5.5.7 P-E loop for Sample (a) at high frequency(b) at low frequency X= 0%, 5%, 10%, 30%. (c) Polarization as a function of weight fraction at high frequency and low frequency.

Fig.5.5.7 (a) shows the ferroelectric study of the composite systems where voltage-dependent polarization is analyzed at room temperature at different frequency regimes as bismuth ferrite is an intrinsic multiferroic compound, it has a simultaneous magnetic and electric ordering at 300 K[184]. It has been observed that the sample exhibits a wider ferroelectric loop at low frequencies and the polarization is reduced at high frequency. This is because the electric field oscillates faster at higher frequencies, which might make it more challenging for the material's internal dipoles to align. As a result, the material's overall polarization decreases at higher frequencies. Ferroelectric and dielectric properties driven by the frequency that was determined for the composite system also show a correlation with the reported data. In Fig.5.5.7 (c) Polarization along with varying weight fraction at high frequency and low frequency is observed where we observed that for x =0% the P_{max} = 18.2 μc/cm^2 at low frequency (10hz) and P_{max} = 0.47 μc/cm^2 at high frequency (250hz). The observed loop indicates lossy capacitive behavior for all samples, however, on introducing the filler it has been observed in Fig.5.5.7 (c) that polarization is maximum for (x= 10%) is P_{max} = 22.13 μc/cm^2 at low frequency (10hz) and P_{max} = 0.89 μc/cm^2 at high frequency (250hz). However, for (x= 5%, 15%), the polarization is measured as P_{max} = 0.44 μc/cm^{2,} and P_{max} = 0.41 μc/cm^2 (at 250 Hz) respectively is observed. A kink is observed for x = 10 % at both frequencies. The existence of conducting charges of a particular polarity, whose polarization response

varies as the voltage is changed from positive to negative polarity, is the primary cause of the huge magnitude of polarization and its associated asymmetry. It has been shown that adding filler to composite samples increases the loop area and charge leakage. It is due to the disorder of the system as observed in electronic properties [232]. The enhanced ferroelectric properties reported may find their practical application in device application.

5.5.6 Optical bandgap

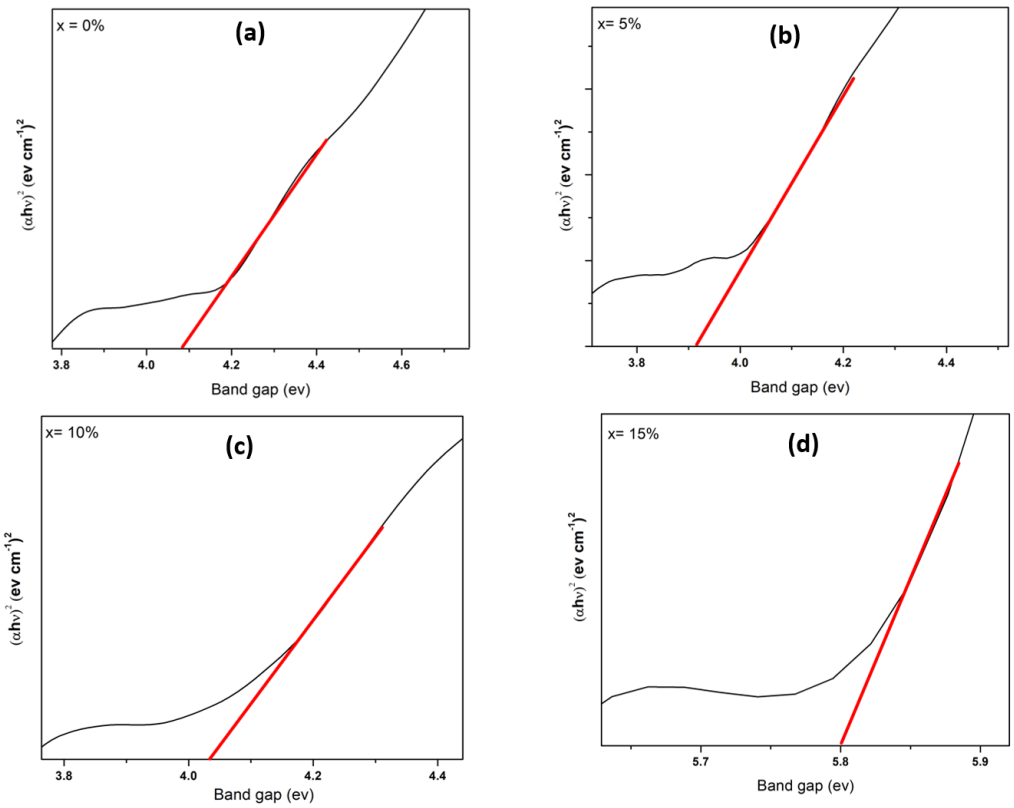

Fig.5.5.8 Band gap calculation for samples (a) X= 0%, (b) X= 5%, (c) X= 10%, (d) X= 15%.

The composites are exposed to absorption and transmission spectra over the wavelength ranges of 200–800 nm to examine the optical performance. The band gap is calculated via Tauc plot method since the band gap and optical transmittance characteristics are correlated. Eq. 8 is used to calculate the band gap [183].

$$\alpha h\nu = B(h\nu - E_g) \quad (8)$$

Where h referred as Planck constant and B is a proportionality constant, E_g is the bandgap, hν signify photon energy, and α is the provided absorption coefficient. From figure 9, the estimated values for the composite system x= (0%, 5%, 10%, and 15%) are

4.08 eV, 3.9 eV, 4.03 eV, and 5.08 eV, respectively. The observed values indicate that at a lower weight percentage, the composite system exhibits a good optical response. At higher concentrations of ZnO, the interaction between the two systems BFO and ZnO and structural defects is held responsible for the increased band gap [233]. The analysis reveals that the composite system has better optical absorption that may find its practical application in photovoltaics.

Conclusion

In this work, $Bi_{0.9}Nd_{0.1}Fe_2O_3$ and zinc oxide are produced by the sol-gel method which is then followed by the construction of composite systems by varying wt% of ZnO nanoparticles. A systematic investigation shows non-monotonic variation of structural, morphological, ferroelectric, and impedance characteristics in Nd-doped BFO/ZnO composite systems. Structural properties confirm the presence of Bismuth ferrite and ZnO phases along with some structural impurity phases. The elemental composition is confirmed by EDX spectra. The observed average particle size is below 100 nm. The complex impedance spectroscopy confirms all the composite exhibit large resistance and capacitive behavior. The dielectric strength was improved by the insertion of filler and the dielectric losses are lowered. The Conductivity shows that the system is not disturbed by the addition of filler and dielectric dispersion was caused by the presence of many conductivity processes, as demonstrated by dielectric measurements. All the composite sample exhibits ferroelectric characteristics, according to the ferroelectric loop analysis. Filler ZnO has enhanced the ferroelectric properties, with maximum polarization at x = 10%. The band gap of composite systems shows better optical absorption resulting in enhanced optoelectronic properties. Consequently, it can be concluded that ZnO addition has improved Nd-doped BFO's overall properties considerably. These composites' stated characteristics indicate that they have a lot of promise for improving magnetic memory and electronic sensor technologies.

Summary

BFO/NaCl-In this study, high-purity bismuth ferrite (BFO) nanoparticles are fabricated using the sol-gel method. The impact of adding the ionic filler NaCl on the matrix's microstructure, shape, and characteristics are examined. The structural and FE-SEM studies verified that secondary phases were formed because of the annealing temperatures. Phase change and an increase in particle size were caused by the addition of NaCl, which also influenced coercivity and magnetic properties which can be advantageous for memory and sensor systems. NaCl incorporation significantly changed the dielectric properties, increasing dielectric permittivity at low frequencies by a factor of 6 according to a complex impedance study. Higher electrical conductivity was produced by the disorder that the filler incorporation produced. These results indicate the potential of altering desired characteristics for electrical and energy storage device applications via halide-based composites.

BFO/CFO- We have successfully mixed bismuth and cobalt ferrite in different proportions to produce composite materials. The sol-gel method creates the individual components and then fabricates them together. The analysis confirmed the expected crystal structures of both materials with some additional impurities. The microstructural analysis observed the formation of a well-connected network (percolating cluster) of cobalt ferrite nanoparticles at a specific ratio. Further electrical investigation revealed that this composite offered good stability and acted like an insulator at low frequencies, referring them as a possible contender for energy storage applications. Additionally, the composite's magnetic characteristics were improved by the inclusion of cobalt ferrite nanoparticles. CFO increases the overall magnetization non-monotonically with maximum Mr = 35.57(emu/gm) and Hc= 1277 Oe. The observed band gap for the composite system is 2.5 to 3 eV. The incorporation of cobalt ferrite nanoparticles modifies the ferroelectric characteristics, according to ferroelectric investigations, a conducting percolating cluster that spans the composite system forms beyond x=30%, transforming the system from a lossy capacitor to an ideal resistor. The investigated system exhibits tremendous promise for the development of magnetic memory devices, photovoltaics, and electronic sensor devices.

Bi(1-x) Ba(x)FeO3- This work showcases the production of Bi(1-x) Ba(x)FeO_3 nanoparticles wit variation of (x = 0, 0.1). The Rhombohedral structure belonging to R3C space group was confirmed by structural analysis. The prepared nanoparticles showed a packed spherical shape with small grain boundaries. The substitution of barium caused the grain size to grow, which influenced the nanoparticles' shape. The Ba-doped system had higher coercivity although there was no change in retentivity. The dielectric study showed that substituting Ba has improved the overall dielectric strength of the material. The findings demonstrate the opportunity of altering electronic and magnetic characteristics at ambient conditions, for targeted device application.

$Bi_{(0.9)}$ $Ba_{(0.1)}$ $Fe_{(1-x-y)}$ $Co_{(x)}$ $Al_{(y)}O_3$- This work explores impact of adding Co and Al as a dopant on the different features of bismuth ferrite (BFO). Changes in impurity phases and lattice constants are observed using XRD analysis. The presence of dopants has an impact on the non-uniform grain distribution, observed in morphological analysis. VSM is utilized for evaluating magnetic properties such as coercivity and retentivity, which show variations because of dopant addition. Impedance spectroscopy analysis of the dielectric response displays changes in the dielectric features, by dropping the dielectric constant and losses. It shows that the introduction of co and Al dopants enhances the suitability of BFO for device applications.

$Bi_{0.99}Nd_{0.01}Fe_2O_3$/ZnO-The study examines composite materials composed of zinc oxide and bismuth ferrite ($Bi_{0.99}Nd_{0.01}Fe_2O_3$) which were fabricated by sol-gel technique. The quantity of ZnO nanoparticles was changed, and the material's subsequent qualities were examined. Their results show that the addition of ZnO has a direct effect on the composites' electrical, optical, morphological, and structural features. Although the formation of several unwanted impurity phases, the materials exhibited interesting characteristics. The ZnO filler reduced dielectric losses and improved electricity properties like capacitance. it is observed that conductivity remained unaffected, and the composites exhibited ferroelectric behaviour with enhanced polarization at a specific ZnO concentration. ZnO was also shown to improve light absorption, indicating improved optoelectronic characteristics. Overall, the study shows that incorporating ZnO significantly improves the properties of Nd-doped bismuth ferrite, which makes these composites desirable choices for use in electrical and magnetic devices.

Scope of future work

The work presented deals with the investigation of structural, electric, optoelectronic, and magnetic properties of the multiferroic composite systems. The composite investigated at room temperature holds immense promise for next-generation devices. It is well understood that temperature has a remarkable impact on electronic and magnetic properties. So, the investigation at high and low order temperatures is necessary to find the stability of such composite for device application. In one of our studies of BFO and CFO where we can measure the ferroelectric polarization at low temperature, it shows enhancement in ferroelectric properties as the temperature is lowered where the system holds its ferroelectric qualities up to the temperature of 150 K. The multiferroic hold potential in photovoltaics and the composite system approach enhanced the optical band gap. Still, a further thorough investigation is required to design composites with strong multiferroic properties that effectively convert absorbed light into electricity (photovoltaic effect), recognize how magnetic and ferroelectric order interact to influence charge transport and light absorption and enhance solar energy conversion efficiency. Additionally, one more key factor will be understanding how to manipulate the interface between different components within the composite to achieve strong connection between the ferroelectric and magnetic order. Unfortunately, additional investigation of these multiferroic composites is obstructed by limitations in currently available instrumentation. Our lack of ability to precisely investigate the properties of the materials at the microscopic level is restricted by the absence of advanced equipment. This result lacks of crucial details about the interplay between magnetic and ferroelectric order, which are believed to be key to their functionalities. Further understanding of this information could lead to breakthroughs in the development of energy-efficient devices for application in multifunctional electronic, magnetic and photovoltaics.

References -

[1] J. Wu, Z. Fan, D. Xiao, J. Zhu, and J. Wang, "Multiferroic bismuth ferrite-based materials for multifunctional applications: Ceramic bulks, thin films and nanostructures," Prog Mater Sci, vol. 84, pp. 335–402, Dec. 2016, doi: 10.1016/J.PMATSCI.2016.09.001.

[2] H. Schmid, "Multi-ferroic magnetoelectrics," http://dx.doi.org/10.1080/00150199408245120, vol. 162, no. 1, pp. 317–338, Jan. 2011, doi: 10.1080/00150199408245120.

[3] N. A. Spaldin and R. Ramesh, "Advances in magnetoelectric multiferroics," Mar. 01, 2019, Nature Publishing Group. doi: 10.1038/s41563-018-0275-2.

[4] H. Liu and X. Yang, "A brief review on perovskite multiferroics," Ferroelectrics, vol. 507, no. 1, pp. 69–85, Jan. 2017, doi: 10.1080/00150193.2017.1283171.

[5] J. A. Quintana-Cilleruelo et al., "Ceramic processing and multiferroic properties of the perovskite YMnO3-BiFeO3 binary system," Journal of the American Ceramic Society, vol. 103, no. 9, pp. 4846–4858, Sep. 2020, doi: 10.1111/JACE.17211.

[6] Y. Selmani, M. Mouatassime, F. Goumrhar, H. Labrim, L. Bahmad, and A. Benyoussef, "Structural, electronic and magnetic properties of the perovskite Ymno3," Solid State Commun, vol. 328, p. 114254, Apr. 2021, doi: 10.1016/J.SSC.2021.114254.

[7] E. Montanari et al., "High-Temperature Polymorphism in Metastable BiMnO3," ACS Publications, vol. 17, no. 25, pp. 6457–6467, Dec. 2005, doi: 10.1021/cm051576w.

[8] V. M. Goldschmidt, "Die Gesetze der Krystallochemie," Naturwissenschaften, vol. 14, no. 21, pp. 477–485, May 1926, doi: 10.1007/BF01507527.

[9] M. Fiebig, T. Lottermoser, D. Meier, and M. Trassin, "The evolution of multiferroics," Jul. 05, 2016, Nature Publishing Group. doi: 10.1038/natrevmats.2016.46.

[10] G. Catalan and J. F. Scott, "Physics and Applications of Bismuth Ferrite," Advanced Materials, vol. 21, no. 24, pp. 2463–2485, Jun. 2009, doi: 10.1002/ADMA.200802849.

[11] S. Hanif et al., "Structural, magnetic, dielectric and bonding properties of BiMnO3 grown by co-precipitation technique," Results Phys, vol. 7, pp. 3190–3195, 2017, doi: 10.1016/j.rinp.2017.08.061.

[12] R. V. Shpanchenko et al., "Synthesis, structure, and properties of new perovskite PbVO3," Chemistry of Materials, vol. 16, no. 17, pp. 3267–3273, Aug. 2004, doi: 10.1021/cm049310x.

[13] M. Fiebig, T. Lottermoser, D. Meier, and M. Trassin, "The evolution of multiferroics," Jul. 05, 2016, Nature Publishing Group. doi: 10.1038/natrevmats.2016.46.

[14] P. Saxena and A. Mishra, "Structural and electrical properties of YMnO3 manganites: Influence of Cr ion doping," J Solid State Chem, vol. 301, p. 122364, Sep. 2021, doi: 10.1016/J.JSSC.2021.122364.

[15] C. Ederer and N. A. Spaldin, “Origin of ferroelectricity in the multiferroic barium fluorides BaMF4: a first principles study,” Phys. Rev., vol. 74, no. 2, p. 024102, 2006, doi: 10.1103/physrevb.74.024102.

[16] A. Chrétien and M. Samouël, “Magnetic properties of compounds BaMF4 and Pb2MF6 (M = Mn, Fe, Co, Ni, Cu, Zn),” Monatsh. Chem., vol. 103, no. 1, pp. 17–23, Jan. 1972, doi: 10.1007/bf00912925.

[17] J. M. Posse, K. Friese, and A. Grzechnik, “Structural stability of BaMF4 (M = Mg, Zn and Mn) at high pressures,” Journal of Physics: Condensed Matter, vol. 23, no. 21, p. 215401, May 2011, doi: 10.1088/0953-8984/23/21/215401.

[18] J. Van Den Brink and D. I. Khomskii, “Multiferroicity due to charge ordering,” Journal of Physics Condensed Matter, vol. 20, no. 43, Oct. 2008, doi: 10.1088/0953-8984/20/43/434217.

[19] Y. J. Kim, S. Konishi, Y. Hayasaka, I. Kakeya, and K. Tanaka, “Magnetic and electrical properties of LuFe2O4 epitaxial thin films with a self-assembled interface structure,” CrystEngComm, vol. 22, no. 6, pp. 1096–1105, Feb. 2020, doi: 10.1039/C9CE01666J.

[20] N. Wang et al., “Structure, Performance, and Application of BiFeO3 Nanomaterials,” Mar. 01, 2020, Springer. doi: 10.1007/s40820-020-00420-6.

[21] V. V. Jadhav et al., “Mixed-phase bismuth ferrite nanoflake electrodes for supercapacitor application,” Applied Nanoscience (Switzerland), vol. 6, no. 4, pp. 511–519, Apr. 2016, doi: 10.1007/s13204-015-0469-8.

[22] S. Ulag et al., “Fabrication of three-dimensional PCL/BiFeO3 scaffolds for biomedical applications,” Mater Sci Eng B Solid State Mater Adv Technol, vol. 261, Nov. 2020, doi: 10.1016/j.mseb.2020.114660.

[23] N. Saikia, R. Chakravarty, S. Bhattacharjee, R. L. Hota, R. K. Parida, and B. N. Parida, “Synthesis and characterization of Gd-doped LaFeO3 for device application,” Mater Sci Semicond Process, vol. 151, Nov. 2022, doi: 10.1016/j.mssp.2022.106969.

[24] Arti, S. Kumar, P. Kumar, R. Walia, and V. Verma, “Improved ferroelectric, magnetic and photovoltaic properties of Pr doped multiferroic bismuth ferrites for photovoltaic application,” Results Phys, vol. 14, p. 102403, Sep. 2019, doi: 10.1016/J.RINP.2019.102403.

[25] M. A. Shahbazi et al., “The versatile biomedical applications of bismuth-based nanoparticles and composites: Therapeutic, diagnostic, biosensing, and regenerative properties,” Feb. 21, 2020, Royal Society of Chemistry. doi: 10.1039/c9cs00283a.

[26] S. Liu et al., “Enhanced microwave absorbing properties of La-modified Bi5Co0.5Fe0.5Ti3O15 multiferroics,” Journal of Materials Science: Materials in Electronics, vol. 30, no. 16, pp. 15619–15626, Aug. 2019, doi: 10.1007/s10854-019-01940-7.

[27] T. Dhiman, C. Singh, M. Puri, H. Kaur, R. Kaur, and S. Bindra Narang, “Microwave characterization of Pb1−xCaxFe0.5Nb0.5O3 multiferroics at X-band,” European Physical Journal B, vol. 88, no. 10, Oct. 2015, doi: 10.1140/epjb/e2015-60527-1.

[28] Y. Q. Kang, M. S. Cao, J. Yuan, and X. L. Shi, “Microwave absorption properties of multiferroic BiFeO3 nanoparticles,” Mater Lett, vol. 63, no. 15, pp. 1344–1346, Jun. 2009, doi: 10.1016/j.matlet.2009.03.010.

[29] S. N. A. Rusly, I. Ismail, K. A. Matori, Z. Abbas, A. H. Shaari, and I. R. Ibrahim, “A Study of Multiferroic BiFeO3/Epoxy Resin Composite as Potential Coating Materials for Microwave Absorption,” Solid State Phenomena, vol. 307, pp. 20–25, 2020, doi: 10.4028/WWW.SCIENTIFIC.NET/SSP.307.20.

[30] Y. Xiong et al., “Effect of Bi1-xCaxFeO3 on microstructure, microwave absorption and magnetic properties,” J Magn Magn Mater, vol. 562, p. 169846, Nov. 2022, doi: 10.1016/J.JMMM.2022.169846.

[31] Y. Q. Kang, M. S. Cao, J. Yuan, and X. L. Shi, “Microwave absorption properties of multiferroic BiFeO3 nanoparticles,” Mater Lett, vol. 63, no. 15, pp. 1344–1346, Jun. 2009, doi: 10.1016/J.MATLET.2009.03.010.

[32] P. Harshapriya, P. Kaur, and D. Basandrai, “Synthesis and characterization of BFO/BTO/ZnO nanocomposites for promising EMI shielding applications,” Inorg Chem Commun, vol. 156, Oct. 2023, doi: 10.1016/j.inoche.2023.111186.

[33] P. Kaur et al., “Composites of Co-Ti-Mn substituted M-type barium hexaferrite and CuO: Structural, optical, electromagnetic and X-band absorption for commercial applications,” J Magn Magn Mater, vol. 588, Dec. 2023, doi: 10.1016/j.jmmm.2023.171402.

[34] P. Harshapriya, P. Kaur, and D. Basandrai, “Influence of La-Ag substitution on structural, magnetic, optical, and microwave absorption properties of BiFeO3 multiferroics,” Chinese Journal of Physics, vol. 84, pp. 119–131, Aug. 2023, doi: 10.1016/j.cjph.2023.03.021.

[35] M. Chauhan, E. Arya, Vibha, A. Kumari, S. Sanghi, and A. Agarwal, “Structural, magnetic, dielectric, magneto-electric and ferroelectric properties of BaTiO3- NiFe2O4 multiferroics,” J Alloys Compd, vol. 965, p. 171360, Nov. 2023, doi: 10.1016/J.JALLCOM.2023.171360.

[36] D. Chauhan, S. K. Pradhan, S. N. Das, and S. Bhuyan, “Electrical characteristics of multiferroic BiFeO3 electronic system,” Mater Today Proc, vol. 74, pp. 659–662, Jan. 2023, doi: 10.1016/J.MATPR.2022.10.207.

[37] R. Sharma, P. Pahuja, and R. P. Tandon, “Structural, dielectric, ferromagnetic, ferroelectric and ac conductivity studies of the BaTiO3–CoFe1.8Zn0.2O4 multiferroic particulate composites,” Ceram Int, vol. 40, no. 7, pp. 9027–9036, Aug. 2014, doi: 10.1016/J.CERAMINT.2014.01.115.

[38] M. Arshad et al., “Superior energy storage performance and excellent multiferroic properties of BaTi1-xGdxO3 ($0 \leq x \leq 0.06$) ceramics,” Mater Res Bull, vol. 169, p. 112504, Jan. 2024, doi: 10.1016/J.MATERRESBULL.2023.112504.

[39] H. Wang et al., “2D Ferroic Materials for Nonvolatile Memory Applications,” Advanced Materials, 2024, doi: 10.1002/ADMA.202305044.

[40] X. Zhang, B. Liu, J. Huang, X. Cao, … Y. Z. preprint arXiv, and undefined 2023, "Nonvolatile spin field effect transistor based on VSi2N4/Sc2CO2 multiferroic heterostructure," arxiv.org, 2024, Accessed: Apr. 16, 2024. [Online]. Available: https://arxiv.org/abs/2311.03690

[41] S. Kharbanda, N. Dhanda, A. Sun, … A. T.-J. of M., and undefined 2023, "Multiferroic perovskite bismuth ferrite nanostructures: a review on synthesis and applications," Elsevier, Accessed: Apr. 16, 2024. [Online]. Available: https://www.sciencedirect.com/science/article/pii/S0304885323002184

[42] M. M. Vopson, "Fundamentals of Multiferroic Materials and Their Possible Applications," Critical Reviews in Solid State and Materials Sciences, vol. 40, no. 4, pp. 223–250, Jul. 2015, doi: 10.1080/10408436.2014.992584.

[43] X. Zhao, S. Menzel, I. Polian, H. Schmidt, and N. Du, "Review on Resistive Switching Devices Based on Multiferroic BiFeO3," Nanomaterials 2023, Vol. 13, Page 1325, vol. 13, no. 8, p. 1325, Apr. 2023, doi: 10.3390/NANO13081325.

[44] R. Tahir et al., "Multiferroic and ferroelectric phases revealed in 2D Ti3C2Tx MXene film for high performance resistive data storage devices," npj 2D Materials and Applications 2023 7:1, vol. 7, no. 1, pp. 1–8, Feb. 2023, doi: 10.1038/s41699-023-00368-2.

[45] M. M. Vopson, "Fundamentals of Multiferroic Materials and Their Possible Applications," Critical Reviews in Solid State and Materials Sciences, vol. 40, no. 4, pp. 223–250, Jul. 2015, doi: 10.1080/10408436.2014.992584.

[46] R. Gonçalves, A. Larrea, M. S. Sebastian, V. Sebastian, P. Martins, and S. Lanceros-Mendez, "Synthesis and size dependent magnetostrictive response of ferrite nanoparticles and their application in magnetoelectric polymer-based multiferroic sensors," J Mater Chem C Mater, vol. 4, no. 45, pp. 10701–10706, Nov. 2016, doi: 10.1039/C6TC04188D.

[47] O. A. Shilova, T. V. Khamova, G. P. Kopitsa, and M. M. Sychov, "Synthesis and study of multiferroic and ferroelectric 'core-shell' powders for application in electronic devices for medicine and ecology," Biocompatible Hybrid Oxide Nanoparticles for Human Health: From Synthesis to Applications, pp. 183–207, Jan. 2019, doi: 10.1016/B978-0-12-815875-3.00010-2.

[48] B. N. Rao, P. Kaviraj, S. R. Vaibavi, A. Kumar, S. K. Bajpai, and A. Arockiarajan, "Investigation of magnetoelectric properties and biocompatibility of CoFe2O4-BaTiO3 core-shell nanoparticles for biomedical applications," J Appl Phys, vol. 122, no. 16, Oct. 2017, doi: 10.1063/1.4993831/149600.

[49] N. D. Ferson, A. M. Uhl, and J. S. Andrew, "Piezoelectric and Magnetoelectric Scaffolds for Tissue Regeneration and Biomedicine: A Review," IEEE Trans Ultrason Ferroelectr Freq Control, vol. 68, no. 2, pp. 229–241, Feb. 2021, doi: 10.1109/TUFFC.2020.3020283.

[50] A. Amirov, “Multiferroic, magnetic, and magnetoelectric nanomaterials for medical applications,” Magnetic Materials and Technologies for Medical Applications, pp. 469–484, Jan. 2022, doi: 10.1016/B978-0-12-822532-5.00003-0.

[51] M. A. Ahmed, E. Dhahri, S. I. El-Dek, and M. S. Ayoub, “Size confinement and magnetization improvement by La3+ doping in BiFeO3 quantum dots,” Solid State Sci, vol. 20, pp. 23–28, 2013, doi: 10.1016/j.solidstatesciences.2013.02.023.

[52] U. Khan et al., “Influence of cobalt doping on structural and magnetic properties of BiFeO3 nanoparticles,” Journal of Nanoparticle Research, vol. 17, no. 11, pp. 1–9, Nov. 2015, doi: 10.1007/S11051-015-3233-9.

[53] G. Wang, S. Nie, J. Sun, S. Wang, and Q. Deng, “Effects of Zr4+ doping on structure, magnetic and optical properties of Bi2Fe4O9 powders,” Journal of Materials Science: Materials in Electronics, vol. 27, no. 9, pp. 9417–9422, Sep. 2016, doi: 10.1007/s10854-016-4987-2.

[54] S. Hait, S. Ghose, and K. Mandal, “Effect of Ba and Y co-doping on the structural and magneto-electric properties of BiFeO3 ceramic,” J Alloys Compd, vol. 822, May 2020, doi: 10.1016/j.jallcom.2019.153614.

[55] S. Godara and B. Kumar, “Effect of Ba-Nb co-doping on the structural, dielectric, magnetic and ferroelectric properties of BiFeO3 nanoparticles,” Ceram Int, vol. 41, no. 5, pp. 6912–6919, Jun. 2015, doi: 10.1016/j.ceramint.2015.01.145.

[56] J. Jiang et al., “The Doping of Alkali Metal for Halide Perovskites,” ES Materials & Manufacturing, 2019, doi: 10.30919/ESMM5F705.

[57] K. P. Remya, R. Rajalakshmi, and N. Ponpandian, “Development of BiFeO3/MnFe2O4ferrite nanocomposites with enhanced magnetic and electrical properties,” Nanoscale Adv, vol. 2, no. 7, pp. 2968–2976, Jul. 2020, doi: 10.1039/d0na00255k.

[58] J. D. Bobić et al., “PZT-nickel ferrite and PZT-cobalt ferrite comparative study: Structural, dielectric, ferroelectric and magnetic properties of composite ceramics,” Ceram Int, vol. 44, no. 6, pp. 6551–6557, Apr. 2018, doi: 10.1016/j.ceramint.2018.01.057.

[59] Y. Tokunaga, N. Furukawa, H. Sakai, Y. Taguchi, T. H. Arima, and Y. Tokura, “Composite domain walls in a multiferroic perovskite ferrite,” Nat Mater, vol. 8, no. 7, pp. 558–562, 2009, doi: 10.1038/nmat2469.

[60] S. V. Baryshnikov, E. V. Charnaya, A. Y. Milinskii, A. A. Antonov, and A. S. Bugaev, “Phase transitions in the (BaTiO3)x/(BiFeO3)1-x composite ceramics: Dielectric studies,” Compos B Eng, vol. 80, pp. 15–19, Jun. 2015, doi: 10.1016/j.compositesb.2015.05.037.

[61] T. Murtaza, M. S. Khan, J. Ali, T. Hussain, and K. Asokan, “Structural, electrical and magnetic properties of multiferroic NdFeO3–SrTiO3 composites,” Journal of Materials Science: Materials in Electronics, vol. 29, no. 21, pp. 18573–18580, Nov. 2018, doi: 10.1007/s10854-018-9975-2.

[62] Z. Li, J. Dai, C. Cheng, W. Feng, and Q. Wang, “Tailoring photocatalytic activity and magnetic properties of BiFeO3/CeO2/Bi2Fe4O9 composites,” Journal of Physics and Chemistry of Solids, vol. 156, Sep. 2021, doi: 10.1016/j.jpcs.2021.110171.

[63] R. Grigalaitis et al., “Dielectric and magnetic properties of BaTiO3 -NiFe 2O4 multiferroic composites,” Ceram Int, vol. 40, no. 4, pp. 6165–6170, May 2014, doi: 10.1016/j.ceramint.2013.11.069.

[64] B. Dhanalakshmi, P. Kollu, B. Parvatheeswara Rao, and P. S. V. S. Rao, “Impedance spectroscopy and dielectric properties of multiferroic BiFeO3/Bi0.95Mn0.05FeO3-Ni0.5Zn0.5Fe2O4 composites,” Ceram Int, vol. 42, no. 2, pp. 2186–2197, Feb. 2016, doi: 10.1016/j.ceramint.2015.10.005.

[65] S. Jauhar, J. Kaur, A. Goyal, and S. Singhal, “Tuning the properties of cobalt ferrite: a road towards diverse applications,” RSC Adv, vol. 6, no. 100, pp. 97694–97719, Oct. 2016, doi: 10.1039/C6RA21224G.

[66] S. Amiri and H. Shokrollahi, “The role of cobalt ferrite magnetic nanoparticles in medical science,” Materials Science and Engineering: C, vol. 33, no. 1, pp. 1–8, Jan. 2013, doi: 10.1016/J.MSEC.2012.09.003.

[67] M. Sajjia, M. Oubaha, M. Hasanuzzaman, and A. G. Olabi, “Developments of cobalt ferrite nanoparticles prepared by the sol–gel process,” Ceram Int, vol. 40, no. 1, pp. 1147–1154, Jan. 2014, doi: 10.1016/J.CERAMINT.2013.06.116.

[68] M. Madhukara Naik, H. S. Bhojya Naik, G. Nagaraju, M. Vinuth, K. Vinu, and R. Viswanath, “Green synthesis of zinc doped cobalt ferrite nanoparticles: Structural, optical, photocatalytic and antibacterial studies,” Nano-Structures & Nano-Objects, vol. 19, p. 100322, Jul. 2019, doi: 10.1016/J.NANOSO.2019.100322.

[69] S. Kour and R. Mukherjee, “Effect of TiO2 as Filler in NaCl: Possible Applications in Ionic Storage Systems,” J Phys Conf Ser, vol. 2267, no. 1, p. 012092, May 2022, doi: 10.1088/1742-6596/2267/1/012092.

[70] I. S. Elashmawi, “Effect of NaCl filler on ferroelectric phase and polaron configurations of PVDF films,” Crystal Research and Technology, vol. 42, no. 4, pp. 389–393, Apr. 2007, doi: 10.1002/CRAT.200610833.

[71] D. K. Sharma, S. Shukla, K. K. Sharma, and V. Kumar, “A review on ZnO: Fundamental properties and applications,” Mater Today Proc, vol. 49, pp. 3028–3035, Jan. 2022, doi: 10.1016/J.MATPR.2020.10.238.

[72] J. J. Beltrán, C. A. Barrero, and A. Punnoose, “Understanding the role of iron in the magnetism of Fe doped ZnO nanoparticles,” Physical Chemistry Chemical Physics, vol. 17, no. 23, pp. 15284–15296, Jun. 2015, doi: 10.1039/C5CP01408E.

[73] A. C. Janaki, E. Sailatha, and S. Gunasekaran, “Synthesis, characteristics and antimicrobial activity of ZnO nanoparticles,” Spectrochim Acta A Mol Biomol Spectrosc, vol. 144, pp. 17–22, Jun. 2015, doi: 10.1016/J.SAA.2015.02.041.

[74] M. Kahouli, A. Barhoumi, A. Bouzid, A. Al-Hajry, and S. Guermazi, “Structural and optical properties of ZnO nanoparticles prepared by direct precipitation method,”

Superlattices Microstruct, vol. 85, pp. 7–23, Sep. 2015, doi: 10.1016/J.SPMI.2015.05.007.

[75] S. Dabas, M. Kumar, D. V. Singh, V. Chaudhary, and S. Sharma, "Progress in Multiferroic and Magnetoelectric Materials for Emerging Technologies in Next Generation Sensing Devices," J Electrochem Soc, vol. 172, no. 2, p. 027512, Feb. 2025, doi: 10.1149/1945-7111/ADB4A8.

[76] S. Ahmed et al., "Investigations of the microstructural and magnetoelectric properties of (1-x)PbZr0.52Ti0.48O3+(x)NiFe2O4 multiferroic composites," Phys Scr, vol. 100, no. 6, Jun. 2025, doi: 10.1088/1402-4896/ADD2A3.

[77] D. Bochenek, P. Niemiec, D. Brzezińska, G. Dercz, and M. Wąs, "Electrophysical Properties of the Three-Component Multiferroic Ceramic Composites," Materials, vol. 17, no. 1, Jan. 2024, doi: 10.3390/ma17010049.

[78] H. Ao et al., "Influence of volume fraction on magnetodielectric effect in CoFe2O4–Ba0.8Sr0.2TiO3 multiferroic fluids," Appl Phys A Mater Sci Process, vol. 130, no. 3, Mar. 2024, doi: 10.1007/s00339-024-07322-z.

[79] Y. Xu, C. Deng, and X. Wang, "Bandgap modulation and phase boundary region of multiferroic Gd, Co co-doped BiFeO3 thin film," AIP Adv, vol. 13, no. 11, Nov. 2023, doi: 10.1063/5.0176617.

[80] M. Yao et al., "Great multiferroic properties in BiFeO3/BaTiO3system with composite-like structure," Appl Phys Lett, vol. 122, no. 15, Apr. 2023, doi: 10.1063/5.0139017.

[81] S. Sharma, A. Kumar, and O. P. Thakur, "Investigations on structural, magnetic, and dielectric properties of Gd-substituted perovskite BiFeO3 multiferroics," Journal of Materials Science: Materials in Electronics, vol. 34, no. 30, Oct. 2023, doi: 10.1007/s10854-023-11464-w.

[82] W. Ben Taazayet, I. M. Zouari, N. Hosni, B. Dkhil, and N. T. Mliki, "Facile synthesis of pure BiFeO3 and Bi2Fe4O9 nanostructures with enhanced photocatalytic activity," Journal of Materials Science: Materials in Electronics, vol. 33, no. 5, pp. 2518–2533, Feb. 2022, doi: 10.1007/s10854-021-07459-0.

[83] A. Mahajan et al., "Effect of processing on the structures and properties of bismuth sodium titanate compounds," J Mater Res, vol. 36, no. 5, pp. 1195–1205, Mar. 2021, doi: 10.1557/s43578-020-00040-1.

[84] R. Verma et al., "Effect of calcination temperature on structural and morphological properties of bismuth ferrite nanoparticles," Ceram Int, vol. 47, no. 3, pp. 3680–3691, Feb. 2021, doi: 10.1016/j.ceramint.2020.09.220.

[85] P. Suresh, B. K. Hazra, B. R. Kumar, T. Chakraborty, P. D. Babu, and S. Srinath, "Lattice effects on the multiferroic characteristics of (La, Ho) co-substituted BiFeO3," J Alloys Compd, vol. 863, May 2021, doi: 10.1016/j.jallcom.2021.158719.

[86] B. Khan et al., "Structural, dielectric, magnetic and magneto-dielectric properties of (1 − x)BiFeO3–(x)CaTiO3 composites," Journal of Materials Science: Materials in

Electronics, vol. 32, no. 13, pp. 18012–18027, Jul. 2021, doi: 10.1007/s10854-021-06344-0.

[87] M. Siddique, N. M. Khan, and M. Saeed, "Photocatalytic Activity of Bismuth Ferrite Nanoparticles Synthesized via Sol-Gel Route," Zeitschrift fur Physikalische Chemie, vol. 233, no. 5, pp. 595–607, May 2019, doi: 10.1515/zpch-2018-1225.

[88] J. Camargo, A. Prado Espinosa, F. Zabotto, L. Ramajo, and M. Castro, "Magnetoelectric interactions in bismuth sodium-potassium titanate-nickel cobalt ferrite lead-free composite ceramics," J Alloys Compd, vol. 826, Jun. 2020, doi: 10.1016/j.jallcom.2020.154129.

[89] D. Zheng et al., "Modified multiferroic properties in narrow bandgap (1-x)BaTiO3-xBaNb1/3Cr2/3O3-δ ceramics," Ceram Int, vol. 46, no. 17, pp. 26823–26828, Dec. 2020, doi: 10.1016/J.CERAMINT.2020.07.158.

[90] S. Sharma, R. K. Dwivedi, J. M. Siqueiros, and O. Raymond Herrera, "Coexistence of two ferroelectric phases and improved room-temperature multiferroic properties in the (0.70)BiFe1 - XCoxO3-(0.30)PbTiO3system," J Appl Phys, vol. 128, no. 12, Sep. 2020, doi: 10.1063/5.0019764.

[91] M. M. Rhaman, M. A. Matin, M. N. Hossain, M. N. I. Khan, M. A. Hakim, and M. F. Islam, "Ferromagnetic, electric, and ferroelectric properties of samarium and cobalt co-doped bismuth ferrite nanoparticles," Journal of Physics and Chemistry of Solids, vol. 147, Dec. 2020, doi: 10.1016/j.jpcs.2020.109607.

[92] N. Wang et al., "Structure, Performance, and Application of BiFeO3 Nanomaterials," Mar. 01, 2020, Springer. doi: 10.1007/s40820-020-00420-6.

[93] M. M. Rhaman et al., "Enhanced electrical conductivity and multiferroic property of cobalt-doped bismuth ferrite nanoparticles," Journal of Materials Science: Materials in Electronics, vol. 31, no. 11, pp. 8727–8736, Jun. 2020, doi: 10.1007/s10854-020-03407-6.

[94] P. Shen et al., "Structure and electrical properties of Zn-doped BiFeO3 films," Int J Appl Ceram Technol, vol. 17, no. 3, pp. 1392–1399, May 2020, doi: 10.1111/ijac.13433.

[95] T. F. Cao, J. Q. Dai, and X. W. Wang, "Physical properties of Al doped BiFeO3 obtained by sol-gel route and two-step sintering process," Ceram Int, vol. 46, no. 6, pp. 7954–7960, Apr. 2020, doi: 10.1016/j.ceramint.2019.12.016.

[96] C. Song et al., "Magnetic and ferroelectric properties of Indium-doped gallium ferrite," J Magn Magn Mater, vol. 469, pp. 8–12, Jan. 2019, doi: 10.1016/j.jmmm.2018.08.032.

[97] J. Peng et al., "The interplay of phases, structural disorder and dielectric behavior in Al doped BiFeO3-BaTiO3 ceramics," J Alloys Compd, vol. 796, pp. 221–228, Aug. 2019, doi: 10.1016/j.jallcom.2019.05.015.

[98] H. Merina Albert, "SYNTHESIS AND CHARACTERIZATION OF BISMUTH FERRITE NANOPARTICLES."

[99] A. Bismibanu, P. R. Vanga, T. Selvalakshmi, M. Ashok, and M. Alagar, “Investigations on Structural, Optical and Multiferroic Properties of Bismuth Ferrite Nanoparticles Synthesized by Sonochemical Method,” J Electron Mater, vol. 47, no. 11, pp. 6373–6377, Nov. 2018, doi: 10.1007/s11664-018-6581-2.

[100] V. M. Gaikwad and S. A. Acharya, “Perovskite-spinel composite approach to modify room temperature structural, magnetic and dielectric behavior of BiFeO3,” J Alloys Compd, vol. 695, pp. 3689–3703, 2017, doi: 10.1016/j.jallcom.2016.11.367.

[101] H. Liu and X. Yang, “A brief review on perovskite multiferroics,” Ferroelectrics, vol. 507, no. 1, pp. 69–85, Jan. 2017, doi: 10.1080/00150193.2017.1283171.

[102] H. Wu and X. Zhu, “Microstructures, magnetic, and dielectric properties of Ba-doped BiFeO3 nanoparticles synthesized via molten salt route,” Journal of the American Ceramic Society, vol. 102, no. 8, pp. 4698–4709, Aug. 2019, doi: 10.1111/jace.16348.

[103] M. M. El-Desoky, M. S. Ayoua, M. M. Mostafa, and M. A. Ahmed, “Multiferroic properties of nanostructured barium doped bismuth ferrite,” J Magn Magn Mater, vol. 404, pp. 68–73, Apr. 2016, doi: 10.1016/J.JMMM.2015.12.020.

[104] L. Wang et al., “Synthesis of BiFeO3 nanoparticles by a low-heating temperature solid-state precursor method,” Mater Res Bull, vol. 48, no. 2, pp. 383–388, Feb. 2013, doi: 10.1016/j.materresbull.2012.10.038.

[105] R. Wongmaneerung, P. Jantaratana, R. Yimnirun, and S. Ananta, “Phase formation and magnetic properties of bismuth ferrite-lead titanate multiferroic composites,” J Supercond Nov Magn, vol. 26, no. 2, pp. 371–379, Feb. 2013, doi: 10.1007/s10948-012-1733-8.

[106] C. Lan, Y. Jiang, and S. Yang, “Magnetic properties of la and (La, Zr) doped BiFeO3 ceramics,” J Mater Sci, vol. 46, no. 3, pp. 734–738, Feb. 2011, doi: 10.1007/s10853-010-4805-9.

[107] Y. Wang, Y. Hu, L. Fei, Y. Zhang, J. Yuan, and H. Gu, “Synthesis of bismuth ferrite nanoparticles via a wet chemical route at low temperature,” J Nanomater, vol. 2011, 2011, doi: 10.1155/2011/797639.

[108] Y. Wang, Y. Hu, L. Fei, Y. Zhang, J. Yuan, and H. Gu, “Synthesis of bismuth ferrite nanoparticles via a wet chemical route at low temperature,” J Nanomater, vol. 2011, 2011, doi: 10.1155/2011/797639.

[109] K. Osińska, A. Lisińska-Czekaj, H. Bernard, J. Dzik, and D. Czekaj, “Dielectric properties of bismuth ferrite - Bismuth titanate ceramic composite,” in Archives of Metallurgy and Materials, 2011, pp. 1093–1104. doi: 10.2478/v10172-011-0122-9.

[110] N. A. Spaldin, S. W. Cheong, and R. Ramesh, “Multiferroics: Past, present, and future,” Phys Today, vol. 63, no. 10, pp. 38–43, Oct. 2010, doi: 10.1063/1.3502547.

[111] S. Ghosh, S. Dasgupta, A. Sen, and H. S. Maiti, “Low temperature synthesis of bismuth ferrite nanoparticles by a ferrioxalate precursor method,” Mater Res Bull, vol. 40, no. 12, pp. 2073–2079, Dec. 2005, doi: 10.1016/j.materresbull.2005.07.017.

[112] N. Ramadass, “ABOa-Type Oxides-Their Structure and Properties-A Bird’s Eye View.”

[113] C. Li et al., “Emerging alkali metal ion (Li+, Na+, K+ and Rb+) doped perovskite films for efficient solar cells: Recent advances and prospects,” J Mater Chem A Mater, vol. 7, no. 42, pp. 24150–24163, 2019, doi: 10.1039/C9TA08130E.

[114] M. Valant, A. Axelsson, N. A.-C. of Materials, and undefined 2007, “Peculiarities of a Solid-State Synthesis of Multiferroic Polycrystalline BiFeO3,” ACS Publications, Accessed: Apr. 04, 2023. [Online]. Available: https://pubs.acs.org/doi/abs/10.1021/cm071730+

[115] C. Cherpin, D. Lister, F. Dacquait, and L. Liu, “Study of the solid-state synthesis of nickel ferrite (NiFe2O4) by X-ray diffraction (XRD), scanning electron microscopy (SEM) and raman spectroscopy,” Materials, vol. 14, no. 10, May 2021, doi: 10.3390/ma14102557.

[116] J. D. Mackenzie, “Applications of the sol-gel process,” J Non Cryst Solids, vol. 100, no. 1–3, pp. 162–168, Mar. 1988, doi: 10.1016/0022-3093(88)90013-0.

[117] A. Dehghanghadikolaei, J. Ansary, and R. Ghoreishi, “Sol-gel process applications: A mini-review Additive manufacturing in industry 4.0 View project Tool wear in high speed machining View project Review View Online Sol-gel process applications: A mini-review,” vol. 2, p. 2008, 2018, doi: 10.11605/j.pnrs.201802008.

[118] S. A. Mhamad, F. Aziz, M. Aziz, S. Chandren, and A. A. Ali, “Rapid Synthesis of Pure Phase Bismuth Ferrite through Modified Sol-gel Auto-ignition Method: Impact of Different Chelating Agents,” ChemistrySelect, vol. 5, no. 43, pp. 13584–13590, Nov. 2020, doi: 10.1002/SLCT.202002827.

[119] S. K. Srivastav and N. S. Gajbhiye, “Low Temperature Synthesis, Structural, Optical and Magnetic Properties of Bismuth Ferrite Nanoparticles,” Journal of the American Ceramic Society, vol. 95, no. 11, pp. 3678–3682, Nov. 2012, doi: 10.1111/J.1551-2916.2012.05411.X.

[120] R. Mahbub et al., “Structural, Dielectric, and Magnetic Properties of Ba-Doped Multiferroic Bismuth Ferrite,” Acta Metallurgica Sinica (English Letters) 2015 28:8, vol. 28, no. 8, pp. 958–964, May 2015, doi: 10.1007/S40195-015-0279-8.

[121] D. Staedler et al., “Cellular uptake and biocompatibility of bismuth ferrite harmonic advanced nanoparticles,” Nanomedicine, vol. 11, no. 4, pp. 815–824, 2015, doi: 10.1016/j.nano.2014.12.018.

[122] V. A. Surdu et al., “Bi1−xeuxfeo3 powders: Synthesis, characterization, magnetic and photoluminescence properties,” Nanomaterials, vol. 9, no. 10, Oct. 2019, doi: 10.3390/nano9101465.

[123] N. A. Spaldin and R. Ramesh, “Advances in magnetoelectric multiferroics,” Mar. 01, 2019, Nature Publishing Group. doi: 10.1038/s41563-018-0275-2.

[124] K. P. Remya, D. Prabhu, R. J. Joseyphus, A. C. Bose, C. Viswanathan, and N. Ponpandian, “Tailoring the morphology and size of perovskite BiFeO3 nanostructures

for enhanced magnetic and electrical properties," Mater Des, vol. 192, Jul. 2020, doi: 10.1016/j.matdes.2020.108694.

[125] T. Hussain, S. A. Siddiqi, S. Atiq, and M. S. Awan, "Induced modifications in the properties of Sr doped BiFeO3 multiferroics," Progress in Natural Science: Materials International, vol. 23, no. 5, pp. 487–492, Oct. 2013, doi: 10.1016/j.pnsc.2013.09.004.

[126] B. Dhanalakshmi, P. Kollu, B. Parvatheeswara Rao, and P. S. V. S. Rao, "Impedance spectroscopy and dielectric properties of multiferroic BiFeO3/Bi0.95Mn0.05FeO3-Ni0.5Zn0.5Fe2O4 composites," Ceram Int, vol. 42, no. 2, pp. 2186–2197, Feb. 2016, doi: 10.1016/J.CERAMINT.2015.10.005.

[127] C. Song et al., "Magnetic and ferroelectric properties of Indium-doped gallium ferrite," JMMM, vol. 469, pp. 8–12, Jan. 2019, doi: 10.1016/J.JMMM.2018.08.032.

[128] W. A. Wani, S. Kundu, K. Ramaswamy, and H. Venkataraman, "Structural, morphological, optical and dielectric investigations in cobalt doped bismuth ferrite nanoceramics prepared using the sol-gel citrate precursor method," J Alloys Compd, vol. 846, Dec. 2020, doi: 10.1016/j.jallcom.2020.156334.

[129] D. Bhadra, M. G. Masud, S. Sarkar, J. Sannigrahi, S. K. De, and B. K. Chaudhuri, "Synthesis of PVDF/BiFeO 3 nanocomposite and observation of enhanced electrical conductivity and low-loss dielectric permittivity at percolation threshold," J Polym Sci B Polym Phys, vol. 50, no. 8, pp. 572–579, Apr. 2012, doi: 10.1002/polb.23041.

[130] H. H. Singh and H. B. Sharma, "Impedance spectroscopy and transport properties of polymer-based flexible nanocomposites," Solid State Commun, vol. 319, p. 114012, Oct. 2020, doi: 10.1016/J.SSC.2020.114012.

[131] W. C. Zheng, D. X. Zheng, Y. C. Wang, D. Li, C. Jin, and H. L. Bai, "Flexible Fe 3 O 4 /BiFeO 3 multiferroic heterostructures with uniaxial strain control of exchange bias," J Magn Magn Mater, vol. 481, pp. 227–233, Jul. 2019, doi: 10.1016/j.jmmm.2019.02.068.

[132] V. Kumar and S. Singh, "Optical and magnetic properties of (1-x)BiFeO3-xCaTiO3 nanoparticles," undefined, vol. 732, pp. 350–357, Jan. 2018, doi: 10.1016/J.JALLCOM.2017.10.236.

[133] Q. Zhang et al., "An etching and re-growth method for the synthesis of bismuth ferrite/MIL-53(Fe) nanocomposite as efficient photocatalyst for selective oxidation of aromatic alcohols," Appl Catal B, vol. 264, May 2020, doi: 10.1016/j.apcatb.2019.118529.

[134] H. Taniguchi, D. Sato, A. Nakano, and I. Terasaki, "Permittivity boosting in 'yellow' (Nb + In) co-doped TiO2," J Mater Chem C Mater, vol. 8, no. 39, pp. 13627–13631, Oct. 2020, doi: 10.1039/d0tc03539d.

[135] M. Kawarasaki, K. Tanabe, I. Terasaki, Y. Fujii, and H. Taniguchi, "Intrinsic Enhancement of Dielectric Permittivity in (Nb + In) co-doped TiO2 single crystals," Scientific Reports 2017 7:1, vol. 7, no. 1, pp. 1–6, Jul. 2017, doi: 10.1038/s41598-017-05651-z.

[136] Z. Tang et al., “Modulations of various alkali metal cations on organometal halide perovskites and their influence on photovoltaic performance,” Nano Energy, vol. 45, pp. 184–192, Mar. 2018, doi: 10.1016/J.NANOEN.2017.12.047.

[137] S. Kour and R. Mukherjee, “Effect of TiO2as Filler in NaCl: Possible Applications in Ionic Storage Systems,” in Journal of Physics: Conference Series, Institute of Physics, Jun. 2022. doi: 10.1088/1742-6596/2267/1/012092.

[138] M. V. Shisode, D. N. Bhoyar, P. P. Khirade, and K. M. Jadhav, “Structural, Microstructural, Magnetic, and Ferroelectric Properties of Ba2 +-Doped BiFeO3 Nanocrystalline Multifferroic Material,” J Supercond Nov Magn, vol. 31, no. 8, pp. 2501–2509, Aug. 2018, doi: 10.1007/s10948-017-4515-5.

[139] A. Mijiti, M. Mamat, F. Xiaerding, Q. Wang, A. Abudurexiti, and L. Aihaiti, “Electron-beam evaporated bismuth ferrite (BiFeO3) thin films and characterization,” Mater Res Express, vol. 8, no. 3, Mar. 2021, doi: 10.1088/2053-1591/abeaba.

[140] M. Sakar, S. Balakumar, P. Saravanan, and S. N. Jaisankar, “Annealing temperature mediated physical properties of bismuth ferrite (BiFeO3) nanostructures synthesized by a novel wet chemical method,” Mater Res Bull, vol. 48, no. 8, pp. 2878–2885, Aug. 2013, doi: 10.1016/j.materresbull.2013.04.008.

[141] J. Article Author et al., “ETH Library Multiferroic bismuth ferrite: Perturbed angular correlation studies on its ferroic α-β phase transition Rights / license: Creative Commons Attribution 4.0 International Multiferroic bismuth ferrite: Perturbed angular correlation studies on its ferroic α-β phase transition,” Phys Rev B, vol. 102, p. 224110, 2020, doi: 10.3929/ethz-b-000463075.

[142] A. Manzoor, S. K. Hasanain, A. Mumtaz, M. F. Bertino, and L. Franzel, “Effects of size and oxygen annealing on the multiferroic behavior of bismuth ferrite nanoparticles,” Journal of Nanoparticle Research 2012 14:12, vol. 14, no. 12, pp. 1–10, Nov. 2012, doi: 10.1007/S11051-012-1310-X.

[143] J. T. Han et al., “Tunable synthesis of bismuth ferrites with various morphologies,” Advanced Materials, vol. 18, no. 16, pp. 2145–2148, Aug. 2006, doi: 10.1002/adma.200600072.

[144] T. Liu, Y. Xu, and C. Zeng, “Synthesis of Bi2Fe4O9 via PVA sol-gel route,” Mater Sci Eng B Solid State Mater Adv Technol, vol. 176, no. 7, pp. 535–539, Apr. 2011, doi: 10.1016/j.mseb.2011.01.009.

[145] T. J. Park, G. C. Papaefthymiou, A. R. Moodenbaugh, Y. Mao, and S. S. Wong, “Synthesis and characterization of submicron single-crystalline Bi 2Fe4O9 cubes,” J Mater Chem, vol. 15, no. 21, pp. 2099–2105, Jun. 2005, doi: 10.1039/b501552a.

[146] Z. Li, J. Dai, C. Cheng, W. Feng, and Q. Wang, “Tailoring photocatalytic activity and magnetic properties of BiFeO3/CeO2/Bi2Fe4O9 composites,” Journal of Physics and Chemistry of Solids, vol. 156, Sep. 2021, doi: 10.1016/J.JPCS.2021.110171.

[147] G. Singh et al., “Magneto-dielectric and multiferroic properties in Bi0.95Yb0.05Fe0.95Co0.05O3,” Phys Scr, vol. 94, no. 6, Apr. 2019, doi: 10.1088/1402-4896/ab03a5.

[148] Ashima, S. Sanghi, A. Agarwal, Reetu, N. Ahlawat, and Monica, "Structure refinement and dielectric relaxation of M-type Ba, Sr, Ba-Sr, and Ba-Pb hexaferrites," J Appl Phys, vol. 112, no. 1, p. 014110, Jul. 2012, doi: 10.1063/1.4734002.

[149] P. Sharma, A. Kumar, T. Jingyou, and G. Tan, "Structural, electrical, and magnetic properties of mullite-type Bi2Fe4O9 ceramic," J Electroceram, vol. 45, no. 4, pp. 148–155, Dec. 2020, doi: 10.1007/s10832-021-00233-y.

[150] M. M. Rhaman et al., "Enhanced electrical conductivity and multiferroic property of cobalt-doped bismuth ferrite nanoparticles," Journal of Materials Science: Materials in Electronics, vol. 31, no. 11, pp. 8727–8736, Jun. 2020, doi: 10.1007/S10854-020-03407-6/TABLES/4.

[151] D. Mishra, B. P. Mandal, R. Mukherjee, R. Naik, G. Lawes, and B. Nadgorny, "Oxygen vacancy enhanced room temperature ferromagnetism in Al-doped MgO nanoparticles."

[152] R. Das, T. Sarkar, and K. Mandal, "Multiferroic properties of Ba2+ and Gd3+ co-doped bismuth ferrite: magnetic, ferroelectric and impedance spectroscopic analysis," J Phys D Appl Phys, vol. 45, no. 45, p. 455002, Oct. 2012, doi: 10.1088/0022-3727/45/45/455002.

[153] B. Neher et al., "Study of the electric properties of palm fiber-reinforced acrylonitrile butadiene styrene composites," Journal of Reinforced Plastics and Composites, vol. 34, no. 15, pp. 1253–1260, Aug. 2015, doi: 10.1177/0731684415591067.

[154] L. F. Lima, A. L. Vieira, H. Mukai, C. M. G. Andrade, and P. R. G. Fernandes, "Electric impedance of aqueous KCl and NaCl solutions: Salt concentration dependence on components of the equivalent electric circuit," J Mol Liq, vol. 241, pp. 530–539, Sep. 2017, doi: 10.1016/j.molliq.2017.06.069.

[155] J. N. Wilson, J. M. Frost, S. K. Wallace, and A. Walsh, "Dielectric and ferroic properties of metal halide perovskites," APL Mater, vol. 7, no. 1, Jan. 2019, doi: 10.1063/1.5079633.

[156] R. Mukherjee, G. Lawes, and B. Nadgorny, "Enhancement of high dielectric permittivity in CaCu3Ti 4O12/RuO2 composites in the vicinity of the percolation threshold," Appl Phys Lett, vol. 105, no. 7, Aug. 2014, doi: 10.1063/1.4893009.

[157] Pritam, A. Arya, and A. L. Sharma, "Dielectric relaxations and transport properties parameter analysis of novel blended solid polymer electrolyte for sodium-ion rechargeable batteries," J Mater Sci, vol. 54, no. 9, pp. 7131–7155, May 2019, doi: 10.1007/s10853-019-03381-3.

[158] H. J. Woo, S. R. Majid, and A. K. Arof, "Dielectric properties and morphology of polymer electrolyte based on poly(ε-caprolactone) and ammonium thiocyanate," Mater Chem Phys, vol. 134, no. 2–3, pp. 755–761, Jun. 2012, doi: 10.1016/j.matchemphys.2012.03.064.

[159] A. Dhahri, E. Dhahri, and E. K. Hlil, "Electrical conductivity and dielectric behaviour of nanocrystalline La0.6Gd0.1Sr0.3Mn0.75Si0.25O3," RSC Adv, vol. 8, no. 17, pp. 9103–9111, 2018, doi: 10.1039/c8ra00037a.

[160] I. G. Austin and N. F. Mott, “Polarons in Crystalline and Non-crystalline Materials,” Adv Phys, vol. 18, no. 71, pp. 41–102, Jan. 1969, doi: 10.1080/00018736900101267.

[161] S. Moharana, M. K. Mishra, M. Chopkar, and R. N. Mahaling, “Enhanced dielectric properties of surface hydroxylated bismuth ferrite–Poly (vinylidene fluoride-co-hexafluoropropylene) composites for energy storage devices,” Journal of Science: Advanced Materials and Devices, vol. 1, no. 4, pp. 461–467, Dec. 2016, doi: 10.1016/j.jsamd.2016.08.008.

[162] K. Funke, “JUMP RELAXATION IN SOLID ELECTROLYTES,” 1993.

[163] C. Tsonos, “Comments on frequency dependent AC conductivity in polymeric materials at low frequency regime,” Current Applied Physics, vol. 19, no. 4, pp. 491–497, Apr. 2019, doi: 10.1016/j.cap.2019.02.001.

[164] G. Chen et al., “Bismuth ferrite materials for solar cells: Current status and prospects,” Mater Res Bull, vol. 110, pp. 39–49, Feb. 2019, doi: 10.1016/J.MATERRESBULL.2018.10.011.

[165] R. Sharma and R. Mukherjee, “Incorporation of Co (x), Al (y) into Bi (0.99) Ba (0.1) Fe (1-x-y) O3 and its effect on the microstructural, magnetic, and dielectric properties,” Mater Today Proc, 2023, doi: 10.1016/j.matpr.2023.03.582.

[166] Y. Li, W. Q. Cao, J. Yuan, D. W. Wang, and M. S. Cao, “Nd doping of bismuth ferrite to tune electromagnetic properties and increase microwave absorption by magnetic-dielectric synergy,” J Mater Chem C Mater, vol. 3, no. 36, pp. 9276–9282, Aug. 2015, doi: 10.1039/c5tc01684c.

[167] B. K. Vashisth et al., “Modified ferroelectric/magnetic and leakage current density properties of Co and Sm co-doped bismuth ferrites,” J Alloys Compd, vol. 698, pp. 699–705, 2017, doi: 10.1016/j.jallcom.2016.12.278.

[168] S. M. Mane, S. A. Pawar, D. S. Patil, S. B. Kulkarni, N. T. Tayade, and J. C. Shin, “Magnetoelectric, magnetodielectric effect and dielectric, magnetic properties of microwave-sintered lead-free x(Co0.9Ni0.1Fe2O4)-(1-x)[0.5(Ba0.7Ca0.3TiO3)-0.5(BaZr0.2Ti0.8O3)] particulate multiferroic composite,” Ceram Int, vol. 46, no. 3, pp. 3311–3323, Feb. 2020, doi: 10.1016/j.ceramint.2019.10.038.

[169] Y. Zhang et al., “Composition and magnetic properties of cobalt ferrite nano-particles prepared by the co-precipitation method,” J Magn Magn Mater, vol. 322, no. 21, pp. 3470–3475, Nov. 2010, doi: 10.1016/j.jmmm.2010.06.047.

[170] P. D. Prasad and J. Hemalatha, “Enhanced dielectric and ferroelectric properties of cobalt ferrite (CoFe2O4) fiber embedded polyvinylidene fluoride (PVDF) multiferroic composite films,” Mater Res Express, vol. 6, no. 9, Jul. 2019, doi: 10.1088/2053-1591/ab30af.

[171] A. Das, S. De, S. Bandyopadhyay, S. Chatterjee, and D. Das, “Magnetic, dielectric and magnetoelectric properties of BiFeO3-CoFe2O4nanocomposites,” J Alloys Compd, vol. 697, pp. 353–360, 2017, doi: 10.1016/j.jallcom.2016.12.128.

[172] K. L. Routray, D. Sanyal, and D. Behera, “Dielectric, magnetic, ferroelectric, and Mossbauer properties of bismuth substituted nanosized cobalt ferrites through glycine nitrate synthesis method,” J Appl Phys, vol. 122, no. 22, Dec. 2017, doi: 10.1063/1.5005169.

[173] K. Kaur, M. Singh, J. Singh, and S. Kumar, “Multiferroic and magnetodielectric properties of (1-x)KNN-xCMgFO ceramic-based composites,” Journal of Asian Ceramic Societies, vol. 8, no. 4, pp. 1027–1035, 2020, doi: 10.1080/21870764.2020.1803534.

[174] H. A. Chinchay-Espino, G. M. Montes-Albino, C. M. Morales-Cruz, S. E. Dobbertin-Sanchez, and S. Rojas-Flores, “Effect of Cobalt Substitution on the Structural and Magnetic Properties of Bismuth Ferrite Powders,” Crystals (Basel), vol. 12, no. 8, Aug. 2022, doi: 10.3390/cryst12081058.

[175] A. J. Shnoudeh et al., “Synthesis, Characterization, and Applications of Metal Nanoparticles,” in Biomaterials and Bionanotechnology, Elsevier, 2019, pp. 527–612. doi: 10.1016/B978-0-12-814427-5.00015-9.

[176] M. Z. Ahsan, F. A. Khan, and M. A. Islam, “Frequency and temperature dependent intrinsic electric properties of manganese doped cobalt ferrite nanoparticles,” Results Phys, vol. 14, Sep. 2019, doi: 10.1016/j.rinp.2019.102484.

[177] S. Banik, K. Das, and I. Das, “Enhancement of the magnetoresistive property by introducing disorder in the (La1−xYx)0.7Ca0.3MnO3 compound,” RSC Adv, vol. 7, no. 27, pp. 16575–16580, 2017, doi: 10.1039/c7ra00744b.

[178] R. Mahbub et al., “Structural, dielectric, and magnetic properties of Ba-doped multiferroic bismuth ferrite,” Acta Metallurgica Sinica (English Letters), vol. 28, no. 8, pp. 958–964, Aug. 2015, doi: 10.1007/s40195-015-0279-8.

[179] W. A. Wani, S. Kundu, K. Ramaswamy, and H. Venkataraman, “Structural, morphological, optical and dielectric investigations in cobalt doped bismuth ferrite nanoceramics prepared using the sol-gel citrate precursor method,” J Alloys Compd, vol. 846, Dec. 2020, doi: 10.1016/j.jallcom.2020.156334.

[180] X. Liu et al., “Nanoparticle geometrical effects on percolation, packing density, and magnetoresistive properties in ferromagnet-superconductor-insulator nanocomposites,” Phys Rev B, vol. 106, no. 22, Dec. 2022, doi: 10.1103/PhysRevB.106.224417.

[181] S. Mane, P. Tirmali, S. Kadam, A. Tarale, C. Kolekar, and S. Kulkarni, “ Dielectric, magnetic, and magnetodielectric properties of x [Co 0.9 Ni 0.1 Fe 2 O 4]-(1− x)[0.5(Ba 0.7 Ca 0.3)TiO 3)-0.5Ba(Zr 0.2 Ti 0.8)O 3] multiferroic composites ,” Journal of the Chinese Advanced Materials Society, vol. 4, no. 4, pp. 269–284, Oct. 2016, doi: 10.1080/22243682.2016.1214924.

[182] R. C. Kambale, P. A. Shaikh, S. S. Kamble, and Y. D. Kolekar, “Effect of cobalt substitution on structural, magnetic and electric properties of nickel ferrite,” J Alloys Compd, vol. 478, no. 1–2, pp. 599–603, Jun. 2009, doi: 10.1016/j.jallcom.2008.11.101.

[183] K. Li, W. Zhang, K. Guo, R. Cui, C. Deng, and X. Wang, “Modulating light absorption and multiferroic properties of BiFeO3-based ferroelectric films by the introduction of

ZnO layer," Mater Res Express, vol. 9, no. 3, Mar. 2022, doi: 10.1088/2053-1591/ac4328.

[184] S. Kour, S. K. Adhikari, M. Palihawadana, and R. Mukherjee, "The Dielectric, Magnetic, and Ferroelectric Analysis of xNi0.5Co0.5Fe2O4:(1 − x)PANI Multiferroic Composites," J Inorg Organomet Polym Mater, Mar. 2023, doi: 10.1007/s10904-023-02602-2.

[185] Y. Zhang, Z. Chen, W. Cao, and Z. Zhang, "Temperature and frequency dependence of the coercive field of 0.71PbMb1/3Nb2/3O3-0.29PbTiO3 relaxor-based ferroelectric single crystal," Appl Phys Lett, vol. 111, no. 17, Oct. 2017, doi: 10.1063/1.4998187.

[186] H. Schmid, "Some symmetry aspects of ferroics and single phase multiferroics*," Journal of Physics: Condensed Matter, vol. 20, no. 43, p. 434201, Oct. 2008, doi: 10.1088/0953-8984/20/43/434201.

[187] T. P. Comyn, D. F. Kanguwe, J. He, and A. P. Brown, "Synthesis of bismuth ferrite lead titanate nano-powders and ceramics using chemical co-precipitation," J Eur Ceram Soc, vol. 28, no. 11, pp. 2233–2238, Jan. 2008, doi: 10.1016/J.JEURCERAMSOC.2008.02.013.

[188] M. K. Sharif et al., "Synthesis and characterization of Zr and Mg doped BiFeO3 nanocrystalline multiferroics via micro emulsion route," J Alloys Compd, vol. 667, pp. 329–340, May 2016, doi: 10.1016/J.JALLCOM.2016.01.184.

[189] K. P. Remya, D. Prabhu, R. J. Joseyphus, A. C. Bose, C. Viswanathan, and N. Ponpandian, "Tailoring the morphology and size of perovskite BiFeO3 nanostructures for enhanced magnetic and electrical properties," Mater Des, vol. 192, Jul. 2020, doi: 10.1016/j.matdes.2020.108694.

[190] H. Liu and X. Yang, "A brief review on perovskite multiferroics," http://dx.doi.org/10.1080/00150193.2017.1283171, vol. 507, no. 1, pp. 69–85, Jan. 2017, doi: 10.1080/00150193.2017.1283171.

[191] G. Dhir, P. Uniyal, and N. K. Verma, "Effect of particle size on multiferroism of barium-doped bismuth ferrite nanoparticles," Mater Sci Semicond Process, vol. 27, no. 1, pp. 611–618, 2014, doi: 10.1016/j.mssp.2014.07.041.

[192] A.-K. A. N. A. M Valant, "Peculiarities of a solid-state synthesis of multiferroic polycrystalline BiFeO3," Chem. Mater., vol. 19, pp. 5431–5436, 2007, doi: 10.1021/cm071730.

[193] A. W. Hull, "A new method of X-ray crystal analysis," Phys. Rev., vol. 10, no. 6, pp. 661–696, 1917, doi: 10.1103/physrev.10.661.

[194] X. Yan, J. Chen, Y. Qi, J. Cheng, and Z. Meng, "Hydrothermal synthesis and characterization of multiferroic Bi1−xLaxFeO3 crystallites," J Eur Ceram Soc, vol. 30, no. 2, pp. 265–269, Jan. 2010, doi: 10.1016/J.JEURCERAMSOC.2009.06.016.

[195] A. Chaudhuri and K. Mandal, "Study of structural, ferromagnetic and ferroelectric properties of nanostructured barium doped Bismuth Ferrite," J Magn Magn Mater, vol. 353, pp. 57–64, 2014, doi: 10.1016/j.jmmm.2013.09.049.

[196] B. Parvatheeswara Rao and K. H. Rao, “Effect of sintering conditions on resistivity and dielectric properties of Ni-Zn ferrites,” Journal of Materials Science 1997 32:22, vol. 32, no. 22, pp. 6049–6054, Nov. 1997, doi: 10.1023/A:1018683615616.

[197] H. Liu and X. Yang, “A brief review on perovskite multiferroics,” Ferroelectrics, vol. 507, no. 1, pp. 69–85, Jan. 2017, doi: 10.1080/00150193.2017.1283171.

[198] Anju, A. Agarwal, P. Aghamkar, V. Singh, O. Singh, and A. Kumar, “Structural transitions and multiferrocity in Ba and Co substituted nanosized bismuth ferrite,” J Alloys Compd, vol. 697, pp. 333–340, 2017, doi: 10.1016/j.jallcom.2016.12.082.

[199] M. M. El-Desoky, M. S. Ayoua, M. M. Mostafa, and M. A. Ahmed, “Multiferroic properties of nanostructured barium doped bismuth ferrite,” J Magn Magn Mater, vol. 404, pp. 68–73, Apr. 2016, doi: 10.1016/j.jmmm.2015.12.020.

[200] R. Das and K. Mandal, “Effect of barium substitution on ferroelectric and magnetic properties of bismuth ferrite,” in IEEE Transactions on Magnetics, Oct. 2011, pp. 4054–4057. doi: 10.1109/TMAG.2011.2159364.

[201] K. V. Kumar, D. Paramesh, and P. V. Reddy, “Effect of Aluminium Doping on Structural and Magnetic Properties of Ni-Zn Ferrite Nanoparticles,” World Journal of Nano Science and Engineering, vol. 05, no. 03, pp. 68–77, 2015, doi: 10.4236/wjnse.2015.53009.

[202] Q. Khan, A. Majeed, N. Ahmad, I. Ahmad, and R. Ahmad, “Structural features and dielectric behavior of Al substituted Cu0.7Ni0.3Fe2O4 ferrites,” Mater Chem Phys, vol. 273, Nov. 2021, doi: 10.1016/j.matchemphys.2021.125028.

[203] T. F. Cao, J. Q. Dai, and X. W. Wang, “Physical properties of Al doped BiFeO3 obtained by sol-gel route and two-step sintering process,” Ceram Int, vol. 46, no. 6, pp. 7954–7960, Apr. 2020, doi: 10.1016/J.CERAMINT.2019.12.016.

[204] P. H. Deepak and B. Pawandeep, “Structural , magnetic , microwave absorption and electromagnetic properties of Y - Ag - doped bismuth ferrite nanoparticles for commercial applications,” Applied Physics A, 2023, doi: 10.1007/s00339-023-06535-y.

[205] H. Maleki, S. Zare, and R. Fathi, “Effect of Nd Substitution on Properties of Multiferroic Bismuth Ferrite Synthesized by Sol-Gel Auto-combustion Method,” J Supercond Nov Magn, vol. 31, no. 8, pp. 2539–2545, 2018, doi: 10.1007/s10948-017-4516-4.

[206] S. Mukherjee, S. Chakraborty, and S. Mukherjee, “A Comparative Study of Pure and Rare Earth Transition Metal Doped Bismuth Ferrite,” pp. 403–408, 2012.

[207] S. Kumari et al., “Evidence of strong magneto-dielectric coupling and enhanced electrical insulation at room temperature in Nd and Mn co-doped bismuth ferrite,” J Appl Phys, vol. 122, no. 14, 2017, doi: 10.1063/1.4994560.

[208] P. Harshapriya, P. Kaur, and D. Basandrai, “Influence of La-Ag substitution on structural , magnetic , optical , and microwave absorption properties of BiFeO 3 multiferroics,” Chinese Journal of Physics, vol. 84, no. February, pp. 119–131, 2023, doi: 10.1016/j.cjph.2023.03.021.

[209] S. G. Nair, J. Satapathy, and N. P. Kumar, “Influence of synthesis, dopants, and structure on electrical properties of bismuth ferrite (BiFeO 3),” Appl Phys A Mater Sci Process, vol. 126, no. 11, pp. 1–14, 2020, doi: 10.1007/s00339-020-04027-x.

[210] L. Thansanga, A. Shukla, N. Kumar, and R. N. P. Choudhary, “Study of effect of Dy substitution on structural, dielectric, impedance and magnetic properties of bismuth ferrite,” Journal of Materials Science: Materials in Electronics, vol. 31, no. 13, pp. 10006–10017, 2020, doi: 10.1007/s10854-020-03545-x.

[211] Y. Li, W. Q. Cao, J. Yuan, D. W. Wang, and M. S. Cao, “Nd doping of bismuth ferrite to tune electromagnetic properties and increase microwave absorption by magnetic-dielectric synergy,” J Mater Chem C Mater, vol. 3, no. 36, pp. 9276–9282, 2015, doi: 10.1039/c5tc01684c.

[212] V. A. Khomchenko et al., “Crystal structure and multiferroic properties of Gd-substituted BiFeO 3,” Appl Phys Lett, vol. 93, no. 26, pp. 1–4, 2008, doi: 10.1063/1.3058708.

[213] Z. Zhou, W. Sun, Z. Liao, S. Ning, J. Zhu, and J. F. Li, “Ferroelectric domains and phase transition of sol-gel processed epitaxial Sm-doped BiFeO3 (001) thin films,” Journal of Materiomics, vol. 4, no. 1, pp. 27–34, 2018, doi: 10.1016/j.jmat.2017.11.002.

[214] J. Sharma, A. Kumar, S. Kumar, and A. K. Srivastava, “Investigation of structural and magnetic properties of Tb–Ni-doped bismuth ferrite nanoparticles by auto-combustion method,” Appl Phys A Mater Sci Process, vol. 123, no. 8, pp. 1–9, 2017, doi: 10.1007/s00339-017-1140-x.

[215] M. V. Shisode, J. S. Kounsalye, A. V. Humbe, R. C. Kambale, and K. M. Jadhav, “Investigations of magnetic and ferroelectric properties of multiferroic Sr-doped bismuth ferrite,” Appl Phys A Mater Sci Process, vol. 124, no. 9, pp. 1–11, 2018, doi: 10.1007/s00339-018-2025-3.

[216] G. D. Hu, X. Cheng, W. B. Wu, and C. H. Yang, “Effects of Gd substitution on structure and ferroelectric properties of BiFe O3 thin films prepared using metal organic decomposition,” Appl Phys Lett, vol. 91, no. 23, pp. 3–6, 2007, doi: 10.1063/1.2822826.

[217] Z. J. Li et al., “Mg-substitution for promoting magnetic and ferroelectric properties of BiFeO3 multiferroic nanoparticles,” Mater Lett, vol. 175, pp. 207–211, 2016, doi: 10.1016/j.matlet.2016.04.016.

[218] R. Das, T. Sarkar, and K. Mandal, “Multiferroic properties of Ba 2+ and Gd 3+ co-doped bismuth ferrite: Magnetic, ferroelectric and impedance spectroscopic analysis,” J Phys D Appl Phys, vol. 45, no. 45, 2012, doi: 10.1088/0022-3727/45/45/455002.

[219] R. Sharma and R. Mukherjee, “Incorporation of Co <inf>(x)</inf>, Al <inf>(y)</inf> into Bi <inf>(0.99)</inf> Ba <inf>(0.1)</inf> Fe <inf>(1-x-y)</inf> O<inf>3</inf> and its effect on the microstructural, magnetic, and dielectric properties,” Mater Today Proc, 2023, doi: 10.1016/j.matpr.2023.03.582.

[220] A. K. Sahu, P. Mallick, S. K. Satpathy, and B. Behera, “Effect on Structural, Electrical and Temperature Sensing behavior of Neodymium Doped Bismuth Ferrite,” Adv Mater Lett, vol. 12, no. 7, pp. 1–7, 2021, doi: 10.5185/amlett.2021.071648.

[221] S. R. Dhanya and J. Satapathy, “Structural, dielectric and impedance analysis of Nd-doped BiFeO3 prepared using solid-state synthesis method,” Journal of Materials Science: Materials in Electronics, vol. 34, no. 5, Feb. 2023, doi: 10.1007/s10854-023-09878-7.

[222] A. Sharma, S. K. Godara, and A. K. Srivastava, “Influence of composition variation on structural, magnetic and dielectric properties of Gd3Fe5O12(x)/MgFe2O4(1−x) composite,” Indian Journal of Physics, vol. 96, no. 14, pp. 4173–4184, Dec. 2022, doi: 10.1007/s12648-022-02365-5.

[223] S. Vats, A. Kumar, S. Kalia, J. Mohammad, and N. Prasad, “Synthesis of bismuth doped cobalt ferrite and its composite with Polyaniline,” in Materials Today: Proceedings, Elsevier Ltd, 2021, pp. 679–682. doi: 10.1016/j.matpr.2021.07.448.

[224] M. ud D. Rather, R. Samad, and B. Want, “Improved magnetoelectric effect in ytterbium doped BaTiO3 –CoFe2O4 particulate multiferroic composites,” J Alloys Compd, vol. 755, pp. 89–99, Jul. 2018, doi: 10.1016/j.jallcom.2018.04.289.

[225] O. Malyshkina, … G. S.-M. E., and undefined 2020, “Effect of sintering temperature on dielectric properties of barium titanate ceramics and composite,” moem.pensoft.net, Accessed: Mar. 29, 2022. [Online]. Available: https://moem.pensoft.net/article_preview.php?id=65576&skip_redirect=1

[226] R. Sharma, P. S. Maji, and R. Mukherjee, “Dielectric and magnetic response of BiFeO3 in the presence of ionic filler at room temperature,” Journal of Materials Science: Materials in Electronics, vol. 35, no. 1, p. 71, Jan. 2024, doi: 10.1007/s10854-023-11773-0.

[227] E. A. Volnistem et al., “Intensifying the photocatalytic degradation of methylene blue by the formation of BiFeO3/Fe3O4 nanointerfaces,” Ceram Int, vol. 46, no. 11, pp. 18768–18777, 2020, doi: 10.1016/j.ceramint.2020.04.194.

[228] S. Martin et al., “Impact of target volume segmentation accuracy and variability on treatment planning for 4D-CT-based non-small cell lung cancer radiotherapy,” Acta Oncol (Madr), vol. 54, no. 3, pp. 322–332, 2015, doi: 10.3109/0284186X.2014.970666.

[229] K. Li, W. Zhang, K. Guo, R. Cui, C. Deng, and X. Wang, “Modulating light absorption and multiferroic properties of BiFeO3-based ferroelectric films by the introduction of ZnO layer,” Mater Res Express, vol. 9, no. 3, 2022, doi: 10.1088/2053-1591/ac4328.

[230] A. Kumari et al., “Role of Bi-excess on structural, electrical, optical, and magnetic properties BiFeO3 nanoparticles,” Journal of Materials Science: Materials in Electronics, vol. 32, no. 19, pp. 23968–23982, Oct. 2021, doi: 10.1007/s10854-021-06860-z.

[231] R. Grigalaitis et al., “Dielectric and magnetic properties of BaTiO3 -NiFe 2O4 multiferroic composites,” Ceram Int, vol. 40, no. 4, pp. 6165–6170, May 2014, doi: 10.1016/j.ceramint.2013.11.069.

[232] A. Jain, A. K. Panwar, A. K. Jha, and Y. Sharma, “Improvement in dielectric, ferroelectric and ferromagnetic characteristics of Ba0.9Sr0.1Zr0.1Ti0.9O3-NiFe2O4

composites," Ceram Int, vol. 43, no. 13, pp. 10253–10262, 2017, doi: 10.1016/j.ceramint.2017.05.053.

[233] S. Sharma, T. T. T. Carol, D. Basandrai, and A. K. Srivastava, "Structural, magnetic, and optical study of La3+–Co2+-substituted Ni2Y-type barium hexaferrites," J Mater Res, vol. 38, no. 8, pp. 2156–2168, Apr. 2023, doi: 10.1557/s43578-023-00946-6.

International conference's

- Participation in International Conference on Advanced Nanostructured Material for Energy Generation, Storage, and Smart Applications.

Agricultural Development Trust's

Shardabai Pawar Mahila Arts, Commerce and Science College, Shardanagar, Baramati.

NAAC Re-Accredited 'A' Grade College Affiliated to Savitribai Phule Pune University.

CERTIFICATE

This is to certify that, *Mr. Rikky Sharma*
from
"Lovely Professional University, Phagwara, Punjab"
has attended
an International Web-Conference organized by Department of Physics on **"Advanced Nanostructured Materials for Energy Generation, Storage and Smart Applications"**
on 09th - 10th October 2020.

Dr. T. P. Gujar, Organizing Secretary | Mr. S. N. Belpatre, Coordinator | Mr. R. B. Deshmukh, Co-Convener | Dr. S. J. Sathe, Convener

Certificate Id.- SPMCANM20_051

- Participated in an International conference on applied sciences by ISSRD.

ISSRD

INTERNATIONAL SOCIETY FOR SCIENTIFIC RESEARCH AND DEVELOPMENT

This is to certify that

Rikky Sharma

has participated in the International Conference on Applied Science Mathematics and Statistics(ICASMS) held in Kharagpur, India on 03rd September, 2021.

ID-ICASMS-KGPR-030921-801L
Listener ID

CHAIRMAN, ISSRD

03rd SEPTEMBER, 2021
CONFERENCE DATE

- Best E-poster Presentation award at International Conference on Advanced Materials for Societal Applications (ICAMSA-2021)

J. C. Bose University of Science and Technology, YMCA, Faridabad

(A HARYANA STATE GOVERNMENT UNIVERSITY)

(Accredited 'A' grade by NAAC)

International Conference

On

Advanced Materials for Societal Applications

(ICAMSA-2021)

Best E-poster Presentation Award

S. No. YMCA/PHY/ICAMSA/PP5

This certificate is awarded to **Rikky Sharma** from **Lovely Professional University** for presenting her paper as **E-poster presentation** on Title **"Investigation of Multiferroic Composite system and Their Possible Application in Electronic Devices and Photovoltaics"** in **International Conference on Advanced Materials for Societal Applications (ICAMSA-2021)** from **26th – 28th October, 2021** organised by **Department of Physics, J. C. Bose University of Science and Technology, YMCA, Faridabad.**

Parmod Kumar
Dr. Parmod Kumar
Organizing Secretary

Dr. Anurag Gaur
Organizing Secretary

ASharma
Dr. Anuradha Sharma
Convenor, ICAMSA-2021

- Oral presentation at the FAS-2021 national conference by NIT Gujrat.

सरदार वल्लभभाई राष्ट्रीय प्रौद्योगिकी संस्थान, सूरत.

Sardar Vallabhbhai National Institute of Technology

Surat-395 007 (Gujarat) INDIA

NATIONAL CONFERENCE on

FUNDAMENTAL & APPLIED SCIENCES (FAS-2021)

Under Institute Diamond Jubilee Celebration

CERTIFICATE

This is to certify that Mr./Mrs./Prof./Dr.

Rikky Sharma

of

Lovely Professional University

has participated and delivered an Oral Presentation in the National Conference on

"FUNDAMENTAL & APPLIED SCIENCES (FAS-2021)"

Organized by Department of Physics, Sardar Vallabhbhai National Institute of Technology, Surat, India In association with Centre for Continuing Education, SVNIT, Surat during October 20 - 21, 2021.

Organizing Secretary

Head of the Department

- Research work presentation at FPMSN-2022 international conference on Physics.

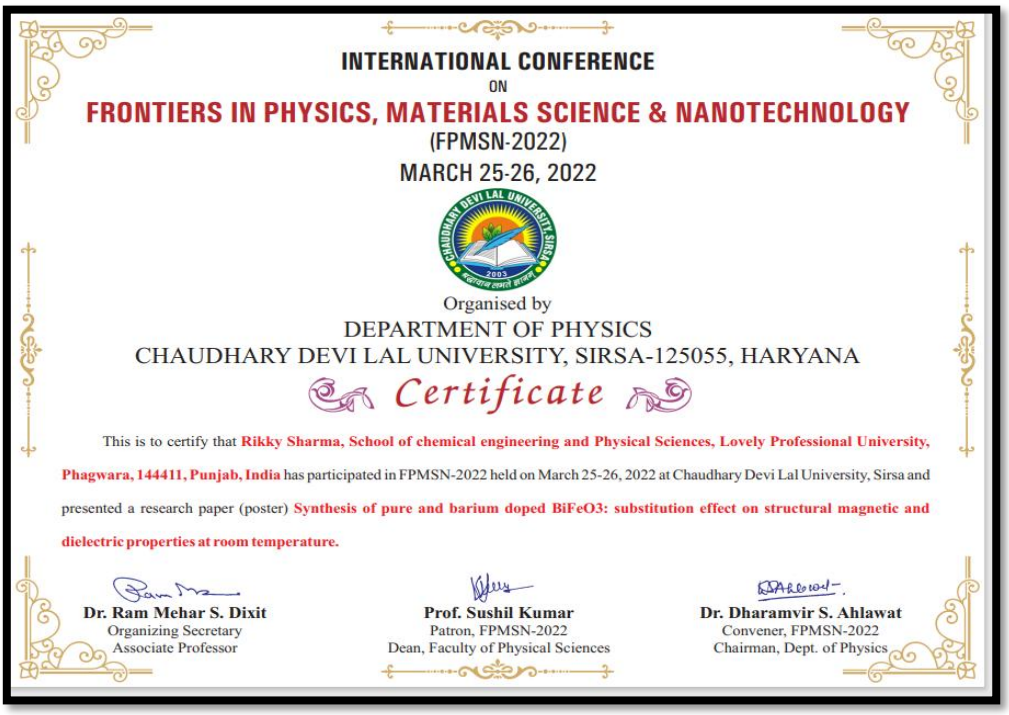

INTERNATIONAL CONFERENCE
ON
FRONTIERS IN PHYSICS, MATERIALS SCIENCE & NANOTECHNOLOGY
(FPMSN-2022)
MARCH 25-26, 2022

Organised by
DEPARTMENT OF PHYSICS
CHAUDHARY DEVI LAL UNIVERSITY, SIRSA-125055, HARYANA

Certificate

This is to certify that **Rikky Sharma, School of chemical engineering and Physical Sciences, Lovely Professional University, Phagwara, 144411, Punjab, India** has participated in FPMSN-2022 held on March 25-26, 2022 at Chaudhary Devi Lal University, Sirsa and presented a research paper (poster) **Synthesis of pure and barium doped BiFeO3: substitution effect on structural magnetic and dielectric properties at room temperature.**

Dr. Ram Mehar S. Dixit
Organizing Secretary
Associate Professor

Prof. Sushil Kumar
Patron, FPMSN-2022
Dean, Faculty of Physical Sciences

Dr. Dharamvir S. Ahlawat
Convener, FPMSN-2022
Chairman, Dept. of Physics

- Research paper presentation at the I3CMETAS-2022 conference.

Certificate No.:- I3CMETAS22/CC/153

PHD CHAMBER OF COMMERCE AND INDUSTRY

SEMS WELFARE FOUNDATION

Conference Certificate

This is to certify that the paper titled

Synthesis Of As-Prepared And Barium Doped Bifeo3: Substitution Effect On Structural Magnetic And Dielectric Properties At Room Temperature.

Authored/Co-authored by:

Rikky Sharma And Rupam Mukherjee

and Presented by:

Rikky Sharma

was presented in the mode of Online/Offline at International Conference On "Contemporary Challenges in Management, Education, Technology & Applied Sciences (I3CMETAS 22)" collaboratively organized by "SEMS & MIMT" held on April, 09 – 10, 2022 at Mangalmay Institute of Management & Technology, Greater Noida, UP

Mr. Atul Mangal, Chairman, MIMT
Mr. Ayush Mangal, Vice Chairman, MIMT
Mr. Arun Kumar Rana, Organizing Secretary, MIMT
Dr. Nitendra Kumar, Organizing Secretary, SEMS

- Research paper presentation at the (CHEMSMART-2022) International Conference.

NATIONAL INSTITUTE OF TECHNOLOGY ROURKELA

(An Institution of National Importance)

CHEMSMART-22

Certificate of Participation

This is to Certify that the Paper titled

Incorporation of Co(x), Al(y)into Bi (0.99) Ba (0.1) Fe (1-x-y) O3 and its effect on the microstructural, magnetic, and dielectric properties.

has been presented by the author(s)

Rikky Sharma

from

Lovely Professional University

In one of the technical sessions of An International Conference on ADVANCES IN SMART MATERIALS, CHEMICAL & BIOCHEMICAL ENGINEERING (CHEMSMART-22) organized by the Department of Chemical Engineering, NIT Rourkela, during December 16-18, 2022.

Dr. Krunal Gangawane
Convener–CHEMSMART-22

Prof. Abanti Sahoo
Chairman –CHEMSMART-22

Workshops

- Participated in a National workshop on recent material trends and devices by NIT Jalandhar.

Certificate ID: YCCMJA-CE000185

Dr B R AMBEDKAR NATIONAL INSTITUTE OF TECHNOLOGY
JALANDHAR, PUNJAB INDIA
(An Institution of National Importance under MHRD, New Delhi, Govt. of India)

One Week Short Term Course on

"Recent Trends in Advanced Materials and Devices"

(September 21, 2020 - September 25, 2020)

Certificate of Participation

This is to certify that Rikky Sharma *from* LPU *has participated in the* One Week Short Term Course *on* ***"Recent Trends in Advanced Materials and Devices"*** *organized by Department of Physics and Department of Electronics & Communication Engineering, Dr B R Ambedkar National Institute of Technology Jalandhar held during September 21, 2020 to September 25, 2020.*

Dr Ashish Raman
Coordinator

Dr Praveen Malik
Coordinator

Dr H M Mittal
Convener

- Participation in an International seminar on National Science Day organized by IISR.

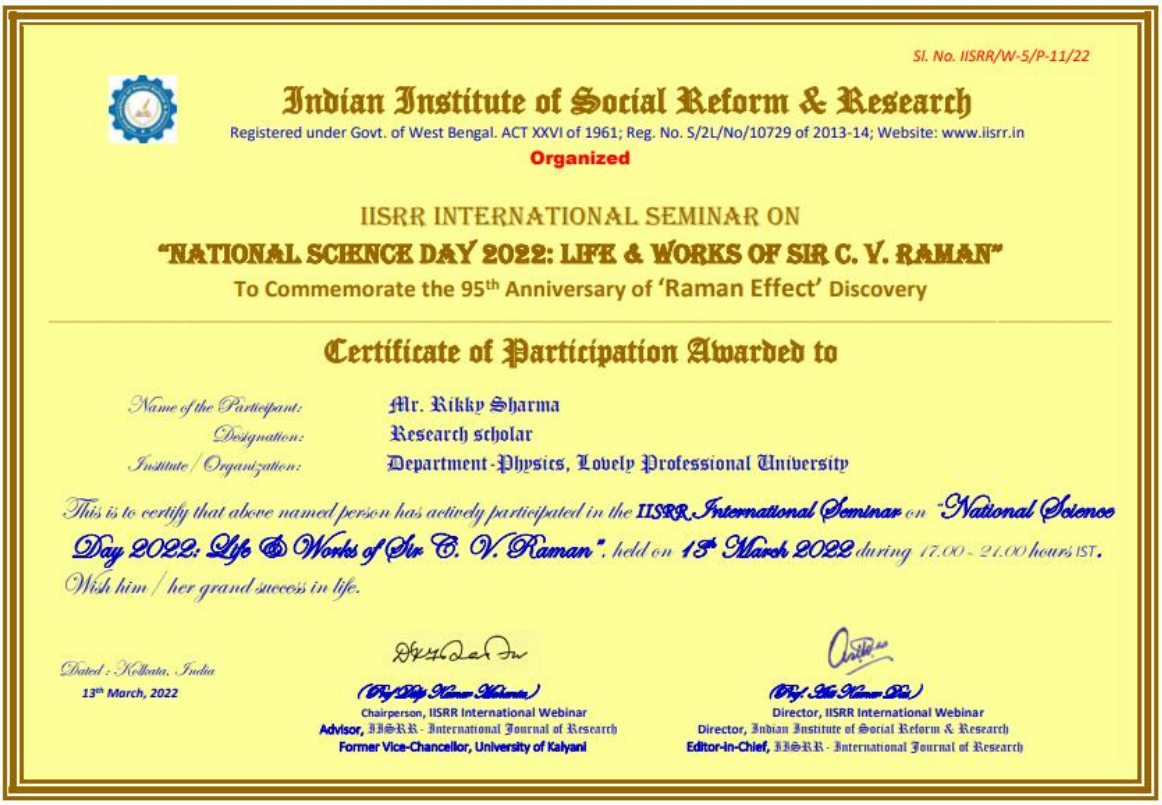

Sl. No. IISRR/W-5/P-11/22

Indian Institute of Social Reform & Research

Registered under Govt. of West Bengal. ACT XXVI of 1961; Reg. No. S/2L/No/10729 of 2013-14; Website: www.iisrr.in

Organized

IISRR INTERNATIONAL SEMINAR ON

"NATIONAL SCIENCE DAY 2022: LIFE & WORKS OF SIR C. V. RAMAN"

To Commemorate the 95th Anniversary of 'Raman Effect' Discovery

Certificate of Participation Awarded to

Name of the Participant: Mr. Rikky Sharma
Designation: Research scholar
Institute / Organization: Department-Physics, Lovely Professional University

This is to certify that above named person has actively participated in the IISRR International Seminar on "National Science Day 2022: Life & Works of Sir C. V. Raman", held on 13th March 2022 during 17.00 - 21.00 hours IST. Wish him / her grand success in life.

Dated : Kolkata, India
13th March, 2022

Chairperson, IISRR International Webinar
Advisor, IISRR - International Journal of Research
Former Vice-Chancellor, University of Kalyani

Director, IISRR International Webinar
Director, Indian Institute of Social Reform & Research
Editor-in-Chief, IISRR - International Journal of Research

❖ Webinar on excellence in teaching, training, and research BIET, CRESIHRD, and ICERS.

❖ Training program on IPR under National Intellectual Property Awareness Mission.

Publications

- **Sharma, R**., Maji, P.S. & Mukherjee, R. Dielectric, and magnetic response of $BiFeO_3$ in the presence of ionic filler at room temperature. J Mater Sci: Mater Electron 35, 71 (2024). https://doi.org/10.1007/s10854-023-11773-0.
- **Sharma, R**., Basandrai, D., Maji, P. S., & Mukherjee, R. Tailoring of dielectric, ferroelectric, and optical properties of Bi0. 99Nd0. 1Fe2O3/ZnO nanocomposite at room temperature. Inorganic Chemistry Communications. (2024), 112526. https://doi.org/10.1016/j.inoche.2024.112526
- **Sharma, R.,** Mukherjee, R., Kaur, M. et al. Compositional-driven variations in magnetic, conductivity, and ferroelectric properties of multiferroic $BiFeO_3$–$CoFe_2O_4$ composite system. Journal of Materials Research (2024). https://doi.org/10.1557/s43578-024-01336.
- **Sharma, R**., & Mukherjee, R. (2023). Incorporation of Co (x), Al (y) into Bi (0.99) Ba (0.1) Fe (1-xy) O3 and its effect on the microstructural, magnetic, and dielectric properties. Materials Today: Proceedings. https://doi.org/10.1016/j.matpr.2023.03.582

Other Publications

- Sharma, B., **Sharma, R.,** Kour, S., Sharma, M. D., Amin, O., Maity, A. R., & Mukherjee, R. (2022). Fractional exponents of electrical and thermal conductivity of vanadium intercalated layered 2H-NbS2 bulk crystal. *Indian Journal of Physics*, *96*(5), 1335-1339..https://doi.org/10.1007/s12648-021-02045-w
- Simrandeep Kour, O. Amin, B. Sharma, M. Kalyan, N. Kumari, **R. Sharma**, and R. Mukherjee. ” Frequency dependent conductivity in vanadium intercalated MnPSe3 bulk single crystal.” Journal of Emerging Technologies and Innovative Research 6 (2019): 738-4
- Kour, Simrandeep, **Rikky Sharma,** Sameena Sulthana, and Rupam Mukherjee. "Measurement Techniques for Determining the Thermal Conductivity of Bulk Samples and Thin Films." In Semiconductor Nanoscale Devices: Materials and Design Challenges, pp. 155-172. Bentham Science Publishers, 2025. DOI: 10.2174/9789815313208125010009

J Mater Sci: Mater Electron (2024) 35:71

Dielectric and magnetic response of $BiFeO_3$ in the presence of ionic filler at room temperature

Rikky Sharma[1], Partha Sona Maji[2], and Rupam Mukherjee[3,*]

[1] Department of Physics, Lovely Professional University Phagwara, Phagwara 144411, Punjab, India
[2] Department of Physics, Amity School of Applied Sciences, Amity University, Rajarhat Newtown, Kolkata 700135, India
[3] Department of Physics, Presidency University, Bangalore, Karnataka 560065, India

Received: 6 May 2023
Accepted: 2 December 2023

ABSTRACT

Composite systems consisting of ionic sodium chloride (NaCl) as a filler with varying weight percentages (x = 0%, 10%, 30%, and 50%) embedded into the matrix of multiferroic bismuth ferrite ($BiFeO_3$) were synthesized. Post-annealed at 750 °C, the XRD analysis reveals that the presence of NaCl leads to the formation of secondary phases. The particle grain size varies in the range of 0.5–1.5 µm as found from FESEM. The VSM study shows the coercive field (Hc) enhancement with maximum H_c = 79.18 Oe is found for the composite system x = 10%. The electrical impedance study reveals that at a low-frequency regime, the real component of dielectric permittivity has relatively increased for the composite systems compared to as-prepared bismuth ferrite (BFO). The dielectric loss increases at low frequency but remains comparable at the high-frequency limit, indicating a possible role in the energy storage application. Exponent (n) for frequency-dependent electrical conductivity is found to be large (n > 1) which is due to various degrees of the proximity of adjacent NaCl grains distributed in a multiferroic matrix.

1 Introduction

The high dielectric constant, low leakage current, high dielectric strength, flexible mechanical properties, and light weight are some of the highly desired properties for application in electrical power systems and green energy storage devices. Ferroelectrics are among the class of material species that show large dielectric constant that originates either from permanent dipole moment or the lone pairs of cations or the crystallographic distortion of the materials. The signature of ferroelectric exhibits spontaneous polarization below ordering temperature [1]. Further, the capability to possess multiferroic behavior with large dielectric permittivity leads to potential applications in different fields, from biomedical science to multifunctional microelectronic devices [2, 3]. Multiferroic materials possess the combined properties of ferroelectricity and ferromagnetism. $BiFeO_3$ is considered as one of the potential candidates for dielectric energy storage devices due to its strong magnetoelectric coupling at room temperature [4]. It is established that the A site Bi^{3+} ($6s^2$) state in BFO is considered to be the lone pair due to which the ferroelectricity originates at high temperature. In contrast, $EuTiO_3$ is found to show multiferroic behavior where ferroelectricity is induced by the tensile strain and negative chemical pressure on the B site of the Ti ion. As BFO is a widely investigated

Address correspondence to E-mail: rupam.mukherjee@presidencyuniversity.in

https://doi.org/10.1007/s10854-023-11773-0
Published online: 08 January 2024

Journal of MATERIALS RESEARCH

Article
DOI:10.1557/s43578-024-01336-2

Compositional-driven variations in magnetic, conductivity, and ferroelectric properties of multiferroic $BiFeO_3$–$CoFe_2O_4$ composite system

Rikky Sharma[1], Rupam Mukherjee[2,a], Mehakpreet Kaur[1], Sanat Kumar Adhikari[3], Madhumita Nath[1,4], Deepak Basandrai[1]

[1] Department of Physics, Lovely Professional University, Phagwara, Punjab 144411, India
[2] Department of Physics, Presidency University, Bangalore, Karnataka 560064, India
[3] UGC-DAE Consortium for Scientific Research Kolkata Centre, Salt Lake, Kolkata 700106, India
[4] Department of Physics, Deshabandhu Mahavidyalaya, Chittaranjan, West Bengal 71331, India
[a] Address all correspondence to this author. e-mail: rupam.mukherjee@presidencyuniversity.in

Received: 30 August 2023; accepted: 1 April 2024

The matrix of multiferroic $BiFeO_3$ $(1-x)$ and $CoFe_2O_4$ (x) as a filler with varying weight fractions ($x = 10$, 30, 50%) was synthesized by the sol–gel technique. The microstructure reveals that the filler at a critical weight fraction of 30% forms a clustering network that spans the entire system. Temperature-dependent dc resistivity of the composite systems confirms the semiconducting behavior where the large change in resistivity is mainly attributed to scattering by grain boundaries between percolating clusters. The VSM analysis implies that saturation magnetization in composite samples with $x = 10\%$ and 50% increases to 17 emu/g and 35 emu/g, respectively. The impedance analysis showed the presence of severe trapped charges that lead to depolarization effect in composites. However, the dielectric loss remains low for all composite systems till 10^4 Hz with the loss peak appearing around 10^5 Hz.

Introduction

Multiferroics are a class of materials that exhibit two or more primary ferroic ordering, thus making them a suitable candidate for various technological applications like spintronics, microsensors, and storage devices [1–4]. $BiFeO_3$, bismuth ferrite (BFO), is one of the well-known multiferroic materials whose lone electron pairs of Bi^{3+} lead to ferroelectric behavior and ordering of Fe^{3+} leads to G-type antiferromagnetic behavior. The simultaneous presence of both electrical and magnetic polarization at room temperature leads to strong magnetoelectric coupling which further offers a wide range of applications in electromagnetic transducers, biomedical applications, and solar cells for energy generation [4–7]. However, the intriguing properties of perovskite-structured BFO are strongly dependent on the fabrication process which has a direct impact on the coupling coefficient, thus making it weak. Moreover, the presence of a large leakage current, high transition temperature, and small magnetization limit its potential usage in scientific applications. Various methods such as substitutional doping, surface modification, and multilayer with imperfect interfaces have been adapted in order to improve the properties of multiferroic BFO materials [8–15]. Further, for better utilization of multiferroic materials in commercial technologies, the magnetoelectric coupling should be large enough in wide temperature range of 200–400 K. The lack of consistent and desired properties in so-far investigated multiferroic materials at wide temperature range has shifted our attention to nano-composite systems. In addition, it has also been reported that as compared to single-phase materials, composite systems are prone to have synergistic effect that leads to remarkable magnetoelectric coupling due to the product tensor properties [16]. The interfacial phenomena between the nanoparticles of the constituent phases in composites can also produce multifunctional miniaturized devices like spintronics with high efficiency and fast electric and magnetic switching. However, magnetoelectric effect in percolation-based composite systems has not been studied in details till date. In our work, $CoFe_2O_4$ (CFO) nanoparticles are embedded into the matrix of BFO in order to investigate the degree of magnetoelectric coupling in the percolative composite system. The CFO is well known for its high magnetic coercivity,

Inorganic Chemistry Communications 165 (2024) 112526

Contents lists available at ScienceDirect

Inorganic Chemistry Communications

journal homepage: www.elsevier.com/locate/inoche

Short communication

Tailoring of dielectric, ferroelectric, and optical properties of $Bi_{0.99}Nd_{0.1}Fe_2O_3$/ZnO nanocomposite at room temperature

Rikky Sharma [a], Deepak Basandrai [a,*], Partha Sona Maji [b], Rupam Mukherjee [c]

[a] Department of Physics, Lovely Professional University Phagwara, 144411, Punjab, India
[b] Department of Physics, Amity School of Applied Sciences, Amity University, Rajarhat Newtown, Kolkata 700135, India
[c] Department of Physics, Presidency University, Bangalore, Karnataka, 560064, India

ARTICLE INFO

Keywords:
Multiferroic
Composite
Impurity phase
Polarization
Bandgap

ABSTRACT

We observe the fine-tuning of electrical and optical properties in a composite nanoparticle system consisting of varying weight fractions of semiconducting ZnO grains (x) embedded into Nd-doped multiferroic $Bi_{0.99}Nd_{0.1}Fe_2O_3$ matrix and annealed at 500 °C. X-ray diffraction (XRD) is used to validate the phase which further reveals the existence of cubic ZnO phases and rhombohedral BFO with some impurity phases. With the aid of SEM and EDX, the morphological and elemental composition of grains are found to be affected by ZnO nanoparticles. To understand the nature of dielectric response impedance analysis is performed which reveals the presence of large resistance offered by a composite maximum of 46.8 KΩ at x = 10 %. The enhancement in dielectric constant and dielectric loss is observed at higher concentrations for (x = 5 %). The Ferroelectric investigation shows that the maximum polarization achieved at low frequency for x = 10 % is 22.13 μc/cm^2. The optical band gap in the composite sample exhibits significant dependence on ZnO concentrations, thus indicating potential application in optoelectronic devices.

1. Introduction

The search for novel compounds with distinct and flexible properties has prompted researchers to look into multifunctional materials that exhibit fine control of electrical and magnetic properties in miniaturized smart devices. Multiferroics are materials that exhibit both ferroelectric and ferromagnetic characteristics concurrently in a single phase[1]. The presence of both the ferroic properties in a material simultaneously has received a lot of attention in the development of non-volatile memory devices, ultrafast optoelectronic devices, spintronics, transducers, solar cells for energy generation [2], biomedical applications [3,4,5,6]. Till date, $BiFeO_3$ (BFO) is one of the most studied single-phase multiferroic materials with ferroelectric and anti-ferromagnetic characteristics at ambient temperature [7]. It has ferroelectricity at 643 K Curie temperature and anti-ferromagnetism at 1143 K Neel temperature. Its perovskite crystal structure is deformed and rhombohedral, of the ABO3 type, with an R3c space group[8]. A-sites in BFO are typically held by Bi^{3+} ions, which promote the stability of ferroelectricity in deformed structures, whereas B- B-sites are filled by transition metal ions (Fe), which contribute to magnetism. The unoccupied d^0 orbital causes ferroelectricity in multiferroics, whereas partially filled d^n orbitals cause ferromagnetism[9]. Ferroelectricity can, however, be formed by the stereochemical activity of Bi^{3+} ions, whereas Fe^{3+} ions cause ferromagnetism in BFO. Many partial replacements of rare-earth ions at Bi^{3+} sites and transition metal ions at Fe^{3+} sites can significantly improve electrical and magnetic characteristics[10]. Ferroelectricity is caused by the displacement of Bi^{3+} and Fe^{3+} cations along the [1 1 1] planar direction, which is off-centered to the oxygen octahedron[10]. Even though BFO exhibits versatile properties for device applications, its practical applicability is limited due to the occurrence of contamination or impurity phases in the synthesis process. During synthesis, the unwanted impurity phases cause some unfavorable characteristics, such as weak magneto-electric coupling, high tangent loss, structural distortion, high current leakage and other secondary phase formations, which subsequently affect the dielectric permittivity, ferroelectric, electrical resistivity, and magnetic hysteresis of the material[11]. To solve the drawbacks of single-phase Bismuth Ferrite, research has been carried out by doping rare earth elements (La, Y, Gd, Sm, Nd, Tb, and so on) at the A-site of Ferroic materials to improve their properties [7,12,13,14,15]. Various reports observe that doping has effectively enhanced the overall properties of the Bismuth ferrite. Shisode et al. has reported synthesis of $Bi_{1-x}Sr_xFeO_3$ (x = 0.05, 0.15, 0.25) by sol–gel

* Corresponding author.
E-mail address: deepakbasandrai@gmail.com (D. Basandrai).

https://doi.org/10.1016/j.inoche.2024.112526
Received 28 March 2024; Received in revised form 25 April 2024; Accepted 9 May 2024
Available online 10 May 2024

ARTICLE IN PRESS

Materials Today: Proceedings xxx (xxxx) xxx

Contents lists available at ScienceDirect

Materials Today: Proceedings

journal homepage: www.elsevier.com/locate/matpr

Incorporation of Co $_{(x)}$, Al $_{(y)}$ into Bi $_{(0.99)}$ Ba $_{(0.1)}$ Fe $_{(1-x-y)}$ O_3 and its effect on the microstructural, magnetic, and dielectric properties

Rikky Sharma, Rupam Mukherjee *

School of chemical engineering and Physical Sciences, Lovely Professional University, Phagwara 144411, Punjab, India

ARTICLE INFO

Article history:
Available online xxxx

Keywords:
Sol-Gel
Magnetism
Dielectric
XRD

ABSTRACT

The work is focused on synthesizing Bi $_{(0.99)}$ Ba $_{(0.1)}$ Fe $_{(1-x-y)}$ Co $_{(x)}$ Al $_{(y)}O_3$ with composition (x = 0, y = 0), (x = 0.1, y = 0) and (x = y = 0.1) using solgel method and investigating magnetic and dielectric properties at room temperature. The obtained Nanoparticles in the form of fine powder have undergone pre-sintering at 200 °C for 2 h and after that sintering at 500 °C for 3 h. The structural and morphological studies were investigated using X-ray diffraction (XRD) and FE-SEM. The XRD analysis reveals the presence of $BiFeO_3$ with rhombohedral R3C group along with the impurity phases. The crystallite size is found to decrease along with the shrinkage in Lattice Constant. The SEM images show the formation of irregular and heterogeneous structures. It has been observed that the addition of Co followed by Al is found to reduce impurity phases. The presence of Co and Al is confirmed by EDX mapping. The VSM (Vibrating sample magnetometer) is used to investigate room-temperature magnetism by plotting the Hysteresis loop. The magnetic study reveals that subsequent addition Co and Al has offered improved magnetic properties attaining maximum Hc =1570 Oe at room temperature. The dielectric response as a function of Frequency from 100 Hz to 10 MHz is observed. The change in the dielectric constant and reduction in dielectric loss are observed.

Selection and peer-review under responsibility of the International Conference on Advances in Smart Materials, Chemical & Biochemical Engineering.

1. Introduction

Due to the presence of two or more fundamental ferroic orderings, multiferroics [1,2] are well-known materials and an excellent choice for a variety of electrical devices [3]. Due to its low band gap and robust magnetoelectric coupling at ambient temperature, bismuth ferrite is a well-known multiferroic with a wide range of applications in electronic devices, medicinal applications, and solar cells [4–8]. Its potential applications are constrained by the presence of a substantial leakage current, a high transition temperature, and a modest magnetization. These materials are more dependable for use in electronic and magnetic devices because they have strong magnetic characteristics and strong, stable electronic properties at room temperature.Many researchers over the world have developed various mechanisms to modify the properties of multiferroic materials such as doping, and composite, anisotropy change, synthesis mechanism [1]. The structure plays a vital role in deciding the properties of the materials by tailoring the microstructure and morphology we can interplay with such material by replacing A and B cations [2]. Although the perovskite Phase in multiferroic Bismuth ferrite is very sensitive the interplay of structural disorder is considered one of the key features to improve electronic properties. Various studies reported that the incorporation of other Anion and Cation enhanced the overall physical properties[3,4]. The incorporation of Ba into Bi is found to influence the multiferroic and dielectric properties [4–7]. This implies that the choice of a suitable dopant can finely tune the required properties. In this study, we have synthesized Bi $_{(0.99)}$ Ba $_{(0.1)}$ Fe $_{(0.99-x-y)}$ Co $_{(x)}$ Al $_{(y)}O_3$ for (x = 0, y = 0), characterization (x = 0.1, y = 0) and (x = y = 0.1)using the sol–gel method as it is having various advantages over another synthesis route[8–10]. According to the researchers, both Al [11–13] and Co[14–16] are effective at changing the electrical and magnetic properties. As a result, the simultaneous insertion of both dopants in our situation is expected to improve the electrical and magnetic characteristics in the presence of Ba. The purpose of the study is to enhance the electronic and room temperature and their significant effect on the microstructure and may find their potential application in device fabrication.

* Corresponding author.
E-mail address: Raddressupam.23644@lpu.co.in (R. Mukherjee).

https://doi.org/10.1016/j.matpr.2023.03.582
2214-7853/
Selection and peer-review under responsibility of the International Conference on Advances in Smart Materials, Chemical & Biochemical Engineering.